

N72-14304

G.V. Logvinovich

HYDRODYNAMICS OF FREE-BOUNDARY FLOWS

**CASE FILE
COPY**

TRANSLATED FROM RUSSIAN

**Published for the National Aeronautics and Space Administration
and the National Science Foundation, Washington, D.C.
by the Israel Program for Scientific Translations**

G.V. Logvinovich

HYDRODYNAMICS OF FREE-BOUNDARY FLOWS

(Gidrodinamika techenii so svobodnymi granitsami)

Izdatel'stvo "Naukova Dumka"
Kiev 1969

Translated from Russian

Israel Program for Scientific Translations
Jerusalem 1972

TT 70-50187
NASA TT F-658

Published Pursuant to an Agreement with
THE NATIONAL AERONAUTICS AND SPACE ADMINISTRATION
and
THE NATIONAL SCIENCE FOUNDATION, WASHINGTON, D. C.

Copyright © 1972
Israel Program for Scientific Translations Ltd.
IPST Cat. No. 5922
ISBN 0 7065 1209 X

Translated by D. Lederman
Edited by P. Greenberg

Printed in Jerusalem by IPST Press
Binding: Wiener Bindery Ltd., Jerusalem

Available from the
U. S. DEPARTMENT OF COMMERCE
National Technical Information Service
Springfield, Va. 22151

Contents

FOREWORD	1
CHAPTER ONE. Principal Properties of Free Boundaries	3
1. The dynamic boundary condition	4
2. The kinematic boundary condition	7
3. Orthogonal free surface	9
4. Steady free boundaries	11
5. Self-similar free boundaries	15
6. The spray root	17
7. The tip of a spray sheet	18
CHAPTER TWO. Some General Properties of Potential Free-Boundary Flows .	19
1. The velocity potential	19
2. The stream function	20
3. Boundary conditions and the general nature of the flows . . .	21
4. Velocity potential at free boundaries	22
5. Equipotential surfaces	24
6. Pressure within the fluid	25
7. Kinetic energy of the fluid	27
8. The energy equation	29
9. The momentum theorem	29
10. Zero-potential surface	32
11. Mass, momentum and energy fluxes through the zero- potential surface	33
12. Green's theorem	34
CHAPTER THREE. Elementary Gases of Free-Boundary Flows	38
Flow with Spherical Symmetry	
1. Spherical flow	38
2. Inertia flow	39
3. Equipotential surface	40
4. Kinetic energy	41

Cavitation in Jets	
5. Two-dimensional expansion of a fluid annulus	42
6. Motion of a thin fluid annulus	43
7. Drag and the reentrant jet	45
8. General treatment of the energy and momentum equations .	47
Planing of a Plate	
9. Steady free boundaries	49
10. Kinetic energy	50
11. Stagnation point	51
12. Lift and drag	52
CHAPTER FOUR. Symmetric Immersion of a Body into a Fluid	54
1. Impact of bouyant bodies	54
2. Immersion and impact	56
Continuous Immersion of a Profile	57
3. Uniform immersion of a wedge (Wagner's problem)	57
4. Small deadrise angles	60
5. Kinematic elements of the free surface	65
6. Graphical representation of the momentum and energy . . .	66
7. Velocity and pressure distributions	68
8. Drag on a cylinder	70
9. Transient drag	71
10. Estimating the transient function	73
11. Some experimental results	75
Uniform Immersion of a Cone	76
12. Immersion of a cone	76
13. Case of small deadrise angles	78
14. Application of the pressure integral for determining the drag on a cone	80
15. Transient drag on a cone	84
Symmetric Immersion of Bodies at Variable Velocity	87
16. Immersion of bodies at variable velocity	87
17. Principal energy and momentum equations	90
18. Application of the Wagner integral to calculation of drag . .	91
19. Axisymmetric immersion of a slender body	94
20. Induced mass of a slender body	95
21. Fall of a body on the surface of a fluid	97
22. Principal equations for compressible fluids	98
23. Simplest case of impact	99
24. Limiting cases of motion	101
CHAPTER FIVE. Developed Cavitation	103
1. Cavity drag	104
2. Shape of an infinite axisymmetric cavity	105

3. Application of the momentum theorem to the determination of the drag and dimensions of a cavity	107
4. Corollaries of the momentum theorem	109
5. General equation for cavity expansion	110
6. Approximation equation of the cavity profile and length	113
7. Cavitation energy	115
8. The principle of "independent expansion" of a cavity	116
9. Cavity sealing and wake flow	118
10. Structural details of cavities in a heavy fluid	118
11. Rising of the cavity	120
12. Cavity downwash in asymmetric flow	122
13. The general case of transverse motion of a cavity	123
14. Equation of motion for the perturbed motion of a cavity	127
15. Effect of the free surface and walls	129
16. Different stages of developed cavitation and the loss of gas from a cavity	129

CHAPTER SIX. Method of Plane Sections and Its Application for

Calculating Hydrodynamic Forces	134
1. Basic conditions and principles	135
2. Approximate calculation of induced masses. Motion in an ideal fluid	137
3. The concept of the pierced layer	140
4. Flow with streamline separation	142
5. Further refinements of the theory	144
6. Forces on a partly wetted body	147
7. Planing. Principal considerations	149
8. Equations for calculating the planing of a profile	152
9. Equations of motion	155
10. Vibrations of a slender body. The flapping wing	156
11. Small vibrations of a solid slender body	157
12. Motion of a flexible body	160

CHAPTER SEVEN. Cavitating Hydrofoils 163

1. Flow past a profile and past finite-span hydrofoils	163
2. Lift and induced drag	166
3. Effect of cavity on the downwash	168
4. Effect of hydrofoil immersion depth	170
5. The lift of a profile at small immersion depth	173
6. Hydrodynamic features of hydrofoils	175
7. Flow past a wedge-shaped profile	176
8. Application of the Sedov theory to cavitating hydrofoils	178
9. Estimating the hydrodynamic features of a noncavity wedge-shaped profile	180

10. Polar diagram of hydrofoil and experimental data	180
11. Fully stalled profile	186
12. Application of wing theory to the calculation of a cavitating plate	188
13. Stalled foil of finite span	189
Bibliography	192

FOREWORD

Many current problems in hydrodynamics are concerned with bodies moving at high velocities in fluids, which inevitably entail the formation of free boundaries. In the majority of cases exact solutions of such problems cannot be found.

This monograph deals with general physical flow properties at the front of a body in a fluid, flows with developed cavitation, planing and other related situations, when allowance must be made for free-boundary effects and surface discontinuity.

Theorems and general approaches to the problem have been concerned to an equal extent with both two- and three-dimensional flows, which allow one, with sufficient generality, to construct a model of the effect under consideration, carry out approximate calculations, interpret experiments, and formulate specific mathematical problems. This being the case, the author almost completely omitted well-known solutions to two-dimensional problems dealing with collisions, free-jet flow past bodies and planing; applicable solutions are therefore quoted as known results which may be found in the literature.

Analysis of complicated flows arising on the formation of free boundaries, in many cases enables one to successfully develop a method for finding comprehensive estimates and for deriving relatively simple formulas with which to compute some effects which cannot be calculated with mathematical exactitude. The author strove, if only to a limited extent, to comply with engineering requirements; different engineering aspects involving the use of simple methods are investigated, and preliminary quantitative estimates of complex phenomena associated with the motion of solid bodies in a fluid are made. Consequently, many results are derived from simple computational formulas.

It is usually difficult to theoretically assess the accuracy of a formula obtained by approximation methods. Therefore, in every section basic experimental data are cited and compared with the approximate theoretical results. Their agreement under specific conditions may serve as a basis for the use of both the results themselves and of the method involved in their derivation. One should bear in mind that very few important practical hydrodynamic problems are solved theoretically with the aid of flow patterns which are fairly close to those in actual flows. In the majority of important cases, in order to extract mathematical solutions, the original flow model is simplified to some extent and the resulting solutions reflect only to a limited extent the actual physical processes involved. This situation may be illustrated by problems on hydrofoils solved in the linear approximation on the assumption that the free surface is plane, and that both the hydrofoil thickness and angle of attack are infinitesimal. In actual fact, for a profile

of finite thickness and finite angle of attack the free surface is to some extent distorted, because the hydrofoil may be raised above the undisturbed level, although this is by no means evident from linear theory. It is generally impossible to construct a nonlinear theory and so it is almost always necessary to set up an experiment which, however, cannot yield scientific and practical data without theoretical analysis of its design and results. For this purpose an approximate computation may prove useful.

The classical results of Keldysh, Lavrent'ev and Sedov directly concerned with continuous motion of fluids, subject to certain modifications, appear to be applicable to discontinuous cavitation flow. In particular, Sedov's thin-wing theory appears to be valid also for a cavitating hydrofoil.

This monograph is based on a paper* by the author bearing the same title.

The section dealing with submersion of a body in a fluid has been supplemented by data on maximum [collapse] cavity dimensions, energy loss in collisions, and on approximations made necessary by the need to make allowance for the fluid's compressibility, compiled on the basis of published work by the author.

The general equations of dynamics of a thin body are solved in the form of a formula for computing the force due to vibrations of rigid and flexible thin bodies. Results for a flexible body explain the swimming mechanism of fish and sea animals, and also allow interesting computations to be undertaken. Subsequent development of this theory to include inhomogeneous wakes of oscillating bodies, analysis of various profiles and refinement of experimental results allows one to explain in detail the mechanism of a flapping wing.

* Logvinovich, G.V. *Gidrodinamika techenii so svobodnymi granitsami* (Hydrodynamics of Free-Boundary Flows).— In: *Trudy TsAGI*, 935. Moskva. 1965.

Chapter One

PRINCIPAL PROPERTIES OF FREE BOUNDARIES

When solid bodies are submerged in a fluid, the free boundaries of the latter are set into motion, which in many cases cannot be neglected. If the body moves at high velocity, but the velocity of the fluid is still substantially smaller than the speed of sound, and the different points at the surface of the body do not simultaneously make contact with the fluid, then the ponderability [weight] and compressibility of the fluid can be neglected. When many points at the body surface come simultaneously into contact with the fluid (impact) the compressibility must be taken into account, since the impact produces compression waves, which carry away a part of the energy. The surface tension forces are inconsequential, if the dimensions of the bodies and the dynamic pressures in the fluid are sufficiently large. The frictional forces are not always negligible; however, they can usually be approximately taken into account and added to the result obtained with these neglected.

Usually the free boundaries of a fluid are limited by the atmosphere. Their motion sets the atmospheric gas into motion, which involves some changes in the pressure at the free boundary. However, in the majority of cases the density of the gas is negligible compared with that of the liquid. Hence the pressure at each point of the free boundary can to a good approximation be regarded as uniform and not time-dependent.

The above considerations make it possible to treat the fluid as ideal, weightless and incompressible, and the pressure at the free boundaries as constant. In an ideal fluid any change in the motion can occur only due to normal pressures applied to the fluid boundaries. Consequently, if the flow was potential before being acted upon by the body, it will remain so also thereafter.

Before passing on to the study of particular cases, we consider the basic general properties of free, constant-pressure boundaries.

The physical properties of moving free boundaries, postulated below, reduce to three conditions: 1) the pressure along the free boundary is constant, and consequently the pressure gradient within the fluid at the free boundary is normal to it; 2) the rate at which a point of the free boundary moves along the normal to it is equal to the projection, on this normal, of the absolute velocity of a fluid particle, coinciding with this point; 3) the fluid particles, once they arrive at the free boundary, remain there during the subsequent motion.

1. The dynamic boundary condition

We assume that the orthogonal coordinate system x, y, z is associated with the quiescent fluid, and let the unit vectors of the coordinate axes be i, j and k . The unit vectors of the outward normal and of two orthogonal tangents to the free boundary at some point ξ , with which the particle under study coincides, are denoted by \bar{e}_s, \bar{e}_n and \bar{e}_τ . The absolute particle velocity is $\bar{u} = \bar{e}_s u_s + \bar{e}_n u_n + \bar{e}_\tau u_\tau$ (Figure 1).

Euler's equation for an ideal fluid not acted upon by mass forces is*

$$\frac{D\bar{u}}{Dt} = -\frac{1}{\rho} \text{grad } p. \quad (1.1)$$

The first boundary condition, which follows from the fact that the pressure is the same at any point of the free surface, reduces to the following equivalent expressions:

$$\bar{e}_n \times \frac{D\bar{u}}{Dt} = \bar{e}_n \times \text{grad } p = 0 \quad (1.2)$$

or

$$\bar{e}_s \frac{Du_s}{Dt} = 0; \quad \bar{e}_\tau \frac{Du_\tau}{Dt} = 0. \quad (1.2a)$$

Consequently, the absolute acceleration of fluid particles at a free, constant-pressure surface is always directed along the normal to this surface.

The motion of fluid particles forming the free boundary is equivalent to frictionless motion of a material point over a moving surface with the normal reaction defined by $\frac{\partial p}{\partial n}$. Hence all the principles studied in dynamics apply also here.

The components of angular velocity of the free surface at the point where the particle is located are denoted by ω_s, ω_n and ω_τ , where s, n and τ are the pertinent axes.

The absolute acceleration of the particle is

$$\begin{aligned} \bar{\omega} = \frac{D\bar{u}}{Dt} = \bar{e}_s \left(\frac{Du_s}{Dt} + u_\tau \omega_n - u_n \omega_\tau \right) + \bar{e}_n \left(\frac{Du_n}{Dt} + u_s \omega_\tau - u_\tau \omega_s \right) + \\ + \bar{e}_\tau \left(\frac{Du_\tau}{Dt} + u_n \omega_s - u_s \omega_n \right). \end{aligned}$$

Expansion of the vector product $\bar{e}_n \times \frac{D\bar{u}}{Dt}$ yields

$$\begin{aligned} \frac{Du_s}{Dt} + u_\tau \omega_n - u_n \omega_\tau = 0, \\ \frac{Du_\tau}{Dt} + u_n \omega_s - u_s \omega_n = 0. \end{aligned} \quad (1.3)$$

The pressure gradient is $p = \bar{e}_s \frac{\partial p}{\partial s} + \bar{e}_n \frac{\partial p}{\partial n} + \bar{e}_\tau \frac{\partial p}{\partial \tau}$, but since it follows from equation (1.2) that $\frac{\partial p}{\partial s} = 0$ and $\frac{\partial p}{\partial \tau} = 0$ we obtain

$$\frac{Du_n}{Dt} + u_s \omega_\tau - u_\tau \omega_s = -\frac{1}{\rho} \frac{\partial p}{\partial n}. \quad (1.4)$$

* The Stokes derivative $\frac{D}{Dt}$ is used in its ordinary sense, i.e., when differentiation pertains to individual fluid particles.

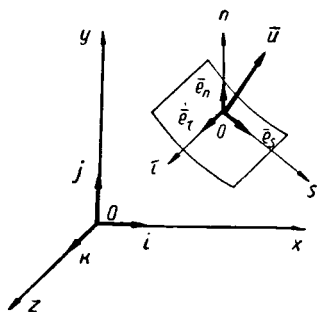


FIGURE 1.

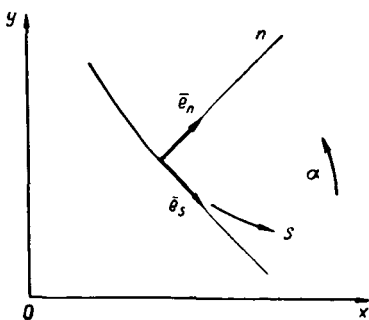


FIGURE 2.

In particular, for plane-parallel motion of a segment of the free surface and assuming that the flow in each plane $z = \text{const}$ is the same, and aligning the s and n axes in this plane in the manner shown in Figure 2, we derive

$u_t = 0$, $\omega_n = 0$, $\omega_t = \frac{D\alpha}{Dt}$, and $\omega_s = 0$, where α is the angle between s and x .

Hence, by virtue of the fact that $e_s \frac{Du}{Dt} = 0$, boundary conditions (1.3) and (1.4) can be written in the form

$$\frac{Du_s}{Dt} = u_n \frac{D\alpha}{Dt}; \quad \frac{Du_n}{Dt} + u_s \frac{D\alpha}{Dt} = -\frac{1}{\rho} \frac{\partial p}{\partial n}. \quad (1.5)$$

It is easy to show that conditions (1.5) hold for any axisymmetrical flow, provided that axes s and n coincide with the plane passing through the axis of symmetry.

All hydrodynamic problems with moving free boundaries can be subdivided into two groups. The first group comprises flows in which new particles do not emerge at the free surface, for example, an infinite submerged wedge or cone without flow separation (Figure 3). In these cases the individual particles can be designated by their initial ($t = 0$) coordinates at the undisturbed free surface (x_0, y_0, z_0) . The subsequent location of the particle, expressed as $x = x(x_0, y_0, z_0, t)$, $y = y(x_0, y_0, z_0, t)$, and $z = z(x_0, y_0, z_0, t)$, defines its trajectory s' .

The second group of problems includes flows in which new particles, until now residing within the fluid, rise to the free surface. These are instances of planing and submersion of wedges and cones with finite dimensions, when free jets or cavities form at the edges of bodies. Obviously these particles can be designated by the time and coordinates of the point at which they are shedded from the solid surface, which again are functions of time. The free surfaces formed by particles situated there at the start of motion will be termed outer free boundaries, while the free boundaries formed by particles shedded by the edges of the body are termed inner free boundaries. We note that in a number of the cases outer free boundaries may coexist simultaneously with the formation of inner boundaries (Figure 4). Thus, the free surface behind the planing step of a gliding [hydrofoil] vessel is an inner free surface, while that at the front and sides of the hydrofoil and wake is an outer free surface.

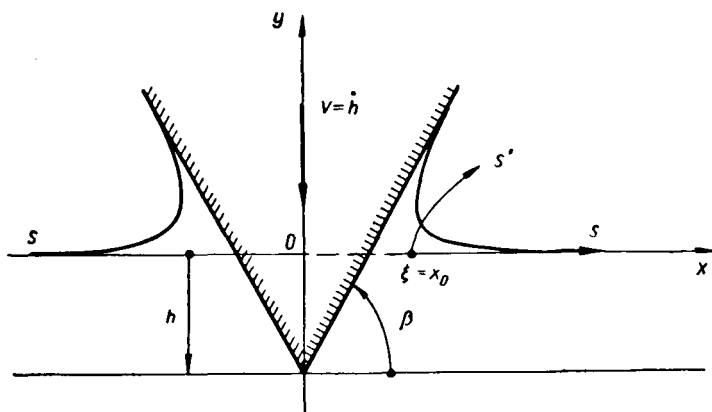


FIGURE 3.

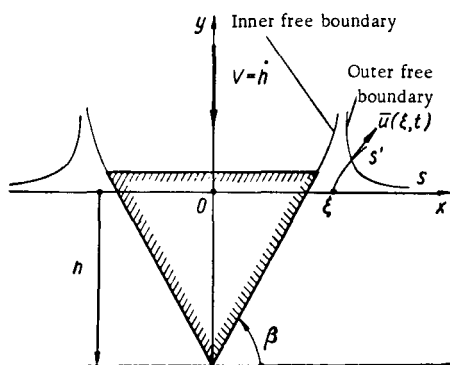


FIGURE 4.

After the particles emerge at the free surface, the behavior of the [individual] parts of these boundaries is the same and obeys the same equations, irrespective as to whether the boundaries are inner or outer. However, if the fluid started moving from rest, then for an outer free boundary at time $t = 0$ the velocities of all the boundary particles will be $u_{x0} = 0$, $u_{y0} = 0$ and $u_{z0} = 0$. For inner free boundaries the particle emerges at the boundary at some time $t > 0$ and has in general nonzero initial velocities.

Each individual fluid particle is designated by ξ , which denotes the set of its initial coordinates. In the particular case of two-dimensional or axisymmetrical flows it is convenient, for outer boundaries, to regard ξ as denoting the initial distance from the particle to the coordinate origin, while the meaning of ξ for inner boundaries will be clarified below.

2. The kinematic boundary condition

Let us consider the two-dimensional motion of a free-surface element of length δs , on which are present particles ξ and $\xi + \delta\xi$ (Figure 5). Let the coordinates of these particles at the time $t = t_1$ be $\xi = s$ and $\xi + \delta\xi = s + \delta s$. Denoting the velocity vector pertaining to each particle by $\bar{u}(\xi, t)$ we find that the absolute velocity of particle ξ is $\bar{u}(\xi, t_1)$ and its displacement over the small time interval δt is $\bar{u}(\xi, t_1) \delta t$. The velocity of particle $\xi + \delta\xi$ at the same instant will be $\bar{u}(\xi + \delta\xi, t_1) = \bar{u}(\xi, t_1) + \frac{\partial \bar{u}}{\partial \xi} \delta\xi$ and its displacement will be $\bar{u}(\xi, t_1) \delta t + \frac{\partial \bar{u}}{\partial \xi} \delta\xi \delta t$. Denoting, as before, the unit vectors along the tangent and normal to the free surface at time t_1 by \bar{e}_s and \bar{e}_n , respectively, we find that at time $t_1 + \delta t$ the distance between the points under study changes by an amount $\bar{e}_s \frac{\partial \bar{u}}{\partial \xi} \delta\xi \delta t$ and the free-surface element in its new position makes an angle $\delta\alpha = \bar{e}_n \frac{\partial \bar{u}}{\partial \xi} \delta t$ with the original position. The distance along the boundary s between particles ξ and $\xi + \delta\xi$ at time $t_1 + \delta t$ will be $\delta s' = \delta s + \bar{e}_s \frac{\partial \bar{u}}{\partial \xi} \delta\xi \delta t$, while at time t_1 , it was $\delta\xi = \delta s$.

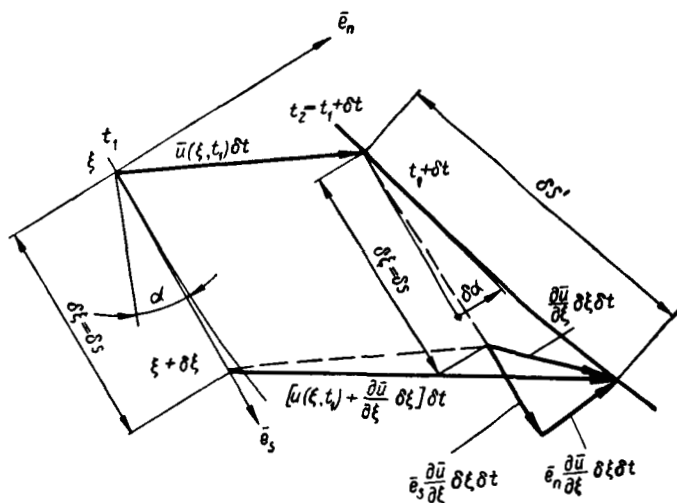


FIGURE 5.

We now introduce the relative elongation of the free surface

$$\varepsilon = \lim_{\delta \rightarrow 0} \left(\frac{\delta s'}{\delta} - 1 \right) = \frac{\partial \bar{u}}{\partial \xi} - 1.$$

As $\delta \rightarrow 0$, we have

$$\delta\alpha = \bar{e}_n \frac{\partial \bar{u}}{\partial \xi} \delta t = \bar{e}_n \frac{\partial \bar{u}}{\partial s} \delta t; \quad \delta s' - \delta s = \bar{e}_s \frac{\partial \bar{u}}{\partial \xi} \delta\xi \delta t$$

and hence

$$\begin{aligned}\frac{D\mathbf{e}}{Dt} &= \bar{\mathbf{e}}_s \frac{\partial \bar{\mathbf{u}}}{\partial s} = \frac{\partial \mathbf{u}_s}{\partial s} - \mathbf{u}_n \frac{\partial \alpha}{\partial s}; \\ \frac{D\alpha}{Dt} &= \bar{\mathbf{e}}_n \frac{\partial \bar{\mathbf{u}}}{\partial s} = \frac{\partial \mathbf{u}_n}{\partial s} + \mathbf{u}_s \frac{\partial \alpha}{\partial s}.\end{aligned}\quad (1.6)$$

Here the partial derivative is used in the sense that the time is held constant while differentiation is performed by moving from one particle to another along the free boundary s . The curvature of this surface is $\frac{\partial \alpha}{\partial s} = \frac{1}{R}$, where $R = R(s, t)$ is the radius of curvature of the free surface in the region of particle ξ under study if $\xi = s$. The first of equations (1.6) yields the theorem on "nonextensibility" of free boundaries.

The distances between particles measured along the free surface remain constant if $\varepsilon = \text{const}$ or $\frac{D\varepsilon}{Dt} = 0$. It follows from the first of equations (1.6) that this condition is satisfied only when vector $\frac{\partial \bar{\mathbf{u}}}{\partial s}$ is orthogonal to element s .

Theorem I. The distances between individual particles along a moving free surface remain constant only when the partial derivative of the absolute velocity vector of the fluid along the free surface, taken along this surface, is orthogonal to the free surface.

Substitution of the right-hand side of the second of equations (1.6) into the first of equations (1.5) yields the Wagner generalized boundary condition

$$\frac{D\mathbf{u}_s}{Dt} = \mathbf{u}_n \left(\bar{\mathbf{e}}_n \frac{\partial \bar{\mathbf{u}}}{\partial s} \right) = \mathbf{u}_n \left(\frac{\partial \mathbf{u}_n}{\partial s} + \mathbf{u}_s \frac{\partial \alpha}{\partial s} \right). \quad (1.7)$$

The fact that free-surface elements δs have no inflection in the vicinity of particle ξ is expressed by the condition $\frac{D\alpha}{Dt} = 0$.

Theorem II. The tangential velocities $\mathbf{u}_s(\xi, t)$ of individual particles at a two-dimensional free boundary moving parallel to itself (Figure 6) cannot be changed by arbitrarily modifying the normal velocity of the boundary.

This theorem is of importance in the study of unsteady motion of bodies with spray sheets forming at their surface.

If the free surface is described by the equation $F(x, y, z, t) = 0$, then the normal velocity of each point of this surface is $/10/$

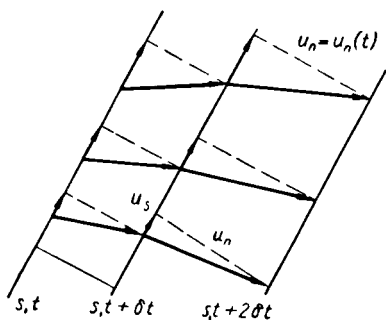


FIGURE 6.

$$v_n = \frac{\frac{\partial F}{\partial t}}{\sqrt{\left(\frac{\partial F}{\partial x}\right)^2 + \left(\frac{\partial F}{\partial y}\right)^2 + \left(\frac{\partial F}{\partial z}\right)^2}}. \quad (1.8)$$

However, velocity v_n pertains to points of surface F , and not to particles ξ at this surface.

3. Orthogonal free surface

A free boundary, for which the particle velocity vector \bar{u} at all its points is directed normal to this surface, will be termed an orthogonal free surface. Certain general theorems hold for such free boundaries.

Theorem III. A continuous free boundary moving at finite velocities and accelerations can be orthogonal to the trajectories of particles belonging to it only if the trajectories of these particles describe straight lines.

Let particle ξ , belonging to free boundary s (Figure 7), move along trajectory s' which has a radius of curvature R' at the point of intersection with s ; the absolute velocity of the particle is $u = \frac{ds'}{dt}$, the accelerations tangential and normal to the trajectory are $\frac{du}{dt}$ and $\frac{u^2}{R'}$, all these accelerations lying in the plane tangent to the trajectory. It is evident that the absolute value of the tangent of the angle between the tangent to the trajectory and w , the vector of absolute acceleration of the particle, is equal to the ratio $\frac{u^2}{R'} : \frac{du}{dt}$. According to dynamic conditions (1.1) and (1.2) vector w is orthogonal to s ; consequently, directions s and s' will be orthogonal when $u \neq 0$, when either $R' \rightarrow \infty$ or $\frac{du}{dt} \rightarrow \infty$ (if R' is finite). This yields the above theorem.

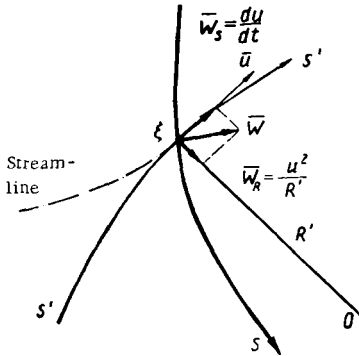


FIGURE 7.

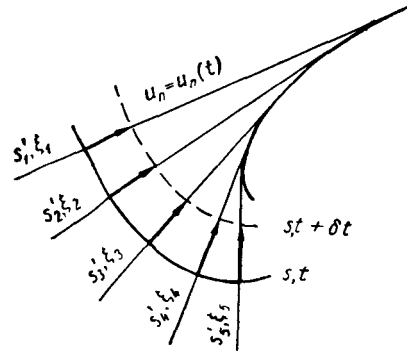


FIGURE 8.

If surface s is orthogonal to particle trajectories s' (Figure 8), then according to Theorem III trajectories s' are straight lines and, therefore, the angular velocity $\frac{D\alpha}{Dt}$ in the vicinity of each particle at surface s is zero, and also the tangential component of absolute velocity u_t is zero. Then it follows from the second of equations (1.6) that $\frac{\partial u_n}{\partial s} = 0$ and, hence, the normal velocity u_n is a function of time, but not of s along the orthogonal free surfaces s .

The difference in velocity potentials at two points of a free surface is $\varphi_2 - \varphi_1 = \int_1^2 u_s ds$. At an orthogonal free surface $u_s = 0$, and so $\varphi_2 - \varphi_1 = 0$ for all points of this surface at any time.

Theorem IV. A free orthogonal surface is an equipotential surface, the potential of which is not a function of s , but may be a function of time.

Continuous closed orthogonal free surfaces, which move with finite and continuous velocities and accelerations, may be either spherical or cylindrical surfaces, which confine a fluid volume from within. Problems of this type are related, in particular, to expansion of gas bubbles in a liquid, and may also include the approximate solution of the problem of flow of a thin jet past a slender circular cone, with developed cavitation past the cone. The solution of the problem of expansion of a spherical cavity due to the pressure of an included gas is known [10]. Both the above problems are considered below, stated somewhat differently and in a more general form.

In proving Theorem III we omitted the case $\frac{du}{dt} \rightarrow \infty$, which corresponds to "impact" origination of flow. For example, suppose the flow which develops upon uniform submersion of a wedge is stopped at some instant, but the free boundaries retain the shape they acquired during submersion. Then ($t = t_1$) the wedge is instantaneously set into motion by applying an impulsive force to it. It is clear that during the infinitesimal period of acceleration of the wedge, the particles at the free surface will be subjected to infinite acceleration which, according to equation (1.1), are directed normal to the curved

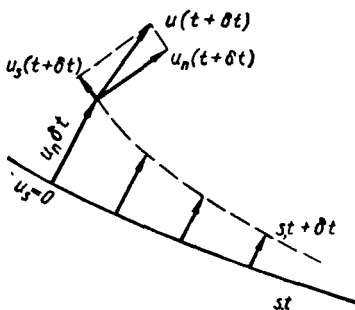


FIGURE 9.

free surface. These accelerations will produce finite velocities \bar{u} of the particles; these velocities will be normal to boundary s and will satisfy the solution of the corresponding boundary-layer problem.

However, surface s is orthogonal immediately following the impact. Since the curvature of surface s is

variable and $\frac{\partial u_s}{\partial s} \neq 0$, it follows from equations (1.5) that, although $u_s = 0$ at time t , the acceleration $\frac{Du_s}{Dt} = u_n \frac{D\alpha}{Dt} \neq 0$;

from equations (1.6) the angular velocity of elements of s at the initial instant will

be $\frac{D\alpha}{Dt} = \frac{\partial u_n}{\partial s}$ when $u_s = 0$. Hence $u_s \neq 0$ at each point of s at subsequent times, and the free boundary ceases to be orthogonal after the impact (Figure 9). The above considerations make it possible to assess the rate of increment of the velocity potential φ at the free surface immediately following the impact. In fact, for some small time interval δt after the impact

$$\delta u_s = \frac{Du_s}{Dt} \delta t = \left[\frac{\partial}{\partial s} \left(\frac{u_n^2}{2} \right) + u_n \frac{\partial \alpha}{\partial s} \right] \delta t \approx \frac{\partial}{\partial s} \left(\frac{u_n^2}{2} \right) \delta t.$$

The second term in the brackets is neglected as a high-order infinitesimal.

Assuming that the free surface extends to infinity, where the velocity potential $\varphi = 0$, we obtain for point s

$$\delta\varphi_s = \frac{u_n^2}{2} \delta t = \left[-\int_s^\infty \frac{\partial}{\partial s} \left(\frac{u_n^2}{2} \right) ds \right] \delta t.$$

The fraction of kinetic energy of the fluid, corresponding to the integral of $\varphi_s u_n ds$ along the free surface, will be $\delta T_s = \left[\frac{\rho}{4} \int_s^\infty u_n^3 ds \right] \delta t$. It is easy to show that quantity $\frac{dT_s}{dt}$ at $t = t_1$ is equal to half the kinetic energy flux through the initial free boundary. The cumulative potential φ_s and energy T_s cannot be changed by subsequently stopping the body. Hence, if the body is stopped some time after it has been set into motion, the fluid will not come to a complete rest. This is precisely the main difference between motions with free boundaries and motion in an infinite fluid.

4. Steady free boundaries

The term steady free boundary is applied to a surface which moves relative to a stationary fluid uniformly and in a straight line, without changing form. In the two-dimensional case the steady surface can be expressed in the x, y coordinate system associated with the quiescent fluid by the equation $F(x - V_x t, y - V_y t) = 0$; this equation is not an explicit function of time t . The steady surface can clearly be treated as stationary in the x', y' coordinate system by setting $x = x' + V_x t$ and $y = y' + V_y t$.

Let us clarify some general properties of steady boundaries. Suppose vector $\vec{V}_s = iV_x + jV_y$ is the translational velocity of the free boundary, and vector \vec{V}_r the relative velocity of a boundary particle in the system of x', y' coordinates. The absolute particle velocity is then $\vec{u} = \vec{V}_s + \vec{V}_r$.

Since the particle must remain all the time at surface s , its relative velocity can be directed only along the arc of this surface; consequently $\vec{V}_r = \vec{e}_s V_s$. The dynamic boundary condition (1.5) thus yields

$$\vec{e}_s \frac{D\vec{u}}{Dt} = \vec{e}_s \left(\frac{d\vec{V}_s}{dt} + \vec{e}_s \frac{DV_s}{Dt} + \vec{e}_s V_s \frac{D\alpha}{Dt} \right) = 0.$$

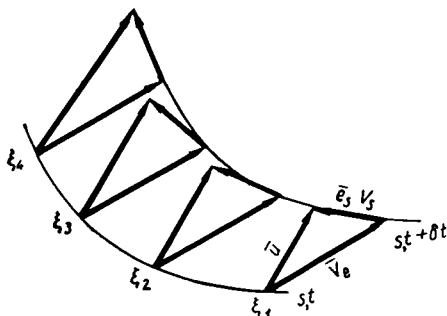


FIGURE 10.

Since it has been assumed that $\frac{d\bar{V}_e}{dt} = 0$, $\frac{DV_s}{Dt} = 0$ for each particle at a steady free boundary at any time. Hence each particle moves with time along boundary s , and velocity V_s along this boundary is constant (Figure 10).

Theorem V (Wagner). The relative particulate velocity along any steady free boundary is constant for all particles at all points on the boundary.

The projections of the absolute velocity of particle ξ on the tangent and normal to the boundary are

$$u_s = \bar{e}_s \bar{u} = \bar{e}_s \bar{V}_e + V_s; \quad u_n = \bar{e}_n \bar{u} = \bar{e}_n \bar{V}_e. \quad (1.9)$$

If surface s contains a point or points where $u_s = 0$ and $u_n = 0$, then it follows from the second of equations (1.9) that the direction of transport [reference-frame] velocity at these points coincides with the direction of the tangent to s . The second of equations (1.9) then yields $V_e + V_s = 0$ (Figure 11).

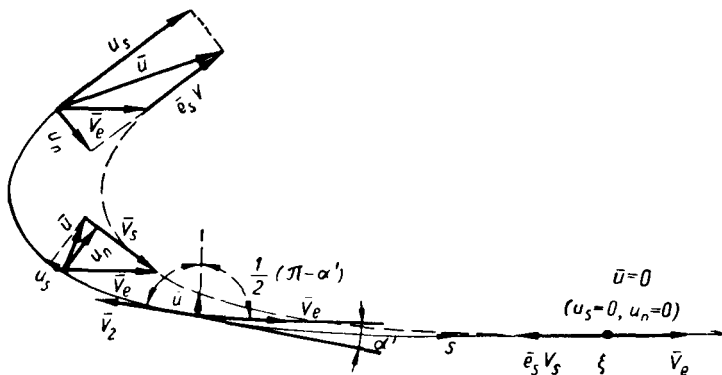


FIGURE 11.

Theorem VI. The relative fluid particle velocity at a steady free surface extending into the quiescent fluid, where the direction of the tangent to the free surface coincides with the direction of the transport [reference-frame] velocity, is always equal in absolute magnitude to the translational velocity and is directed opposite to it.

If $V_e + V_s = 0$, then, setting angle $(s, \bar{V}_e) = \alpha'$, we find (see Figure 11) that $u_n = V_e \sin \alpha'$; $u_s = V_e (\cos \alpha' - 1) = -2V_e \sin^2 \frac{\alpha'}{2}$, and the absolute magnitude of the velocity is $u = 2V_e \sin \frac{\alpha'}{2}$. The ratio of R' , the radius of curvature of the trajectory, to the radius of curvature R of surface s will then be $\frac{R'}{R} = 4 \sin \frac{\alpha'}{2}$. Obviously, the angle between the directions of the transport [reference-frame] and absolute velocity is $\frac{1}{2}(\pi - \alpha)$, i. e., half the angle between \bar{V}_e and \bar{V}_r .

Theorem VII. The absolute velocity vector of every particle at each point of a steady free boundary extending into the quiescent fluid, bisects the angle between the transport and relative velocities.

We determine the distance between particles. Substituting the expression for \bar{u} into the first of equations (1.6) we obtain

$$\frac{D\epsilon}{Dt} = \bar{e}_s \frac{\partial \bar{u}}{\partial s} = \bar{e}_s \frac{\partial \bar{V}_s}{\partial s} + \frac{\partial V_s}{\partial s}.$$

The transport velocity is constant over the entire surface and therefore

$\frac{\partial \bar{V}_s}{\partial s} = 0$. The relative velocity V_s is constant according to Theorem V; hence $\frac{\partial V_s}{\partial s} = 0$, from which $\frac{D\epsilon}{Dt} = 0$. This implies that ϵ is constant along s .

If $\epsilon = 0$ at one point of surface s , then $\epsilon = 0$ over the entire free boundary.

Theorem VIII. The distance between fluid particles along a steady free surface always remains constant.

This theorem is clarified by Figure 12. Lines s_1, s_2, s_3 depict respectively equal trajectories of particles ξ_1, ξ_2 and ξ_3 , which are initially located at the undisturbed boundary, coinciding with the x axis. Free boundary s intersects these trajectories during the subsequent instants of time t_1, t_2 and t_3 , so that distance $\Delta \xi$ between the particles remains constant.

We note that Theorems V through VIII lend themselves to elementary proof by "reversing the motion," i. e., by regarding surface s as stationary and the liquid as moving with velocity \bar{V}_s . Then the free surface will be a streamline at which the relative velocity is constant on the basis of Bernoulli's equations. However, the only approach used here is that of study of the "absolute" motion relative to a fluid at rest at infinity.

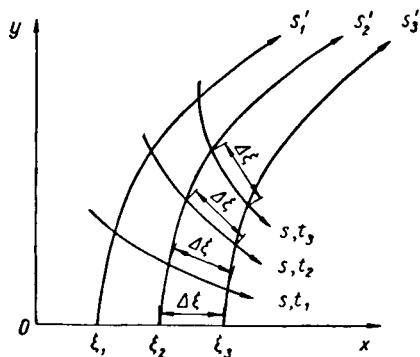


FIGURE 12.

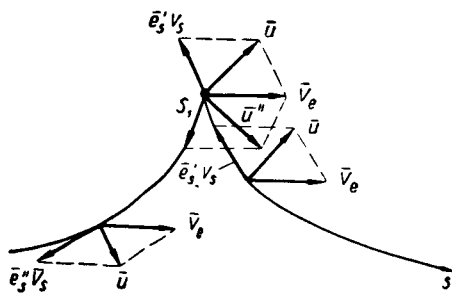


FIGURE 13.

Let us investigate whether a steady free surface can have cusps. Assume that a steady free boundary has a cusp s_1 (Figure 13), and let surface s at all its points far from point s_1 coincide with the direction of the transport velocity \bar{V}_s , and let the absolute velocities of particles at these surface regions be zero. It follows from Theorems V and VI that in this case the relative velocity V_s in the forward part of s is directed toward point s_1 , while that in the rear part of s_1 is directed away from this

point. Consequently, particle ξ , which at a given time corresponds to the cusp s_1 , should simultaneously have velocities $\vec{u}' = \vec{V}_s + \vec{e}_s' V_s$ and $\vec{u}'' = \vec{V}_s + \vec{e}_s'' V_s$, which are not equal, since unit vectors \vec{e}_s' and \vec{e}_s'' from both sides of the cusp are different. Hence it follows that particle ξ_1 should rotate. But the points contained within the cusp are irrotational, since the fluid is assumed to be ideal and moving only by virtue of normal pressures. Consequently, rotation at point s_1 is impossible.

Theorem IX. A steady free surface serving as the boundary of an irrotational fluid cannot have cusps.

It is known that trochoidal waves have a cusp and move at constant velocity without losing their shape. Consequently, in this case the free surface is steady and also has a cusp. This apparent contradiction to Theorem IX is due to the fact that the trochoidal wave has a nonzero vortex, while Theorem IX is valid for a free surface bounding irrotational flow.

We shall show that a closed steady free boundary cannot move through a fluid at rest. Let us assume that a space within the fluid is bounded by a closed surface s , moving with constant velocity \vec{V}_s within a fluid at rest and satisfying all the conditions for steady boundaries. If the absolute particle velocity at a single point of s is given, then vector equation $\vec{u} = \vec{V}_s + \vec{e}_s V$ will yield the velocity V , which, according to Theorem V, is constant along the entire boundary s . If $V_s \neq 0$, then the velocity circulation at the free surface will be nonzero, thus giving rise to the Zhukovskii force which, however, should be zero, since by the statement of the problem the pressure at each point of the free surface is the same. Thus velocity V_s should be equal to zero, while the absolute particulate velocities at surface s should be $\vec{u} = \vec{V}_s$. Obviously, this condition can be satisfied when curve s bounds a region filled with fluid undergoing translational motion. When the outer space is filled with fluid, vector \vec{u} of each particle ξ coincides with the direction of the streamline passing through this particle (Figure 14). The above condition can be satisfied only when the entire fluid undergoes translational motion with velocity \vec{V}_s or (with the problem as stated here) $\vec{V}_s = 0$, since \vec{V}_s is by definition the transport velocity relative to a fluid at rest.

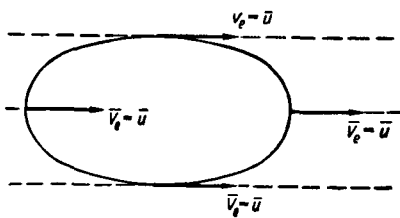


FIGURE 14.

Theorem X. A fluid volume at rest at infinity cannot contain a closed steady free surface moving with nonzero transport velocity.

Steady free boundaries arise ahead of a planing plate or on uniform translational motion of a body within a fluid accompanied by formation of

a cavity behind it. In particular, Theorem X without the solution of the potential problem explains the phenomenon of reentrant jets* *ab* (Figure 15) during cavitating flow past a plate or some other body. Physical experience shows that reentrant jets are unstable, break up, migrate to the boundaries of the cavity, and are carried away by the flow. In the idealized statement of the problem pressure p_k within the cavity is lower than the pressure at infinity, and so the absolute value of the relative velocity is $V_s =$

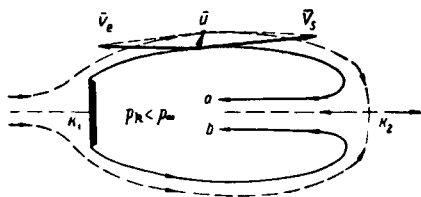


FIGURE 15.

number is $\sigma = \frac{p_0 - p_k}{\frac{\rho V_s^2}{2}} > 0$. Absolute velocity vector \vec{u} no longer bisects the angle between V_s and \vec{V}_s ; the free surface proper is formed by particles shed from the edges of the plate and acts as an inner free boundary. However, all the general results pertaining to free boundaries are applicable also in this case.

5. Self-similar free boundaries

A free boundary which remains geometrically similar to itself at any time is called a self-similar free boundary (Figure 16). Such free boundaries arise, for example, upon symmetrical submersion of a wedge or cone, if one considers the boundary within the plane passing through the axis of symmetry.

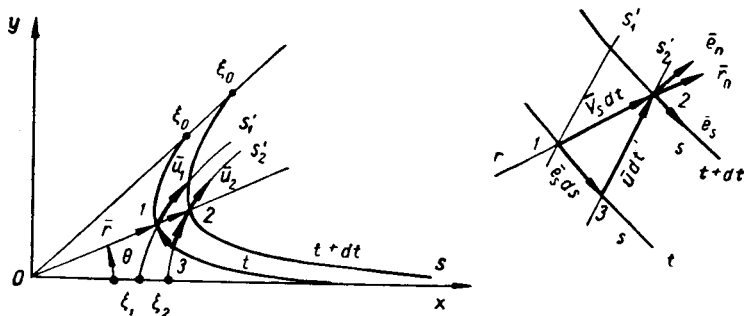


FIGURE 16.

To retain geometrical similarity each linear dimension of a self-similar free surface should increase (or decrease) at a rate proportional to this linear dimension. If the equation of the free surface in polar

* [First discovered by Efros, D.A.— DAN SSSR, Vol.51, No.4, pp.267—270. 1946; and Vol.60, pp.29—31. 1948.]

coordinates r, θ is expressed in the form $r = hf(\theta)$, where h is some linear scale, then the absolute magnitude of the radial velocity of the boundary at $\theta = \text{const}$ will be $V_r = \frac{r}{h} \dot{h}$, and the radial velocity vector will be $\bar{V}_r = \bar{r}_0 V_r$, where \bar{r}_0 is the unit vector in the r direction. We shall measure free-surface arc s from ray OA , along some fluid particle slides. The absolute velocity of fluid particle ξ at surface s is composed of the radial velocity \bar{V}_r and relative tangential velocity $\bar{V}_s = \bar{e}_s V_s$ along the free surface. The absolute velocity vector of particle ξ has the form

$$\bar{u} = \bar{V}_r + \bar{V}_s = \bar{r}_0 \frac{r}{h} \dot{h} + \bar{e}_s V_s. \quad (1.10)$$

We shall now examine the properties of a self-similar free boundary propagating with constant velocity $\dot{h} = \frac{h}{t}$ or $V_r = \frac{r}{t}$ for each value of θ .

Figure 16 shows two positions of the free boundary at times t and $t + dt$; it is assumed that particle ξ_0 is initially ($t = 0$) at the center of similarity O , while the free surface coincides with the x axis. From the self-similarity of flow we have that absolute velocities $\bar{u}(\xi, t)$ of the fluid at points 1 and 2 where the radius-vector \bar{r} meets $s(t)$ and $s(t + dt)$ are equal, i.e., $\bar{u}_1 = \bar{u}_2$. Passing from point 1 to point 3 along a line with constant t , and then from point 3 to point 2 with constant s , we find

$$\bar{u}_2 = \bar{u}_1 + \frac{\partial \bar{u}}{\partial s} ds + \frac{\partial \bar{u}}{\partial t} dt. \quad (1.11)$$

This transition can be expressed differently, as $\bar{e}_s ds + \bar{u} dt = \bar{V}_r dt$. From this, using the vectorial definition of velocity given by equation (1.10), we find

that $V_s = -\frac{ds}{dt} = -\frac{s}{t}$. Substitution of this result into equation (1.11),

making use of the fact that $\bar{u}_1 = \bar{u}_2$, yields

$$\frac{\partial \bar{u}}{\partial s} \cdot \frac{s}{t} + \frac{\partial \bar{u}}{\partial t} = 0. \quad (1.12)$$

The vector $\bar{u}(\xi, t)$ satisfies $\frac{\partial \bar{u}}{\partial t} = \frac{D\bar{u}}{Dt}$. Hence if dynamic boundary condition $\bar{e}_s \frac{D\bar{u}}{Dt} = 0$ is satisfied, then the kinematic condition $\frac{De}{Dt} = \bar{e}_s \frac{\partial \bar{u}}{\partial s} = 0$ is satisfied simultaneously. This condition shows that a moving free surface has constant length and that distances between individual particles remain constant ($\xi = s$).

Theorem XI. Distances between particles at a self-similar plane or axisymmetrical free surface propagating with constant velocity remain constant.

This theorem and all the previous deviations pertain in substance to self-similar outer free boundaries, which are produced on self-similar submersion of bodies, when an undisturbed free surface is broken by a body and particles which find themselves at the point of discontinuity continue moving along the edges of the body (Figure 3). A more detailed analysis of properties of self-similar free boundaries which arise on submersion of bodies into a fluid is given in Chapter Four.

6. The spray root

The immersion of bodies, planing, and some other cases are accompanied by the formation of spray sheets near the body surface. The free surface far from the body does not usually curve much, but the curvature in the vicinity of the spray-sheet base increases sharply, and angle α made by the free surface with the horizontal attains high values over a small segment of s . It will subsequently be seen that small such regions [the spray root] are important in the formation of the flow and in the force exerted by the body on the fluid. In this connection we shall clarify the principal properties of the spray root for two-dimensional or axisymmetrical flows.

To calculate the tangent of the absolute particulate velocity u , one can in general integrate the first of equations (1.5), which expresses the dynamic boundary condition. This yields

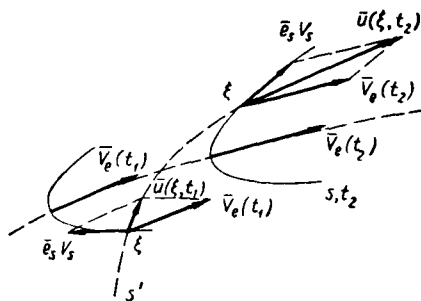
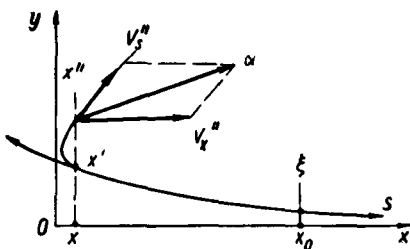
$$u_{s_1} - u_{s_2} = \int_{\alpha_1}^{\alpha_2} u_n d\alpha. \quad (1.13)$$

It should, however, be remembered that velocities u_n and u_s pertain to the same particle ξ ; here $u_n = u_n(\xi, t)$ and $\alpha = \alpha(\xi, t)$. Hence in order to carry out integration, an expression must first be found for $u_n = u_n(\xi, \alpha)$. In general this is difficult. In the particular case of a steady free surface (see Section 4), when the transport velocity of the boundary (for example, \bar{V}_s) is constant and equal to iV_x , the free surface is given by $y = f(x)$ in the moving coordinate system, and as $x \rightarrow \infty$, $y \rightarrow 0$ and $y' \rightarrow 0$, Theorem VI holds. Since in this case the tangential relative velocity $V_s = -V_x$ is constant along s , while the normal velocity of the particle is $u_n = (\vec{e}_n i) V_x = -V_x \sin \alpha$, we find that $u_s(\xi, \alpha) = -\int_0^\alpha V_x \sin \alpha d\alpha = -V_x (1 - \cos \alpha)$.

It was taken into account while integrating that as $x \rightarrow \infty$, $u_s \rightarrow 0$ and $\alpha \rightarrow 0$. This result (mentioned in Section 5) shows that the absolute tangential velocity at a steady surface depends only on the angle of turn α and not on the form of the equation of the free surface. In the case of an accelerating free surface it is also possible to integrate equation (1.2) or (1.7), but the calculations become complicated even in the simplest of cases.

Denoting the spray-root surface length by Δs and the transport acceleration by w_s , it can be shown that when $\frac{w_s \Delta s}{V_s^2} \ll 1$, the tangential velocity u , after traversing the curved region is determined exactly as for a steady surface.

Theorem XII (Wagner). The relative tangential velocity of particles along a short spray-root surface segment is approximately constant and in value is close to the transport velocity of the curving segment proper. This theorem is illustrated in Figures 17 and 18.



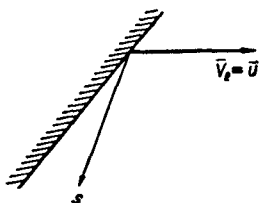
7. The tip of a spray sheet

The point at which the free boundary of the fluid is in contact with solid boundaries of the body is called the tip of the spray sheet (Figure 19).

The following theorem is easily proved from continuity and flow irrotation conditions.

Theorem XIII (Wagner). The absolute velocity of fluid particles at the tip of a spray sheet is equal to the absolute velocity of the tip proper.

A spray-sheet tip forms either at the surface of a body which is in contact with the free surface, or in the region when the outer and inner free surfaces merge upon formation of free jets (splashes).



The above theorems as such do not yield solutions to specific problems. In effect they only define the kinematics of the motion, since the utilization of the dynamic boundary layer does not go beyond using the condition of orthogonality of the absolute acceleration vector of a surface particle to the free surface. However, the limitations imposed by these theorems together with other hydrodynamic conditions make it possible to derive useful results and to gain helpful insight into the flow pattern even before solving the problem.

Chapter Two

SOME GENERAL PROPERTIES OF POTENTIAL FREE-BOUNDARY FLOWS

In this chapter we shall consider some general properties of potential and in general unsteady flows of an ideal fluid with moving free boundaries. It should be remembered that in the overwhelming number of practical problems involving the motion of bodies on fluid surfaces the free boundaries have a complicated curvilinear shape, and it is virtually impossible to solve the Laplace equation exactly. This requires certain simplifications, the proper selection of which necessitates a detailed study of the flow. It is assumed that the reader is familiar with the theory of potential flows, and hence attention is paid primarily to features inherent to free-boundary flows. Particular attention is paid to clarification of some fine points in the equations of hydrodynamics and, in addition, to constructing a physical, clear flow pattern.

1. The velocity potential

Mathematically, the velocity potential φ is defined as a function of coordinates x, y, z and of time t , the gradient of which is equal to the velocity vector \vec{v} at this point of space. Thus, $\vec{v} = \text{grad } \varphi$ or

$$v_x = \frac{\partial \varphi}{\partial x}; \quad v_y = \frac{\partial \varphi}{\partial y}; \quad v_z = \frac{\partial \varphi}{\partial z}. \quad (2.1)$$

It is known from potential theory that function φ is singular in a simply-connected space, possesses neither a maximum nor a minimum within the fluid, and that the potential field is devoid of vortices and sources.

The fact that each elementary volume of the space should be supplied by the same amount of fluid which is discharged from it is expressed for an incompressible fluid by the continuity equation

$$\text{div } \vec{v} = \frac{\partial v_x}{\partial x} + \frac{\partial v_y}{\partial y} + \frac{\partial v_z}{\partial z} = 0.$$

For potential flows substitution of components $\frac{\partial \varphi}{\partial x}$, $\frac{\partial \varphi}{\partial y}$ and $\frac{\partial \varphi}{\partial z}$ into the above expression yields the Laplace equation

$$\Delta \varphi = \frac{\partial^2 \varphi}{\partial x^2} + \frac{\partial^2 \varphi}{\partial y^2} + \frac{\partial^2 \varphi}{\partial z^2} = 0. \quad (2.2)$$

This form of the Laplace equation is retained also in the coordinate system moving with the flow. Any point x, y, z of the velocity field $\vec{v}(x, y, z, t)$ for which $\Delta\varphi = 0$ (equation (2.2)) does not contain sources or vortices.

It is sometimes convenient to consider the continuity condition for some finite portion of space x, y, z filled by a fluid and confined by a closed surface Σ . Surface Σ may be stationary as well as mobile, free or solid. If the absolute velocities of transport of surface Σ along the inner normal to it are denoted by V_n , while the absolute fluid velocities are designated as previously by \vec{v} , then the general continuity equation will express the fact that the flow of a fluid volume within region Σ should be equal to the rate of growth of the volume of region Σ proper. If \vec{e}_n is taken to denote the unit vector of the inner normal, then the fluid volume entering volume Σ per unit time through surface element $\delta\Sigma$ is $-(V_n - \vec{e}_n \vec{v}) \delta\Sigma$, while the rate of growth of the volume of region Σ is $\iint_{\Sigma} V_n d\Sigma$. Integrating the first expression over the entire surface Σ and equating the result to the second integral, we obtain the general continuity equation

$$\iint_{\Sigma} \vec{e}_n \vec{v} d\Sigma = 0. \quad (2.3)$$

This equation does not contain the proper motion of boundaries of region Σ . It is important to remember that the general continuity equation does not stipulate absence of vortices and sources within this region. The presence within region Σ of a closed vortex or source and sink of equal strengths (a doublet) will not contradict equation (2.3). Hence the flow satisfying this equation may be both potential and nonpotential [rotational] in all or some parts of space Σ , while the flow satisfying condition (2.2) in region Σ is potential at all points of this region.

2. The stream function

Stream function ψ expresses the fluid flux per unit time through a given surface. In the planar case $\delta\psi = -v_x \delta y$ and $\delta\psi = v_y \delta x$; consequently,

$$v_x = \frac{\partial\psi}{\partial y} = -\frac{\partial\psi}{\partial y}, \quad v_y = \frac{\partial\psi}{\partial x} = \frac{\partial\psi}{\partial x}.$$

In the axisymmetrical case, with the y axis serving as the axis of symmetry and \tilde{x} denoting the distance between the point and this axis, we have $\delta\psi = v_{\tilde{x}} \delta\tilde{x}$. For reference, we now present the Laplace equation for φ and the continuity equation for ψ in the case of axisymmetrical flow with y as the axis of symmetry. Since \tilde{x} is the distance from the point to the above axis of symmetry, these equations assume the form

$$\begin{aligned} \frac{\partial^2\varphi}{\partial y^2} + \frac{\partial^2\varphi}{\partial \tilde{x}^2} + \frac{1}{\tilde{x}} \cdot \frac{\partial\varphi}{\partial \tilde{x}} &= 0; \\ \frac{\partial^2\psi}{\partial y^2} + \frac{\partial^2\psi}{\partial \tilde{x}^2} - \frac{1}{\tilde{x}} \cdot \frac{\partial\psi}{\partial \tilde{x}} &= 0. \end{aligned} \quad (2.4)$$

The stream function at free boundaries will be treated as the flux passing through area element δS of the free boundary per unit time when this area element has been instantaneously stopped, while the particles continue moving with velocity \bar{u} .

The positive direction here is that of the flow moving into the fluid volume under study. If u_n is directed outward from the free surface, we have there $\delta\psi = \bar{e}_n \bar{u} \delta S < 0$, since the inner normal is regarded as positive. Figure 20 shows the pattern of streamlines extending from the inner to the outer boundary.

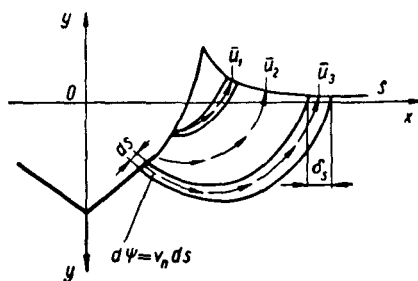


FIGURE 20.

3. Boundary conditions and the general nature of the flows

The boundary conditions at a surface of a solid body consist in the fact that the normal component of V_n of the velocity of a point on the body is equal to the normal component of the absolute fluid velocity at this point (impermeability of the solid surface). For potential flow this means

that $\frac{\partial\varphi}{\partial n} = V_n = \bar{e}_n(\bar{V} + [\bar{\omega} \times \bar{r}])$ for each value of t , where \bar{V}_c is the velocity of some center, fixed relative to the body, while $\bar{\omega}$ and \bar{r} are respectively the angular velocity vector of the body and the radius vector of a point on the body surface with origin at this center.

At free boundaries also $\frac{\partial\varphi}{\partial n} = u_n$,* but usually free boundaries must be defined from the condition that pressure p at them is specified or usually constant (see Chapter One).

The Laplace equation can in general have an infinite number of solutions. However, it is known that the Laplace equation $\Delta\varphi = 0$ has a unique solution for each time t , if the values of φ or $\frac{\partial\varphi}{\partial n}$ are specified at known boundaries of region Σ , or if values of φ are specified at one part of surface Σ and those of $\frac{\partial\varphi}{\partial n}$ at the other.

* The symbol u is reserved for denoting the absolute velocities at outer free boundaries, while v is used for designating absolute velocities within the fluid and at solid boundaries. In Chapter One the inner normal was treated as positive for the free boundary, for which reason the sign of u_n is reversed here.

For free boundary flows, where the problem of determining the shape (equation) of the free boundary is difficult as such, it is impossible in many cases to obtain a unique solution of the Laplace equation for each instant of time. However, the fact that the Laplace equation $\Delta\varphi = 0$ has in principle a unique solution under the aforementioned conditions makes it possible to prove Wagner's theorem on the uniqueness of the flow in the presence of free boundaries.

Let us assume that when a body of specified shape is submerged in a fluid, when only outer free boundaries form, we have given at time t_0 the velocity \bar{V} of all the points of the body, and consequently

$\frac{\partial\varphi}{\partial n} = \bar{e}_n \bar{V}$ at the surface of the body, the equation of the free surface

$s(x, y, z, t_0)$ and the velocity distribution at it $\bar{u}(s, t_0)$, i.e., $u_n = \frac{\partial\varphi}{\partial n}$ on s

at time t_0 , and that these values satisfy the corresponding boundary value problem $\Delta\varphi = 0$ and hence uniquely define the potential field

$\varphi(x, y, z, t_0)$ within the entire fluid region. The values of $\frac{Du_s}{Dt}$ at t_0 are

determined from the boundary condition $\frac{Du_s}{Dt} = u_n \left(\frac{\partial\bar{u}}{\partial s} \bar{e}_n \right)$ (see equation (1.7)),

since u_n and $\frac{\partial\bar{u}}{\partial s} \bar{e}_n$ are known for t_0 , while the values of $\frac{Du_s}{Dt}$ at the

subsequent time $t_0 + dt$ are found from the expression

$$u_s(s, t_0 + dt) = u_s(s, t_0) + \frac{Du_s}{Dt} dt.$$

Integration of this new value of u_s along s yields $\varphi(s, t_0 + dt) = \varphi(s, t_0) + d\varphi$; vectors $\bar{u}dt$ define the new location of the boundary $s(t_0 + dt)$. Solving

again the Laplace equation $\Delta\varphi = 0$ for boundary conditions $\frac{\partial\varphi}{\partial n} = \bar{e}_n \bar{V}$ at the

surface of the body and $\varphi(s, t_0 + dt)$ on $s(t_0 + dt)$ we derive the value of

$u_n(t_0 + dt)$ on s , and consequently also of $\frac{\partial\bar{u}}{\partial s} \bar{e}_n$ for $(t_0 + dt)$, etc.

Theorem XIV (Wagner). When the shape of the body, shape of free boundaries and the velocity potential field of the fluid are given at the initial time, while the shape of the body and the law governing its motion are specified for the subsequent time instants, the hydrodynamic problem has a unique solution for each subsequent time instant.

This theorem also applies to the case of emergence of new fluid particles at the free boundary.

4. Velocity potential at free boundaries

The velocity potential in a simply connected space can be expressed as a linear velocity integral, taken along any reconcilable curve drawn between points A and B . Denoting a contour element of length by ds and the fluid velocity at points of this element by \bar{v} , and denoting the tangential velocity vector by \bar{e}_s , we have

$$\varphi_B - \varphi_A = \int_A^B \bar{e}_s \bar{v} ds = \int_A^B (v_x dx + v_y dy + v_z dz).$$

Referring point A to infinity, where the fluid is at rest, φ_A can be regarded as equal to an additive constant, which will be treated as equal everywhere to zero. We note that, in order to regard φ_A as equal to zero, we require a law governing the decrease in the tangent to the fluid velocity distribution $v_s = \bar{v}_s$ upon approaching the point of infinity. In particular, for a two-dimensional source at the origin the fluid velocity decreases along radius r as $\frac{1}{r}$ and the integral $\int \frac{dr}{r} = \ln r + C$ does not tend to zero or to a constant value at infinity. However, it will be shown below that potentials of this kind are not encountered in the submersion phenomena under study.

If contour s , along which the tangential velocity v_s is integrated, is a fluid contour, i.e., each of its points moves in space with the same velocities as the fluid at this point, then the elementary component $v_s ds$ of the velocity flux along this contour changes with time due to changes in v_s , as well as due to changes in the length of element ds /10/. Hence

$$\frac{D}{Dt}(v_s dx) = dx \frac{Dv_s}{Dt} + v_s dv_s,$$

since

$$\frac{D}{Dt} dx = dv_s.$$

Constructing similar expressions along other axes, if the mass forces have potential U and pressure p is a function only of density ρ , and also making use of the fact that the Euler equation for the x axis yields

$$\frac{Dv_x}{Dt} = -\frac{\partial U}{\partial x} - \frac{1}{\rho} \frac{\partial p}{\partial x}, \text{ then}$$

$$\frac{D}{Dt}(\varphi_B - \varphi_A) = \frac{D}{Dt} \int_A^B v_x dx + v_y dy + v_z dz = \left[-U - \int \frac{dp}{\rho} + \frac{v^2}{2} \right]_A^B. \quad (2.5)$$

From this follows the known theorem due to Lord Kelvin on the constancy of circulation in a closed fluid contour. In fact, if the contour is closed, then points A and B coincide and the right-hand side of equation (2.5) vanishes. Then the integral on the left-hand side expresses circulation Γ of velocity in a closed contour. Since $\frac{D\Gamma}{Dt} = 0$, the circulation in this contour remains constant.

When a region containing a weightless and incompressible fluid is bounded by free boundaries s , consisting of a fluid (streamline) and extending into the region where the fluid is at rest (where $\varphi = 0$), point A can be placed at boundary s in the far region; consequently $\frac{v_A^2}{2} = 0$. Pressure p along the entire boundary is assumed to be constant, and the potential of mass forces is zero when weight is neglected, i.e., $U = 0$. The upper limit of integration of equation (2.5) can be associated with some fluid particle ξ at the free surface s and then the integral on the left-hand side can be treated as the "potential of particle ξ ." Equation (2.5) yields

$$\frac{D\varphi(\xi, t)}{Dt} = \frac{1}{2} u^2(\xi, t). \quad (2.6)$$

Equation (2.6) serves as the boundary condition for any free surface under the above conditions.

The elementary length of the trajectory of each surface particle ξ is $ds' = u^2(\xi, t) dt$. If the potential at point x_0, y_0, z_0 where particle ξ is situated at time t_0 is φ_0 , but the velocity $u_0 \neq 0$, and then at time t the particle has moved together with the free boundary s and arrived at point x, y, z , then the potential at this point $\varphi(x, y, z, t)$ or $\varphi(\xi, t)$ (these two definitions are fully equivalent due to the single-valuedness of the potential field) is determined by integrating equation (2.6) with respect to time:

$$\varphi(\xi, t) = \varphi_0(\xi, t_0) + \frac{1}{2} \int_{t_0}^t u^2(\xi, t) dt = \varphi_0(\xi, t_0) + \frac{1}{2} \int_{\xi_0}^{\xi} u(\xi, t) ds'. \quad (2.7)$$

Expression (2.7) is sometimes convenient in the study of the motion of free boundaries. If the fluid starts moving from rest, it can always be assumed that $\varphi_0 = 0$.

Defining impact initiation of a flow as the onset of flow due to the application of infinite pressures during an infinitesimal period at some boundary segment, we conclude from equation (2.7) that the velocity potential of surface particles of an ideal incompressible fluid does not change during impact.

Impact pressure p at solid boundaries can be as high as desired. Integrating equation (2.5) with respect to time, and making use of the fact that impact duration τ is infinitesimal while the velocity u over the integration interval is finite, we derive

$$\varphi_B - \varphi_A = -\frac{1}{\rho} (p_{iB} - p_{iA}),$$

where $p_i = \int_0^\tau p dt$ is the impulsive pressure. Consequently, the potential difference at the ends of a streamline can also be treated as the result of the application of a difference in impulsive pressures at points B and A .

5. Equipotential surfaces

The potential $\varphi(\xi, t)$ of a particle at a free surface s increases with time (see equation (2.7)), but within the fluid there can exist close to s a surface

τ , at which potential φ remains constant ($\varphi(\tau) = \text{const}$). Let us determine the velocity of propagation of surface τ . The flow pattern is depicted in Figure 21.

It was previously pointed out that streamlines l and trajectories s' have a common tangent at free surface s . Let δl be an infinitesimal segment of the streamline directed to particle ξ at free surface s . Neglecting the quantity $\frac{\partial u}{\partial t}$ along this element, we have

$$\varphi(\xi, t) - \varphi_\tau = \int_{\delta l} u(l, t) dl = u(\xi, t) \delta l \quad \text{as } \delta l \rightarrow 0.$$

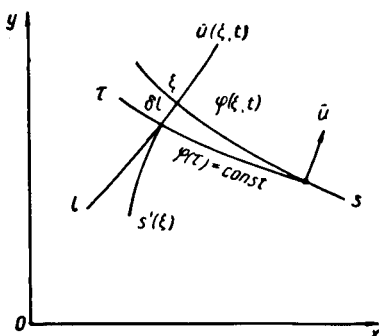


FIGURE 21.

Differentiation with respect to time yields

$$\frac{D}{Dt} [\varphi(\xi, t) - \varphi_\tau] = \frac{D}{Dt} (u \delta l) = \frac{Du}{Dt} \delta l + u \frac{D\delta l}{Dt}.$$

The difference between the velocities of the ends of element δl will be $\frac{D\delta l}{Dt} = u - V_\eta$, where the normal velocity of propagation of surface τ is denoted by V_η . By definition, $\varphi_\tau = \text{const}$; hence

$$\frac{D\varphi(\xi, t)}{Dt} = \frac{Du}{Dt} \delta l + u(u - V_\eta).$$

Equating the above equation to equation (2.6), we find that $\frac{Du}{Dt} \delta l + u(u - V_\eta) = \frac{1}{2} u^2$ or $V_\eta = \frac{1}{2} u$, if $\frac{Du}{Dt} \delta l \rightarrow 0$. Consequently, an equipotential surface infinitely close to free surface s propagates in the same direction as s , but at a velocity half that of particles at s .

Theorem XV. The absolute velocities of an equipotential surface infinitely close to a free surface propagating at finite and continuous velocities and accelerations have the same directions along streamlines, but equal half the velocity of surface particles situated on the same streamline.

This theorem has an interesting corollary. If the fluid started moving from rest, then the velocity potential at the free surface (as everywhere in the fluid) is initially zero. In the region close to the body the velocity potential at free boundary s will change with time (increase), but will remain zero at an infinite distance from the free surface. Hence surface τ , at which $\varphi = 0$, is always infinitesimally close to the initial free boundary s_0 during all subsequent times at infinity. Since at large (but not infinite) distances from the body the elevation of surface s over s_0 is small and the particulate velocities \bar{u} are directed approximately along normals to s , it can be claimed that surface $\varphi = 0$ during its motion always divides the space between the instantaneous position of s and its initial position s_0 into two approximately equal parts, as long as the distance between s and s_0 is small compared with the distance traveled by the body which set the fluid in motion. Theorem XV makes it possible to construct a net of surfaces φ and ψ in the vicinity of free surface s , if the surface proper and velocity \bar{u} at the surface are given.

6. Pressure within the fluid

The pressure p at point x, y, z in the coordinate system associated with a fluid at rest is defined by the Cauchy-Lagrange integral

$$\frac{\partial \varphi}{\partial t} + \frac{v^2}{2} + \int \frac{dp}{\rho} + U = F(t). \quad (2.8)$$

For a heavy and incompressible fluid $\int \frac{dp}{\rho} = \frac{p}{\rho}$ and $U = 0$; if the fluid is at rest at infinity in such a manner that as $r \rightarrow \infty$ we have $\frac{\partial \varphi}{\partial t} \rightarrow 0$ and also $\varphi \rightarrow 0$ (or $\varphi \rightarrow \text{const}$), and all of its free boundaries are acted upon by a

constant pressure p_0 , then function $F(t)$ can be treated as constant and equal to p_0/ρ . Then this equation simplifies to

$$\frac{\partial \varphi}{\partial t} + \frac{v^2}{2} + \frac{\rho}{\rho} \left|_{x,y,z,t} = \frac{p_0}{\rho} \right|_{r \rightarrow \infty}$$

Here potential $\varphi = \varphi(x, y, z, t)$, pressure p and absolute velocity v are determined at a point (x, y, z) stationary in space for the same time t at which $\frac{\partial \varphi}{\partial t}$ is determined. Obviously the pressure at free surface s is p_0 ; hence the condition $\frac{\partial \varphi}{\partial t} + \frac{v^2}{2} = 0$ is another form of the dynamic boundary condition for points in (x, y, z) space which, for given t , coincide with surface s .

If velocity potential φ' is specified as a function of time t and coordinates x', y', z' in a coordinate system moving relative to system x, y, z , i.e., $\varphi = \varphi(x', y', z', t)$, then coordinates x', y', z' for each fixed point of space x, y, z will be time-dependent and the potential at a point x, y, z will change both due to its explicit time dependence and due to changes in coordinates x', y', z' . This must be taken into account when calculating $\frac{\partial \varphi}{\partial t}$ for substitution into equation (2.8).

Assuming that system x', y', z' coincides with stationary system x, y, z at a given time t and that the components of the velocity at which an arbitrary point of the moving coordinate system moves relative to the stationary coordinate system are V_x, V_y , and V_z , we derive for infinitesimal subsequent time intervals $x = x' + V_x t$; $y = y' + V_y t$ and $z = z' + V_z t$. Since $\varphi(x, y, z, t) = \varphi(x', y', z', t)$ due to uniqueness of the potential field and coincidence of the coordinate axes, differentiation of the second expression as a composite function yields

$$\frac{\partial \varphi}{\partial t|_{x,y,z,t}} = \frac{\partial \varphi}{\partial t|_{x',y',z',t}} + \frac{\partial \varphi}{\partial x'} \frac{dx'}{dt} + \frac{\partial \varphi}{\partial y'} \frac{dy'}{dt} + \frac{\partial \varphi}{\partial z'} \frac{dz'}{dt}.$$

At the time under consideration we have $\frac{\partial \varphi}{\partial x'} = \frac{\partial \varphi}{\partial x}$ and similarly for the other [two] directions; from the previous definition of the coordinates we have

$$\frac{dx}{dt} = -V_x; \quad \frac{dy}{dt} = -V_y; \quad \frac{dz}{dt} = -V_z.$$

The transport [reference-frame] velocity of a point in the moving coordinate system is $\bar{V}_* = \bar{V}_0 + \bar{\omega} \times \bar{r}'$, where \bar{V}_0 is the velocity vector of the origin of the moving system, $\bar{\omega}$ is the vector of angular velocity at which the moving coordinate system rotates relative to the stationary system, while \bar{r}' is the radius vector of the point in the x', y', z' coordinate system. Hence the transport velocity of the point can be expressed in the form

$$\begin{aligned} \bar{V}_* = iV_x + jV_y + kV_z = \bar{V}_0 + \bar{\omega} \times \bar{r}' = i[V_x + (z'\omega_y - y'\omega_z)] + \\ + j[V_y + (x'\omega_z - z'\omega_x)] + k[V_z + (y'\omega_x - x'\omega_y)]. \end{aligned}$$

Finally the equation for pressure, if the velocity potential is specified in the moving coordinate system, has the following form for the previously mentioned conditions:

$$\begin{aligned} \frac{\partial \varphi}{\partial t} \Big|_{x',y',z',t} - \frac{\partial \varphi}{\partial x} [V_x + (z'\omega_y - y'\omega_z)] - \frac{\partial \varphi}{\partial y} [V_y + (x'\omega_z - z'\omega_x)] - \\ - \frac{\partial \varphi}{\partial z} [V_z + (y'\omega_x - x'\omega_y)] + \frac{1}{2} \left\{ \left(\frac{\partial \varphi}{\partial x} \right)^2 + \left(\frac{\partial \varphi}{\partial y} \right)^2 + \left(\frac{\partial \varphi}{\partial z} \right)^2 \right\} + \frac{\rho}{\rho} \Big|_{x',y',z',t} = F(t). \quad (2.9) \end{aligned}$$

The prime in the expression for $\frac{\partial' \varphi}{\partial t}$ means that the partial derivative is taken of φ , specified in the moving coordinate system, while the differentiation is carried out with constant values of coordinates x' , y' , z' . It is assumed that any point of the free boundary at any time is acted upon by a pressure $p - p_0 = \text{const.}$

If particle ξ at surface s is placed at some instant at the origin of the stationary coordinate system, and one of the axes is directed along the tangent to trajectory s' , then we obtain from equation (2.6)

$$\frac{D\varphi}{Dt} = \frac{\partial \varphi}{\partial t} + \frac{\partial \varphi}{\partial s'} \cdot \frac{ds'}{dt}.$$

Since $\frac{\partial \varphi}{\partial s'} = u$ and $\frac{ds'}{dt} = u$, substitution of these quantities into equation (2.6) yields a boundary condition for these points of space x, y, z which, at the time under study, coincide with the boundary. This condition can be expressed in the form $\frac{\partial \varphi}{\partial t} + \frac{u^2}{2} = 0$ (as was pointed out above).

The particle potential $\varphi(\xi, t)$ can also be treated as a potential specified in a moving coordinate system, whose origin is at all times associated with particle ξ , while assuming for simplicity that the direction of one of the axes of the moving system coincides with the tangent to the trajectory. Formally equation (2.9) then yields the boundary condition

$$\frac{\partial' \varphi(\xi, t)}{\partial t} - \frac{\partial \varphi}{\partial s'} \cdot \frac{ds'}{dt} + \frac{u^2}{2} = \frac{D\varphi(\xi, t)}{Dt} - \frac{u^2}{2} = 0.$$

This form of the boundary condition is equivalent to equation (2.6), since by definition

$$\frac{D\varphi(\xi, t)}{Dt} = \frac{\partial' \varphi(\xi, t)}{\partial t}.$$

7. Kinetic energy of the fluid

The instantaneous value of the kinetic energy of a fluid bounded by a surface Σ is

$$T = -\frac{\rho}{2} \iint_{\Sigma} \varphi \frac{\partial \varphi}{\partial n} d\Sigma. \quad (2.10)$$

The values of φ and $\frac{\partial \varphi}{\partial n}$ in this expression pertain to points of instantaneous location of boundary surface Σ at the time for which the energy is calculated; the sign convention is such that the normal directed into the fluid is positive. If the fluid fills an infinite half-space and its motion is induced by a body moving at the surface, one must select as this surface the free boundary s , wetted surface s_b of the body and some surface s_∞ , lying at infinite distance from the disturbed region, extending from the free surface and bounding the fluid region under study.

By estimating the order of magnitude of the reduction in φ and

$\frac{\partial \varphi}{\partial n}$ and the order of magnitude of the growth of surface s_∞ with increasing distance to it, it is shown that the energy integral (2.10) taken over this

surface can be as small as desired, if the value of r_∞ is sufficiently large. Hence in the cases under study the integration extends only to surface $s + s_k = \Sigma$.

Equation (2.10) is usually derived by means of Green's theorem (see below and also /10/), but it can also be obtained from simple considerations of mechanics (Figure 22). Let us assume that region Σ is simply connected and the fluid motion within it is potential. Consequently, region Σ contains no sources or vortices, and each streamline may pass only from one point on the boundary to another. We consider an infinitesimally thin flow tube which defines an area element $\delta\Sigma_1$ at its origin at the inner boundary, while the absolute fluid velocity at this point of the boundary is v_1 . At the point where the tube under study again arrives at the boundary it defines an area $\delta\Sigma_2$ and the fluid velocity is v_2 . Denoting an element of flow tube length by δl , the velocity by v and the cross-sectional area of the tube by δF , we can express the kinetic energy of mass $\rho\delta l\delta F$ as $(\rho\delta l\delta F) \frac{v^2}{2}$. The continuity equation yields $v_1\delta\Sigma_1 \cos(\widehat{v_1, n_1}) = v\delta F = -v_2\delta\Sigma_2 \cos(\widehat{v_2, n_2})$, where $\frac{\partial\varphi_1}{\partial n} = v_1 \cos(\widehat{v_1, n})$, while $\int_1^2 v dl = \varphi_2 - \varphi_1$; consequently, the kinetic energy of the fluid contained within the entire flow tube is

$$\frac{\rho}{2}(\varphi_2 - \varphi_1) \frac{\partial\varphi_1}{\partial n} \delta\Sigma = -\frac{\rho}{2} \varphi_1 \frac{\partial\varphi_1}{\partial n} \delta\Sigma_1 - \frac{\rho}{2} \varphi_2 \frac{\partial\varphi_2}{\partial n} \delta\Sigma_2.$$

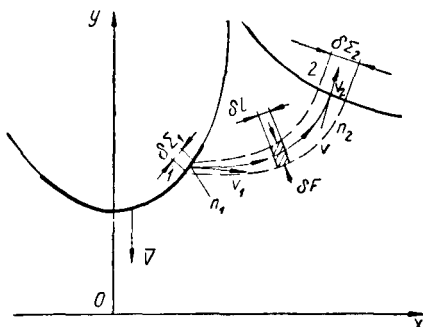


FIGURE 22.

Integration over the entire surface Σ includes surfaces Σ_1 and Σ_2 and formally yields equation (2.10). However, in some cases it is convenient to use the formula

$$T = -\frac{\rho}{2} \iint_{\Sigma} (\varphi_1 - \varphi_2) \frac{\partial\varphi_1}{\partial n} d\Sigma, \quad (2.11)$$

where, for example, φ_1 and $\frac{\partial\varphi_1}{\partial n}$ pertain to the solid surface, while φ_2 applies to the ends of the same streamlines emerging at the free surface. In this sense equation (2.10) can be regarded as the energy integral over the flow tubes.

8. The energy equation

The energy equation for an inviscid fluid mass is

$$\frac{D}{Dt}(T + U) = \iint_{\Sigma} p V_n d\Sigma. \quad (2.12)$$

Internal energy U in the cases under study is the potential energy of mass forces and the deformation energy of the fluid. For a weightless incompressible ideal fluid $U = 0$.

It is of importance that the surface in formula (2.12) bounds some fluid of constant mass which moves together with the boundaries of Σ , since the fluid particles do not penetrate these boundaries. Hence V_n is the normal velocity of the boundaries proper of region Σ (positive along the inner normal), while p is the external pressure at these boundaries.

Since the fluid is incompressible and there is no mass flux through surface Σ , the volume of closed region Σ should remain constant and $\iint_{\Sigma} V_n d\Sigma = 0$. Obviously, the constant pressure p_0 acting on all the boundaries of Σ cannot change the kinetic energy of the fluid mass, and so only the excess pressure $p - p_0 = \Delta p$ is important in (2.12).

As in Section 7, it is shown by estimating the order of magnitude of the reduction in p and V_n with increasing distance from the center of disturbances, that the contribution to integral (2.12) of the parts of surface Σ located at infinity is infinitesimal.

By assumption, excess pressure $p - p_0$ is nonzero only at s_k , the wetted surface of the body. Suppose some central point, fixed relative to the body surface, moves with velocity \bar{V}_0 , while the angular velocity of the body is $\bar{\omega}$, then the normal velocity of point \bar{r} on the body surface is $\bar{n}(\bar{V}_0 + \bar{\omega} \times \bar{r}) = V_n$. In formula (2.12) it is clear that $\int_{s_k} p V_n ds = \int_{s_k} (p - p_0) \bar{n}(\bar{V}_0 + \bar{\omega} \times \bar{r}) ds = \bar{P}\bar{V}_0 + \bar{M}\bar{\omega}$, where \bar{P} is a force vector, while \bar{M} is the momentum vector of the pressure forces exerted on the fluid by surface s_k of the body, reduced to the above central point.

Thus, (2.12) yields for a weightless incompressible fluid ($U = 0$) the energy equation

$$\frac{DT}{Dt} = \bar{P}\bar{V} + \bar{M}\bar{\omega}, \quad (2.13)$$

which expresses the law of conservation of energy (the work of external forces is equal to the rate of increment of the fluid energy). For an incompressible weightless ideal fluid the entire energy can only exist in the form of kinetic energy T .

Equations (2.12) and (2.13) for an ideal incompressible fluid are equivalent to equations of dynamics of a system of material points with ideal constraints. However, these constraints are not always holonomic.

9. The momentum theorem

The momentum theorem for that part of weightless fluid bounded by surface Σ which moves together with the particles has the same meaning

as for a system of material points, the motion of which is studied in theoretical mechanics. Denoting the principal momentum vector and the principal vector of the moment of momentum [angular momentum] of all the particles within region Σ by \bar{K} and \bar{K}_m , respectively, and assuming also that $\bar{e}_n d\Sigma = d\bar{\Sigma}$, we obtain

$$\frac{d\bar{K}}{dt} = \iint_{\Sigma} (p - p_0) d\bar{\Sigma}; \quad \frac{d\bar{K}_m}{dt} = \iint_{\Sigma} (p - p_0) (\bar{r} \times d\bar{\Sigma}). \quad (2.14)$$

The right-hand sides of equations (2.14) express the sums of external forces and external moments acting on the fluid mass bounded by fluid boundary Σ , which reduce to integrals of pressure forces and of moments of pressure forces at surface Σ .

The linear and angular momenta of fluid within volume dQ , which is located at the given instant at point \bar{r} , are respectively $d\bar{K} = \text{grad } \varphi dQ$ and $d\bar{K}_m = (\bar{r} \times \text{grad } \varphi) dQ$. Hence, for the entire region under study

$$\bar{K} = \varrho \iiint_Q \text{grad } \varphi dQ; \quad \bar{K}_m = \varrho \iiint_Q (\bar{r} \times \text{grad } \varphi) dQ.$$

The Gauss theorem yields

$$\begin{aligned} \iiint_Q \text{grad } \varphi dQ &= - \iint_{\Sigma} \varphi d\bar{\Sigma}; \\ \iiint_Q (\bar{r} \times \text{grad } \varphi) dQ &= - \iint_{\Sigma} \varphi (\bar{r} \times d\bar{\Sigma}), \end{aligned}$$

where φ is the boundary value of the velocity potential at the time under study.

For the motion of a body at the surface of a fluid, treated below, one always encounters parts of free boundary s and wetted surface s_k of the body, at which the fluid particles move with high velocities, which decrease when moving away from the surface and tend to zero at infinite distance from the region of disturbances. It will therefore be assumed that the closed surface Σ consists of surface s_k , surface s which starts from the surface of the body and extends over large distances from it, where surface s is closed by an infinitely removed part of surface Σ , which is designated by s_∞ . We now clarify how the momentum theorem is to be used in these cases and what is the mechanical meaning of individual terms of the general formulas (2.14).

The Gauss theorem yields

$$\bar{K} = \varrho \iiint_Q \text{grad } \varphi dQ = - \varrho \iint_{s_k + s} \varphi d\bar{s} - \varrho \iint_{s_\infty} \varphi d\bar{s} = \bar{B} + \bar{B}_\infty. \quad (2.15)$$

Momenta \bar{B} and \bar{B}_∞ of external forces pertain respectively to surface $s_k + s$ and s_∞ , and are equal to corresponding integrals in formula (2.15). The velocity potential φ is determined from equation (2.7) by integration with respect to time. Assuming that the motion started from rest at $t = 0$, when the potential of each particle was zero, we derive the potential of some particle on the bounding surface at time t :

$$\varphi = - \frac{p_t}{\varrho} + \frac{1}{2} \int_0^t u^2 dt.$$

Here $p_i = \int_0^t (p - p_0) dt$ is the impulsive pressure.

At the infinitely removed part of surface s_∞ we have

$$\bar{B}_\infty = -\varrho \iint_{s_\infty} \varphi d\bar{s} = \iint_{s_\infty} p_i d\bar{s} - \iint_{s_\infty} \left(\frac{1}{2} \int_0^t u^2 dt \right) d\bar{s}. \quad (2.16)$$

In the second integral of the right-hand side the particulate velocity \bar{u} decreases with increase in distance r from the center of disturbances not slower than $\frac{1}{r^2}$, while the area of surface s_∞ increases as a function of r^2 .

Consequently, for a region of disturbances of arbitrary size it is always possible to select within an infinite half-space large distances r such that this integral, which decreases not slower than $\frac{1}{r^2}$, will be as small as desired for an arbitrary, but finite time t .

We now subtract \bar{B}_∞ from each part of equality (2.15):

$$\bar{K} - \bar{B}_\infty = -\varrho \iint_{s_k + s} \varphi d\bar{s} = \bar{B}. \quad (2.17)$$

By the initial condition, surface Σ moves together with the fluid; consequently it bounds a constant fluid volume. Surface Σ is acted upon by constant pressure p_0 and additional variable pressure $p - p_0$, which is determined by the motion of the boundaries. The impulsive pressure p_i at free boundaries s is zero. The integral of excess pressure over the solid boundaries of the body reduces to the force

$$\bar{P} = \iint_{s_k} (p - p_0) d\bar{s} = \frac{D\bar{B}}{Dt},$$

with which the body acts on the fluid. The pressure force at an infinitely removed part of the boundary applied externally is $\bar{P}_\infty = \frac{D\bar{B}_\infty}{Dt}$. Thus, differentiation of (2.17) yields the final formula of the momentum theorem in the form

$$\frac{D}{Dt} (\bar{K} - \bar{B}_\infty) = -\varrho \frac{D}{Dt} \iint_{s_k + s} \varphi d\bar{s} = \frac{D\bar{B}}{Dt} = \bar{P}. \quad (2.18)$$

The magnitude of the actual momentum \bar{K} of all the fluid particles in region Σ , as the momentum of reaction forces \bar{B}_∞ external to Σ , depends on the shape of the removed part s_∞ of the boundary and in this sense they are indeterminate. Hence, the "momentum" vector, or the momentum of pressure forces applied to the fluid through the surface of a body moving on it, is determined from expression (2.17) and may not equal the actual momentum of all the fluid particles.

It is similarly shown that the vector of the "moment of momentum" or the impulsive moment of external pressure forces on the fluid relative to point $\bar{r} = 0$, is

$$\bar{I}_m = -\varrho \iint_{s_k + s} \varphi (\bar{r} \times d\bar{s}) = \int_0^t \left[\iint_{s_k + s} (p - p_0) (\bar{r} \times d\bar{s}) \right] dt = \int_0^t \bar{M} dt.$$

It also follows from this definition that

$$\bar{P} = \iint_{\Sigma} (p - p_0) d\bar{\Sigma}; \quad \bar{M} = \iint_{\Sigma} (p - p_0) (\bar{r} \times d\bar{\Sigma}).$$

According to boundary condition (2.6), we have

$$\bar{P} = -\varrho \frac{D}{Dt} \iint_{s_k+s} \varphi d\bar{s} = \iint_{s_k} (p - p_0) d\bar{s}.$$

The momentum theorem for steady flows will be applied below to specific problems.

10. Zero-potential surface

During any submersion of a solid body into a fluid initially at rest, for which we assume at zero time ($t = 0$) that $\varphi = 0$, there will exist at all its points during each subsequent time instant ($t > 0$) within the fluid

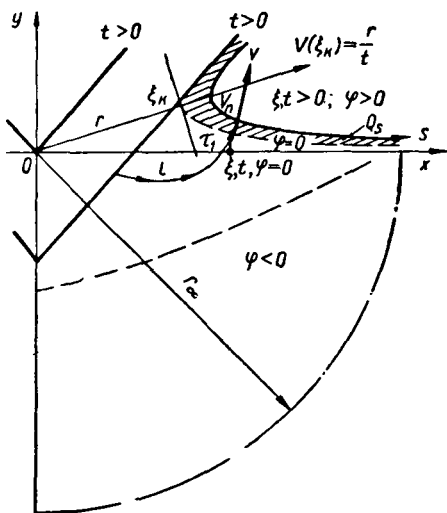


FIGURE 23.

a surface τ , at which during the entire motion $\varphi = 0$. At time $t = 0$ free surface s is a surface at which $\varphi = 0$. During subsequent periods positive potentials will be "accumulated" at surface s ; hence, according to Theorem XV, surface $\varphi = 0$ from the very start will move in the same direction as surface s , and at all times will divide the fluid region which rose above the initial level into two parts: one between s and τ , in which $\varphi > 0$, and another, where $\varphi < 0$ (Figure 23).

The pressure at surface τ (where $\varphi = 0$) is defined by equation (2.9). Since at surface τ we have $\frac{\partial \varphi}{\partial t} = 0$,

$$\frac{p_\tau - p_0}{\varrho} = V_n v - \frac{v^2}{2}. \quad (2.19)$$

When the pressure within the fluid is greater than or equal to p_0 , we derive that the normal velocity of transport of surface τ proper is $V_n \geq \frac{1}{2} v$, where v is the fluid velocity at surface τ . Here it is clear that velocity $\bar{v} = \text{grad} \varphi$ is orthogonal to surface τ . Consequently, for any continuous submersion of a body into a fluid initially at rest, surface τ , at which $\varphi = 0$, is always contained within the fluid and intersects the surface of the body or inner free boundaries. The latter statement will be illustrated below.

Suppose a hemisphere with radius $r \rightarrow \infty$ is drawn from the center of disturbances at the free surface within the fluid in such a manner that it intersects the free surface; on this hemisphere, by definition, $\varphi \rightarrow 0$. If surface τ , at which $\varphi = 0$, passes from the line of intersection of the hemisphere and the free boundary such that it does not intersect the body or the inner free boundaries, then the hemisphere and surface τ bound a region with fluid at rest; consequently, the velocity of surface τ proper and of the fluid at it will be zero. Then surface τ will be equivalent to a solid surface, at which $\frac{\partial \varphi}{\partial n} = 0$, but it is possible that $\varphi \neq 0$, which is incompatible with the definition of surface τ and the entire formulation of the problem.

When the body is extracted from the fluid at rest (without break in continuity) positive potentials arise at the free surface, at the surface of the body, and everywhere within the fluid; surface $\varphi = 0$ in this case no longer lies within the fluid.

We now clarify the location of the maximum pressure point. Euler's vector equation in the moving coordinate system τ, η , associated with a point on surface τ , can be expressed in the two-dimensional case as two scalar equations:

$$\omega = -\frac{1}{\rho} \cdot \frac{\partial p}{\partial \tau};$$

$$\frac{\partial v}{\partial t} + (v - V_\eta) \frac{\partial v}{\partial \eta} = -\frac{1}{\rho} \cdot \frac{\partial p}{\partial \eta},$$

where ω is the angular velocity with which system τ, η rotates relative to the stationary coordinate system, which at the time under consideration coincides with axes τ, η .

When $v - V_\eta = 0$, particle ξ_k always remains at surface τ . If then the trajectory of this particle is rectilinear and it moves with constant velocity,

$\frac{\partial v}{\partial t} = 0, \omega = 0$; thus $\frac{\partial p}{\partial \tau} = 0, \frac{\partial p}{\partial \eta} = 0$, and particle ξ_k is always situated at the maximum-pressure point. It is assumed that there are no singular points anywhere within the fluid, the excess pressure is positive, surface τ is continuous, has a single-valued curvature and extends from the surface of the body to infinity, where it coincides asymptotically with the initial free surface. These conditions, in particular, are satisfied by flows with self-similar and steady free boundaries.

Theorem XVI. For uniform motions with self-similar or steady free boundaries one of the pressure maxima is always located at the zero-potential surface and at that point on this surface where the transport velocity of the surface is equal to the absolute velocity of the fluid.

11. Mass, momentum and energy fluxes through the zero-potential surface

To fix ideas, we shall consider the case when surface τ ($\varphi = 0$) lies within the fluid, while the free surface moves outward and extends from particle ξ_k to infinity, where it coincides with the undisturbed level. We

fix at the free surface particle ξ , approached by streamline l which is orthogonal to surface τ and intersects it at point τ_1 (see Figure 23).

If the volume of the region bounded by surfaces τ , l and s is denoted by Q_s , then $\frac{dQ_s}{dt} = \int_{\tau_1} (v - V_n) d\tau$; however, the limit of integration can be variable, since streamline l may intersect surface τ in different points at different times.

Momentum \bar{B}_s of the fluid within region Q_s increases due to transport of momentum $q(v - V_n) v d\tau dt$ and work of pressure forces on surface τ , equal to $(p_\tau - p_0) d\tau dt$. As a result, equation (2.19) gives

$$\frac{d\bar{B}_s}{dt} = q \int_{\tau} \frac{v^2}{2} d\tau = \bar{\Pi}. \quad (2.20)$$

This formula makes no allowance for increase in momentum due to pressure forces acting on surface l_1 between τ and s .

The increment of kinetic energy T_s in region Q_s is also composed of the energy transport $q(v - V_n) \frac{v^2}{2} d\tau dt$ and work of pressure forces $(p_\tau - p_0) v d\tau dt$. Consequently

$$\frac{dT_s}{dt} = q \int_{\tau} V_n \frac{v^2}{2} d\tau = E \quad (2.21)$$

In many cases of submersion of bodies and their motion at free surfaces it is possible to locate (using additional considerations) a region of possible location of surface $\varphi = 0$ and certain features of this surface. Then formulas (2.20) and (2.21) sometimes provide useful results.

12. Green's theorem

Omitting the proof [10], Green's theorem for two arbitrary functions φ and φ' , which are continuous and have continuous first and second derivatives within a connection region Q , bounded by surface Σ , can be expressed as

$$\begin{aligned} \iint_{\Sigma} \varphi \frac{\partial \varphi}{\partial n} d\Sigma &= - \iiint_Q \left(\frac{\partial \varphi}{\partial x} \cdot \frac{\partial \varphi'}{\partial x} + \frac{\partial \varphi}{\partial y} \cdot \frac{\partial \varphi'}{\partial y} + \frac{\partial \varphi}{\partial z} \cdot \frac{\partial \varphi'}{\partial z} \right) \times \\ &\quad \times dx dy dz - \iint_Q \varphi \Delta \varphi' dx dy dz; \\ \iint_{\Sigma} \varphi' \frac{\partial \varphi}{\partial n} d\Sigma &= - \iiint_Q \left(\frac{\partial \varphi'}{\partial x} \cdot \frac{\partial \varphi}{\partial x} + \frac{\partial \varphi'}{\partial y} \cdot \frac{\partial \varphi}{\partial y} + \frac{\partial \varphi'}{\partial z} \cdot \frac{\partial \varphi}{\partial z} \right) \times \\ &\quad \times dx dy dz - \iint_Q \varphi' \Delta \varphi dx dy dz. \end{aligned} \quad (2.22)$$

If φ and φ' are velocity potentials of two different irrotational flows, then for an incompressible fluid $\Delta \varphi = 0$ and $\Delta \varphi' = 0$. The equality of the first integrals on the right-hand side yields the relationship

$$\iint_{\Sigma} \varphi \frac{\partial \varphi'}{\partial n} d\Sigma = \iint_{\Sigma} \varphi' \frac{\partial \varphi}{\partial n} d\Sigma. \quad (2.23)$$

When $\varphi = \varphi'$ and $\Delta\varphi = 0$, each of equations (2.22) upon being multiplied by $-\frac{\rho}{2}$, will yield an expression for the kinetic energy of the fluid in region Σ in terms of values of φ and $\frac{\partial\varphi}{\partial n}$ at the boundaries (see equation (2.10)).

Using equation (2.23) we can prove that the effect of infinity due to any local disturbance at the free surface is equal to the effect of a doublet placed at the center of disturbance (Figure 24).

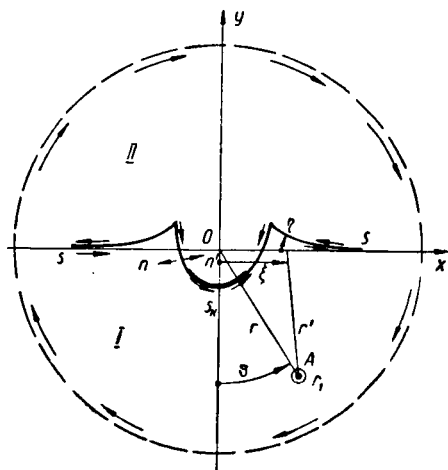


FIGURE 24.

We limit ourselves to the two-dimensional case. Potential φ' can be represented as $\ln r'$, since $\ln r'$ satisfies the Laplace equation $\Delta(\ln r') = 0$ if r' is the distance from point A (Figure 24) to any point of space x, y (within as well as outside the fluid). By assumption, point A lies in fluid-filled region I , and consequently when integrating over boundaries Σ of this region point A should be excluded. This can be done by drawing a circle of radius r_1 with center at point A . The contribution of the first integral around this circle, if $d\Sigma_1 = r_1 d\omega$, will be $\int_{\omega \rightarrow 2\pi} \varphi \frac{1}{r_1} r_1 d\omega \rightarrow 2\pi \varphi_A$ as $r_1 \rightarrow 0$, and the corresponding contribution of the second integral will be zero, since there are no sources or sinks outside circle r_1 . Integration of (2.23) only over the boundaries of region I gives

$$\varphi_A = -\frac{1}{2\pi} \int_{\Sigma} \varphi \frac{\partial \varphi'}{\partial n} d\Sigma + \frac{1}{2\pi} \int_{\Sigma} \varphi' \frac{\partial \varphi}{\partial n} d\Sigma.$$

Function φ is harmonic within region I , as well as within region II external to the fluid, and so allowance must be made in calculating φ_A that region II with boundary Σ' also has a potential φ . But for region II point A is an external point and for any point of the boundary of region II the

value of radius r' at point A is finite. It therefore follows from (2.23) that

$$0 = -\frac{1}{2\pi} \int_{\Sigma'} \frac{\partial \varphi'}{\partial n'} d\Sigma' + \frac{1}{2\pi} \int_{\Sigma'} \varphi' \frac{\partial \varphi}{\partial n'} d\Sigma'.$$

To calculate φ_A the last two expressions should be added. However, when integrating along the contour of region II it should be traversed in the same direction as the contour of region I . But $\frac{\partial}{\partial n} = -\frac{\partial}{\partial n'}$, hence, reversing the direction of traverse of contour II , after replacing $\frac{\partial}{\partial n'}$ by $\frac{\partial}{\partial n}$, φ_A can be calculated by traversing $s_k + s^*$ twice during the integration. Substitution of the values of φ and $\frac{\partial \varphi}{\partial n}$ at the boundaries of the disturbed region into the integrals gives

$$\varphi_A = -\frac{1}{\pi} \int_{s_k+s} \varphi \frac{\partial \varphi'}{\partial n} ds + \frac{1}{\pi} \int_{s_k+s} \varphi' \frac{\partial \varphi}{\partial n} ds. \quad (2.24)$$

In the preceding formulas we omitted integration over circles s_∞ and s'_∞ . However, the radii of these circles can be made as large as desired, and the value of φ_A cannot depend on the magnitude of these radii as $r_\infty \rightarrow \infty$.

Hence in the first integral we should have $\varphi_\infty \rightarrow C (= 0)$, since $\frac{\partial \varphi'}{\partial n} \cdot \frac{1}{r_\infty} \cdot ds_\infty = r_\infty d\omega$.

In the second integral, since $\varphi_\infty = \ln r' \rightarrow \infty$ as $r_\infty \rightarrow \infty$, $\int_{s_\infty} \frac{\partial \varphi}{\partial n} ds \rightarrow 0$; here this

integral should decrease with increasing r_∞ much more rapidly than the increase in $\ln r_\infty$. Thus, integration over all the infinitely far boundaries can be dispensed with by setting the additive constant for φ at infinity equal to zero.

All these considerations are similar in the three-dimensional case, for which φ' should be represented by function $1/r'$. The expression for the potential at point A then takes the form

$$\varphi_A = \frac{1}{2\pi} \iint_{s_k+s} \varphi \frac{\partial \varphi'}{\partial n} ds + \frac{1}{2\pi} \iint_{s_k+s} \varphi' \frac{\partial \varphi}{\partial n} ds. \quad (2.25)$$

Let us find the first term of the series expansion of φ about point A at infinity.

In the two-dimensional case $r' = \sqrt{(x+\xi)^2 + (y-\eta)^2}$, where x and y are coordinates of point A ; ξ and η are the coordinates of the contour of the disturbed part of boundaries s_k and s . When for the disturbed region $\xi, \eta \ll r'$, we have approximately, for $\xi \rightarrow \pm \infty$ and $\varphi \rightarrow 0$,

$$r' = r \left(1 - \frac{x\xi}{r^2} - \frac{y\eta}{r^2} + \dots \right); \quad \ln r' = \ln r - \frac{x\xi}{r^2} - \frac{y\eta}{r^2} + \dots,$$

where $r = \sqrt{x^2 + y^2}$.

Since distance r from the origin of coordinates x, y to point A is constant,

$$\frac{\partial \varphi'}{\partial n} = -\frac{x}{r^2} \cdot \frac{\partial \xi}{\partial n} - \frac{y}{r^2} \cdot \frac{\partial \eta}{\partial n}.$$

* Here, as above, s_k are the boundaries of the body, s denotes the free surfaces, and s_∞ designates surfaces at infinity; $\Sigma = s_k + s + s_\infty$.

where

$$\frac{\partial \xi}{\partial n} = \cos(\widehat{n, x}) \quad \text{and} \quad \frac{\partial \eta}{\partial n} = \cos(\widehat{n, y}).$$

Substitution of these expressions into (2.24) yields

$$\psi_A = \frac{1}{\pi} \int_{s_k + \xi} \psi \left(\frac{x}{r^2} \cos(\widehat{n, x}) + \frac{y}{r^2} \cos(\widehat{n, y}) \right) ds - \frac{1}{\pi} \int_{s_k + \xi} \left(\frac{x \xi}{r^2} + \frac{y \eta}{r^2} \right) \frac{\partial \psi}{\partial n} ds.$$

If the flow is symmetrical about the y axis, then $s \cos(\widehat{n, x})$ and ξ at symmetrical points are of the same magnitude and opposite sign, while ψ and $\frac{\partial \psi}{\partial n}$ are equal. We denote by ϑ the angle between the negative y direction and the direction of r ; then $\frac{-y}{r} = \cos \vartheta$. The momentum of the external force, or the momentum of the fluid along the axis, is $B_y = -\varrho \int_{s_k + \xi} \psi \cos(\widehat{n, y}) ds$, while the streamline element is $d\psi = \frac{\partial \psi}{\partial n} ds$. For the two-dimensional case

$$\varphi_A = \frac{\cos \vartheta}{\pi \varrho} \left(\frac{B_y}{\varrho} + \int_{s_k + \xi} \eta d\psi \right). \quad (2.26)$$

If the y axis is the axis of symmetry of the flow, then in the three-dimensional case, using formula (2.25), we find similarly

$$\varphi_A = \frac{\cos \vartheta}{2\pi \varrho^2} \left(\frac{B_y}{\varrho} + \int_{s_k + \xi} \eta d\psi \right). \quad (2.27)$$

We recall that the positive directions in (2.26) and (2.27) are those of the normal and of the normal velocity directed into the fluid. When the fluid is acted upon by forces along the negative y axis, $B_y < 0$, and the integral in parentheses is also negative. The integral in (2.26) and (2.27) can be termed the static moment of the streamline relative to the undisturbed level.

Theorem XVII. The effect of any local motion of the boundaries of a fluid-filled half-space at distances larger than the disturbed region and large compared with the actual dimensions of this region, is equivalent to the effect of a corresponding doublet.

For example, if a half-submerged cylinder of radius R floats on a horizontal free surface and acquires downward velocity vertical velocity V due to impact, the momentum component along the y axis will be $B_y =$

$$= -\frac{\pi}{2} R^2 \varrho V \quad (\text{the positive } y \text{ direction is upward}). \quad \text{In integral (2.26)}$$

$\eta = -R \cos \theta$; $d\psi = VR \cos \theta d\theta$, at surface s we have $\eta = 0$. Hence

$$\int_{s_k} \eta d\psi = -VR^2 \int_{-\frac{\pi}{2}}^{+\frac{\pi}{2}} \cos^2 \theta d\theta = -\frac{\pi}{2} R^2 V.$$

The potential at a far point within the fluid is $\varphi = \frac{-VR^2 \cos \theta}{r}$; the expression for φ is the same as for a cylinder performing translational motion within an infinite fluid.

For asymmetrical flow the doublet axis is not vertical. It can be shown by similar considerations that the moment of impulsive forces at the boundaries under the same conditions will reduce to a higher-order doublet. However, this point is not considered here.

Chapter Three

ELEMENTARY CASES OF FREE-BOUNDARY FLOWS

Spherical and cylindrical flows of an ideal incompressible fluid are the free-boundary flows which are simplest for study. If flow starts from rest due to the application of normal pressures at the boundaries, it is potential. According to Theorems III and IV, free boundaries in these cases are orthogonal; it follows that the velocity potential at each point of a free boundary at a given time has the same value $\frac{\partial \varphi}{\partial s} = 0$. Many of the conclusions and methods presented in the previous chapters can be illustrated and developed by a study of these cases. At the end of this chapter we shall consider flow with steady free boundaries which arises, in particular, on steady planing or on developed cavitation. Some of the presented results are important in their own right, while others illustrate the material of the first two chapters, but sometimes result in a new treatment of physical phenomena.

FLOW WITH SPHERICAL SYMMETRY

1. Spherical flow

Let us imagine an infinite region, filled with an incompressible, weightless ideal fluid, which contains a spherical cavity $R = R(t)$ filled with gas at pressure p . At infinity the pressure tends to the constant value $p \rightarrow p_0 = \text{const}$ and the fluid is at rest ($\text{grad } \varphi \rightarrow 0$). Since the density of the gas within the sphere is negligible compared with the density of the fluid, the motion of the gas within the sphere is neglected.

Initially ($t = 0$) the entire fluid was at rest and the velocity potential may be assumed to be zero ($\varphi = 0$) at any point in the fluid-filled space.

The spherical symmetry of the flow makes it possible to represent each fluid particle $\xi = r$ as a spherical layer with surface $4\pi\xi^2$ and thickness $\delta\xi$ at the initial time. Denoting the radius of this layer during subsequent times by $r = r(t)$, we can express the particle volume for these times as $4\pi r^2 \delta r|_t = 4\pi \xi^2 \delta \xi|_{t=0}$. The continuity equation in Lagrangian form expresses the physical fact that the volume of each incompressible-fluid particle remains constant during motion. Consequently

$$\frac{D}{Dt} (r^2 \delta r) = 2r \dot{r} \delta r + r^2 \dot{\delta r} = 0.$$

Taking the limit as $\delta r \rightarrow dr$ and $\delta t \rightarrow dt$ and integrating, we find that $d(r\dot{r}^2) = 0$ for each time instant and for all the particles; thus the particulate velocity is $\dot{r} = \frac{A(t)}{r^2}$ and the particulate velocity potential is $\varphi(r) = -\int_1^{\infty} \dot{r} dr = -\frac{A(t)}{r}$. These expressions are also valid for a surface ($r = R$) particle, for which the spherical coordinate is $R = R(t)$. Hence $A(t) = \dot{R}R^2$ and the velocity potential is $\varphi(r) = -\frac{\dot{R}R^2}{r}$; the potential at the free surface $r = R$ is $\varphi(R) = -\dot{R}R$. Pressure $p(r)$ can be determined directly from equation (2.8) by referring point A to infinity.

The total derivative of the potential has the form

$$\frac{D\varphi(r)}{Dt} = -\frac{\dot{R}R^2 + 2R\dot{R}^2}{r} + \frac{\dot{R}R^2}{r^2} \dot{r}.$$

Since by assumption $r_A \rightarrow \infty$ and $p_A \rightarrow p_0$, and also because $\dot{R}R^2 = r^2\dot{r}$, we have

$$\frac{\Delta p(r)}{\rho} = \frac{p(r) - p_0}{\rho} = (2\dot{R}^2 + R\ddot{R}) \frac{R}{r} - \frac{1}{2} \dot{r}^2. \quad (3.1)$$

At the free surface $r = R$

$$\frac{\Delta p(R)}{\rho} = \frac{p(R) - p_0}{\rho} = \frac{3}{2} \dot{R}^2 + R\ddot{R}. \quad (3.2)$$

In the Eulerian treatment [10] this problem amounts to expressing the flow through any stationary sphere of radius r' as $4\pi r'^2 v_r$, where $v_r = v_r(r', t)$ is the radial velocity. Since the continuity equation is now expressed in the stationary coordinate system $\frac{\partial}{\partial t} (r'^2 v_r) = 0$. From this $v_r = \frac{A(t)}{r'^2}$, and we again derive $\varphi(r', t) = -\frac{\dot{R}R^2}{r'}$. It is clear that the velocity and pressure potentials for point $r' = r$ do not depend on the point of view from which the flow is observed.

2. Inertia flow

This case is possible when the pressure within the sphere is $p(R) = p_0$, i.e., is equal to the pressure at infinity. The equation of motion of the free boundary is obtained from equation (3.2) by setting its left-hand side equal to zero. Separation of the variables R and \dot{R} yields the condition $R^3 \dot{R}^2 = \text{const}$; this constant can be defined as $R_0^3 \dot{R}_0^2$, if R_0 and \dot{R}_0 respectively are the initial sphere radius and the initial radial velocity of its boundaries. Excess pressure $\Delta p(r)$ within the fluid is obtained from equation (3.1) by subtracting from it the right-hand side of equation (3.2) set equal to zero; here making use of the continuity equation $\frac{\dot{R}}{r} = \frac{r^2}{R^2}$, we obtain

$$\frac{\Delta p_1(r)}{\rho} = \frac{1}{2} \dot{R}^2 \left(\frac{R}{r} - \frac{R^4}{r^4} \right). \quad (3.3)$$

If we move from the boundary of sphere R along its radius, the pressure will first increase, attain a maximum at point $\frac{R}{r} = \sqrt[3]{4}$ and then, as R/r

decreases further, will decrease tending to zero, as $\frac{R}{r} \rightarrow 0$ when $r \rightarrow \infty$.

We note that the distribution of pressure Δp_1 along r does not depend on the direction of velocity \dot{R} .

Omitting the restriction that $\Delta p(R) = 0$ and proceeding as in the derivation of formula (3.3), we obtain

$$\frac{\Delta p(r)}{\rho} = \frac{R}{r} \cdot \frac{\Delta p(R)}{\rho} + \frac{1}{2} R^2 \left(\frac{R}{r} - \frac{R^4}{r^4} \right). \quad (3.4)$$

The positive or negative pressure within the sphere propagates through the fluid as R/r , and positive pressure $\Delta p_1(r)$ (obtainable from (3.3) by substituting into it velocity \dot{R} , corresponding to the actual motion of the boundaries) is everywhere added to it. The pressure distribution is depicted in Figure 25, where

$$\Delta \tilde{p} = \Delta \tilde{p}_0 + \Delta \tilde{p}_1; \quad \Delta \tilde{p}_1 = \frac{R}{r} - \left(\frac{R}{r} \right)^4; \quad \Delta \tilde{p}_0 = \frac{R}{r} \cdot \frac{2\Delta p(R)}{\rho \dot{R}^2} = \frac{R}{r} \Delta \tilde{p}(R).$$

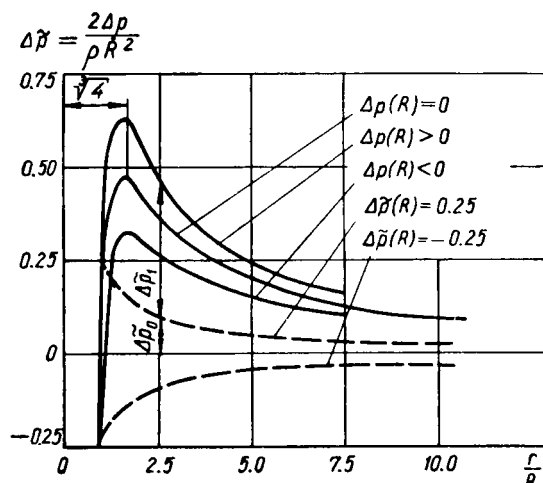


FIGURE 25.

3. Equipotential surface

Let us assume that potential φ on a spherical surface of radius $r_\varphi(t)$ remains constant, the absolute velocity of this surface is $V_\eta = \frac{dr_\varphi}{dt} = \dot{r}_\varphi$ and the velocity of fluid particles at it is $v_\varphi = \frac{\partial \varphi}{\partial r} = \frac{\dot{R}R^2}{r_\varphi^2}$. In order that potential $\varphi = -\frac{\dot{R}R^2}{r_\varphi}$ at sphere $r_\varphi(t)$ remains constant, it is required that the condition

$$\frac{d\varphi}{dt} = -\frac{\dot{R}R^2 + 2R\dot{R}^2}{r_\varphi} + \frac{\dot{R}R^2}{r_\varphi^2} \dot{r}_\varphi = 0$$

be satisfied, whence, using equation (3.2), we derive

$$\dot{r}_\varphi = \dot{R} \frac{r_\varphi}{R} \left(\frac{1}{2} + \frac{\Delta p(R)}{qk^2} \right).$$

This expression corresponds to Theorem XVI if $\Delta p(R) = 0$. Under this condition the equipotential surface which is infinitely close to the free surface $\left(\frac{r_\varphi}{R} \rightarrow 1\right)$, propagates in the same direction as surface R , but at a velocity equal to one half of \dot{R} . When moving by inertia ($\Delta p(R) = 0$) the rate of propagation of the equipotential surface is equal to the fluid velocity at this surface provided that $\left(\frac{r_\varphi}{R}\right)^3 = 2$; if $\frac{r_\varphi}{R} > \sqrt[3]{2}$, the rate of

propagation of the corresponding equipotential surface will be higher than the particle velocity at the surface.

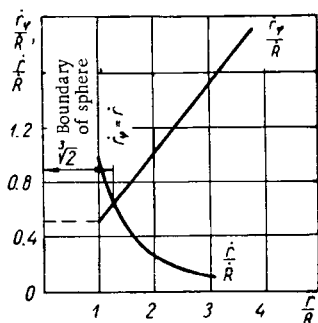


FIGURE 26.

The potential $\varphi(R) = -\frac{\text{const}}{\sqrt{R}}$; conse-

quently, as the sphere expands by inertia, its absolute value decreases. It may be imagined that free surface R overtakes the equipotential surface and "engulfs" it, with the potentials of both surfaces becoming equal at the time of "engulfment." The velocities of the equipotential surface and of the fluid as a function of r/R are shown in Figure 26.

4. Kinetic energy

The kinetic energy for the entire fluid can be calculated either by direct integration with respect to spherical layers, or from (2.10):

$$T = -\frac{\rho}{2} \int_{4\pi} \varphi(R) \dot{R} R^2 d\omega = 2\pi \rho R^3 \dot{R}^2. \quad (3.5)$$

The spherical coordinate r of each particle is determined from the continuity equation $r^3 - R^3 = \text{const}$. Consequently, the entire fluid mass can be treated as a system of material points with holonomic constraints, with radius R serving as the generalized coordinate of a system with one degree of freedom.

We denote the generalized force referred to coordinate R by Q_R . The Lagrangian equation of the second kind for generalized coordinate R has the form

$$\frac{d}{dt} \frac{\partial T}{\partial \dot{R}} - \frac{\partial T}{\partial R} = Q_R. \quad (3.6)$$

Substitution into formula (3.6) of the expression for the kinetic energy from (3.5) yields the equation of motion

$$4\pi R^3 \rho \left(\frac{3}{2} R^2 + R \ddot{R} \right) = 4\pi R^2 \Delta p(R) = Q_R \quad (3.7)$$

The generalized force has thus been found to be the total excess pressure at the inner boundaries of the sphere; naturally, equation (3.7) is identical with equation (3.2).

If an adiabatically expanding gas is held at $t = 0$ within a sphere with $R = R_1$ and $\dot{R} = 0$, then the internal pressure will be defined by the adiabatic equation $pR^{3\kappa} = p_1 R_1^{3\kappa}$ with index κ . Since $V_a = \dot{R}$ and $dR = \dot{R}dt$, integration of energy equation (2.12) for a weightless fluid ($U = 0$) yields

$$\dot{R}^2 = \frac{2}{\rho R^3} \int_{R_1}^R \left\{ p_1 \left(\frac{R_1}{R} \right)^{3\kappa} - p_0 \right\} R^2 dR. \quad (3.8)$$

Substitution of \dot{R}^2 from (3.8) and of $\Delta p(R) = p_1 \left(\frac{R_1}{R} \right)^{3\kappa} - p_0$ into equation (3.4) gives the pressure distribution within the fluid at each point r for given R .

CAVITATION IN JETS

5. Two-dimensional expansion of a fluid annulus

Let us imagine a two-dimensional flow when the region occupied by the fluid is bounded by two concentric circles: an inner circle with $R_a = R_a(t)$ and an outer circle with $R_b = R_b(t)$.

We denote the distance from a particle to the center by $r = r(t)$, where $R_a \leq r \leq R_b$; the pressure at the inner and outer boundaries are designated respectively by p_a and p_b , and $p_b - p_a$ by Δp . The volume of fluid between particle R_a and r remains constant; hence

$$\frac{D}{Dt} (r^2 - R_a^2) = 2(r\dot{r} - R_a\dot{R}_a) = 0,$$

whence $\dot{r} = \frac{\dot{R}_a R_a}{r}$ and the potential difference is expressed as

$$\varphi(r) - \varphi(R_a) = \int_{R_a}^r \dot{r} dr = \dot{R}_a R_a \ln \frac{r}{R_a}.$$

Substitution of the expressions for potentials and velocities into equation (2.5) yields an expression for the pressure at any point of the fluid:

$$\frac{p(r) - p(R_a)}{\rho} = -(\dot{R}_a R_a + \dot{R}_a^2) \ln \frac{r}{R_a} + \frac{1}{2} \dot{R}_a^2 \left(1 - \frac{R_a^2}{r^2} \right). \quad (3.9)$$

The kinetic energy of the entire fluid at time t is calculated most simply by integration along flow tubes (see formula (2.11)):

$$T = -\frac{\rho}{2} [\varphi(R_a) - \varphi(R_b)] \dot{R}_a 2\pi R_a = \pi \rho R_a^2 \dot{R}_a^2 \ln \frac{R_b}{R_a}. \quad (3.10)$$

If velocity \dot{R}_a and pressure difference Δp are finite, then

$\left\{ \frac{p_b - p_a}{\rho} - \frac{1}{2} \dot{R}_a^2 \left(1 - \frac{R_a^2}{R_b^2} \right) \right\} \frac{1}{\ln \frac{R_b}{R_a}}$ decreases without limit as $\frac{R_b}{R_a} \rightarrow \infty$. Hence,

when the fluid extends to infinity ($R_b \rightarrow \infty$), while inner boundaries \dot{R}_a have nonzero velocity R_a , then for an arbitrary value of Δp the expansion of the cavity is governed by the expression $\dot{R}_a R_a + R_a^2 = 0$. Solving this equation gives $\dot{R}_a R_a = \text{const}$. It follows from (3.10) that if $\frac{R_b}{R_a} \rightarrow \infty$, then T , the kinetic energy, also tends to infinity, since $\ln \frac{R_b}{R_a} \rightarrow \infty$. Hence no finite externally applied pressures operating over a finite time are able to change the pressure at the inner boundaries of a cylindrical cavity in an infinite fluid.

6. Motion of a thin fluid annulus

We denote the annulus thickness by δ ($\delta = R_b - R_a$), and assume that ratio δ/R_a is very small. Retaining terms containing δ/R to the first power, we derive the continuity equation for the entire annulus in the form $S = R\dot{\delta} = \text{const.}$ The pressure difference $\Delta p = p_b - p_a$ at the boundaries is found from (3.9) to be $\frac{\Delta p}{\rho} = -R\dot{\delta}$. Elimination of δ from the last two expressions yields an approximate equation of motion for the annulus,

$$\ddot{R} + \frac{\Delta\rho}{\rho S} R = 0. \quad (3.11)$$

Let us consider a circular cone with small vertex angle $\frac{\pi}{2} - \beta$, placed with its longitudinal axis symmetrically into a thin jet of diameter d and velocity V_0 (Figure 27). Then a thin annular jet appears past the base of the cone and, if the internal pressure is lower than the external pressure, it will form a thin-walled cavity. Cavities of this kind are in fact sometimes observed; in the rear part, where the jets merge, the flow is no longer potential, and gas bubbles are expelled from this part of the cavity, with the result that the pressure within the cavity is lower than the outside pressure.

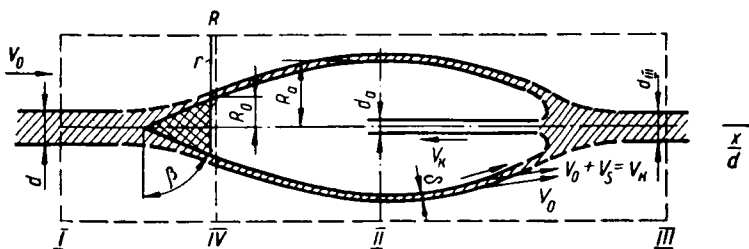


FIGURE 27.

Each length element dx of such a cavity can, to a known approximation, be treated as a thin cylindrical annulus, the motion of which in the radial direction is defined by the equation $\ddot{R} + \frac{\Delta p}{\rho S} R = 0$ with the initial conditions

$t = 0 \begin{cases} R = R_0 \\ \dot{R} = \dot{R}_0 \end{cases}$, where R_0 is the cone base radius, while $\dot{R}_0 = V \sin\left(\frac{\pi}{2} - \beta\right)$. The origin of the longitudinal axis of symmetry (x axis) can be placed at the center of the cone base, in which case $t = \frac{x}{V}$ approximately, since $\cos\left(\frac{\pi}{2} - \beta\right) \approx 1$, and the absolute velocity along the outer surface of the jet is constant by Bernoulli's equation. It follows from the continuity equation that the area is $S \approx \frac{d^2}{8}$. Denoting the cavitation number by $\sigma = \frac{2\Delta p}{\rho V^2}$, solving the equation of radial motion of the annulus and substituting the above quantities, we can derive an approximate expression for the cavity contour,

$$\frac{R(x)}{d} = \frac{\sin\left(\frac{\pi}{2} - \beta\right)}{2\sqrt{\sigma}} \sin\left(2\sqrt{\sigma} \frac{x}{d}\right) + \frac{R_0}{d} \cos\left(2\sqrt{\sigma} \frac{x}{d}\right), \quad (3.12)$$

where $R(x)$ is the inner radius of the cavity, while the outer radius $R + \delta$ of the cavity can be found by calculating δ from the continuity equation $2\pi S = 2\pi R\delta = \frac{\pi}{4} d^2$. It is clear that formula (3.12) was derived by neglecting the difference in the tangential velocity at the inner and outer boundaries, and, consequently, this conclusion is suitable only for low σ and sharp cones; here equation (3.12) cannot describe correctly the shape of the boundaries in the trailing part of the cavity, where \dot{R}/V_0 is no longer a small quantity.

If the x axis is vertical and the velocity within the jet is low, then consideration must be given to gravity forces, which in this case is relatively easy. In our theory the radial expansion of an elementary annulus is treated as being independent of the longitudinal drift of this annulus and from these considerations time t is expressed in terms of x . Denoting the velocity at the cone base by V_0 and retaining the origin of the x axis at its previous location, we obtain from the free-fall equation

$$x = V_0 t + \frac{gt^2}{2} \quad \text{or} \quad t = \frac{V_0}{g} \left(\sqrt{1 + \frac{2gx}{V_0^2}} - 1 \right).$$

Hence

$$\begin{aligned} \frac{R(x)}{d} = & \frac{\sin\left(\frac{\pi}{2} - \beta\right)}{2\sqrt{\sigma}} \sin\left(2\sqrt{\sigma} \left[\sqrt{1 + \frac{2gx}{V_0^2}} - 1 \right] \frac{V_0^2}{gd}\right) + \\ & + \frac{R_0}{d} \cos\left(2\sqrt{\sigma} \left[\sqrt{1 + \frac{2gx}{V_0^2}} - 1 \right] \frac{V_0^2}{gd}\right). \end{aligned} \quad (3.13)$$

Equation (3.13) reduces to equation (3.12) if $V_0 \rightarrow \infty$ or if the Froude numbers $\frac{V_0}{\sqrt{gd}}$ and $\frac{V_0}{\sqrt{gx}}$ are high. It is not difficult to determine the motion of the fluid also when the axis of the cone is oriented arbitrarily relative to the terrestrial vertical. For this it is possible to use (with the same degree of accuracy) the above principle of "independence of expansion"

of each transverse layer of the fluid for its longitudinal motion. It is evident that the center of gravity in a gravitational field will move in space in the same manner as a material point with initial velocity \bar{V}_0 .

7. Drag and the reentrant jet

The forces acting on a cone streamlined by a thin jet and the diameter of the reentrant jet can be calculated by means of the energy and momentum theorem. As to the reentrant jet we note that, according to Theorem X, the inner boundary of a cavity, when the cavity is considered in its absolute motion relative to a stationary fluid column, will be a steady surface, which cannot be closed. Hence, a reentrant jet, whose cross-sectional area is denoted by F_c , must be directed from the trailing end of the cavity to its leading end.

According to Theorem V, the relative particulate velocity V_s along the inner boundaries is constant. However, since by assumption pressure p_k within the cavity is lower than pressure p_0 in the free flow, the relative particulate velocity $V_s = V_k$ at the inner boundary is higher than the particulate velocity at the outer boundaries, where $V_s = V_0$, i. e., it is equal to the velocity in the jet (or equal in magnitude to the transport velocity in the absolute motion of the cone relative to a stationary fluid column). Velocity V_k can be obtained from the Bernoulli equation constructed for a streamline passing through a far point ahead of the cone and along the cavity

boundary; it is found that $p_0 - p_k = \frac{\rho V_0^2}{2} \left(\frac{V_k^2}{V_0^2} - 1 \right)$ or $V_k = V_0 \sqrt{1 + \sigma}$. The

absolute relative velocity at any point in the flow is $V_k = V_0 + v_s$, where v_s is the additional velocity; at the inner boundaries $v_s = v_k = V_k - V_0 \approx \frac{1}{2} \sigma V_0$.

We now draw control surface I - III, associated with the cone (see Figure 27), moving the bases of this surface far ahead of the cone and far back from the cavity. It is clear that the kinetic energy of absolute motion of the fluid (column stationary, cone in motion) within control surface I - III increases only due to energy transport by the jet toward the cone. Denoting by X the force which overcomes the drag, we obtain from the energy equation

$$\frac{dT}{dt} = XV_0 = \rho V_k F_c \frac{(V_0 + V_k)^2}{2} - F_c V_k (p_0 - p_k) = [\rho F_c V_k (V_k + V_0)] V_0 = \frac{dB}{dt} V_0$$

where $\rho V_k F_c$ is the mass of fluid passing per unit time through the cross-sectional area of the reentrant jet, i. e., through surface II in the direction of the cone, while $V_0 + V_k$ is the absolute velocity of these particles, equal to the sum of transport velocity V_0 and the relative velocity V_k ; the jet moves in a region with pressure $p_k < p_0$, which results in the appearance of the term $F_c V_k (p_0 - p_k)$.

We now substitute in the last equation the above expression for velocity V_k and thus derive the cross-sectional area of the reentrant jet,

$$F_c = \frac{X}{\rho V_0^2} \cdot \frac{1}{\sqrt{1 + \sigma} |1 + \sqrt{1 + \sigma}|} \rightarrow \frac{X}{2 \rho V_0^2} \cdot \frac{1}{1 + \frac{3}{4} \sigma} \Big|_{\sigma \rightarrow 0} \quad (3.14)$$

It is assumed here and subsequently that the reentrant jet does not reach the base of the cone and is somehow removed from the flow region. Actually, however, it breaks up at the rear part of the cavity into droplets, which are deposited on the inner boundaries of the cavity and are carried away from it by the flow. The loss of gas bubbles from the cavity is associated with this breakup and ejection from the cavity of sprays from the reentrant jet. Hence the flow shown in Figure 27 can actually be obtained at relatively low V_0 if gas is continuously supplied to the cavity. But then the jet in the rear part of the cavity is replaced by foam which is carried away by the flow, and the flow in the rear part of the cavity is no longer potential due to mixing of the gas with the fluid.

Applying the momentum theorem to the relative motion of the fluid through control surface $I - II$ on the assumption that the jet is removed from the cavity within surface $II - III$ and exerts no force on the cone, we can derive an expression for the drag of the cone. In fact, denoting the cross sections of the control surface by $F_I = F_{II}$, the flow cross section by F'_I and F'_{II} and the maximum (frontal) cross section of the cavity by S_k , we have

$$X = F'_I \rho V_0^2 + F_I p_0 - \int_{F'_{II}} \rho (V_0 + v_x)^2 dF - \int_{F_{II}} p_{II} dF.$$

The pressure integral in plane II is composed of pressure p_0 , acting on area $F_{II} - F'_{II} - S_k$, the pressure integral over the jet cross section, which is obtained from the Bernoulli equation

$$\int_{F'_{II}} p_{II} dF = \int_{F'_{II}} \left[p_0 + \frac{\rho V_0^2}{2} - \frac{\rho}{2} (V_0 + v_x)^2 \right] dF,$$

and, finally, the pressure p_k in the cavity, acting on surface $S_k = \pi R_k^2$. Substitution of these expressions for calculating the pressure integral

together with the continuity equation $F'_I V_0 = \int_{F'_{II}} (V_0 + v_x) dF$ into the preceding

expression for the drag X , we obtain the final expression for this latter quantity:

$$X = S_k (p_0 - p_k) - \int_{F'_{II}} \frac{\rho v_x^2}{2} dF. \quad (3.15)$$

We note that the result expressed by equation (3.15) does not apply only to the case of a cone placed in a thin jet, but also to the case when the fluid within the cavity extends to infinity ($d \rightarrow \infty$).

To evaluate the integral in formula (3.15) we assume, as an approximation, that the additional velocity v_x varies linearly from the value of v_k at the inner boundary to zero at the outer boundary. Thus $v_x = v_k (1 - \frac{\zeta}{\delta})$, where ζ is the distance along axis R from the inner boundary to some point inside the jet. Substitution of this velocity distribution into the continuity equation yields

$$F'_I V_0 = \int_0^\delta (V_0 + v_x) 2\pi (R + \zeta) d\zeta,$$

whence

$$\frac{d^2}{8} \approx R\delta \left(1 + \frac{1}{4} \sigma\right).$$

The integral in (3.15) can be expressed approximately as

$$\int_{F'_{II}} \frac{\partial v_x^2}{2} dF = \frac{\partial v_k^2}{2} \int_0^\delta 2\pi(R + \zeta) \left(1 - \frac{\zeta}{\delta}\right)^2 d\zeta \approx \frac{\partial V_0^2}{2} \cdot \frac{\pi d^2}{4} \cdot \frac{\sigma^2}{12}.$$

The drag is

$$X = S_k(p_0 - p_k) - \frac{\partial V_0^2}{2} \cdot \frac{\pi d^2}{4} \cdot \frac{\sigma^2}{12}.$$

The drag can also be estimated approximately by drawing the rear part of control surface $I - IV$ in the immediate vicinity of the cone base. Carrying out elementary calculations and retaining terms which are a function of σ only to the first power, we derive the approximate expression

$$(1 + \sigma) \frac{1 - \cos\left(\frac{\pi}{2} - \beta\right)}{2\sigma} \approx \frac{R_k^2}{d^2} - \frac{R_0^2}{d^2} \quad (3.16)$$

The drag of the cone is expressed approximately in the form

$$X = \frac{\pi d^2}{4} \cdot \frac{\partial V_0^2}{2} 2 \left[1 - \cos\left(\frac{\pi}{2} - \beta\right) \right] + \pi R_0^2 (p_0 - p_k) \approx \frac{\pi d^2}{4} \cdot \frac{\partial V_0^2}{2} \mu_z + \pi R_0^2 \Delta p,$$

where $\frac{\pi}{2} - \beta = \mu \rightarrow 0$.

Figure 27 shows the flow of a jet of weightless fluid past a circular cone for the case $(\frac{\pi}{2} - \beta) = 0.4$, cavitation number $\sigma = 0.01$, and $d = 2R_0 = 1$ cm. The cavity outline was calculated from (3.12), while the reentrant jet is expressed by (3.14). From the preceding expression for X the drag coefficient referred to the cone base area πR_0^2 will be, for the problem at hand,

$$c_x = \frac{d^2}{2R_0^2} \left[1 - \cos\left(\frac{\pi}{2} - \beta\right) \right] + \sigma \approx 0.03.$$

The boundary segments calculated from the above expressions are shown by solid curves in Figure 27.

8. General treatment of the energy and momentum equations

We consider the case $\frac{\delta}{R} \rightarrow 0$ and $\sigma \rightarrow 0$. However, the flow still remains as shown in Figure 27, i.e., the presence of a reentrant jet. Then the equation $\ddot{R} + \frac{\Delta p}{\rho S} R = 0$ of the radial motion of the annulus becomes asymptotically exact. Multiplying both terms of this equation by $2\pi \dot{R} \rho S$ and making

use of the fact that $2\pi S = 2\pi R\delta$, we have

$$2\pi q R \delta \dot{R} \frac{d\dot{R}}{dt} + 2\pi R \frac{dR}{dt} \Delta p = 0.$$

The first term represents the time derivative of the kinetic energy T of the fluid per unit length of cavity generatrix, while the second term, corresponding to the expression $\frac{d}{dt} (\pi R^2 \Delta p) = \frac{dU'}{dt}$, can be regarded as the derivative of the potential energy U' , also referred to unit length of the cavity generatrix.

Hence the equation of expansion of the annulus is equivalent to the energy equation in the form $\frac{d}{dt} (T' + U') = 0$, or $T' + U' = \text{const}$ for any annular element of cavity length. When the cone moves in its absolute motion through distance dx , provided that the fluid column can be treated as stationary, the force overcoming the drag performs work Xdx and an element of annular cavity with length dx , containing energy $(T' + U') dx$, moves away from the base plane. Consequently, $T' + U' = X$. The instant when the annular element reaches its maximum expansion and $\dot{R} = 0$ corresponds to the first term of (3.15) for the frontal cross section. Upon subsequent compression the energy contained within the fluid annulus also remains unchanged and is transferred to the reentrant jet in the rear part of the cavity.

Denoting the kinetic energy of absolute motion of the fluid for time t_0 by T_0 , and the momentum in the direction of absolute cone motion by B_0 , we have for any subsequent time t

$$T = T_0 + \int_{t_0}^t X V_0 dt; \quad B = B_0 + \int_{t_0}^t X dt. \quad (3.17)$$

It was pointed out above that when the cone moves relative to the stationary fluid column in the crosshatched part of the volume (see Figure 27), the energy and momentum do not change, and the increments in T and B occur due to the reentrant jet moving into the cavity. If the absolute velocity of the cone is $\dot{x} = V_0 = \text{const}$ and during time $t - t_0$ it travels through distance x , then we have an added mass $qF_c x$ of the fluid in the jet, whose absolute velocity is $2\dot{x}$. Thus

$$T = T_0 + qF_c x \frac{(2\dot{x})^2}{2} = T_0 + qF_c x (2\dot{x}) \dot{x};$$

$$B = B_0 + qF_c x (2\dot{x}).$$

These equations yield the identical result, valid for any uniform motion of a body relative to a stationary fluid:

$$T - T_0 = (B - B_0) \dot{x}, \quad (3.18)$$

where the momentum vector B is directed as velocity \dot{x} ; here, from the condition of axial symmetry, B is the principal vector of the absolute momentum of the fluid.

9. Steady free boundaries

Steady planing and developed cavitation can serve as examples of flows with steady free boundaries. The formation of a cavity behind a body is equivalent to the formation of a free boundary behind a planing surface in

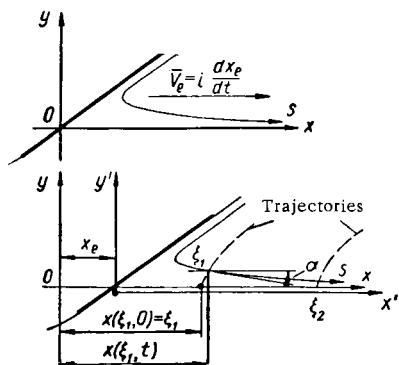


FIGURE 28.

the sense that new fluid particles move from the body edge to the free surface. First we consider in detail the properties of free boundaries consisting of the same particles, which arise ahead of planing bodies (Figure 28).

Retaining the notation of Section 4, Chapter One, we restrict ourselves to the case when the transport velocity \bar{V}_e has the same direction as the undisturbed boundary. The absolute velocities of particle ξ along the normal and tangent to the free boundary will then be $u_n = V_e \sin \alpha$ and $u_s = V_e (\cos \alpha - 1)$, where α is the angle between s and the x axis, if it is assumed that \bar{V}_e is in the positive x direction, which is also the positive direction of s . According to Theorem VIII for a steady free boundary the distances

between particles at the boundary remain constant; consequently $s_2(\xi_2) - s_1(\xi_1) = \xi_2 - \xi_1$, where ξ is the abscissa of particles at the undisturbed free surface.

The potential difference between particles ξ_2 and ξ_1 is defined as

$$\varphi(\xi_2, t) - \varphi(\xi_1, t) = \int_1^2 u_s ds = V_e \int_1^2 (\cos \alpha - 1) ds = V_e (x - s) \Big|_1^2.$$

If it is assumed that $\varphi(\xi_2, t) \rightarrow 0$ as $\xi_2 \rightarrow \infty$ (consequently, x and s separately tend to infinity), and also that $s_2 - x_2 \rightarrow 0$, the preceding expression yields

$$\varphi(\xi, t) = V_e (x - \xi), \quad (3.19)$$

where x is the abscissa of particle ξ at time t , while ξ is the abscissa of the same particle at time $t = 0$, i. e., at the time when the particle was still at infinite distance from the planing surface. Consequently, $x - \xi$ is simply the absolute travel of particle ξ along the x axis.

It is known that normal velocities at a free boundary at large distances ahead of a planing plate (in the two-dimensional case) are approximately the same as those ahead of a corresponding lifting vortex. Consequently, if at the time under study the vortex coincides with the origin of the stationary coordinate system x, y , then as $x \rightarrow \infty$

$$u \approx u_n \approx V_e \frac{\text{const}}{x}.$$

However, $dt = -\frac{dx}{V_e}$; hence formula (2.7) yields*

$$\varphi(\xi, t) = \frac{1}{2} \int_0^t u^2 dt \approx \frac{1}{2} \text{const } V_e \int_{x=\xi}^{\infty} \frac{dx}{x^2} \approx \frac{1}{2} \text{const } \frac{V_e}{x}.$$

Under these conditions the rise in the level of the free surface is $y_s \approx \int_0^t u dt$, and consequently it is logarithmically infinite. For a plate with finite span formula (2.7) is applicable directly in the vertical plane of symmetry. But for any three-dimensional flow the reduction in velocity u with increasing distance from a planing plate occurs more rapidly than $\frac{1}{x}$, and therefore everywhere at a free surface from the point where it starts curving the potential of any particle is positive and finite, while the level rise y_s can be as large as desired.

10. Kinetic energy

In the two-dimensional case the kinetic energy of the fluid in any region is obtained from the expression $T = -\frac{\rho}{2} \int \varphi \frac{\partial \varphi}{\partial n} ds$ (see Section 7, Chapter Two). If T is referred to a layer of unit thickness (along the z axis), in our case $\frac{\partial \varphi}{\partial n} = -u_n$ and, in addition, $\sin \alpha ds = -dy$; hence, substituting the above values of u_n and φ into the expression for T , we obtain $\frac{\partial \varphi}{\partial n} ds = -V_e \sin \alpha ds = V_e dy$. Integration from s to $s \rightarrow \infty$ yields

$$T = \frac{\rho}{2} V_e^2 \int_0^{y_s} (x - \xi) dy. \quad (3.20)$$

In keeping with the meaning of integration in (3.20) one should, at some instant of time, integrate the particle travel $(x - \xi) = f(y_s)$ along the free surface. However, the steady state of the free surface means that the trajectories of all the particles are identical, hence geometrically the integral $\int_0^{y_s} (x - \xi) dy$ is the area bounded by the trajectory of particle ξ , segment of the y axis drawn from the start of the trajectory, and segment $x - \xi$ connecting point y_s , ξ , which is the instantaneous location of particle ξ , with the y axis. The geometric construction is shown in Figure 29, in which this region is shaded.

To calculate the energy T , expression $\varphi \frac{\partial \varphi}{\partial n}$ should be integrated over a closed contour, since we restricted ourselves in deriving (3.20) to integration only along the free boundary from particle ξ to $\xi = s \rightarrow \infty$. The interpretation is that (3.20) expresses the kinetic energy of the fluid within a region bounded by surface $\varphi = 0$, free surface s extending from particle ξ to infinity, and a streamline (in absolute motion), which arrives at particle ξ and intersects the plane $\varphi = 0$. In Figure 29 this area is shaded by continuous and dashed lines.

* In general the moving and stationary coordinates are related by the expression $x = x' - V_e t$; since here $x = x'$, we have dropped the prime of x in the integrand.

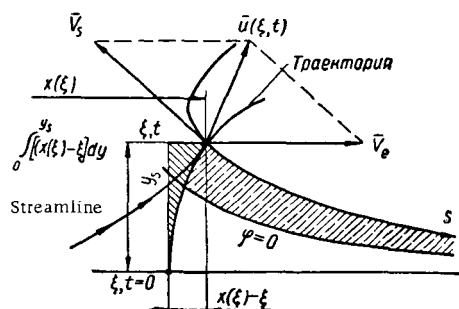


FIGURE 29.

The particle travel $x(\xi) - \xi$ decreases with increasing x' not slower than $\frac{1}{x'^2}$; the surface rise y_s is proportional to $\ln x'$. Hence the integral in (3.20) decreases as $\frac{1}{x'^2}$ with increasing x' . Consequently, the kinetic energy of fluid particles in the surface region is always finite.

11. Stagnation point

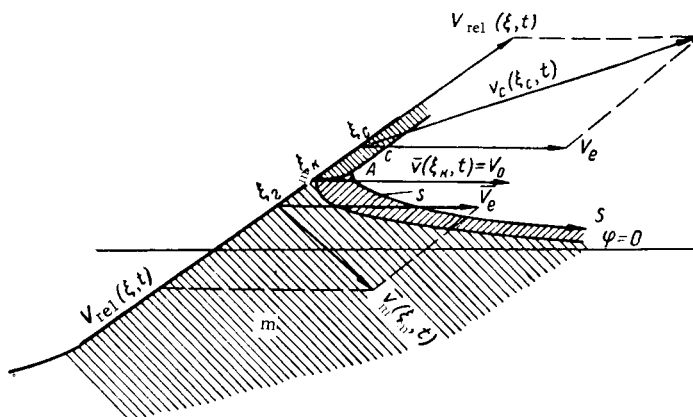
The excess pressure at the stagnation point is $\Delta p_k = \frac{\rho V_s^2}{2}$; the velocity of a fluid particle situated at the stagnation point relative to the planing surface is zero. Consequently, the same particle ξ_k is always located at the stagnation point. Here the absolute velocity $\bar{v}(\xi_k, t)$ of this particle has the same direction and magnitude as the transport velocity \bar{V}_e . All the particles at the planing surface which do not coincide with the stagnation point move away from it. The normal velocities of particles close to the stagnation point are identical. Hence those particles ξ_c , which are located in the region of the spray sheet, have absolute velocity $v(\xi_c, t) > v(\xi_k, t)$, while for particle ξ_m , located in the main flow, $v(\xi_m, t) < v(\xi_k, t)$ (Figure 30).

The pressure at the stagnation point is maximum and $\frac{\partial \Delta p}{\partial s} = 0$. Hence according to (2.5) the rate of growth of the potential of particles infinitely close to the stagnation point is

$$\frac{D}{Dt} \varphi(\xi, t) = -\frac{\Delta p_k}{\rho} + \frac{v^2(\xi, t)}{2} = \frac{v^2(\xi, t)}{2} - \frac{v^2(\xi_k, t)}{2}.$$

Consequently potential $\varphi(\xi_c, t)$ for particles ξ_c increases, and for particles ξ_m of the main flow the potential $\varphi(\xi_m, t)$ decreases. For particle ξ_k located at the stagnation point $\frac{D}{Dt} \varphi(S_k, t) = 0$. For a particle at infinity ($\xi \rightarrow \infty$), at the free surface $\Delta p = 0$, while u is a quantity of the same order of magnitude as $\frac{1}{\xi}$; hence as $\xi \rightarrow \infty$ we also have $\frac{D}{Dt} \varphi(\xi \rightarrow \infty, t) = 0$. It follows that the rate of increase in the potential difference between the stagnation point

17



Therefore surface $\varphi=0$, ahead of a planing plate bisecting at infinity the distance between the instantaneous position of the free surface and the undisturbed level, is always located above the undisturbed level and approaches the planing plate at the stagnation point, where the excess pressure has a maximum.

We assume that the plate is planing at velocity V_* , directed along the x axis which coincides with the undisturbed level of the fluid. The angle of attack of the plate is denoted by α . The normal force P_n on the plate can be determined from various points of view. It follows from the energy equation that the increment in the kinetic energy of the entire fluid is equal to the work of internal forces. In steady motion of a plate the kinetic energy of fluid particles changes only due to the sliding off of a spray sheet with thickness δ from the leading edge of the plate. Neglecting the pressure gradient within the spray sheet and making use of the fact that the relative velocity at the free surface is $V_* = V_*$ (Theorem VI), we find that the mass of fluid leaving (per unit time) a unit plate span at the forward edge is $\rho\delta V_*$ and that it carries away energy $\rho\delta V_* \frac{v_*^2}{2}$. Velocity v_* is the absolute velocity of particles at the forward edge of the spray

* This assertion is quite rigorous if we treat steady planing as the limiting case of self-similar entry of a plate into the fluid, when the velocity is directed at angle θ to the undisturbed level. Then, as $\theta \rightarrow 0$, there will exist (according to the condition of self-similarity) a single particle ξ_* for which $\varphi_* = 0$ at time $t = 0$, and condition $\Delta p - \frac{\rho V_*^2}{2} = 0$ is always satisfied. Hence for all $t > 0$ we have $\varphi(\xi_*, t) = 0$.

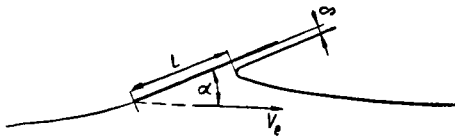


FIGURE 31.

sheet; consequently $v_e = 2V_e \cos \frac{\alpha}{2}$ (Figures 30 and 31). From the energy equation $\frac{dT}{dt} = P_n \sin \alpha V_e = \rho \delta V_e \frac{v_e^2}{2}$ we derive the expression for the normal force

$$P_n = \rho \delta V_e^2 \operatorname{ctg} \frac{\alpha}{2}. \quad (3.21)$$

Formula (3.21) can be regarded as the generalization of Zhukovskii's formula (for a plate placed perpendicularly to the flow), that the pressure force on the surface is $\rho Q V_e$, where Q is the fluid volume carried away by the spray sheet per second.

If $\alpha = \frac{2}{\pi}$ and $Q = \delta V_e$, then (3.21) expresses Zhukovskii's result. The analogy established by Wagner between a planing surface and an airfoil yields the expression for the lift

$$Y = \pi \sin \alpha \frac{\rho V_e^2}{2} L = P_n \cos \alpha,$$

where L is the wetted length (see Figure 31). Comparison of this expression with expression (3.21) shows that $\frac{\delta}{L} = \frac{\pi}{4} \alpha^2$ if $\alpha \rightarrow 0$.

Formula (3.21) can also be obtained from a Lagrangian equation of the second kind. Suppose initially the kinetic energy of the fluid in the entire region is T_0 . The plate will move during time t through a distance $x = V_e t$ and energy T_0 will be increased by the amount $\rho \delta x \frac{v_e^2}{2}$. Since $v_e = 2V_e \cos \frac{\alpha}{2}$, while $V_e = \dot{x}$, the energy at time t will be $T = T_0 + \rho \delta x \dot{x}^2 2 \cos^2 \frac{\alpha}{2}$. The generalized force referred to the x coordinate is $X = P_n \sin \alpha$. Substitution of the above expressions into the Lagrangian equation $\frac{d}{dt} \frac{\partial T}{\partial \dot{x}} - \frac{\partial T}{\partial x} = X$ again yields (3.21). We note that the above applies only to steady motion, when $\ddot{x} = 0$ and $\alpha = \text{const}$.

If the plate moved before time t at constant velocity $\dot{x} = \dot{x}_1$ and the corresponding force was P_{n1} , and then during time interval $t_2 - t_1$ the plate acquired the velocity $\dot{x} = \dot{x}_2$, then with time, as $t_2 < t \rightarrow \infty$, if $\dot{x}_2 = \text{const}$, the force will acquire a new steady value $P_n \rightarrow P_{n2}$, which is also obtainable from (3.21). The transition from one steady motion to another involves a change in the kinetic energy of the entire fluid, and not only of the energy in the spray sheet. Hence, during such a transition force P_n will no longer be obtainable from (3.21) and cannot be calculated from the Lagrangian equation, since the constraints for the particles will no longer be holonomic.

The ideal fluid flows examined in this chapter can be calculated exactly. Steady planing of a flat plate was already studied in great detail by conformal mappings. An analogy between planing and the motion of an airfoil was established by Wagner; the problem was developed further by Sedov. However, the equations used here are more general and can be used in many different cases, in particular those for which an exact solution cannot be obtained. Comparison of general relationships for a flow which can be calculated exactly in a particular case allows one to obtain a general idea of the flow pattern and to construct an approximate computational scheme for another flow which cannot be calculated exactly.

Chapter Four

SYMMETRIC IMMERSION OF A BODY INTO A FLUID

In studies of high-velocity entry of bodies into water it is often possible to treat water as an ideal and incompressible fluid. However, in all cases, even on the assumptions which are made, exact calculation of the forces and configuration of free boundaries are found to be virtually impossible. It is hence very important to use relatively simple examples to examine the details of these kinds of flows, clarify the principal governing relationships, and work out effective methods for theoretical estimates which would agree with experimental results.

The entire immersion process can be subdivided into three stages: from initial contact to separation of the spray roof region from the body surface; from spray-root separation to cavity formation; and steady cavitating flow. In the present chapter we consider the first and second stages of immersion of symmetric bodies and profiles, which possess the property that initial contact with the free surface occurs at a single central point.

1. Impact of buoyant bodies

Problems involving impact of buoyant bodies are stated as follows. It is assumed that the fluid is ideal, incompressible and fills some part of the space bounded by the specified free surface s . A body (or contour in the two-dimensional problem) whose surface s_b is also specified floats at the fluid surface. Before impact the body and the fluid are at rest. Impact means imparting to the body a velocity \bar{V} over an infinitesimal time interval $\Delta t \rightarrow 0$ by applying to the body an infinite force $\bar{P} \rightarrow \infty$. Since the fluid is set in motion from rest by normal pressures, the motion is potential. As is known, if the Cauchy-Lagrange integral

$$\frac{\partial \varphi}{\partial t} + \frac{v^2}{2} + \frac{p}{\rho} + U = F(t)$$

is integrated over this infinitesimal time interval Δt , it is found that the integrals of terms which retain finite values within the integration interval drop out as $\Delta t \rightarrow 0$, and as a result one derives the expression

$$\rho \varphi = - \int_0^{\Delta t} p dt = - p_i$$

where p_i is the impulsive pressure.

At the free surface s we have $p_i = 0$; consequently, following the impact the velocity potential φ at it is equal to zero (or to a nonzero additive constant). The fluid velocity normal to surface s_k at the body surface after the impact should equal the normal component of the body velocity, and therefore the boundary condition at surface s_k is $\frac{\partial \varphi}{\partial n} = \bar{e}_n \bar{V}$. At infinite distance from the body the fluid motion vanishes; hence $\text{grad } \varphi \rightarrow 0$, and velocity potential φ tends to zero or some constant value.

The problem of impact on a buoyant body thus reduces to a boundary-value problem of a mixed type, when the value of potential φ is given over a part of boundaries s , while the value of $\frac{\partial \varphi}{\partial n}$ is given at a part of boundary s_k ; boundaries s and s_k are known, and we require the potential function satisfying the Laplace equation $\Delta \varphi = 0$ within the fluid-occupied region, and boundary conditions at surfaces s and s_k . Methods for solving problems of this type are known and have been incorporated in all courses on hydro-mechanics; at present a large number of particular results were obtained for two- as well as three-dimensional flows. Hence, without dwelling in detail on the theory of impact of buoyant bodies, we shall note only the principal results.

In all these cases the ensemble of impulsive pressures applied to the fluid by the surface of the body, reduces to the principal momentum vector \bar{B} and the principal vector of the impulsive momentum, i. e., the vector of the moment of momentum [angular momentum] \bar{M} of the fluid, expressed in terms of induced inertias, the components of which can have different values along different axes. It is known that reduced masses and moments of inertia depend on the shape and dimensions of the body, and on the form of the free surface (if the body floats), and are proportional to the density ρ of the fluid and are independent of the velocity following the impact. In particular, for vertical symmetric impact (along the y axis) of a buoyant body $B_x = 0$, $\bar{M} = 0$, while $B_y = m_y^* V_y$ and the kinetic energy of the fluid is $T = m_y^* \frac{V_y^2}{2} = \frac{1}{2} B_y V_y$. For a plate of width $2c$, aligned along the x axis, the induced mass per unit length z on impact in the y direction is $m_y^* = \frac{\pi}{2} \rho c^2$; for a disk with radius c in the x, z plane on a like impact we have $m_y^* = \frac{4}{3} \rho c^3$; the values of induced inertias for other cases can be found in the literature and will be subsequently utilized without proof as known results.

In 1952 Gurevich /5/, as well as Berman, Parkhomovskii and others, solved a number of problems involving impact of profiles in developed cavitated flow. Solutions for two-dimensional flows are found by means of conformal mappings.

From the standpoint of mechanics these problems are equivalent to problems of impact of a body on an infinite fluid, or of a body floating at the free surface, the only difference being that even before the impact the free surface assumed a shape produced by cavitated flow. In these cases the induced mass found from solving the impact problem cannot be treated as a universal constant. The continuous motion of a profile or of a body with developed cavitation behind it cannot be constructed by superposition of infinitesimal, but infinitely frequent, impacts.

It is easy to show that for arbitrary motion within an unbounded region of a closed surface, it is always possible to draw on such a surface a closed curve on which the velocity potential would be equal to its value at infinity (for example, zero). An equipotential surface extending to infinity can be drawn from this curve at the body surface and this equipotential surface can always be treated as the free surface in the problem of impact by one-half of the body. In this sense problems with impact of a buoyant body are equivalent to problems of the motion of a body within an infinite fluid; when the buoyant body is impacted tangentially to the free surface, this is equivalent to the shifting of one-half of a symmetric body relative to its other half within an infinite fluid.

2. Immersion and impact

Comparison between the theory of continuous immersion and impact entry of buoyant bodies shows that these two phenomena are entirely different. This assertion is supported by the following considerations.

1. The theory of impact of buoyant bodies ignores the migration of the free boundaries during impact, and hence the potential at the free boundaries during this time remains unchanged (in particular, $\phi = 0$). This motion of free boundaries cannot be neglected in continuous immersion; the velocity potentials at the boundaries differ substantially from zero and may markedly exceed the potential at the body surface.

2. The fact that potentials at the free boundaries are not zero means that the fluid flow arising on continuous immersion cannot be obtained instantaneously only by the body impact, even if the boundaries in both these cases are the same. This flow forms with immersion of the body and contains within it implicitly the immersion history.

3. The relationship between the momentum and energy for symmetric impact and for immersion are different. In the case of impact of a buoyant body $T = \frac{1}{2} V_\infty B_\infty$, and consequently Wagner's integral is $I_w = 2T - VB_\infty = 0$.

On uniform immersion this integral is equal to the kinetic energy of the entire fluid and determines the drag. The concept of the induced mass on immersion of a body also has a different meaning than on impact. In the presence of free boundaries it is impossible to formally construct the equation of motion of the body on the assumption of steadiness in the frequently used form $\frac{d}{dt} [(m + m^*) V] + kV^2 = 0$. The induced mass m^* and the drag coefficient k are found to be related and depend not only on the instantaneous state of motion of a body with mass m , but also on the history of this motion.

Even in the simplest case of uniform immersion of a rectilinear wedge the rigorous mathematical solution of the problem cannot be fully completed. The equation of the free boundaries remains indeterminate, and this in turn makes it impossible to formulate the corresponding boundary-value problem. But even if the equation of the free surface could be found, difficulties would arise in solving the Laplace equation when a part of the boundaries has a complex curved shape. The problem in more complicated cases is even more difficult. Hence, subsequently, we shall attempt to circumvent these difficulties by seeking suitable approximate solutions to problems of this type.

CONTINUOUS IMMERSION OF A PROFILE

3. Uniform immersion of a wedge (Wagner's problem)

We assume that an infinite wedge is immersed symmetrically into a fluid (Figure 32). The general conditions are as follows: the fluid is ideal, weightless and incompressible, with density ϱ . The initially quiescent fluid fills the lower half-space x, y, z at $y < 0$. The coordinate origin is placed at the point where the wedge vertex first comes into contact with the free surface; the depth of immersion is h , and the rate of immersion is $\dot{h} = V = \text{const}$. Since the fluid motion starts from rest due to normal forces, it has a velocity potential φ at each instant of time and at each point in the fluid-filled space. All the results pertain to unit wedge length along the z axis.

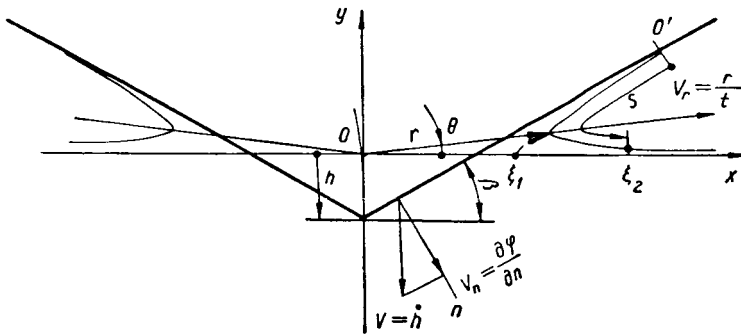


FIGURE 32.

At infinity $\text{grad } \varphi \rightarrow 0$, and it can be shown that the effect of the flow at $r^2 = x^2 + y^2 \rightarrow \infty$ is equivalent to a doublet of the form $\varphi = -\frac{M r^2 \cos \theta}{r} + C$, where M is a constant. We hence set the additive constant C equal to zero and assume that $\varphi \rightarrow 0$ as $r \rightarrow \infty$. At the wedge's solid surfaces the boundary condition is $\frac{\partial \varphi}{\partial n} = V \cos \beta$, where β is the deadrise angle.

The pressure p at each point of the free surface is constant and equal to p_0 , the pressure at infinity. The free surface proper is in motion and always consists of the same fluid particles. The free-surface arc, measured from the tip O' of the spray sheet, is denoted by s . Then the dynamic boundary condition, which follows from constancy of pressure at the free boundary, is $\frac{\partial p}{\partial s} = 0$ or $\bar{e}_s \frac{D\bar{u}}{Dt} = 0$, where \bar{u} is the absolute velocity vector at the boundary (\bar{e}_s and \bar{e}_n are unit tangential and normal vectors). Since $\bar{u} = \bar{e}_s u_s + \bar{e}_n u_n$, the dynamic condition is reduced to the form $\frac{Du_s}{Dt} = u_n \frac{D\alpha}{Dt}$, where α is the angle of rotation of the free surface. The kinematic conditions at the free boundary reduce to two equations (for the relative elongation $\frac{De}{Dt} = \bar{e}_s \frac{\partial u}{\partial s}$ and for the

rates of rotation $\frac{D\alpha}{Dt} = e_n \frac{\partial \bar{u}}{\partial s}$) of a boundary segment, consisting of the same particles. These conditions are general and valid for any free boundaries; they will subsequently be used.

The self-similarity of the flow is obvious, since the linear dimension (for example h) is determined only by the scale. Consequently, the free boundary translates while remaining similar to itself. Hence in polar coordinates r, θ , for each $\theta = \text{const}$ a point on the boundary is transported along radius r at constant velocity $V_r = \frac{r}{t} = \frac{r}{h} V$, while the arc length of the free surface up to this point increases at the rate $\frac{s}{t}$, which is also constant. Obviously, the velocity \bar{u} of different fluid particles which arrive at different times at point $\frac{r}{t} = \text{const}$ and $\theta = \text{const}$ is the same. Hence, if $u_s = u_s(s, t)$, the dynamic boundary condition for a point at the free surface propagating along r in a given direction is $\frac{\partial u_s}{\partial s} = \frac{u_n}{R}$, which is the first kinematic boundary condition (see (1.6)). Consequently, the distance along the free surface between individual particles remains unchanged throughout the motion (Theorem XI).

Denoting the individual particles of the free surface by their initial abscissas ξ at the undisturbed surface, we have $\xi = s$. The absolute velocity of a particle at a self-similar point A is $\bar{u} = \bar{V}_r + \bar{V}_s$; the absolute magnitude of the velocity is $V_s = \frac{s}{t}$, and this velocity is directed toward the spray-sheet tip (Figure 33).

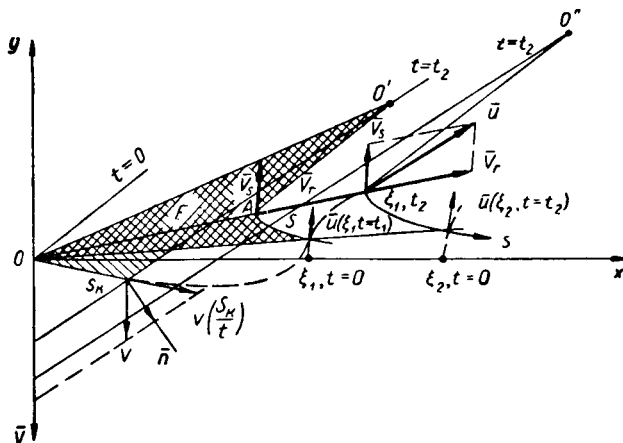


FIGURE 33.

The potential and stream functions at the free surface are given by

$$\frac{\partial \varphi}{\partial s} = u_s = V_r \cos(\widehat{r, s}) - V_s = \frac{r}{t} \cdot \frac{\partial r}{\partial s} - \frac{s}{t};$$

$$\varphi_\infty - \varphi(s) = \int_s^\infty u_s ds = \frac{r^2 - s^2}{2t} \Big|_s^\infty.$$

Integration is carried out for a fixed time t . At infinity, where $r = s \rightarrow \infty$ as $u_s \rightarrow 0$, it is assumed that $\varphi_{(\infty)} = 0$, which yields

$$\varphi(s, t) = \frac{r^2 - s^2}{2t}. \quad (4.1)$$

The stream function at the boundaries will be treated as positive if velocity $\frac{\partial \varphi}{\partial n}$ is directed along the inward normal; the stream function at the free boundaries is negative. At the free boundary

$$d\psi = -u_n ds = -\frac{r}{t} \sin(\widehat{r, s}) ds,$$

since $\sin(\widehat{r, s}) = \frac{rd\theta}{ds}$, we have $\psi(s, t) = -\frac{2F}{t}$, where F is the area of a curved sector, bounded by free-surface arc s and radii connecting the ends of this arc to the similarity [homothetic] center. The same expression for the stream function is valid also for the wedge generatrix s_k ; hence the condition $\psi(s_k, t) + \psi(s, t) = 0$ defines the ends of the same streamline.

The pressure at each homothetic point is

$$\frac{p - p_0}{\rho} = -\frac{\partial \varphi}{\partial t} + \frac{\partial \varphi}{\partial r} \cdot \frac{dr}{dt} - \frac{1}{2} u^2. \quad (4.2)$$

If $\frac{r}{t} = \text{const}$ and $\theta = \text{const}$, then $\frac{\partial \varphi}{\partial t} = \frac{\varphi}{t}$, and so $\Delta p = p - p_0 = \text{const}$ at each point. It is of importance that the boundary condition at the free surface ($\Delta p = 0$) coincides with the kinematic condition $\bar{u} = \bar{V}_r + \bar{V}_\theta$. If the pressure force of the wedge on the fluid is $P_h(t)$, by virtue of the fact that the pressure at homothetic points is invariable while the distances between them increase in proportion to time t , we have $\frac{P_h}{t} = \text{const}$.

The energy and momentum of the fluid are determined from the preceding condition for the force:

$$T = \int_0^t \left(\frac{P_h}{t} \right) t V dt = \frac{P_h V t}{2}; \quad B_h = \int_0^t \left(\frac{P_h}{t} \right) t dt = \frac{P_h t}{2}. \quad (4.3)$$

It is noteworthy that this yields the condition $T = VB_h$, relating the energy and momentum, which is in general characteristic for any symmetric uniform immersion. If we would stop the motion at some instant, while retaining the same boundaries as for uniform immersion with a homothetic center, and by impacting on the wedge we would impart to it momentum B'_h and velocity V , then the kinetic energy would be $T' = \frac{1}{2} VB'_h$. At all the free boundaries immediately following the impact φ and u_s would then be zero.

The energy and momentum can also be calculated in terms of φ and $\frac{\partial \varphi}{\partial n}$ at the boundaries:

$$T = -\frac{\rho}{2} \int_{s_k+s} \varphi \frac{\partial \varphi}{\partial n} ds; \text{ on } s_k \quad \frac{\partial \varphi}{\partial n} = V \cos \beta; \quad (4.4)$$

$$B_h = -\rho \int_{s_k+s} \varphi \cos(\widehat{n, h}) ds; \text{ on } s_k \quad \cos(\widehat{n, h}) = \cos \beta.$$

Multiplying the second integral of (4.4) by V and subtracting from it twice the kinetic energy T , we derive Wagner's integral, thus eliminating integration over the solid boundaries:

$$T = VB_h = \rho \int_s \left(V dx - \frac{\partial \varphi}{\partial n} ds \right). \quad (4.5)$$

Since $P_h = \frac{DB_h}{Dt}$, while B_h is proportional to t^2 , the derivative has associated with it the factor $\frac{2}{t}$:

$$P_h = \frac{2\rho}{t} \int_s \left(dx + \frac{d\psi}{V} \right). \quad (4.6)$$

Wagner, in determining the position of the free boundary by successive approximations, used this formula to calculate the drag of a wedge with deadrise angle 18° and found it to be approximately $P_h = 16 \pi \rho V^2 h$.

Dimensional analysis formally yields for the drag the expression $P_h = \rho V^2 h f(\beta)$, however, this theory does not aid in calculating function $f(\beta)$.

4. Small deadrise angles

It is clear that $\theta < \beta$ for any point on free boundary s , and so for $\beta \rightarrow 0$, $r \rightarrow \xi = s$. We denote by c the distance along the x axis from the homothetic center to the spray-root point (Figure 34). Obviously, the rise of the spray-root point (at which the tangent to s is parallel to the y axis) will be equal to $c(\operatorname{tg} \beta) - h - \delta$, and for all $x > c$ the rise of the free-surface level is $y_s < c(\operatorname{tg} \beta) - h - \delta$.

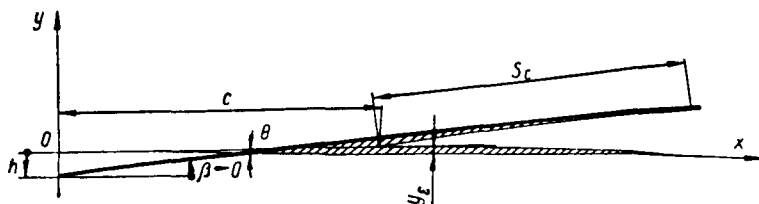


FIGURE 34.

If we retain c constant and decrease β until it vanishes, then $c(\operatorname{tg} \beta) \rightarrow 0$ and $y_s = 0$ for all $x > c$, since $h < c(\operatorname{tg} \beta)$. Hence as $\beta \rightarrow 0$ the free surface

outside the spray sheet is infinitely close to plane $y = 0$; the boundary conditions at the wedge surface within width $\pm c$ and at the free surface for $x > c$ are equivalent to boundary conditions at a plate floating on the free surface and impacted vertically. The difference between these flows consists in the fact that in the case of a wedge the equivalence to the plate does not hold at the spray-sheet root and a fluid stream, carrying kinetic energy and momentum fluxes from the principal region into the spray sheet.

In order to determine the energy and momentum, the entire region containing the fluid can be divided into two parts: the bulk of the fluid and the region of the spray sheet. In the bulk of the fluid, from equivalence with impacting on a floating plate at $\beta \rightarrow 0$, the kinetic energy of the fluid is

$$T_1 = \frac{\pi}{2} \rho c^3 \frac{V^3}{2},$$

and the vertical component of the fluid momentum is

$$B_h = \frac{\pi}{2} \rho c^2 V.$$

When $\beta \rightarrow 0$ the length of the spray sheet is $s_c \rightarrow c$, while the absolute velocity of every fluid particle in it equals $\frac{2c}{t}$. It is possible to replace the entire region of the spray sheet by an equivalent triangular spray sheet with base thickness δ . The mass of the fluid in two spray sheets is then $\rho \delta c$, the kinetic energy carried by them being

$$T_2 = \rho \delta c \left(\frac{2c}{t} \right)^2 \frac{1}{2},$$

and the vertical component of momentum is

$$B_{h2} \approx -\rho \delta c \left(\frac{2c}{t} \right) \beta.$$

Since $B_h = B_{h1} + B_{h2}$, for $\beta \rightarrow 0$, we have $B_h \rightarrow B_{h1}$ and $P_t \rightarrow \pi \rho V \frac{c^3}{t}$.

As a result of the fact that $T = V B_h$, for $\beta \rightarrow 0$, we have $T_1 \rightarrow T_2$. Consequently

$$\frac{\delta}{c} = \frac{\pi}{8} \left(\frac{h}{c} \right)^2.$$

The determination of width c is based on the previously mentioned analogy with impacting a plate floating on the free surface. Since the boundary conditions for both cases are identical, due to the uniqueness of the solution of the Laplace equation the velocity potentials at the boundaries will also be identical. The potential for a plate of width $\pm c$ is

$$\varphi = -V \sqrt{c^2 - x^2},$$

and the normal velocities at the free boundaries are

$$u_n = V \left(\frac{1}{\sqrt{1 - \left(\frac{c}{x} \right)^2}} - 1 \right).$$

Particle ξ rises above the initial level until, at time t , it reaches the side wall of the wedge or, more precisely, passes onto the surface of the spray sheet, in which case $c = x$. Hence

$$\int_0^t u_n dt + h = c(\operatorname{tg} \beta). \quad (4.7)$$

Setting $t = t(c)$, we have $dt = \frac{dt}{dc} dc$. Substitution of the expression for dt into (4.7) yields the integral equation

$$x \int_{\frac{c}{x} \rightarrow 1}^{\frac{c}{x}} \frac{dh}{dc} \cdot \frac{d\left(\frac{c}{x}\right)}{\sqrt{1 - \left(\frac{c}{x}\right)^2}} = c(\operatorname{tg} \beta)_{c \rightarrow x}. \quad (4.8)$$

For a rectilinear wedge $\frac{dh}{dc} = \text{const}$ while $\int_0^1 \frac{d\xi}{\sqrt{1 - \xi^2}} = \arcsin \xi \Big|_0^1 = \frac{\pi}{2}$. Therefore

$$\frac{dc}{dh} = \frac{\pi}{2} \cdot \frac{1}{\operatorname{tg} \beta}. \quad (4.9)$$

Wagner [31] regards function $\frac{dh}{dc}$ as purely geometrical for both rectilinear and curvilinear wedges.

It can be shown by a direct check that if the profile relative to the vertical centerline of the wedge is

$$\eta = ax + a_1 x^3 + a_2 x^5 + a_3 x^7 + \dots,$$

then integral equations (4.7) and (4.8) are satisfied provided

$$\frac{dh}{dc} = \frac{2}{\pi} a + a_1 c + a_2 \frac{4}{\pi} c^3 + \frac{3}{2} a_3 c^5 + \frac{16}{3\pi} a_4 c^7 + \dots$$

These two expressions can be used to find $c = f(h)$ for curvilinear profiles. An example is a wedge with straight sides $a = \operatorname{tg} \beta$ and $a_1, a_2, \dots = 0$; this proves the validity of (4.9).

For a profile outlined by a quadratic parabola we have $\eta = a_1 x^2$ and $\frac{dh}{dc} = a_1 c$, from which $h = a_1 \frac{c^2}{2}$, since at the point of initial contact $h = 0$ and $c = 0$. If a circular cylinder with radius R is immersed into the fluid, then, as long as ratio $\frac{h}{R}$ is very small, the arc of its circumference can be treated approximately as a segment of a parabola provided $a_1 = \frac{1}{2R}$. Hence $c^2 = 4Rh$ and, since we are using the expanding-plate analogy, the vertical momentum component is

$$B_y = \frac{\pi}{2} \rho c^2 h = 2\pi \rho h^2 R,$$

and the drag at $V = h = \text{const}$ is

$$P_v = \frac{dB}{dt} = 2\pi\sigma R h^2. \quad (4.10)$$

Using formula (4.9) and proceeding as before, the drag of a rectilinear wedge is found to be

$$P_v = \pi\sigma h^3 \left(\frac{\pi}{2\lg\beta} \right)^2. \quad (4.10a)$$

We note that (4.10) and (4.10a) express the limiting result, which is closer to reality, the smaller the values of $\frac{h}{R}$ for a cylinder and of β for a wedge.

Attempts to obtain a satisfactory approximation for force P_v at nonzero β from the expanding-plate analogy were made by a number of investigators. However, published results are not free of certain contradictions in applying the Cauchy-Lagrange integral. Hence, a detailed study will be made in subsequent sections of the method of the pressure integral and it will be correlated with the theory of self-similar immersion of a wedge. It will be shown by a number of examples that the use of this method makes it possible to obtain approximate, but sufficiently accurate, formulas for calculating the flow corresponding to immersion of bodies.

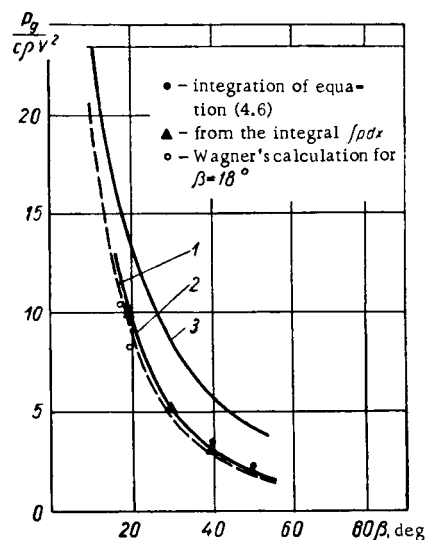


FIGURE 35.

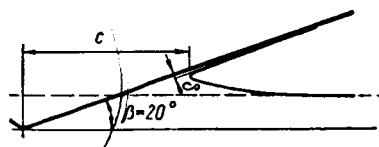


FIGURE 36.

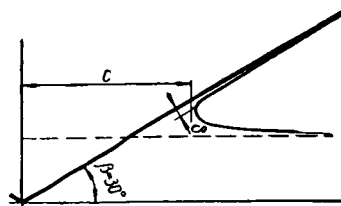


FIGURE 37.

Wagner [31], in his classic work, calculated (by the method of successive approximations) the drag P_v for $\beta = 18^\circ$, using (4.6). Then, using the results of (4.10a) [so-called expanding-plate analogy] and the

case $\beta \rightarrow \frac{\pi}{2}$, obtained by solving the problem for impact on a floating wedge, he suggested the approximating expression

$$P_\nu = \pi Q V^2 h \left(\frac{\pi}{2\theta} - 1 \right)^2. \quad (4.11)$$

Pierson's calculations /28/ generally confirmed Wagner's results. Figure 35 shows the results of these calculations. Curve 1 is calculated from Wagner's formula $\frac{P}{\rho g V^2} = 2 \operatorname{tg} \beta \left(\frac{90}{\beta} - 1 \right)$; curve 2 was obtained from Pierson's formula $\frac{P}{\rho g V^2} = 5.9 \left(\frac{57.3}{\beta + 30} \right)^{3.75}$, while curve 3 was constructed from (4.10a) with h replaced by $\frac{2c}{\pi} \operatorname{tg} \beta$. Figures 36 through 39 depict free-surface profiles calculated by Pierson.

It was shown by experiments carried out by Zhuravlev and Golovin /14/, in which the instantaneous resistance to energy of metal wedges into water was measured by piezoelectric transducers, that under conditions when the aspect ratio can be assumed to be large, the results calculated from (4.11) are in satisfactory agreement with experimental data. It is interesting to note that (as these experiments also showed) the force attains its maximum when a wedge of width $2a$ is submerged to a depth $h = \frac{2}{\pi} \operatorname{atg} \beta$. This is an indirect proof of the main postulate of Wagner's theory. In general, comparison of results obtained from Wagner's approximate immersion theory with experimental data shows that these are in satisfactory agreement, allowing one to apply these methods to the solution of new problems.

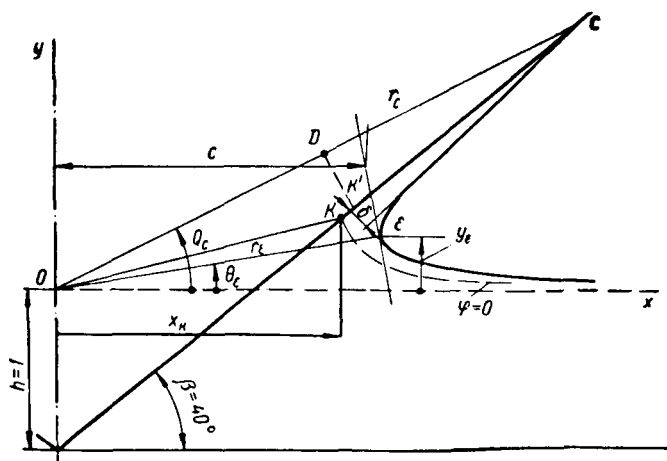


FIGURE 38.

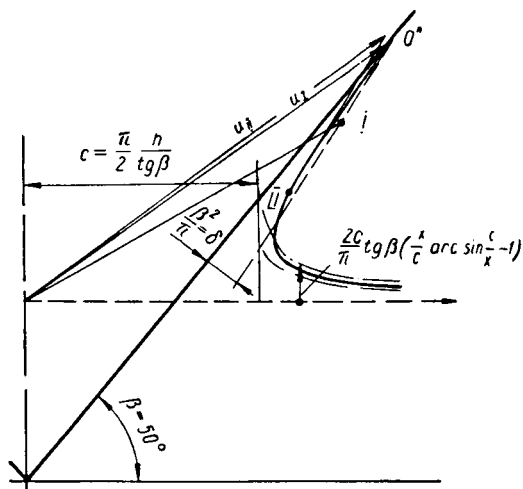


FIGURE 39.

5. Kinematic elements of the free surface

To construct an approximate theory of immersion of various bodies it is very important to estimate the kinematic parameters of the spray-root area and of the spray sheet at the free surface.

The velocity distribution at salient points of the flow can be determined by simple measurement of the segment lengths, using the results of free-surface calculations from /28/, displayed in Figures 36–39. We assume that $h = 1$, $h' = 1$, $t = 1$ and also $c = \frac{\pi}{2 \operatorname{tg} \beta}$. The asymptotic solution as $\beta \rightarrow 0$ yields the following limiting relationships (see the notation of Figure 38):

$$\frac{\beta - \theta_c}{\beta} = \frac{1}{\pi}; \quad \frac{y_e}{c} = \left(1 - \frac{2}{\pi}\right) \beta - \frac{\beta^2}{2\pi}; \quad \frac{s_e}{c} = 1;$$

$$\frac{S_{ce}}{c} = \frac{u_{se} t}{c} = 1; \quad \frac{u_{sc} t}{c} = (1 + \cos \beta).$$

Table 1 lists quantities measured from Figures 36–39 and calculated from formulas giving the limiting relationships.

TABLE 1

β	$\frac{\beta - \theta}{\beta}$	$\frac{x_e}{c}$	$\frac{y_e}{c}$		$\frac{r_e}{c}$	$\frac{r_c}{c}$	$\frac{S_{ce}}{c}$	$\frac{u_{sc} t}{c}$		$\frac{\theta_e}{\beta}$
			measured	calculated				measured	calculated	
0	0.318	1.000	—	0	1.000	2.00	1.00	—	2.00	0.362
20	0.32	1.015	0.093	0.110	1.01	1.95	0.98	1.94	1.94	0.312
30	0.31	1.030	0.146	0.145	1.05	1.97	1.00	1.88	1.86	0.267
40	0.29	1.035	0.181	0.173	1.05	1.87	0.97	1.78	1.77	0.260
50	0.30	1.065	0.242	0.230	1.077	1.83	1.02	1.74	1.64	0.250

The following should be noted. The tangential velocity within the spray sheet is defined as the projection of the transport velocity of the spray-sheet tip onto the edge of the wedge, i. e., $u_{se} = \frac{r_c}{l} \cos(\widehat{OCA})$. Had the free surface been stationary [relative to the wedge] and moved along the x axis with velocity $\frac{dc}{dt}$, the principal boundary condition (see Sections 4 and 6 of Chapter One) would have yielded $u_{se} = \frac{dc}{dt} (1 + \cos \beta)$. It is seen from the data listed in Table 1 that, at least up to $\beta = 40^\circ$, the results of the asymptotic theory ($\beta \rightarrow 0$) and of more exact calculations are in very close agreement.

Let us now clarify the location on the lateral surface of the wedge of point K , at which $\varphi = 0$. The potential at point C is $\varphi_c = \frac{r_c^2}{2l}$; moving along

the lateral surface of the wedge to point K we obtain $\varphi_K = \varphi_c - \int_K^C u_s ds = 0$.

Within the integration interval $u_s < u_{se}$, and consequently $K'C < KC$; here segment $K'C$ is derived from the expression

$$\frac{r_c^2}{2l} = K'C \frac{r_c}{l} \cos(\widehat{OCA}).$$

Thus, point K with $\varphi = 0$ is situated close to point K' , but within segment $K'A$; projection of point K' onto r_c (point D) bisects this segment.

6. Graphical representation of the momentum and energy

Once the free-surface shape is known, it is possible to construct a diagram which graphically explains the application of Wagner's formula (4.6) and makes it possible to approximate the as yet unknown potential distribution. If the instantaneous values of potentials $\frac{\varphi}{V_c}$ at boundaries are constructed as a function of $\frac{x}{c}$, then we obtain the scheme shown in

Figure 40a. The potential for the free boundaries is calculated from the formulas of Section 3 of the present chapter. At the lateral side of the wedge, in the spray-sheet region where $\Delta p \approx 0$, the potential is easily calculated from the known velocities and configuration of the spray.

The potential at segment OK is unknown and should be selected to satisfy the conditions of the problem. The vertical component of the momentum is

$$B_h = -\rho \int_{s_h+s} \varphi dx = 2\rho c^3 V (S_1 - \Delta S),$$

where S_1 and ΔS are surfaces bound by the curve $\frac{\varphi}{V_c} = f\left(\frac{x}{c}\right)$.

Figure 40b is a plot of velocity potential $\frac{\psi}{V_c}$ as a function of $\frac{x}{V_c}$. When calculating the kinetic energy along flow tubes,

$$T = -\frac{\rho}{2} \int_{\psi_k + \psi_s} \varphi d\psi = -\frac{\rho}{2} \int_{\psi_k} (\varphi_k - \varphi_s) d\psi,$$

the free-surface velocity potentials φ_s in Figure 40b are referred to the starting points of the streamlines at the wedge surface; obviously, the difference in ordinates of the crosshatched regions S_1 and S_2 is equal to the differences in the relative potentials at the ends of the streamline, for which $\frac{x}{c} = \frac{\psi_k}{V_c}$. It is clear that the entire crosshatched area is proportional to the kinetic energy and that the equality

$$T = \rho c^2 V^2 (S_1 + S_2)$$

is here valid.

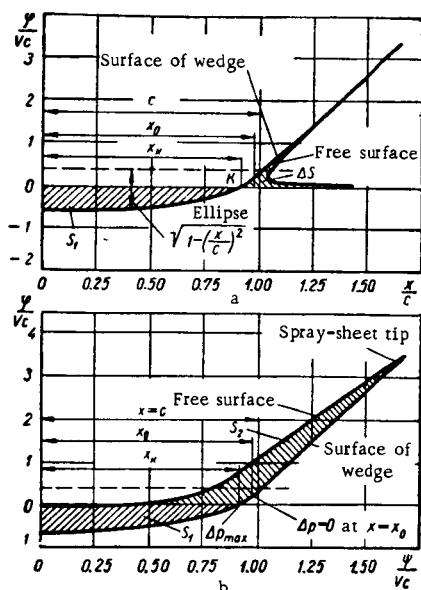


FIGURE 40.

Wagner's integral (4.5) is $I_w = 2T - B_h V = T$. Substitution of values of T and B_h into this expression shows that area S_1 disappears from the Wagner integral and $I_w = 2\rho c^2 (S_2 + \Delta S)$. However, to calculate the pressure distribution at the wedge surface it is necessary to know the potential distribution at segment x_h , which cannot be calculated by ordinary methods.

Using the expanding-plate analogy, it can be approximately assumed that the curve bounding area S_1 is an arc of an ellipse, selected to satisfy the following conditions:

a) at point K , $\varphi = 0$,

$$\frac{\partial \varphi}{\partial x} = \frac{x_h}{c} \cdot \frac{dc}{dt};$$

b) at point $\zeta_0 = \frac{x_0}{c}$, $\varphi > 0$,

$$\frac{\partial \varphi}{\partial x} = 2 \frac{x_0}{c} \cdot \frac{dc}{dt},$$

the excess pressure $\Delta p = 0$;

c) from point ζ_0 to the spray-sheet tip the potential varies linearly along a straight line tangent to the ellipse at point ζ_0 .

It is evident that all these conditions can be satisfied by expressing the potential along segment $\pm \zeta_0$ in the form

$$\varphi = -cV[\sqrt{1-\zeta^2} - \sqrt{1-\zeta_k^2}]. \quad (4.12)$$

The area can be determined from

$$S_1 = \int_0^{\zeta_k} [\sqrt{1-\zeta^2} - \sqrt{1-\zeta_k^2}] d\zeta = \frac{1}{2} \{ \arcsin \zeta_k - \zeta_k \sqrt{1-\zeta_k^2} \} \approx \frac{\pi}{4} - \sqrt{1-\zeta_k^2}.$$

In general area ΔS is unknown, but some basis exists for the assumption that $\Delta S \approx 0$ for small β .

From the theory of self-similar immersion

$$P_h = \frac{DB_h}{Dt} = \frac{2B_h}{t} = 4qcV \frac{c}{t} \left(\frac{\pi}{4} - \sqrt{1-\zeta_k^2} \right).$$

Substitution of the expression for c yields

$$P_h = \pi q h V^2 \left(\frac{\pi}{2 \lg \beta} \right)^2 \left(1 - \frac{4}{\pi} \sqrt{1-\zeta_k^2} \right). \quad (4.13)$$

Quantity ζ_k for a wedge when $V = \text{const}$ can be determined from the velocity condition at stagnation point K , at which the fluid velocity is identical with the transport velocity at point K proper (see Theorem XVII). The potential distribution for curved surfaces (a cylinder, say) can be assumed to be the same as for a wedge, but determination of ζ_k is a more complex problem, since $\frac{dc}{dh}$ is variable and Theorem XVII is not directly applicable to point K . However, for slightly-curved profiles ζ_k is determined in the same manner as for a wedge.

7. Velocity and pressure distributions

Formula (4.12) defines the velocity potential only at the wedge surface; hence when differentiating with respect to space coordinates we should remain at the

edge surface s_k . Since $x = s \cos \beta$ the tangential velocity is $v_s = V \frac{\zeta}{\sqrt{1-\zeta^2}} \cos \beta$.

The x and y components of the fluid velocity are given by the expressions

$$v_x = v_s \cos \beta + v_n \sin \beta = V \cos^2 \beta \left(\frac{\zeta}{\sqrt{1-\zeta^2}} + \operatorname{tg} \beta \right),$$

$$v_y = v_s \sin \beta - v_n \cos \beta = V \cos^2 \beta \left(\frac{\zeta}{\sqrt{1-\zeta^2}} \operatorname{tg} \beta - 1 \right),$$

which, however, do not reflect the physical reality in the vicinity of the wedge vertex, at which is situated the stagnation point where $v_x = 0$ and $v_y = -V$. In order to avoid contradictions, the vertex can be assumed to be somewhat rounded, and $\operatorname{tg} \beta$ in this region can be treated as the derivative of the ordinate of the contour profile with respect to the horizontal axis.

By the problem statement, at point K , $v_x = \zeta_k \frac{dc}{dt}$ and $\frac{y_k}{x_k} = \frac{v_{y_k}}{v_{x_k}}$. Since $y_k = x_k \operatorname{tg} \beta - h$ and $\frac{h}{x_k} = \frac{h}{\zeta_k c} = \frac{1}{\zeta_k} \cdot \frac{dh}{dc}$,

$$\sqrt{1-\zeta_k^2} = \frac{\frac{dh}{dc}}{1 + \operatorname{tg}^2 \beta - \frac{dh}{dc} \operatorname{tg} \beta}.$$

For small β , $\sqrt{1-\zeta_k^2} \approx \frac{dh}{dc}$.

We now derive an equation for the pressure distribution over the surface of a wedge or of some weakly curved profile. Since the velocity potential $\varphi = -cV(\sqrt{1-\zeta^2} - \sqrt{1-\zeta_k^2})$ has been specified in the moving coordinate system, the partial derivative of φ with respect to time for points stationary in the space, coinciding at the time in question with the boundary, will be

$$\frac{\partial \varphi}{\partial t} = \frac{\partial' \varphi}{\partial t} - \frac{\partial \varphi}{\partial y} \cdot \frac{dy}{dt}. \text{ Also } \frac{dy}{dt} = -V; \text{ when } \beta \rightarrow 0, \frac{\partial \varphi}{\partial y} \rightarrow -V, \text{ while } \frac{\partial' \varphi}{\partial t} =$$

$$= -\frac{dc}{dt} V \frac{1}{\sqrt{1-\zeta^2}} + \frac{dc}{dt} V \sqrt{1-\zeta_k^2} = -\frac{V^2 \frac{dc}{dh}}{\sqrt{1-\zeta^2}} + V^2. \text{ The above expressions were}$$

obtained using the fact that $\sqrt{1-\zeta_k^2} \approx \frac{dh}{dc}$.

The square of the absolute velocity of the fluid is

$$v^2 = V^2 + V^2 \frac{\zeta^2}{1-\zeta^2} = \frac{V^2}{1-\zeta^2}.$$

Substitution of the above expressions into the Cauchy - Lagrange integral

$$\frac{\Delta p}{\rho} = -\frac{d\varphi}{dt} - \frac{1}{2} v^2 = -\frac{\partial' \varphi}{\partial t} + V^2 - \frac{1}{2} v^2$$

yields an approximate expression for Δp at the contour surface:

$$\frac{\Delta p}{\rho} = \frac{dc}{dt} \cdot \frac{V}{\sqrt{1-\zeta^2}} - \frac{V^2}{2} \cdot \frac{1}{1-\zeta^2}. \quad (4.14)$$

The value of Δp is zero at point ζ_0 , which is found from the expression

$$\frac{1}{2} \cdot \frac{dh}{dc} = \sqrt{1 - \zeta_0^2}.$$

The drag can be found by integrating Δp over the width $\pm \zeta_0 c$. Carrying out the required computations and using the approximate expression for ζ_0 , we derive the final expression for the pressure exerted by the profile on the fluid:

$$P_h = \int_{-\zeta_0 c}^{+\zeta_0 c} \Delta p dx = \pi \rho V^2 c \frac{dc}{dh} \left[1 - \frac{1}{\pi} \frac{dh}{dc} \left(1 + \ln 4 \frac{dc}{dh} \right) \right]. \quad (4.15)$$

All the expressions obtained for the drag of wedges with low β are also valid for slightly curved profiles, since points ζ_0 and ζ_* are defined in terms of $\frac{dh}{dc}$. Expressions obtained from the estimated momentum (4.13) and from the pressure integral (4.15) are in principle approximate to the same degree as Wagner's formula (4.11). Check calculations show that for a wedge with β up to 30° ($\frac{dh}{dc}$ up to 0.4), the values of drag calculated from formulas (4.13) and (4.15) are close but exceed somewhat the drag calculated from Wagner's formula (4.11).

8. Drag on a cylinder

The drag acting on unit length of a circular cylinder of radius R , being immersed into a fluid with constant velocity V , for the limiting case of $\frac{h}{R} \rightarrow 0$ was calculated above (see formula (4.10)). Since $c^2 = 4Rh$ and

$\frac{dc}{dh} = \frac{2R}{c} = \sqrt{\frac{R}{h}}$ hold approximately for small h/R , formula (4.15) gives

$$P_y = 2\pi \rho V^2 R \left[1 - \frac{1}{\pi} \sqrt{\frac{h}{R}} \left(1 + \ln 4 \sqrt{\frac{R}{h}} \right) \right]. \quad (4.16)$$

The variation in the relative drag $\bar{P}_y = \frac{P_y}{2\pi \rho V^2 R}$ as a function of $\frac{h}{R}$ is given in Table 2.

TABLE 2

$\frac{h}{R}$	0.0	0.01	0.04	0.09	0.16
\bar{P}	1.0	0.85	0.745	0.66	0.58

It is interesting that the force attains its maximum on initial contact at $h = 0$ and then decreases rapidly. Evidently, at some value of h/R the spray-sheet root breaks off the cylindrical surface and an unsteady transient results (Figure 41).

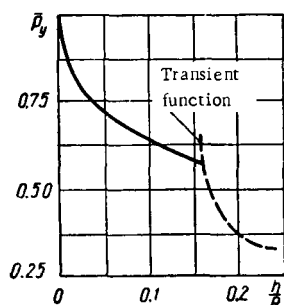


FIGURE 41.

It should be noted in conclusion that potential $\phi = -cV\sqrt{1-\xi^2}$ was used by many investigators, starting with Wagner, for calculating the pressure distribution. Two points of view prevailed. According to the first, due to Wagner [31], it was assumed that potential ϕ is confined to the x axis and that there is no vertical velocity. The Cauchy-Lagrange integral yields the following expression for the pressure distribution:

$$\frac{p-p_0}{\rho} = V^2 \frac{dc}{dh} \cdot \frac{1}{\sqrt{1-\xi^2}} - \frac{1}{2} V^2 \frac{\xi^2}{1-\xi^2}.$$

The second point of view made allowance for the fact that the potential $\phi = -cV\sqrt{1-\xi^2}$ pertains to the moving surface of a plate. In calculating $\frac{\partial \phi}{\partial t}$ at stationary points in space for substitution into the Cauchy-Lagrange integral, it is necessary to take into account the transport velocity; hence $\frac{\partial \phi}{\partial t} = -V^2 \frac{dc}{dh} \cdot \frac{1}{\sqrt{1-\xi^2}} + V^2$. The square of the absolute velocity is $v^2 = V_x^2 + V_y^2 = V^2 + V^2 \frac{\xi^2}{1-\xi^2} = V^2 \frac{1}{1-\xi^2}$. The Cauchy-Lagrange integral yields the following expression for the pressure distribution along a moving plate:

$$\frac{p-p_0}{\rho} = V^2 \frac{dc}{dh} \cdot \frac{1}{\sqrt{1-\xi^2}} + \frac{1}{2} V^2 \frac{1-2\xi^2}{1-\xi^2}.$$

A situation resulted when the same phenomenon was described by two different equations; the question had to be resolved as to which of them is valid. Our preceding analysis shows that in order to match the assumed potential distribution with conditions at points ξ_k and ξ_0 , ϕ should be expressed by equation (4.12) or, in the more general form,

$$\phi = -cV [f(\xi) - f(\xi_k)]_{|\xi| \leq \xi_k}.$$

It is found that this representation of the potential, which yields equation (4.14), is, from the point of view of the pressure distribution, equivalent to confining ϕ to the x axis and making allowance for v^2 .

9. Transient drag

Suppose a wedge with deadrise angle β is immersed uniformly into a fluid with velocity h , but that the edges of the wedge are bounded and have width $2l$ (Figure 42). It is clear from the previous discussion that as long as the

tip of the spray sheet does not reach the wedge base l , the flow is self-similar. For small β the length of the spray sheet is approximately c , and the depth of wedge immersion at which the spray-sheet tip reaches the base l is determined from the simple expression

$$h = \frac{2}{\pi} \cdot \frac{l \operatorname{tg} \beta}{1 + \cos \beta}.$$

Starting with this time, as the wedge is immersed further, fluid particles belonging to the spray sheet will start rolling off the edges of the wedge and internal free boundaries will begin to form. However, at the initial stage of this process, as long as the particles rolling off the edges belong to the thin spray sheet, it can be expected that the law governing the rise in drag will not change substantially. However, as the spray-sheet root approaches the edges of a wedge with width $2l$, the formation of internal free boundaries will start increasingly to affect the fluid flow and this will produce a marked change in the increase of the drag, which up to then obeyed approximately the Wagner formula. At high $\frac{h}{l}$, the flow about the wedge approximates steady streaming (cavitated) flow and the drag may be close to the Bobylev drag [10].

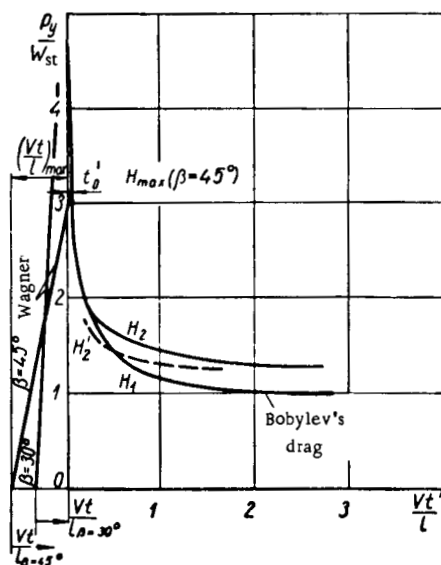


FIGURE 42.

These considerations show that, up to a value of h at which $l \approx c = \frac{\pi h}{2 \operatorname{tg} \beta}$, the drag will increase linearly according to the Wagner law; this will be followed by a transient process with the drag $P = P\left(\frac{h}{l}\right)$ decreasing and

approaching the Bobylev drag W with increasing $\frac{h}{l}$ (as $\frac{h}{l} \rightarrow \infty$). The term "transient function" is applied to the expression

$$H\left(\frac{h}{l}\right) = \frac{P\left(\frac{h}{l}\right)}{W\left(\frac{h}{l} \rightarrow \infty\right)}. \quad (4.17)$$

Drags P and W are proportional to $gh^{\frac{3}{2}}$, and so function H can depend only on $\frac{h}{l}$ for given β ; drag W is also highly dependent on β .

It is impossible to derive an exact expression for the transient function, and hence we shall give below only some more or less satisfactory estimates of it.

10. Estimating the transient function

We shall consider uniform immersion of a wedge with very small dead-rise angle ($\beta \rightarrow 0$), with base width $2l$. It is assumed that upon termination of self-similar immersion over a width $\pm c$ in the coordinate system moving with the wedge (x axis parallel to the free surface and y axis directed upward), the velocity potential at the wedge surface and in the immediate vicinity of the inner free boundary is expressed in the same manner as at the surface of a plate with width $2c$ moving perpendicularly to its plane with velocity \dot{h} .

Thus $\varphi = -\dot{h}c \sqrt{1 - \left(\frac{x}{c}\right)^2}$, where $c = c(t)$. The physical basis for this assumption consists in the fact that at the start of the transient stage the tangential velocity of particles at the edges $x = l$ of the wedge is very high compared with \dot{h} , and the normal velocity of the boundaries varies continuously on transition from the wedge surface to the inner free boundary.

At the point where the particles roll onto the internal free boundary at $x = l$ we have $\Delta p = 0$, since it is assumed that all the free boundaries are subjected to a constant pressure p_0 .

Applying the Cauchy-Lagrange integral to the moving point $x = \text{const}$, we obtain an expression for Δp at the wedge surface:

$$\frac{\Delta p}{\rho} = -\frac{\partial \varphi}{\partial t} - \frac{\partial \varphi}{\partial y} \dot{h} - \frac{1}{2} \left[\left(\frac{\partial \varphi}{\partial x} \right)^2 + \left(\frac{\partial \varphi}{\partial y} \right)^2 \right]. \quad (4.18)$$

The normal velocity of the wedge surface is

$$\dot{h} \cos \beta = -v_y \cos \beta + v_x \sin \beta,$$

where $v_x = \frac{\partial \varphi}{\partial x}$ and $v_y = \frac{\partial \varphi}{\partial y}$ are the absolute fluid velocities in the x and y directions. Substitution of the expression for v_y into formula (4.18) yields

$$\frac{\Delta p}{\rho} = -\frac{\partial \varphi}{\partial t} + \frac{1}{2} \dot{h}^2 - \frac{1}{2} v_x^2 (1 + \tan^2 \beta). \quad (4.19)$$

where $\operatorname{tg}^2 \beta$ can be neglected for small β .

We now use equation (4.2) to determine the function $c = c(t)$ from the condition

that $\Delta p = 0$ at $x = l$. For the point $x = \text{const}$, $\frac{\partial \varphi}{\partial t} = -\frac{hc \frac{dc}{dt}}{\sqrt{c^2 - x^2}}$ and $\frac{\partial \varphi}{\partial x} = \frac{h_x}{\sqrt{c^2 - x^2}}$; for the point $x = l$, after substitution of the expressions for $\frac{\partial \varphi}{\partial t}$ and $\frac{\partial \varphi}{\partial x}$ into equation (4.19) we obtain the differential equation

$$\frac{dc^2}{dt} + \sqrt{c^2 - l^2} - \frac{l^2}{\sqrt{c^2 - l^2}} = 0. \quad (4.20)$$

The most convenient initial conditions for solving equation (4.20) are $h_1 = 0$ for $t_1 = 0$, when $l = c$. The immersion depth h_1 is thus no longer measured from the origin, but from the location of the wedge apex at the time when the spray root with abscissa c reaches the wedge base l (in the Wagner approximation). Under these conditions, upon substituting $\sqrt{\frac{c^2}{l^2} - 1} = \sin u$, equation (4.20) gives

$$\frac{h_1}{2l} = \frac{\dot{h}_1}{2l} = \int_0^u \left(\frac{1}{\cos u} - \cos u \right) du = \ln \operatorname{tg} \left(\frac{\pi}{4} + \frac{1}{2} \arcsin \sqrt{\frac{c^2}{l^2} - 1} \right) - \sqrt{\frac{c^2}{l^2} - 1}. \quad (4.21)$$

Ratio $\frac{c}{l} \rightarrow \sqrt{2}$ as $u \rightarrow \frac{\pi}{2}$, and for this value of the ratio h is infinite.

The drag P is calculated by integrating Δp over the wedge width $\pm l$:

$$P = \int_{-l}^{+l} \Delta p dx = \frac{1}{2} \rho \dot{h}^2 \int_{-l}^{+l} \left(\frac{\frac{dc^2}{dt}}{\sqrt{c^2 - x^2}} - \frac{x^2}{c^2 - x^2} + 1 \right) dx.$$

Integration of (4.20) yields

$$P = \rho l \dot{h}^2 \left[\left(\frac{1}{\sqrt{\frac{c^2}{l^2} - 1}} - \sqrt{\frac{c^2}{l^2} - 1} \right) \arcsin \frac{l}{c} + \left(2 - \frac{c}{2l} \ln \frac{1 + \frac{l}{c}}{1 - \frac{l}{c}} \right) \right]. \quad (4.22)$$

The drag given by expression (4.22) depends on the ratio $\frac{c}{l}$, by means of

which the relative immersion depth $\frac{h_1}{l}$, corresponding to the given value of P , is determined from equation (4.21).

From physical considerations the first term in brackets of equation (4.22) expresses that part of the force which is defined by integrating $\frac{\partial \varphi}{\partial t}$ from the pressure equation over the width, while the second term is proportional to the square of the velocity. When $\frac{c}{l} \rightarrow \sqrt{2}$, $\frac{h_1}{l} \rightarrow \infty$, the inertia force defined by the first term in brackets of equation (4.22) approaches zero, and the transient drag approaches the steady drag expressed by the second term of equation (4.22). It was calculated that the limiting value of the second

term in brackets of equation (4.22), when $\frac{c}{l} \rightarrow \sqrt{2}$, is approximately $\frac{\pi}{4}$, while the drag on a plate in free-streamline flow is 0.88 (it was assumed in our derivation that $\beta \rightarrow 0$, corresponding to a plate). This difference in limiting values follows from our hypothesis on the distribution of horizontal fluid velocities over the width of the plate.

In the first approximation we determine the transient function from equation (4.22) as the ratio of the transient drag $P\left(\frac{h}{l}\right)$ to $W = P\left(\frac{h}{l} \rightarrow \infty\right)$. This yields

$$H_1\left(\frac{h}{l}\right) = \frac{\left(\frac{1}{\sqrt{\frac{c^2}{l^2}-1}} - \sqrt{\frac{c^2}{l^2}-1}\right) \arcsin \frac{l}{c} + 2\left(1 - \frac{c}{4l} \ln \frac{1+\frac{l}{c}}{1-\frac{l}{c}}\right)}{2\left(1 - \frac{1}{2\sqrt{2}} \ln \frac{\sqrt{2}+1}{\sqrt{2}-1}\right)}. \quad (4.23)$$

From this the true transient drag is $P\left(\frac{h}{l}\right) = H_1\left(\frac{h}{l}\right)W(\beta)$, where $W(\beta)$ is the Bobylev drag for a wedge of base $2l$ and deadrise angle β . We note that the transient function has been defined for $\beta \rightarrow 0$, i. e., for a plate; in general, for wedges with different β allowance should be made for $\operatorname{tg} \beta$ in (4.19) and (4.20). However, it may be assumed approximately that H_1 is not a function of β and expresses the drag variation after the force increase corresponding to self-similar immersion ceases. The transient function is plotted in

Figure 42. Different values of β , C_W , $\left(\frac{P}{W_{st}}\right)_{\max}$ and $\left(\frac{Vt}{l}\right)_{\max}$ are listed in Table 3.

TABLE 3

β , deg	C_W	$\left(\frac{P}{W_{st}}\right)_{\max}$	$\left(\frac{Vt}{l}\right)_{\max}$
7.5	0.855	37.4	0.084
10	0.844	26.7	0.112
15	0.830	18.6	0.171
30	0.745	6.18	0.361
40	0.637	3.14	0.637

11. Some experimental results

It can be shown theoretically that the above theory of the transient function is close to reality; here some of the assumptions were selected so that they "compensate" one another to some degree. Now we shall compare the theoretical results with experimental data. First we shall refine the general scheme for calculating the drag. We now again start measuring h from the point of initial contact with the undisturbed level. Up to now, as long as $h < \frac{2l}{\pi} \operatorname{tg} \beta$, the drag rise obeys the Wagner law $P = \pi \rho h \dot{h}^2 \left(\frac{\pi}{2\beta} - 1\right)^2$.

If we express the Bobylev drag by the expression $W = C_w l \rho \dot{h}^2$, then $\frac{P}{W} = \frac{\pi}{C_w} \cdot \frac{h}{l} \times$

$\times \left(\frac{\pi}{2\beta} - 1\right)^2$; $\frac{P}{W}$ attains its maximum at $\frac{h}{l} = \frac{2}{\pi} \operatorname{tg} \beta$ at which point the straight line $\frac{P}{W}$ on the plot of $H_1 = f\left(\frac{h}{l}\right)$ should intersect the curve of $H_1\left(\frac{h}{l}\right)$, provided h is replaced by $h_1 = h - h_0$. The value of h_0 should be determined from the condition that

$$H_1\left(\frac{h_1}{l}\right) = \frac{\pi}{C} \operatorname{tg} \beta \left(\frac{\pi}{2\beta} - 1\right)^2.$$

Experimental studies of immersion of wedges were carried out by Golovin and Zhuravlev /14/ with special equipment in which the instantaneous drag was measured by piezoelectric transducers. The conclusions which follow from a series of experiments using metal wedges with deadrise angles β equal to 5, 10, 15, 30 and 45° are as follows: a) the drag on a wedge attains its maximum at $\frac{h}{l} = \frac{2}{\pi} \operatorname{tg} \beta$, irrespective of the aspect ratio;

b) the drag for large aspect ratios $\frac{L}{2c}$ during the period it rises to the maximum ($c = l$) is equal to the Wagner drag $P = \pi \rho h \dot{h}^2 \left(\frac{\pi}{2\beta} - 1\right)^2$; c) after attaining the maximum the drag variation is governed approximately by the transient function.

Two-dimensional flow attendant on immersion of a wedge cannot be attained experimentally, since any real wedge has some length L and width $2l$. Hence the actual drag, when approaching the maximum, will always be smaller than its value for two-dimensional flow. However, at the initial immersion stage, when L is much greater than the wetted wedge width $2c$, the value of $\frac{dP}{dh}$ can be determined from the slope of the curve on the oscillogram, thus checking Wagner's formula. This was done precisely in /14/, where a graph has been constructed showing the effect of the wedge aspect ratio $\frac{L}{2c}$ on the ratio of the real to the Wagner force.

UNIFORM IMMERSION OF A CONE

12. Immersion of a cone

The flow arising on uniform immersion of a cone along its axis of symmetry (Figure 43) with velocity V is self-similar. In general the theory of immersion of a cone is analogous to the same theory for a wedge. The velocity and pressure at geometrically similar points remain unchanged at any time, the linear dimensions increase proportionally to t , the momenta and kinetic energy are proportional to t^3 and P_v is proportional to t^2 . The relationships for the vertical momentum and the kinetic energy of the fluid are

$$\left. \begin{aligned} B_y &= \int_0^t \left(\frac{P_y}{t^3} \right) t^2 dt = \frac{1}{3} P_y t, \\ T &= \int_0^t \left(\frac{P_y}{t^3} \right) t^2 V dt = \frac{1}{3} V P_y t, \\ \frac{P_y}{t^3} &= \text{const.} \end{aligned} \right\} \quad (4.24)$$

Since the vertical momentum component is

$$B_y = -\rho \int_{S_n + S_c} \varphi \cos(n, y) dS,$$

the drag is

$$P_y = \frac{DB_y}{Dt}$$

and the value of B_y is proportional to t^3 ; $\frac{DB_y}{Dt}$ is proportional to $3t^2$ and so the ratio of the derivative to the integral is $\frac{3}{t}$. Thus

$$P_y = -\frac{3\rho}{t} \int_{S_n + S} \varphi \cos(n, y) dS = \rho V^4 t^2 f(\beta), \quad (4.25)$$

where S is the surface. A similar result can be obtained directly by applying the dimensionality theory in the manner presented by Sedov /20/.

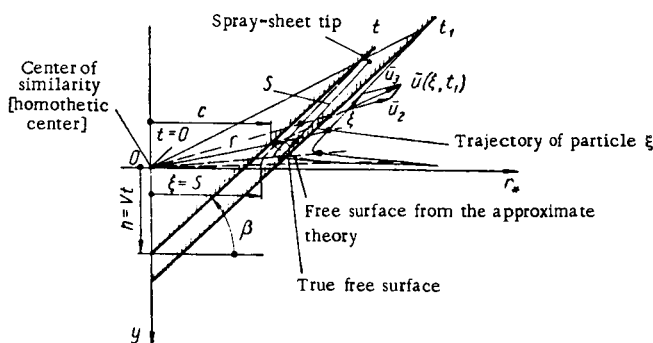


FIGURE 43.

The normal velocity at the cone surface in the expression for kinetic energy

$$T = -\frac{\rho}{2} \iint \varphi \frac{\partial \varphi}{\partial n} dS$$

is $\frac{\partial \varphi}{\partial n} = V \cos \beta$, while in the expression for the momentum at the same surface $\cos(\hat{n}, \hat{y}) = \cos \beta$. Hence integration over the solid boundaries can be eliminated by expressing B_y in terms of Wagner's integral, extending only over the free boundaries of the fluid S_c ; this momentum is

$$B_y = \varrho \int_{S_c} \varphi \left(\cos(\hat{n}, \hat{y}) - \frac{1}{V} \cdot \frac{\partial \varphi}{\partial n} \right) dS. \quad (4.26)$$

From this, applying (4.24), we derive an expression for the drag in terms of φ , $\frac{\partial \varphi}{\partial n}$ and $\cos(\hat{n}, \hat{y})$ at free surface S_c . Here the area element is $dS = 2\pi r_* ds$, and a free-surface arc element is $ds \cos(\hat{n}, \hat{y}) = dr_*$, where r_* is the distance from the point to the y axis of symmetry.

The kinematic conditions at the free surface will be the same as in two-dimensional flow upon immersion of a wedge. Hence the velocity potential at the free boundary is also $\varphi = \frac{r^2 - s^2}{2t}$, where r is the distance from the homothetic center to the free-surface point. The distances between free-surface points remain unchanged along s (in the r_*, y plane), but the fluid particles will stretch in direction perpendicular to s . For a cone, as previously for a wedge, the drag can in principle be obtained from Wagner's integral by the method of successive approximations. In addition to the condition $\text{div } \vec{v} = 0$, the condition of equal volumes displaced by the cone and lifted above the undisturbed level should be satisfied at each point of the fluid-filled space (see Figure 43).

13. Case of small deadrise angles

For a regular cone with deadrise angle β , when $\beta \rightarrow 0$, the velocity at which the pressure surface c expands can be determined from the same Wagner considerations as for the wedge in the two-dimensional case. Let us assume that everywhere at $r > c$, at each instant, the distribution of vertical velocities at the free surface is the same as on vertical impact on a disk of radius c , floating on the surface. Fluid particle ξ at point r_* moves vertically upward and, at time t , when $r_* = c$, reaches the generatrix of the cone, moving toward it with velocity V . If v denotes the vertical velocity of particle rise above the undisturbed level, we may obtain a relationship valid for that value of t at which $r_* = c$:

$$\int_0^t v dt + Vt = c(\text{tg } \beta). \quad (4.27)$$

The velocity of particle ξ is $v = Vf\left(\frac{r_*}{c}\right)$, on the assumption that f is not an explicit function of t . The radius of the pressure surface is $c = c(t)$. Since $c = \frac{dc}{dt}t$ and $\frac{dc}{dt} = \text{const}$, we have

$$\int_0^t \left(1 + \frac{v}{V}\right) \frac{dh}{dc} dc = r_* \text{tg } \beta$$

or

$$\frac{dc}{dt} = \frac{V}{\operatorname{tg} \beta} \left[1 + \int_0^1 f\left(\frac{r_*}{c}\right) d\left(\frac{c}{r_*}\right) \right]. \quad (4.28)$$

Velocity distribution function $f\left(\frac{r_*}{c}\right)$ outside radius c is obtained directly from the known solution of the problem on translational motion of a disk in an unbounded fluid.

As is known [10], in elliptical coordinates, $y = c\mu\zeta$ and $r_* = c(1 - \mu^2)^{\frac{1}{2}}(\zeta^2 + 1)^{\frac{1}{2}}$ and the velocity potential of the disk is $\varphi = \frac{2V}{\pi} c\mu(1 - \zeta \operatorname{arctg} \zeta)$.

In the plane of the disk for $r_* > c$ the curves of $\zeta = \text{const}$ are orthogonal to this plane (at $\mu = 0$); therefore

$$v = -\frac{\partial \varphi}{\partial y} = -\frac{\partial \varphi}{\partial \mu} \cdot \frac{\partial \mu}{\partial y} = \frac{2V}{\pi} (1 - \zeta \operatorname{arctg} \zeta) \frac{1}{\zeta}.$$

Since $\zeta = \left[\left(\frac{r_*}{c}\right)^2 - 1\right]^{\frac{1}{2}}$, formula (4.28) yields

$$\begin{aligned} \frac{dc}{dt} &= \frac{V}{\operatorname{tg} \beta} \left\{ 1 + \frac{2}{\pi} \int_0^1 \left[\frac{d\left(\frac{c}{r_*}\right)}{\sqrt{\left(\frac{r_*}{c}\right)^2 - 1}} - \operatorname{arctg} \sqrt{\left(\frac{r_*}{c}\right)^2 - 1} d\left(\frac{c}{r_*}\right) \right] \right\} = \\ &= \frac{V}{\operatorname{tg} \beta} \left\{ 1 + \frac{2}{\pi} - \frac{2}{\pi} \int_0^1 \left[\operatorname{arctg} \sqrt{\left(\frac{r_*}{c}\right)^2 - 1} \right] d\left(\frac{c}{r_*}\right) \right\} = \frac{4}{\pi} \cdot \frac{V}{\operatorname{tg} \beta}. \end{aligned}$$

The "momentum" of the fluid set into motion by the floating disk to which velocity V has been imparted normal to its surface is

$$B_y = \frac{4}{3} \rho c^3 V,$$

and consequently the drag is

$$P_y = 4\rho c^2 \frac{dc}{dt} V.$$

Since $c = \frac{dc}{dt} t = \frac{4}{\pi \operatorname{tg} \beta} Vt$ and the depth of immersion of the cone apex is $h = Vt$, we finally obtain

$$P_y = 4\rho V^4 t^2 \left(\frac{4}{\pi \operatorname{tg} \beta}\right)^3 = 4\rho V^2 h^2 \left(\frac{4}{\pi \operatorname{tg} \beta}\right)^3. \quad (4.29)$$

For a finite cone with base radius a the maximum value of c is limited by the value of a . Hence the maximum drag is

$$P_{y\max} = 4\rho V^2 a^2 \left(\frac{4}{\pi \operatorname{tg} \beta}\right).$$

Formulas (4.28) and (4.29) are limiting relationships, which hold as $\beta \rightarrow 0$.

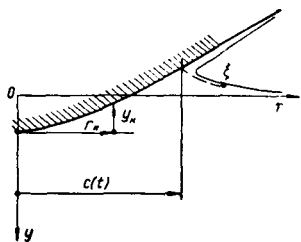


FIGURE 44.

Equation (4.27) can also be written for a cone of revolution of some arbitrary shape (Figure 44). Let us follow some particle ξ , situated at constant distance r_* from the y axis, when the pressure surface c increases from zero to $c = r_*$. At any instant the particle rise velocity at the outer fluid surface is

$$v(r_*, t) = Vf\left(\frac{r_*}{c}\right), \text{ where } r_* = \text{const, and } c = c(t).$$

Since the equation of the cone generatrix relative to its apex is $y_k = y_k(r_*)$, and since

$$Vdt = \frac{V}{\frac{dc}{dt}} dc = \frac{dh}{dc} dc = F(c) dc, \text{ we derive the}$$

integral equation

$$\int_0^t \left(1 + \frac{v\left(\frac{r_*}{c}\right)}{V}\right) \frac{dh}{dc} dc = y_k(r_*). \quad (4.30)$$

Lotov obtained a solution of equation (4.30) for the velocity distribution over the free surface with a corresponding disk:

$$\frac{dh}{dc} = \frac{d}{dc} \left[\frac{1}{c} \int_0^c \frac{r_* y_k(r_*) dr_*}{\sqrt{c^2 - r_*^2}} \right]. \quad (4.30a)$$

This form is convenient for practical calculations.

It follows from equations (4.30) and (4.30a) that, for each given form of the body generatrix $y_k(r_*)$ when $f\left(\frac{r_*}{c}\right) = \frac{v}{V}$ is not an explicit time function, the

entire problem has a unique solution, and thus function $\frac{dh}{dc} = F(c)$ together with the Laplace equation and boundary conditions express the holonomic geometric relationship between $n \rightarrow \infty$ particles of a system of mass points with $n-1$ constraint equations, with the result that the entire system has one degree of freedom. The limitation on the applicability of equation (4.30) consists in the fact that the above velocity distribution function $f(r_*, c)$ rigorously applies to the plane of the disk when $r > c$, while actually one obtains a curved free surface and a velocity distribution different from the above. Actually, the particle constraints for immersion of solids into a fluid are not holonomic, and hence equation (4.30) is the closer to the reality, the smaller $\frac{dh}{dc}$.

14. Application of the pressure integral for determining the drag on a cone

It was found from a study of the pressure integral for uniform immersion of a wedge that, according to the expanding-plate analogy, the expression for the drag on a wedge is very close to that determined from Wagner's integral. Hence the drag on a symmetric circular cone at not too large β

can, as in the case of a wedge, be calculated using the analogy between the flow about a cone and the flow ahead of a disk of radius $c = c(t)$ performing translational motion with velocity V .

Unlike the classical statement of the problem on uniform translational motion of a disk perpendicular to its plane, we assume here that only positive pressures remain equal at the pressure surface of the disk (which is assumed to be equivalent to the cone), while starting from point r_* where $\Delta p = 0$, the tangential velocity along the generatrix becomes constant and the potential increases linearly along the spray sheet. This approach makes it possible in principle to obtain agreement between the main postulates of the exact theory of motion with a homothetic center and the approximate identification of the flow ahead of a cone with the flow ahead of a disk. It can be shown that both theories become identical as $\beta \rightarrow 0$.

Using the expression for the potential at the leading surface of the disk,

$$\varphi = -\frac{2}{\pi} V \sqrt{c^2 - r_*^2},$$

referred to the coordinate system moving with the disk, and the expression

$$\frac{\Delta p}{\rho} = -\frac{\partial \varphi}{\partial t} + \frac{r_*}{t} \cdot \frac{\partial \varphi}{\partial r_*} - \frac{1}{2} \left[V^2 + \left(\frac{\partial \varphi}{\partial r_*} \right)^2 \right]$$

at points $\frac{r}{t} = \text{const}$ at the surface of the equivalent disk, we derive the expression

$$\frac{\Delta p}{\rho} = \frac{2}{\pi} \cdot \frac{Vc}{t} \cdot \frac{1}{\sqrt{1-\zeta^2}} - \frac{V^2}{2} \left(1 + \frac{4}{\pi^2} \cdot \frac{\zeta^2}{1-\zeta^2} \right). \quad (4.31)$$

It was assumed in formula (4.31) and subsequently that $\frac{r_*}{c} = \zeta$. It should be noted that this formula does not contain the above expression for φ , from which $\varphi = 0$ when $r = c$, but the partial derivative

$$\left. \frac{\partial \varphi}{\partial t} \right|_{\text{move}} - \frac{r_*}{t} \cdot \frac{\partial \varphi}{\partial r_*} = \left. \frac{\partial \varphi}{\partial t} \right|_{\text{stat}}$$

where $\left. \frac{\partial \varphi}{\partial t} \right|_{\text{stat}}$ is determined in the coordinate system associated with the stationary fluid. Hence the assumed expression for φ is used only in the sense that $\frac{\partial' \varphi}{\partial t} = \frac{\partial \varphi}{\partial c} \cdot \frac{dc}{dt}$. The disk analogy is applied only to the expressions for $\frac{\partial \varphi}{\partial c}$ and $\frac{\partial \varphi}{\partial r}$; the point r at which Re potential φ vanishes is not determined by the pressure equation. Equation (4.31) is similar to equation (4.14).

Since it is assumed that at the generatrix of the cone $\Delta p \gg 0$, point ζ_0 at which $\Delta p = 0$ is determined from (4.31) by the expression

$$\frac{c}{Vt} = \frac{4}{\pi} \cdot \frac{1}{\lg \beta} = \frac{\pi}{4} \sqrt{1-\zeta_0^2} \left(1 + \frac{4}{\pi^2} \cdot \frac{\zeta_0^2}{1-\zeta_0^2} \right). \quad (4.32)$$

For small $\operatorname{tg} \beta$, approximately

$$1 - \zeta_0 \approx \frac{1}{32} \operatorname{tg}^2 \beta; \quad 1 - \zeta_0^2 \approx \frac{1}{16} \operatorname{tg}^2 \beta.$$

The resultant drag can be determined by the integral of pressure Δp over the projection of the cone surface on the plane $y = \text{const}$:

$$P_y = \int_0^{\zeta_0} \Delta p 2\pi r_* dr_* = 4QV^2 h^2 \left\{ \left(\frac{4}{\pi \operatorname{tg} \beta} \right)^3 (1 - \sqrt{1 - \zeta_0^2}) - \right. \\ \left. - \frac{1}{2\pi} \left(\frac{4}{\pi \operatorname{tg} \beta} \right)^3 \left[\ln \frac{1}{1 - \zeta_0^2} + \zeta_0 \left(\frac{\pi^2}{4} - 1 \right) \right] \right\}. \quad (4.33)$$

Dividing the right- and left-hand sides of (4.33) by the limiting drag obtained from formula (4.29), we have

$$K(\beta) = \frac{P_y}{4QV^2 h^2 \left(\frac{4}{\pi \operatorname{tg} \beta} \right)^3} = 1 - \frac{\operatorname{tg} \beta}{4} \left[\frac{4 + \pi^2}{8} + \ln \frac{4}{\operatorname{tg} \beta} \right]. \quad (4.34)$$

If the cone is not infinite and has a base radius a , then at time t_m the spray-sheet root will attain the radius $\xi_0 c = a$ and P_y has a maximum. It follows that $a = \frac{4Vt_m}{\pi \operatorname{tg} \beta}$, and so the maximum drag is

$$P_{y\max} = 4QV^2 a^2 K_m(\beta) = 4QV^2 a^2 \left(\frac{4}{\pi \operatorname{tg} \beta} \right) K(\beta). \quad (4.35)$$

For uniform immersion of the cone

$$P_y(t) = P_{y\max} \left(\frac{t}{t_m} \right)^3,$$

where

$$t_m = \frac{\pi a \operatorname{tg} \beta}{4V}.$$

The kinetic energy T of the fluid upon immersion of a cone is equal (as for the wedge) to the product of velocity V and vertical momentum

component B_y . We refer the entire kinetic energy $T = \frac{1}{2} VB_y = \frac{4}{3} Qc^3 \frac{V^2}{2}$

(as $\beta \rightarrow 0$) to the spray sheet and assume that the spray length is c and the thickness at the root is δ . Since by similarity the section cut through the spray sheet by a plane through the y axis should be approximately triangular, the volume of fluid in the spray is found to be $\frac{2}{3} \delta c^3$. The absolute velocity in

the spray sheet (when $\zeta > \zeta_0$), as for a wedge, is $2 \frac{dc}{dt} = \frac{8}{\pi} \cdot \frac{V}{\operatorname{tg} \beta}$; hence the energy equation yields $\frac{\delta}{c} = \frac{\pi^2}{32} \operatorname{tg}^2 \beta$. Moreover, for relatively large β the spray-sheet volume can be determined from the general energy equation

$$T = VB_y$$

by assuming that energy $\frac{1}{2} T^*$ is contained within the spray, while the velocities of all the fluid particles within the spray are the same and are given vectorially by $\vec{u} = \vec{u}_r + \vec{u}_s$. For points in the spray close to the root of the sheet $u_s = u_r = \frac{dc}{dt}$, but vectors \vec{u}_r and \vec{u}_s are directed relative to one another approximately at angle β . Hence $u = 2 \frac{dc}{dt} \cos \frac{\beta}{2}$. Formula (4.24) yields

$$T = \frac{1}{3} P_\mu h. \text{ Denoting the spray-sheet volume by } q, \quad \frac{1}{6} P_\mu(h) h = \frac{6q}{2} u^2.$$

In general, the conclusions following from matching the exact theory to approximations obtained from the expanding-plate analogy in the case of a wedge and from the disk analogy in the case of a cone are qualitatively fully identical and differ only by numerical coefficients.

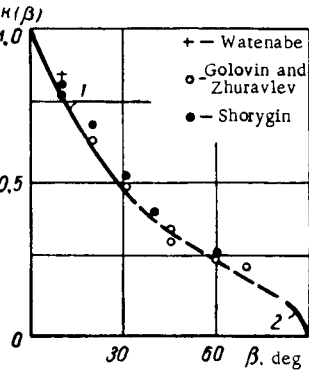


FIGURE 45.

Experiments carried out with metal cones in which the forces were measured by piezoelectric transducers show that this theory is in satisfactory agreement with experimental results. Table 4 lists three values of the maximum drag obtained experimentally and theoretically from (4.35), as well as the time t_m , obtained by these two methods.*

The entry velocity V was close to 4 m/sec, the diameter $2a$ was 80 mm for cones with β equal to 10 and 20°, and 60 mm for the cone with $\beta = 15^\circ$. Agreement between theoretical and experimental results was obtained not only for maximum values, but also for the entire drag-time curve.

Averaged values of $K(\beta)$ calculated from the latest experimental results due to Shorygin /14/ are given in Table 5.

TABLE 4

β , deg	P_m , dyne		t_m , sec	
	experimental	theoretical	experimental	theoretical
10	63.0	59.2	0.00134	0.00138
15	19.7	19.8	0.00161	0.00165
20	24	22.6	0.00280	0.00286

TABLE 5

β , deg	0	10	20	30	40	50	60	70
$K(\beta)$	1.00	0.82	0.68	0.51	0.40	0.30	0.25	0.22

* The experiments were performed by Golovin and Zhuravlev /12, 13/.

The above approximate theory yields results close to experimental results at angles β approximately equal to 30° . The experimental results obtained by various investigators are plotted in Figure 45. Segment 1 of the curve corresponds to (4.34), while segment 2 was plotted from a formula obtained by Sagomonyan which, in our notation, has the form

$$K(\beta) = \left(\frac{\pi}{4}\right)^4 \mu \ln \frac{1}{\mu} \text{ and is valid for small angles } \mu = \frac{\pi}{2} - \beta \rightarrow 0.$$

15. Transient drag on a cone

After the tip of the spray sheet reaches the cone base a , fluid particles, which up to now moved along the cone generatrix, will be shed from the edges. However, fluid particles belonging to the spray sheet already move at a steady velocity and consequently their separation from the edges should not affect the law governing the rise in drag. A cavity starts to form from the time the spray root reaches the cone base ($c \rightarrow a$), and this will result in the reconstruction of the flow and in changing the relationship $P_y = P_y(h)$. As the immersion depth increases, the drag will tend to the value of steady drag on a cone moving with developed cavitation behind it, i. e., at $h \rightarrow \infty$ we have $P_y(h) \rightarrow W(h \rightarrow \infty)$.

As for a wedge, the transient function is $H\left(\frac{h}{a}\right) = \frac{P_y\left(\frac{h}{a}\right)}{W}$. To estimate the function $H\left(\frac{h}{a}\right)$ we assume potential φ at the surface of a disk with radius $c^* > a$ is expressed in the same manner as on the surface of a disk (cone with $\beta \rightarrow 0$) at $a > c$. Here radius c^* is actually some linear time-dependent variable. The condition for determining $c^* = c^*(t)$ consists in the fact that $\Delta p = 0$ when $r_* = a$. Since the potential $\varphi = -\frac{2}{\pi} V \sqrt{c^{*2} - r_*^2}$ is taken in the moving coordinate system and pertains to the surface of a hypothetical disk with radius $c^* > a$, the equation for pressure at disk surface a is

$$\frac{\Delta p}{\rho} = -\frac{\partial \varphi}{\partial t} + V^2 - \frac{1}{2} \left[V^2 + \left(\frac{\partial \varphi}{\partial r} \right)^2 \right]_{r_* = a}.$$

At the edge of the disk $r_* = a$, $\Delta p = 0$, and upon substitution for $\frac{\partial \varphi}{\partial t}$ and $\frac{\partial \varphi}{\partial r_*}$ (discarding the asterisk over c)

$$\frac{\Delta p}{\rho} = \frac{2}{\pi} V \frac{c \frac{dc}{dt}}{\sqrt{c^2 - r_*^2}} + \frac{V^2}{2} \left(1 - \frac{4}{\pi^2} \frac{r_*^2}{c^2 - r_*^2} \right). \quad (4.36)$$

The condition that $\Delta p = 0$ at $r_* = a$ yields a differential equation for $c = c(t)$:

$$\frac{d\left(\frac{c}{a}\right)^2}{d\left(\frac{Vt}{a}\right)} = \frac{1}{\frac{\pi}{2} \sqrt{\left(\frac{c}{a}\right)^2 - 1}} - \frac{\pi}{2} \sqrt{\left(\frac{c}{a}\right)^2 - 1}. \quad (4.37)$$

Integration, subject to the initial condition that $\frac{c}{a} = 1$ at $t = 1$, gives

$$\frac{Vt}{a} = \frac{8}{\pi^2} \left\{ \ln \operatorname{tg} \left[\frac{\pi}{4} + \frac{1}{2} \arcsin \frac{\pi}{2} \sqrt{\left(\frac{c}{a}\right)^2 - 1} \right] - \frac{\pi}{2} \sqrt{\left(\frac{c}{a}\right)^2 - 1} \right\}. \quad (4.38)$$

Here, as for the wedge, linear variable c does not increase together with the infinite expansion of the cavity radius, but attains a limiting value $c = a \sqrt{1 - \frac{4}{\pi^2}}$ as $\frac{Vt}{a} \rightarrow \infty$. This is a natural result of the schematically assumed potential distribution over the plane of the disk ($\beta \rightarrow 0$) and the region in the proximity of its edges ($r = a + \epsilon$, where $\epsilon \ll a$); formally these approximations are valid when $v_s \gg V$. It is clear that while the distributions of potentials φ and velocities $\frac{\partial \varphi}{\partial r}$ obtained from the assumed expression for φ may be close to the actual distributions at the disk surface, the potential distribution at the cavity boundaries is quite different. An approximate distribution of φ in the meridional plane r, y is shown schematically in Figure 46.

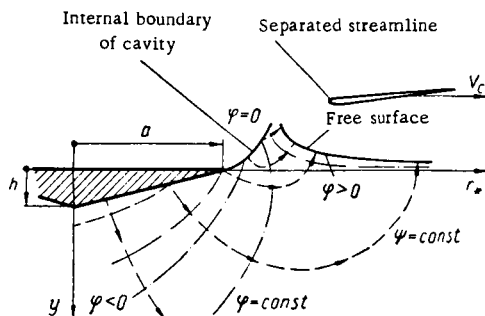


FIGURE 46.

The resultant drag is obtained as the integral, over the area of disk a , of the projections of excess-pressure forces on the y axis. Substitution of $\frac{dc}{dt}$ from equation (4.37) into (4.36) yields

$$\begin{aligned} P_y &= \int_0^a \Delta p 2\pi r \cdot dr = \pi a^2 \frac{\rho V^2}{2} \left\{ \frac{4}{\pi} \left[\frac{1}{\frac{\pi}{2} \sqrt{\left(\frac{c}{a}\right)^2 - 1}} - \frac{\pi}{2} \sqrt{\left(\frac{c}{a}\right)^2 - 1} \right] \times \right. \\ &\quad \times \left[1 - \sqrt{1 - \left(\frac{a}{c}\right)^2} \right] \frac{c}{a} + \left[1 + \frac{4}{\pi^2} + \frac{4a^2}{\pi^2 c^2} \ln \left(1 - \frac{a^2}{c^2} \right) \right] \Big\} = \\ &= P_y^* \left(\frac{c}{a} \right) + P_y^* \left(\frac{c}{a} \right). \end{aligned} \quad (4.39)$$

From the physical point of view the first term in braces of (4.39) gives the unsteady drag coefficient corresponding to $\frac{\partial \varphi}{\partial t}$ in the pressure equation, while

the second term corresponds to $\frac{1}{2} v^2$; however, these terms are related.

As the cone immersion depth increases ($Vt \rightarrow \infty$) the first term tends to zero, while the second increases to the steady drag W .

The cavitation drag coefficient of a disk as $Vt \rightarrow \infty$ is $c_x = 0.82$, while the limiting value of the last bracket in (4.39) is approximately 0.7, which coincides with the drag coefficient of a cone for which $\beta = 15^\circ$.

On the assumption that the transition drag does not essentially depend on β , we define the transient function as

$$H_1\left(\frac{Vt}{a}\right) = \frac{P_v'\left(\frac{Vt}{a}\right) + P_v^*\left(\frac{Vt}{a}\right)}{P_{v(\infty)}^*},$$

where the relationship between $\frac{c}{a}$ in (4.39) and $\frac{Vt}{a}$ is derived from (4.38).

Then the true transient drag on a cone is obtained from the expression

$$P_{v \text{ tr}} = H_1\left(\frac{Vt}{a}\right) W, \quad (4.40)$$

where the true steady cavitation drag on a cone, $W = c(\beta) \pi a^2 \frac{\rho V^2}{2}$, should be determined independently of equation (4.39).

The values of the transient function calculated from the preceding formulas are listed in Table 6.

TABLE 6

$\frac{Vt}{a}$	0.025	0.05	0.1	0.2	0.3	0.4	0.5	1.0
$H_1\left(\frac{Vt}{a}\right)$	2.7	1.86	1.57	1.36	1.24	1.16	1.11	1.02

As for a wedge, the transient function H_1 for a cone tends to infinity as $\frac{Vt}{a}$ approaches zero. High values of H_1 correspond to small β , at which the maximum value of P_v is very high.

It is clear from the preceding that in calculating the entire process of immersion of a cone during the time up to $t_m = \frac{\pi}{4} \cdot \frac{a \operatorname{tg} \beta}{V}$ drag P_v increases as a square of the time and its maximum at time t_m is determined from expression (4.35). Then the drag decreases according to the transient function. Consequently, the time scales of t_m and t are shifted relative to one another by an amount given by $P_v(t)_{\max} = H_1\left(\frac{Vt}{a}\right) W$.

We note in conclusion that the principal results of this theory are in agreement with experimental data, particularly with respect to t_m and $P_{v \text{ max}}$. The experimental verification of the calculated value of H_1 for a cone is more difficult than for a wedge as a result of a sharp drop in the drag after the maximum. At this stage a cathode-ray oscillograph was used for

recording elastic transient oscillations of the system, which are superimposed on the transition drag. The graph of the transient function $\frac{P_v}{W} = H\left(\frac{Vt}{a}\right)$ is plotted in Figure 47. The theoretical results (curve 1) are compared with experimental data (curve 2) in Figure 48. The drag coefficients of cones with different cone angles are given in Table 7.

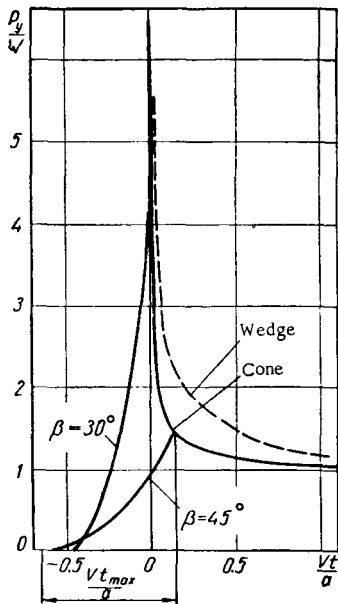


FIGURE 47.

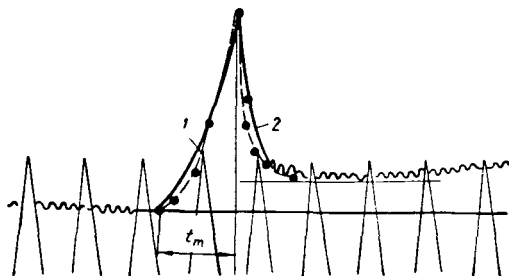


FIGURE 48.

TABLE 7

β , deg	5	10	15	20	30	45
C_x	0.78	0.75	0.715	0.68	0.607	0.465
$K_m(\beta)$	12.8	5.65	3.35	2.25	1.05	0.3

SYMMETRIC IMMERSION OF BODIES AT VARIABLE VELOCITY

16. Immersion of bodies at variable velocity

To better clarify the features of flow of an ideal incompressible fluid brought about by a body being immersed through its free surface, let us imagine that the fluid is continuous. We imagine that a wedge is immersed into such a fluid with constant velocity \dot{h} and, when the apex reaches depth h ,

the wedge is instantaneously stopped by an impulsive force applied only to the wedge. Until the wedge was stopped the velocity potential φ , being accumulated at the free surface differed from zero. Since the impulsive pressures at the free surface at the time of stopping are zero, potentials φ_i remain unchanged as a result of stopping the body. The pressure gradients during impact are directed normal to the free surface, and therefore also the tangential velocities u_t remain unchanged (see Theorem II). It follows that stopping the wedge does not result in instantaneously stopping the fluid flow, as would have happened in the case of a body moving inside the fluid.

Let us assume that the velocity potential of flow being induced by the continuous immersion of the body is $\varphi = \varphi_1 + \varphi_2$. Potential φ_1 corresponds to impact excitation of flow due to the instantaneous configuration of free boundaries (at the free surface $\varphi_1 = 0$). The accumulating potential φ_2 differs from zero at the free surface S and does not depend explicitly on the body velocity; consequently, at the surface of the body $\frac{\partial \varphi_2}{\partial n} = 0$. According to Green's theorem

$$\int_{S_k+S} \varphi_1 \frac{\partial \varphi_2}{\partial n} dS = \int_{S_k+S} \varphi_2 \frac{\partial \varphi_1}{\partial n} dS.$$

The first integral is equal to zero, since at the solid boundaries $\frac{\partial \varphi_2}{\partial n} = 0$, while at the free boundaries $\varphi_1 = 0$. Consequently, the integral in the right-hand side is also zero.

The kinetic energy T of the fluid and the vertical component of the momentum B can now be represented as a sum of two terms:

$$T = -\frac{\rho}{2} \iint_{S_k} \varphi_1 \frac{\partial \varphi_1}{\partial n} dS - \frac{\rho}{2} \iint_S \varphi_2 \frac{\partial \varphi_2}{\partial n} dS = T_1 + T_2;$$

$$B = -\rho \iint_{S_k} \varphi_1 dx - \rho \iint_{S+S_k} \varphi_2 dx = B_1 + B_2.$$

Only the energy T_1 and momentum B_1 can change instantaneously with a change in \dot{h} ; these two former quantities can be represented in the term of "impact" induced mass m^* using the ordinary expressions

$$T_1 = m^* \frac{\dot{h}^2}{2}; \quad B_1 = m^* \dot{h}.$$

Formally the impact induced mass m^* can be calculated by solving the boundary-value problem for each configuration of boundaries, as is the case with the induced mass of a floating body.

From the energy and momentum equations the pressure force of the body on the fluid is expressed by two equations:

$$P = \frac{1}{h} \cdot \frac{DT}{Dt}; \quad P = \frac{DB}{Dt}.$$

The time derivatives of T_1 and B_1 are

$$\frac{DT_1}{Dt} = m^* \ddot{h} + \frac{\dot{h}^2}{2} \cdot \frac{dm^*}{dt}$$

$$\frac{DB_1}{Dt} = m^* \ddot{h} + \dot{h} \frac{dm^*}{dt}.$$

The time derivatives of T_2 and B_2 can be treated as the energy and momentum fluxes to the spray sheet. Denoting the mass flux by ϱQ , we find that $\frac{DT_2}{Dt} = \varrho Q \frac{u_{sc}^2}{2}$ and $\frac{DB_2}{Dt} = -\varrho Q u_{sc} \sin \beta$; velocity u_{sc} and the spray-sheet slope β can be determined from the spray-root analogy. We thus have two independent equations for the pressure force of the body on the fluid: the energy equation

$$P = m^* \ddot{h} + \frac{1}{2} \dot{h} \frac{dm^*}{dt} + \varrho Q \frac{u_{sc}^2}{2h};$$

the momentum equation

$$P = m^* \ddot{h} + \dot{h} \frac{dm^*}{dt} - \varrho Q u_{sc} \sin \beta,$$

which contain the three unknowns P , m^* and Q . Hence we make the additional requirement that at $\dot{h} = 0$ each of these equations should express the force upon uniform immersion, always expressible as

$$P_0 = \dot{h} \frac{dM_0}{dt}.$$

We note that M_0 has the dimensions of the induced mass and can be determined quite easily from the expression for the force during uniform immersion.

It should, however, be remembered that M_0 , which shall be termed the "apparent" induced mass, being multiplied by the acceleration \ddot{h} does not yield the reaction force of the fluid on the acceleration of the body. Thus, at $\dot{h} = 0$,

$$\frac{a}{dt} \left(M_0 - \frac{1}{2} m^* \right) = \varrho Q \frac{u_{sc}^2}{2h^2};$$

$$\frac{a}{dt} (M_0 - m^*) = -\varrho Q \frac{u_{sc} \sin \beta}{h}.$$

If $\frac{u_{sc}}{2h \sin \beta} = k$, then upon elimination of ϱQ

$$\frac{dm^*}{dt} = \frac{2(1+k)}{2k+1} \frac{dM_0}{dt}.$$

Integration of both parts of this equation with respect to the variable M_0 gives

$$m^* = \int_0^{M_0} \frac{2(1+k)}{2k+1} dM_0. \quad (4.41)$$

Returning to the starting equations, we find that the pressure exerted by the body on the fluid is determined from the general formula

$$P = m^* \dot{h} + \frac{dM_0}{dt} \dot{h}. \quad (4.42)$$

In particular, the value of k in the integrand of (4.41) is constant for a wedge, and that when $\beta \rightarrow 0$, $k \rightarrow \infty$, and when $\beta \rightarrow \frac{\pi}{2}$, $k \rightarrow \frac{1}{2} \left(\frac{\pi}{2} - \beta \right) = \frac{1}{2} \mu$,

hence $\beta \rightarrow 0$; $m^* \rightarrow M_0$; $\beta \rightarrow \frac{\pi}{2}$; $m^* \rightarrow 2M_0$. Formulas (4.41) and (4.42) are equally valid for symmetric immersion of two-dimensional profiles and for the immersion of axisymmetric bodies.

35

17. Principal energy and momentum equations

The preceding conclusions make it possible to calculate the energy and momentum of the fluid in the free stream (T_1 and B_1) and in the region of the spray sheet (T_2 and B_2). It follows directly from equations presented in the preceding section that $T_1 = B_1 \frac{\dot{h}}{2}$; hence Wagner's integral is

$$I_w = 2T - B\dot{h} = 2T_2 - B_2\dot{h}.$$

On uniform immersion

$$T_1 = \left(M_0 - \frac{1}{2} m^* \right) \dot{h}^2, \quad B_1 = (M_0 - m^*) \dot{h}.$$

It follows from Section 16 that in all cases $m^* > M_0 > \frac{1}{2} m^*$. For bodies close to a plate or disk (wedge or cone at $\beta \rightarrow 0$), $m^* \geq M_0$; hence $T_1 \geq T_2$ while $B_1 \geq 0$. The energy for the immersion of such flat bodies is divided approximately equally between the main flow and the region of the spray sheet, while the momentum of the main flow comprises the principal contribution to the expression for the force.

Using the tangential velocity u_{∞} estimated from the spray-root analogy for $\beta \rightarrow 0$ and $\beta \rightarrow \frac{\pi}{2}$, it can be shown that for the entire range of β the integrand in (4.41) can be approximated by

$$\frac{1+k}{2k+1} \approx 1 - \frac{1}{2} \cos \beta. \quad (4.43)$$

Consider the immersion of a wedge. It follows from Wagner's formula that $M_0 = \frac{\pi}{2} \rho h^2 \left(\frac{\pi}{2\beta} - 1 \right)^2$; substitution into the principal equation (4.42) yields

$$P = \pi \left(\frac{\pi}{2\beta} - 1 \right)^2 \left[\rho h \dot{h}^2 + \left(1 - \frac{1}{2} \cos \beta \right) \rho h^2 \dot{h} \right]. \quad (4.44)$$

The expressions for calculating the forces attendant to nonuniform immersion can be obtained for any body, if the force attendant to uniform immersion is known and, conversely, from a known induced mass m^* , calculated for the case of impact on a floating body, one can determine the force attendant to uniform immersion.

For "slender" bodies when $\frac{dc}{dh} \rightarrow 0$, the drag is given approximately by the formula

$$P \approx m^* \ddot{h} + \frac{1}{2} \dot{h} \frac{dm^*}{dt}. \quad (4.45)$$

In the sense of the derivation of the preceding equations, m^* is the impact induced mass, determined for the case of impact on a body floating on the free surface, distorted by the preceding continuous immersion.

For very slender bodies ($\beta \rightarrow \frac{\pi}{2}$) $M_0 \rightarrow \frac{1}{2} m^*$; hence the momentum of the main flow is $B_1 = m^* \dot{h}$, while the momentum of the spray-sheet region is found to be halved, i. e., $B_2 = -\frac{1}{2} m^* \dot{h}$. The kinetic energy in the region of the spray sheet is close to zero, and the main part of the kinetic energy is concentrated within the main region of the flow.

For symmetric immersion of a circular cone it can apparently be assumed that, as for the wedge, $\frac{1+k}{2k+1} \approx 1 - \frac{1}{2} \cos \beta$. Hence, from the preceding formulas,

$$m^* = 2 \left(1 - \frac{1}{2} \cos \beta \right) M_0.$$

The apparent induced mass for a cone is $M_0 = \frac{1}{3} \rho h^3 f(\beta)$, where

$f(\beta) = 4 \left(\frac{4}{\pi \lg \beta} \right)^3 K(\beta)$. Here the value of function $K(\beta)$ is shown in Figure 45.

According to (4.42), the final expression for the drag is

$$P = \left[\rho h^2 \ddot{h}^2 + \rho h^3 \dot{h} \frac{2}{3} \left(1 - \frac{1}{2} \cos \beta \right) \right] f(\beta). \quad (4.46)$$

Formula (4.46) can be used for practical calculation of P ; however, this expression disregards the friction force.

18. Application of the Wagner integral to calculation of drag

Consider the rectilinear immersion of a solid body into a half-space filled by a weightless incompressible fluid. As above, the wetted surface of the body is denoted by S_k and the free surface by S . The body moves with velocity \bar{V} ; the velocity potentials at surfaces S_k and S are respectively denoted by Φ_k and Φ_s .

The kinetic energy of the fluid is determined from formula (2.7). Since the normal velocity of the fluid at surface S_k is $\frac{\partial \varphi_k}{\partial n} = \bar{n}\bar{V}$, division of integral (2.7) into two integrals over S_k and S gives

$$2T = -\varrho \bar{V} \int_{S_k} \varphi_k \bar{n} dS - \varrho \int_S \varphi_S \frac{\partial \varphi_S}{\partial n} dS = 2T_k + 2T_S.$$

The momentum of the fluid according to (2.14) is

$$\bar{B} = -\varrho \int_{S_k} \varphi_k \bar{n} dS - \varrho \int_S \varphi_S \bar{n} dS = \bar{B}_k + \bar{B}_S.$$

Elimination of the integral $\varrho \int_{S_k} \varphi_k \bar{n} dS$ from the first and second expressions yield the Wagner integral:

$$I_w = 2T - \bar{V} \bar{B} = \int_S \bar{V} \varrho \varphi_S \bar{n} dS - \varrho \int_S \varphi_S \frac{\partial \varphi_S}{\partial n} dS = 2T_S - \bar{V} \bar{B}_S, \quad (4.47)$$

which does not involve integration of φ_k and $\frac{\partial \varphi_k}{\partial n}$ over the solid boundaries.

We now note some properties of Wagner's integral.

1. The Wagner integral attendant to the impact excitation of flow from rest is zero for any free-boundary configuration. On impact excitation of flow, $\varphi_s = 0$ at the free surface both before and after impact. Hence

$T = \frac{1}{2} \bar{V} \bar{B}$ while $I_w = 0$. The energy and momentum in this case can be expressed in terms of induced masses, which are uniquely determined by the configuration of the wetted surface of the body and of the free boundaries before impact.

2. The Wagner integral for uniform motion ($\bar{V} = \text{const}$) is equal to the kinetic energy of the fluid which, in turn, is equal to the scalar product of the momentum and velocity vectors. Integration of the energy equation (2.13) for $\omega = 0$ and $\bar{V} = \text{const}$ yields

$$T = \bar{V} \int_0^t \bar{P} dt = \bar{V} \bar{B}.$$

Substituting this result into (4.47) gives $I_w = T$. Differentiation of the Wagner integral with consideration of the fact that $\frac{d\bar{B}}{dt} = \bar{P}$ yields

$$\frac{dI_w}{dt} = 2 \frac{dT}{dt} - \frac{d\bar{V}}{dt} \bar{B} - \bar{V} \frac{d\bar{B}}{dt} = \bar{P} \bar{V} - \frac{d\bar{V}}{dt} \bar{B}.$$

At $\bar{V} = \text{const}$, $\frac{dI_w}{dt} = \frac{dT}{dt} = \bar{P} \bar{V}$, where \bar{P} is the vector of the pressure force on the fluid.

Expanding the expression for $\frac{dI_w}{dt}$ and substituting the value of \bar{B} into the last equation, we have

$$\bar{P}\bar{V} = -\varrho \frac{d\bar{V}}{dt} \int_{S_k} \varphi_k \bar{n} dS + \varrho \bar{V} \frac{d}{dt} \int_S \varphi_s \bar{n} dS - \varrho \frac{d}{dt} \int_S \varphi_s \frac{\partial \varphi_s}{\partial n} ds, \quad (4.48)$$

or, using the preceding expressions for the integrals,

$$\bar{P}\bar{V} = \frac{d\bar{V}}{dt} \bar{B}_k + 2 \frac{d}{dt} T_s - \bar{V} \frac{d}{dt} \bar{B}_s. \quad (4.48a)$$

Figure 49 depicts the flow pattern on entry of the body into the fluid. The space occupied by the fluid can be divided into three regions, designated respectively I, II and III. Region I (main flow) is bounded by surface S_k of the body, streamlines moving from points C , where free boundaries form, to the zero-potential surface τ and then along it to infinity. Integrals

$T_k = -\frac{\varrho}{2} \int_{S_k} \varphi_k \frac{\partial \varphi_k}{\partial n} dS$ and $\bar{B}_k = -\varrho \int_{S_k} \varphi_k \bar{n} dS$ express the kinetic energy and momentum of the fluid in region I; the energy T_k and momenta \bar{B}_k shall be termed bound. Region II (region of the cavity) is bounded by the inner free boundaries CK , segments KD of the zero-potential surface and streamlines CD .

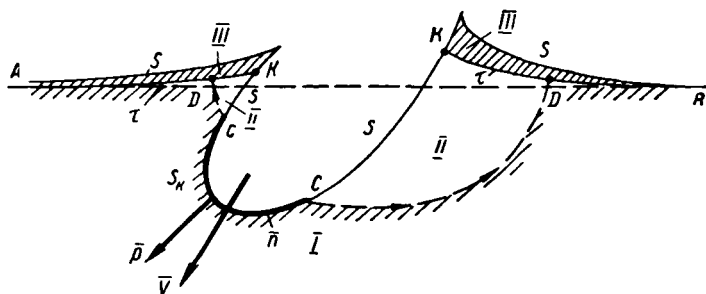


FIGURE 49.

Region III (surface region) is bounded by the zero-potential surface and the free surface, situated above it. According to Sections 10 and 11 of Chapter Two, if the excess pressure at the zero-potential surface is zero, the rate of propagation of surface τ is equal to half the velocity of the fluid at this surface and the volume of region III is equal to half of the volume displaced by the body and the cavity from the initial fluid region. When the zero-potential surface intersects the inner surface of the cavity or the surface of the slender body these conditions are also approximately satisfied; the results show that in this case $\frac{dT_s}{dt} = E$, $\frac{d\bar{B}_s}{dt} = \bar{\Pi}$, where E and $\bar{\Pi}$ respectively are the energy and momentum fluxes through the zero-potential surface τ , while T_s and \bar{B}_s are the kinetic energy and momentum contained in region III. For slender bodies formula (4.48a) makes possible a quite simple calculation of the pressure exerted by the body on the fluid.

19. Axisymmetric immersion of a slender body

For immersion of a slender body (Figure 50) $\tilde{x} = f(y)$, the preceding equations can be simplified and hence some specific results can be obtained.

In addition, this case illustrates the application of general principles presented in the preceding sections. We note that in this case the cavity region II does not exist and only regions I and III are present. From equation (4.48a) the pressure exerted by the body on the fluid is

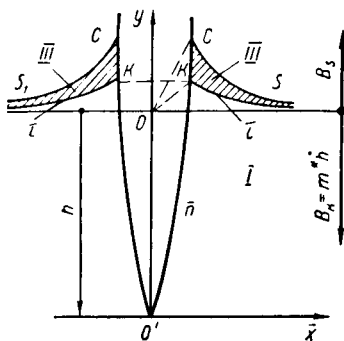


FIGURE 50.

$$P = -\rho \int_{S_k} \frac{h}{h} \varphi_k \bar{n} dS + 2 \frac{1}{h} \cdot \frac{dT_s}{dt} - \frac{dB_s}{dt}.$$

The projection of an element of the body surface S_k on the horizontal plane is $dS_{xk} = \bar{n} dS$; the velocity potential at the body surface can be expressed in the form $\varphi_k = -h \tilde{\Phi}(\tilde{x})$, the distribution function $\tilde{\Phi}(\tilde{x})$

being unknown. Integral $-\frac{\rho}{h} \int_{S_k} \varphi_k \bar{n} dS =$

$= \rho \int_{S_k} h \tilde{\Phi}(\tilde{x}) dS_{xk} = m^*(h, \tau)$ clearly expresses the induced mass in the direction of h . Thus, the first term in the expression for the force is $m^* \dot{h}$. The bound

energy and momenta, respectively, are $T_k = m^* \frac{\dot{h}^2}{2}$ and $B_k = m^* \dot{h}$. However,

the induced mass $m^*(h, \tau)$ depends not only on the shape of the body, but also on the location of surface τ , and this surface is unknown. It is virtually impossible to obtain an exact solution of the problem, but an approximate solution can be obtained. For this we must disregard the forces acting on the fluid along segments KC and use expressions for the energy and momentum fluxes through the zero-potential surface. The pressure force exerted on the fluid can be determined, on the one hand, from equation (4.48a) and, on the other, from the expression $P = \frac{d}{dt} (B_k + B_s)$. Using the expressions for the energy flux E and momentum flux Π_y through the zero-potential surface, we derive

$$P = m^* \dot{h} + \frac{2E}{h} + \Pi_y = m^* \dot{h} + \dot{h} \frac{dm^*}{dt} - \Pi_y. \quad (4.49)$$

For a slender body the value of E can be neglected, compared with Π_y , as being a higher-order infinitesimal. Hence for a slender body we have approximately $\dot{h} \frac{dm^*}{dt} - 2\Pi_y = 0$ or $B_k - 2B_s = 0$, i. e., the momentum of the main flow B_k is directed downward and is twice as large as the momentum of the surface region, which is directed upward. Equation (4.49) yields a limiting expression for the pressure force exerted by the body on the fluid, obtained above in Section 17 by a different method:

$$P \approx m^* \dot{h} + \frac{1}{2} \dot{h} \frac{dm^*}{dt}.$$

Finally, to calculate force P one may (using the method of sources and sinks) calculate velocity v at surface τ and then find Π_y by direct integration. Here it is necessary to satisfy the general continuity equation, according to which the volume of the surface region is equal to half the volume displaced by the body from the initially undisturbed fluid. The second method of calculating P consists in finding the induced mass m^* . This question is examined in the following section.

It can be found from the spray-root analogy that the horizontal and vertical velocities of point C are approximately the same, while the tangential velocity of point K is approximately halved. If the body contour $\tilde{x} = f(y)$ is specified, then point C is determined from the condition $\tilde{x}_C \approx f(h + \tilde{x}_C)$, while the distance from point K to the tip of the body is

$$h' = h + \frac{1}{2}\tilde{x}_C.$$

For a slender body surface τ is close to the horizontal plane. Hence the induced mass of the same body, floating on the horizontal surface and submerged to depth h' , is very close to the sought induced mass m^* .

20. Induced mass of a slender body

Figure 51 shows a slender body whose contour is described by the equation $R = f(\eta)$. This body floats on the free surface AB of a fluid filling the lower half-space. If a velocity \dot{h} is imparted impulsively to this body then, according to the above, the velocity potentials at the free surface will be zero and, using the symmetry principle for calculating the flow, we may supplement the lower part of the body by its mirror image in the upper half-space and consider the motion of this "doubled" body, at velocity \dot{h} , in an infinite medium.

The velocity potential at infinity ($r \rightarrow \infty$) is now calculated from (2.26) or (2.27), respectively, for the two-dimensional or axisymmetric case. The integral $-\int_{S_k+S} \eta d\psi = +Q\dot{h}$ is equal to the "true" volume Q of the

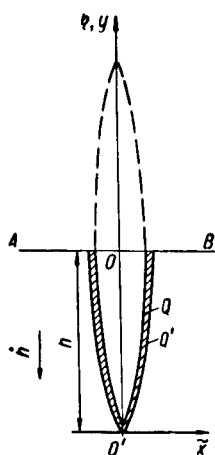
submerged part of the body, while the velocity potential (for axisymmetric flow) is

$$\Psi_{(r \rightarrow \infty)} = \frac{\cos \theta}{2\pi r^2} \left\{ \frac{1}{\epsilon} B_y - \dot{h} Q \right\} = -\frac{\dot{h} \cos \theta}{2\pi r^2} \left\{ \frac{m^*}{\epsilon} + Q \right\}.$$

FIGURE 51.

This value corresponds to the potential induced by the "true" body, supplemented by its mirror-image transform for motion in the y direction with velocity \dot{h} .

As is known, the flow of a fluid induced by a slender axisymmetric body can be represented by a system of sources distributed along the longitudinal axis. Let the density of sources at the axis of symmetry be $\gamma(\eta)$ and let this source distribution correspond to the body $R = f(\eta)$. It is possible to select another body $R' = f'(\eta)$ which is defined by the condition that $\gamma(\eta) = h 2\pi R' \frac{dR'}{d\eta}$.



The velocity potential of a single source is $\frac{-\gamma(\eta)}{4\pi r'}$, where $r' = r + \eta \cos \theta$, while r is the distance from the coordinate origin to the distant point. Since $\frac{\eta}{r} \rightarrow 0$ when $r \rightarrow \infty$, we obtain for the potential

$$\Phi_{r \rightarrow \infty} = -\frac{1}{4\pi r} \int_{-h}^{+h} \gamma(\eta) d\eta - \frac{\cos \theta}{4\pi r^2} \int_{-h}^{+h} \gamma(\eta) \eta d\eta = -\frac{h \cos \theta}{2\pi r^2} Q'.$$

The integral in the first term is zero, since the total source flux should be zero. The integral in the second term is the moment of the doublet.

Substitution of the expression for $\gamma(\eta)$ yields

$$\int_{-h}^{+h} \gamma(\eta) \eta d\eta = h \int_{-h}^{+h} 2\pi R' \frac{dR'}{d\eta} \eta d\eta = h \int_{-h}^{+h} 2\pi R' \eta dR' = 2Q'h \quad (4.50)$$

Quantity Q' shall be termed the "fictitious" volume. Since sources $\gamma(\eta)$ correspond to the "true" body, $\varphi = \psi'$ (as $r \rightarrow \infty$). Since $B_y = -m^*h$, we have finally

$$\frac{m^*}{Q} = Q' - Q. \quad (4.51)$$

Theorem XIX. The volume of the induced mass corresponding to the longitudinal motion of a slender body is equal to the difference in the fictitious and real volumes of the body.

For a body with given shape $R = f(\eta)$ one determines, somehow, by one of the available methods its corresponding system of sources $\gamma(\eta)$ and then finds the value of Q' from (4.50). The sources and sinks yield the relationship

$$\pi R^2 h + \int_0^{R(\eta)} 2\pi x v_y dx = \int_{-h}^{\eta} \gamma(\eta) d\eta = \pi R'^2 h.$$

Since $d(Q' - Q) = \pi(R'^2 - R^2) d\eta$, the expression for the volume of the induced mass has the form

$$\frac{m^*}{Q} = 2\pi \int_{-h}^0 d\eta \int_0^{R(\eta)} \frac{v_y}{h} x dx.$$

where

$$v_y = -\frac{1}{4\pi} \cdot \frac{\partial}{\partial y} \int_{-h}^{+h} \frac{\gamma(\eta) d\eta}{\eta^2 + x^2}.$$

The induced mass m^* pertains to body Q . However, for a very slender body m^* can be approximately referred also to body Q' . The volume of the induced mass is crosshatched in Figure 51. In general the longitudinal induced mass for slender bodies of revolution amounts to only several

per cent of the volume of the submerged part of the body. Thus, Sagomonyan derived the following expression for the drag on immersion of a slender cone with vertex angle 2μ : $P = \pi \rho h^2 \dot{h}^2 \mu^4 \ln \frac{1}{\mu}$. The induced mass can be determined from equation (4.45): $m^* = \frac{2\pi}{3} \rho h^3 \mu^4 \ln \frac{1}{\mu}$. The ratio of the volume of the induced mass to that of the body is $\frac{m^*}{\rho Q} = 2\mu^3 \ln \frac{1}{\mu}$; if $\mu = 0.1$, this ratio is equal to 0.046.

It follows from equation (4.49) that for a slender body, when E can be neglected, $\dot{h} \frac{dm^*}{dt} = \Pi_y$. Hence, for a body immersed with constant velocity, the pressure force is

$$P = \Pi_y = \int_k^{\infty} \frac{\rho \dot{v}_y^2}{2} 2\pi x dx. \quad (4.52)$$

The integration is carried out over the free surface from the body surface R to infinity.

The free-surface velocity distribution can be found by the method of sources and sinks. Thus, if a unit source Q is immersed vertically with constant velocity h , the pressure on the stream surface containing the entire flow starting with the source will, for immersion a of the source,

be $\Pi_y = \frac{\rho Q^2}{16\pi a^2} \cos^4 \theta_1$, where the source strength is determined from the expression $\pi R^2 \dot{h} + Q(1 - \cos \theta_1) = Q$, while $\frac{R}{a} = \tan \theta_1$. For a slender body angle θ_1 is small, and approximately $P_0 = \Pi_y = \rho \pi R^2 h^2 \frac{1}{16} \cdot \frac{R^2}{a^2}$.

21. Fall of a body on the surface of a fluid

Consider the simplest case of symmetric fall of a body with mass M_b on the surface of a fluid. Suppose, at the first contact ($t = 0$), the body has velocity V_0 . If we neglect the weight of the body and the fluid, the equation of motion has the form

$$M_b \frac{dV}{dt} = -P.$$

Drag P is a function of the shape of the body and for the shape at hand $P = P(h, \dot{h}, \ddot{h})$.

Integration with respect to time using initial conditions yields the following expressions for the momentum and energy:

$$M_b (V - V_0) = - \int_0^t P dt = -B(t);$$

$$M_b \left(\frac{V^2}{2} - \frac{V_0^2}{2} \right) = - \int_0^t P V dt = -T(t).$$

These equations make it possible, in principle, to calculate for each instant the velocity $V(t)$, momentum $B(t)$ and kinetic energy $T(t)$ of the fluid. However, these quantities cannot be expressed in terms of the instantaneous values of the induced mass by the expressions $B = m^* V$ and $T = m^* \frac{V^2}{2}$, since here the two equations (energy and momentum) are incompatible. If we still use these expressions for B and T , then, from the momentum equation, the velocity following impact will be $V = V_0 \frac{1}{1+\mu}$, where $\mu = \frac{m^*}{M_b}$. Here the kinetic energy of the body-fluid system following impact will be smaller than the kinetic energy of the body preceding impact by the "lost" energy $\frac{M_b V_0}{2} \frac{\mu}{1+\mu}$. But loss of energy is incompatible with potentiality of impact-induced flow. For cases of immersion of sharp-nosed bodies this "paradox" is eliminated for an incompressible fluid by allowance for the momentum and energy of the spray sheet, as shown in Section 16. It remains to clarify the question of impact of bodies coming in contact with the fluid simultaneously over their entire surface, such as a disk or plate. If the body and fluid are incompressible, then formally, from the known impact theory, the entire momentum and the entire kinetic energy are determined by the induced mass, there is no spray, and the above "paradox" cannot be eliminated. A more detailed study shows that allowance for compressibility must be made in the case of simultaneous contact of the surface of the body and the fluid. The "lost" energy is found to be carried away by a shock wave and its magnitude does not depend on the speed of sound.

22. Principal equations for compressible fluids

Flows with velocity potential $\varphi = \varphi(x, y, z, t)$ obey the continuity equation $\frac{\partial \varrho}{\partial t} + \text{div}(\varrho \bar{v}) = 0$, where $\bar{v} = \text{grad } \varphi$, and the Cauchy-Lagrange integral is

$$\frac{\partial \varphi}{\partial t} + \frac{1}{2} v^2 + \int \frac{dp}{\varrho} - U = F(t).$$

The pressure ratio s for quite poorly compressible fluids is very small; hence $\varrho = \varrho_0(1+s)$ and $p = p_0 + \kappa s$, where κ is the bulk elasticity modulus ($\kappa = \varrho_0 \frac{dp}{d\varrho}$), while ϱ_0 and p_0 are respectively the density and pressure of the undisturbed fluid. For $s \ll 1$ the pressure function is

$$\int \frac{dp}{\varrho} = \frac{\kappa}{\varrho_0} \int \frac{ds}{1+s} \approx \frac{\kappa}{\varrho_0} s + \text{const} = c^2 s + \text{const} = \frac{p}{\varrho_0} + \text{const},$$

where c is the speed of sound.

It can be shown by estimating the terms in the expression for pressure attendant to short-duration impact that, for $v \ll c$, the term $\frac{1}{2} v^2$ is small compared with $\frac{\partial \varphi}{\partial t}$ and $\int \frac{dp}{\varrho}$; for a fluid at rest at infinity $F(t) = \frac{p_0}{\varrho_0}$. Hence differentiation of the pressure equation yields

$$\frac{\partial^2 \varphi}{\partial t^2} + \frac{1}{\varrho_0} \cdot \frac{\partial p}{\partial t} = 0.$$

To the same degree of approximation we set in the continuity equation $\operatorname{div}(\varrho \vec{v}) = \varrho_0 \operatorname{div} \vec{v}$. Since $\frac{\partial \varrho}{\partial t} = \frac{1}{c^2} \cdot \frac{\partial p}{\partial t}$, we derive $\frac{1}{\varrho_0} \frac{\partial p}{\partial t} + c^2 \Delta \varphi = 0$. Eliminating $\frac{1}{\varrho} \cdot \frac{\partial p}{\partial t}$ from these expressions yields the known wave equation

$$\frac{\partial^2 \varphi}{\partial t^2} = c^2 \Delta \varphi. \quad (4.53)$$

In the case of spherical symmetry, when $\varphi = \varphi(r, t)$, the wave equation has the form

$$\frac{\partial^2 (\varphi r)}{\partial t^2} = c^2 \frac{\partial^2 (\varphi r)}{\partial r^2} \quad (4.54)$$

Equations (4.53) and (4.54) pertain to the field of acoustics.

23. Simplest case of impact

Imagine a tapered tube with small solid angle Ω , bounded by rigid walls and filled with fluid at all directions $r > R$. A mass impacts at free surface $R\Omega$ with velocity V_0 . The solution of wave equation (4.54) for diverging waves has the form

$$\varphi = \frac{A}{r} f(ct - r + R).$$

The excess pressure in the fluid is given by the expression

$$\Delta p = p(r, t) - p_0 = -\varrho \frac{\partial \varphi}{\partial t} = -\varrho \frac{Ac}{r} f'(ct - r + R)$$

(the prime denotes differentiation with respect to the argument).

The radial velocity is

$$v = \frac{\partial \varphi}{\partial r} = -\frac{A}{r^2} f(ct - r + R) - \frac{A}{r} f'(ct - r + R).$$

Noting that $-\varrho \varphi(r, t) = \int_0^t \Delta p(r, t) dt$ and using the expression for the radial velocity, we derive the known expression

$$v(r, t) = \frac{\Delta p(r, t)}{\varrho c} + \frac{1}{\varrho r} \int_0^t \Delta p(r, t) dt.$$

Now we establish the relationship obeyed by mass m after impact. Considering, due to smallness of Ω , the motion along the axis of symmetry, we have the equation of motion

$$m \frac{dv}{dt} = -\Delta p(R, t) S$$

The impacted surface is $S = R^2 \Omega$, the induced mass is $\varrho R^3 \Omega$, and $\mu = \frac{\varrho R S}{m}$ is the ratio of the induced mass to the mass of the impacting body. Using the expression $m[v_0 - v(R, t)] = S \int_0^t \Delta p(R, t) dt$ and the expression for $v(R, t)$, and setting $\tau = \frac{ct}{R}$, we have the equation

$$\frac{dv}{d\tau} + (1 + \mu)v - v_0 = 0 \quad (4.55)$$

The solution of this equation with initial conditions $t = 0$ and velocity $v = v_0$ is

$$v = \frac{v_0}{1 + \mu} (1 + \mu e^{-(1+\mu)\tau}). \quad (4.56)$$

It is found that if on contact $v = v_0$, then with time, as the wave front moves deeper into the fluid, $v \rightarrow \frac{v_0}{1 + \mu}$, which corresponds to the case of "hard" impact. Obviously, as in Section 21, the kinetic energy of the body as $t \rightarrow \infty$ is

$$E = m \frac{v_0^2}{2} \cdot \frac{1}{(1 + \mu)^2}.$$

The kinetic energy of the fluid is

$$T = m \frac{v_0^2}{2} \cdot \frac{\mu}{(1 + \mu)^2}.$$

and the "lost" energy is

$$E_{\text{lost}} = m \frac{v_0^2}{2} \cdot \frac{u}{1 + \mu}.$$

We shall show that the "lost" energy is equal to the sum of the potential and kinetic energies carried away by the shock wave. The potential energy of compression of a volume of fluid is $\frac{\kappa s^2}{2}$, and the kinetic energy is $\frac{\varrho u^2}{2}$,

where $u = \frac{\Delta p}{\varrho c}$, while the pressure in the acoustic wave at $r = R$ is

$\Delta p = \varrho_0 c v_0 e^{-(1+\mu)\frac{ct}{R}}$. Calculations yield

$$E_{\text{lost}} = S \int_0^{\frac{ct}{R}} \left(\frac{\kappa s^2}{2} + \frac{\varrho u^2}{2} \right) d(ct) = m \frac{v_0^2}{2} \cdot \frac{\mu}{1 + \mu} (1 - e^{-2(1+\mu)\frac{ct}{R}}).$$

As was pointed out, the "lost" energy as $ct \rightarrow \infty$ does not depend on the value of c . Postulating that the fluid is incompressible, we assume that the speed of sound is infinite. This eliminates the previously mentioned "paradox."

The above case is of interest only as an example for gaining insight into the process of impact. Actually impact of a body on a fluid is accompanied by generation of shock waves which move into the fluid as well as into the body. For bodies of complex configuration these shock waves are partially reflected from structural elements and set the impacting body into complex oscillations. The study of oscillations of a body and conditions of its strength on impact on water is a complex scientific and engineering problem.

24. Limiting cases of motion

Experiments were carried out in which a disk with a very small mass was shot out perpendicular to the water surface in such a manner that it impacted on the surface over its entire plane. The experiments were carried out in two versions. In the first a spike was placed in the water, at small depth, below the center of the disk. This spike stopped the disk when the latter hit it. In the second version the spike was removed. High-speed photography showed that after hitting the spike (first version) a spray sheet rises from the edges of the disk and a cavity forms behind the latter. After the disk stopped, the cavities tore away from the disk and within a short time the cavity became almost spherical. When the spike was taken away (second version) the disk removed some of the surface of the cavity, the shape of which also tended to become spherical with time. Analysis of experimental data showed that the kinetic energy $\rho \pi R^3 \dot{R}^2$ corresponding to inertial expansion of a hemisphere remains virtually constant during the entire expansion of the spherical cavity, and equal to the kinetic energy lost by the disk.

The problem of the limiting motion of a light disk of mass m_0 and radius R_n at the boundaries of the cavity was solved theoretically. For a near-spherical axisymmetric cavity the deviation of its spherical coordinates from a sphere with radius R can be expressed by a series in the form $r - R = \xi_1 P_1(\cos \vartheta) + \dots + \xi_n P_n(\cos \vartheta)$, containing Legendre functions. The velocity potential is also expressed by a series containing functions of the form

$\frac{1}{n+1} \cdot \frac{R^{n+2}}{2^{n+1}} P_n(\cos \vartheta)$. Retaining only semiquadratic terms in the pressure

equation, defining the velocities as $v_n = \xi_n + 2 \frac{\dot{R}}{R} \xi_n$ and using the equation of motion of a disk, we can find an approximate solution to the problem in the form of equations:

$$\frac{3}{2} \dot{R}^2 + \left(R + \frac{m_0}{2n\rho R^2} \right) \ddot{R} = 0;$$

$$R \ddot{\xi}_n + 3 \dot{R} \dot{\xi}_n + (1-n) \ddot{R} \xi_n = -(n+1)(2n+1) \frac{m_0 \ddot{R}}{2n\rho R^2}.$$

Since we considered cavities in the lower half-space (impact through a hole in a screen), the second equation is valid only for even n .

Without dwelling on the details of the solution, we only point out its results: a) the cavity shape tends to spherical as the body penetrates deeper into the fluid, when the body and fluid are weightless, while the pressure inside the cavity is equal to that in the quiescent fluid; b) the induced mass of a disk at the boundaries of an expanding cavity increases in proportion to the bubble [cavity] radius R ; c) as the cavity shape tends to spherical, the travel of the disk center is greater than the bubble radius by an amount tending to $\frac{m_0}{\pi \rho R_n^2}$.

The general methods and specific equations presented in this chapter allow one to calculate the hydrodynamic forces acting on immersing bodies. In addition to forces, it is also possible to calculate approximately the flow and the shape of the free surface. It is of importance that the integral effects, as the total forces, momenta and energy, do not depend markedly on the potential distribution over the surface of the body, but instead it is necessary to select a flow pattern which satisfies all the general equations and physical conditions within certain flow regions. This pertains particularly to the spray root.

Consideration must be given to the important features of free-boundary flows. The most important of these consists in the fact that the potential is "accumulated" at the moving free boundaries during the entire motion. Hence a free-boundary flow cannot in general be stopped or induced instantaneously and is not determined uniquely by the value of normal velocities at the boundaries of a moving body. The induced mass has the same physical sense as in the case of bodies fully immersed in an infinite fluid; the magnitude of the associated mass is no longer a universal constant for a given body but depends also on the history of the motion. An ideal incompressible fluid with free boundaries can be treated as a system of material points with ideal constraints, but in general these constraints are not holonomic. The displacements of the body are no longer generalized coordinates in the Lagrange equations, and the application of these equations is in general impossible.

Obviously, features of free-boundary flows must be taken into account in solving specific problems. In spite of the fact that above we considered constant-pressure free boundaries, the same considerations apply to a greater or lesser extent to any surfaces of discontinuity moving from the surface of a body into a fluid.

Chapter Five

DEVELOPED CAVITATION

Developed cavitation arises behind bodies rapidly immersed into a fluid or moving within a fluid at sufficiently high velocities; developed cavitation sets in also at moderate velocities, if gas is injected at the rear of the body.* A detailed physical description and analysis of mechanical aspects of the development of cavitation and, in particular, of developed cavitation are given by Sedov /19/.

Since it is generally impossible to obtain exact solutions to individual problems, the subsequent presentation is based on approximate estimates, supported by experimental data. The gist of what follows was presented in /14/, where the main experimental data are also given.

A developed cavity behind a body when observed visually appears to be formed in its leading part by smooth free jets separating from the body surface. Only in the trailing part of the cavity, where its boundaries join, does one see a bubbling foam mass, which is carried away from the cavity together with the gas and vapor. It was found by high-speed photography with small exposure times that the cavity boundaries, even in the leading part, are hardly ever particularly smooth; they are mottled by small disturbances, projections and droplets. Hence below, in our study of "macroproperties" of cavities, these will be schematized by assuming the free boundaries in the leading part to be smooth. This representation corresponds to the ordinary formulation of jet flow problems.

An important physical characteristic of cavitation flow is the cavitation number, which is defined as the ratio of the pressure difference between the free stream (p_0) and the cavity (p_k) to the velocity head $q = \rho \frac{V^2}{2}$. The cavitation number is therefore $\sigma = \frac{2(p_0 - p_k)}{\rho V^2}$. Developed cavities, the major part of which is free of foam, form when $\sigma < 0.1 - 0.2$.

In fact developed cavitation phenomena are affected to some extent by viscosity, surface tension, boiling temperature, dissolved-gas content and, at very high velocities, fluid compressibility. However, for fluids, such as water, at velocities not exceeding several hundreds of meters per second, moderate body dimensions and temperatures far from the boiling point, all the above factors are practically inconsequential. This makes it possible to treat the fluid, in general estimates of mechanical properties of cavitation flows, as ideal and incompressible. A schematic of a cavity in a flow past a disk is shown in Figure 52.

* In the USSR, in 1945, Epshtein obtained developed cavitation by the injection of gas.

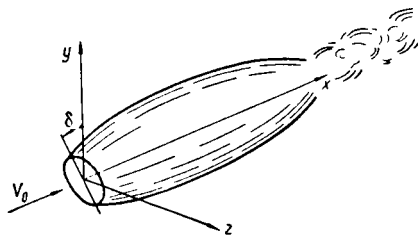


FIGURE 52.

1. Cavity drag

Experiments in cavitation [water] tunnels show that the drag coefficient of each body placed in a cavitation flow depends on the body shape and on the cavitation number. For bodies with smooth outlines (sphere, ellipsoid, etc.), Epshtein and Tseitlin noted that the line of streamline separation from a body surface is not given uniquely by specifying the body shape and cavitation number, and its location depends on the properties of fluid adhesion to a body, absolute flow velocity, and various other causes. The shifting of the separation line for bodies with smooth outlines somewhat affects the drag coefficient.

When the body has fixed streamline separation lines (disk, cone, etc.), the drag coefficient in an ideal incompressible and weightless fluid depends solely on the cavitation number:

$$c_x = \frac{W_0}{S_n \frac{V^2}{2}} = f(\sigma), \quad (5.1)$$

where the drag coefficient is referred to area S_n , bounded by the streamline separation line; for a disk with diameter $d_n = 2R_n$ this area is $S_n = \pi R_n^2$. The drag coefficient attains its maximum value at $\sigma = 0$ ($c_x = c_{x0}$); for a disk and cones, the flow past which occurs along the axis of symmetry, the values of c_{x0} are listed in Table 8.

TABLE 8.

β , deg	0	5	10	15	20	30	45
c_{x0}	0.82	0.78	0.75	0.715	0.68	0.607	0.465

Epshtein reduced experimental data and showed that the drag coefficient of a disk at nonzero cavitation numbers is expressed by the simple formula $c_x \approx c_{x0}(1 + \sigma) = 0.82(1 + \sigma)$. Apparently the same relationship applies for blunt-nosed cones, but for very sharp cones and wedges it is more proper to use Sedov's formula, $c_x \approx c_{x0} + \sigma/19$. Experimental data for a disk and cones can also be found in [29].

Special experiments showed that if the disk is inclined at angle δ to the undisturbed flow surface, then the pressure force acting normally on the disk is $W_n = W_0 \cos \delta$, where W_0 is the drag of the disk, the plane of which is perpendicular to the direction of the undisturbed flow. Quantity W_0 is obtained from (5.1). Projecting force W_n on moving x and y axes, lying in the plane of angle δ , we have

$$W_x = W_0 \cos^2 \delta; \quad W_y = W_0 \cos \delta \sin \delta. \quad (5.2)$$

Experiments show that expressions (5.2) are valid only for $\delta < 45-50^\circ$.

Note. The drag of a disk at $\delta=0$ can be calculated from Bernoulli's theorem, if the distribution $v_r(r)$ of radial velocities at the disk surface is known.

The drag, which is equal to the pressure difference at the leading and trailing surface of a disk with radius R_n , can be expressed in the form

$$W_0 = \int_0^{R_n} p 2\pi r dr - \pi R_n^2 p_k = \pi R_n^2 (p_0 - p_k) + \frac{\rho V_0^2}{2} \int_0^{R_n} \left(1 - \frac{v_r^2}{V_0^2}\right) 2\pi r dr.$$

To obtain agreement between this expression and the observational results of Epshtein we assume that $\frac{v_r}{V_k} = f\left(\frac{r}{R_n}\right)$ does not depend on the cavitation number, while the velocity at the cavity boundaries is $V_k = V_0 \sqrt{1+\sigma}$. Substitution of $f\left(\frac{r}{R_n}\right) = f(u)$ in the preceding expression for the drag yields

$$W_0 = \pi R_n^2 \frac{\rho V_0^2}{2} \left[(1+\sigma) \left(1 - \int_0^1 f^2(u) du\right) \right].$$

Function $\frac{v_r}{V_k} = f(u)$ can be expressed approximately by a parabola in the form $\frac{v_r}{V_k} = u^n$, selected so that $c_{x_0} = 1 - \int_0^1 f^2(u) 2u du = 0.82$; calculations yield $n = 4.55$. Fedorov's experiments with measuring the pressure distribution at a drained disk showed that the above velocity distribution is close to that actually observed.

2. Shape of an infinite axisymmetric cavity

Axisymmetric flow of an infinite fluid past a disk at $\sigma = 0$ corresponds to the well-known Kirchhoff two-dimensional free-streamline flow. However, in the two-dimensional case one can obtain an exact solution, while its corresponding axisymmetrical problem cannot be solved completely, and the cavity outline is known only approximately.

The shape of an axisymmetrical finite-drag half-body was studied independently by Gurevich /4/ and Levinson /1/. They derived the result that a half-body whose profile is $R = f(x)$, placed in an infinite parallel stream along its x axis of symmetry, can have a finite drag if at infinity ($x \rightarrow \infty$) the equation of the profile has the form $\tilde{R} = \frac{\sqrt{x}}{\sqrt{\ln x}} \text{ const.}$ Here the

constant is ≈ 1.34 if it is assumed that the disk radius is $R_n = 1$, while $\tilde{x} = \frac{x}{R_n}$ and $\tilde{R} = \frac{y}{R_n}$ are understood to denote the relative cylindrical coordinates of the contour.

Another derivation of the contour equation of an axisymmetrical cavity can be obtained from energy considerations. We can assume that the kinetic energy of absolute motion of a fluid per unit length of the cavity meridian is constant, and equal to the work of external forces which overcome the drag while the body travels through a unit path. For a uniformly moving body the cavity is treated as a wake, which contains the energy expended in overcoming the body drag. The specific energy content far past the body should be constant and its only form in the case under study should be kinetic.

When $\rho_k = \rho_0$ ($\sigma = 0$), the absolute velocity of boundary particle ξ is $v_0 = V_0 \sin \frac{\alpha}{2}$ while the normal velocity is $v_n = V_0 \sin \alpha = \dot{R}$, where α is the angle between the tangent to the cavity boundary and the x axis, and R and \dot{R} are respectively the distance from the x axis and the radial velocity of point ξ in its absolute motion (Figure 53).

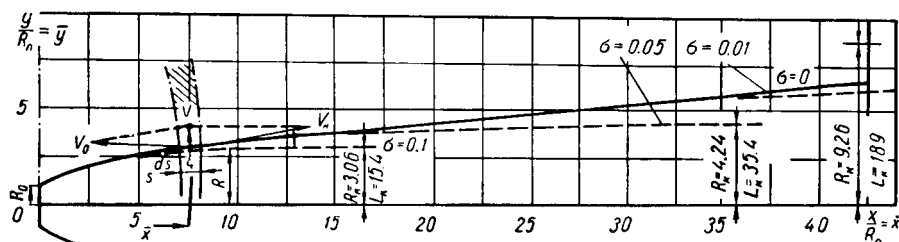


FIGURE 53.

The kinetic energy of the fluid within a flow tube starting from points s and $s + ds$ at the cavity boundary will, by assumption, be

$$dT = -\frac{e}{2} \varphi 2\pi R \dot{R} ds = W V_0 dt. \quad (5.3)$$

The relative velocity V_* of the boundary particle is equal to the translational velocity V_0 of the body; hence we can set $V_0 dt = V_* dt = ds$ in (5.3). The variable part of the potential at points in space coinciding with the boundary is $\varphi = -\frac{\Psi}{\pi Q} \cdot \frac{1}{RR}$. Substituting φ into boundary condition $\frac{\partial \varphi}{\partial t} + \frac{1}{2} v^2 = 0$, and replacing v by \dot{R} by virtue of the smallness of angle α , we have

$$-\frac{W}{\pi Q} \cdot \frac{d}{dt} \left(\frac{1}{P\dot{P}} \right) + \frac{1}{2} \dot{R}^2 = 0.$$

Hence

$$\dot{R} = \frac{\sqrt{\frac{W}{\pi Q}}}{R \sqrt{\ln R + A}}. \quad (5.4)$$

Constant of integration A can be determined if angle α at some point (R_1, x_1) is known. This condition is necessary in order that angle α at this point be small.

It was seen from processing photographs of the cavity formation behind a disk, that the profile of the leading part of the cavity

$\left(\frac{x}{R_n} < 3-5\right)$ can be expressed approximately as $R = R_n \left(1 + 3 \frac{x}{R_n}\right)^{1/3}$, and this expression is valid for small cavitation numbers ($\sigma < 0.1$).

Selecting $\frac{x_1}{R_n} = 2$ as a matching point we have $\frac{dR_1}{dx} \left(1 + 3 \frac{x_1}{R_n}\right)^{-2/3} = 0.274$ and $R_1 = 1.92 R_n$. Substitution into (5.4) yields $A = 0.845 - \ln R_n$. The cavity profile equation for $\frac{x}{R_n} > 2$ has the form

$$\frac{x}{R_n} = 2 + \sqrt{\frac{2}{c_{x0}}} \int_2^{\tilde{R}} \tilde{R} \sqrt{\ln \tilde{R} + A d \tilde{R}}, \quad (5.5)$$

where $\tilde{R} = \frac{R(x)}{R_n}$.

The numerical values of coordinates of the cavity profile calculated from formula (5.5) are listed in Table 9. The profile is shown to scale in Figure 53; theoretical and experimental data are compared in /4/.

TABLE 9.

$\frac{x}{R_n}$	0	0.5	1.0	2.0	5.0	7.5	10	15	20	25
$\frac{R}{R_n}$	1.0	1.36	1.59	1.92	2.57	2.95	3.30	3.85	4.35	4.8

Note. The matching point $\tilde{x}_1 = 2$ was selected arbitrarily. It would have been more natural to subject the solution with constant A to the condition that small variations in \tilde{x}_1 or \tilde{R}_1 do not change the value of A ; this condition corresponds to $\frac{dA}{d\tilde{R}} = 0$. The empirical equation of the profile yields the expression $\tilde{R}^{-2} = \frac{dR}{dx}$ which, after substitution into (5.4) and differentiation, yields a condition for determining the matching point $\frac{dA}{d\tilde{R}} = \tilde{R}_1 c_{x0} - \frac{1}{\tilde{R}_1} = 0$. This yields $\tilde{R}_1 = 1.1$. However, then the requirement that $\frac{dR}{dx}$ be small at the matching point is not satisfied.

3. Application of the momentum theorem to the determination of the drag and dimensions of a cavity

Some useful information on flows with developed cavitation can be obtained by applying the momentum theorem. Consider a steady axisymmetric cavity with nonzero cavitation number. We denote the pressure in the flow at infinity by p_∞ , which is higher than pressure p_* within the

cavity. The stream velocity at infinity is V_0 ; as a result of disturbances in the vicinity of the cavity the stream velocity components are $V_x = V_0 + v_x$ and $V_y = v_y$, where v_x and v_y are the perturbed velocities.

The contour of a physical cavity behind a body (mouthpiece) NN with wake form in the trailing part is shown by solid lines in Figure 54. The wake flow behind the cavity, consisting of foamy, bubbling fluid, vapor and gas or, in some cases, of a vortex system, affects the entire cavitation flow. This effect will be estimated later; at present we shall consider the Ryabushinskii model, when a symmetric cavity is formed between two identical mouthpieces NN and $N'N'$ (dashed lines), so that the cavity is symmetric relative to the plane KK .

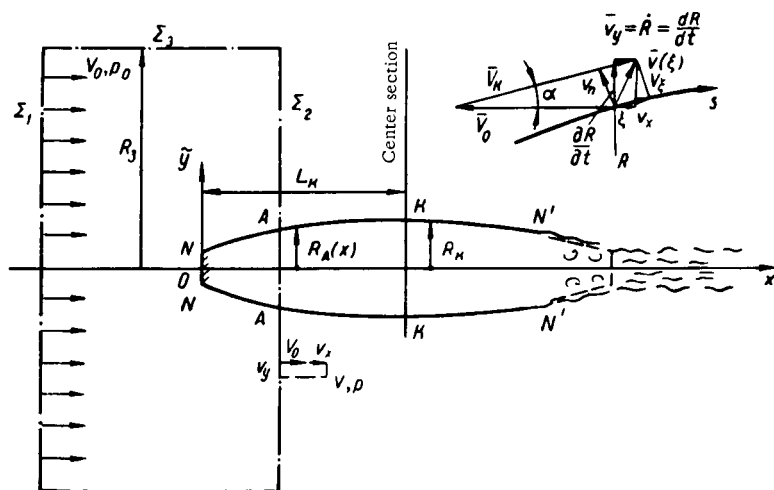


FIGURE 54.

We apply the momentum theorem to a control surface formed by infinite plane Σ_1 far ahead of the cavity and plane Σ_2 , intersecting the cavity along line AA . The momentum theorem takes the form

$$\dot{W}_0 = \int_{\Sigma_1} (\rho V_0^2 + p_0) d\Sigma_1 - \int_{\Sigma_2 - \pi R_A^2} [\rho (V_0 + v_x)^2 + p] d\Sigma_2 - \pi R_A^2 p_k. \quad (5.6)$$

Application of the Bernoulli theorem yields an expression for pressure p in plane Σ_2 at $\tilde{y} \geq R_A$:

$$p = p_0 - \rho V_0 v_x - \frac{\rho v_x^2}{2} - \frac{\rho \tilde{v}_y^2}{2},$$

where the perturbed radial velocity is given by $\tilde{v}_y^2 = v_y^2 + v_z^2$. By virtue of axial symmetry this velocity is identical at all planes passing through the x axis.

The continuity equation for the fluid region bounded by planes Σ_1 , Σ_2 and the cavity is

$$\pi R_A^2 V_0 = \int_{\Sigma_1 - \pi R_A^2} v_x d\Sigma_1.$$

Substitution of the expression for p and of the continuity equation into (5.6) gives

$$W_0 = S_x(p_0 - p_k) + \int_{S_x}^{\infty} \left(\frac{\rho \tilde{v}_y^2}{2} - \frac{\rho \tilde{v}_x^2}{2} \right) d\Sigma_2 = S_x \Delta p + I_y(x) - I_x(x). \quad (5.7)$$

For a specified value of $p_0 - p_k = \Delta p$ formula (5.7) expresses the drag W_0 in terms of the cross-sectional area of the cavity $S_x = \pi R_A^2$ and of the distribution of perturbed velocities v_x and \tilde{v}_y within the fluid in plane Σ_2 .

It is assumed in the derivation of (5.7) that planes Σ_1 and Σ_2 of the control surface extend to infinity. Actually, however, it is more correct to close the control surface by segment Σ_3 of the cylinder surface. Then the momen-

tum $- \rho \int_{x_1}^x \tilde{v}_y (V_0 + v_x) 2\pi R_3 dx$ should be added to the first part of (5.6), the flow rate $\int_{x_1}^x \tilde{v}_y 2\pi R_3 dx$ (where x_1 is the abscissa of plane Σ_1 and x is the abscissa of plane Σ_2) should be added to the right-hand side of the continuity equation. If we consider a finite cavity, then its effect at infinity is equivalent to a doublet, while the absolute velocity at distance r is of the order of $\frac{1}{r^2}$. If we maintain the difference $x - x_1$ constant and allow R_3 to increase without limit, then the integrals of segments of control surface Σ_2 will decrease as $\frac{1}{r^2}$ and can be neglected.

4. Corollaries of the momentum theorem

Obviously, drag W_0 of mouthpiece NN (Figure 54) does not depend on the abscissa of control surface Σ_2 . Hence if this plane is drawn through the maximum cross section KK of the cavity, we derive the known formula

$$W_0 = c_{x0} S_{\max} q (1 + \sigma) = S_k \Delta p - \int_{S_k}^{\infty} \frac{\rho v_x^2}{2} d\Sigma_2 = S_k \Delta p k. \quad (5.8)$$

The drag coefficient referred to the maximum cross section of the cavity is $c_{xk} = \sigma k$. In formula (5.8) $k = 1 - \frac{1}{S_k \Delta p} \int_{S_k}^{\infty} \frac{\rho v_x^2}{2} d\Sigma_2$. It is usually assumed that $k = k(\sigma)$; however, the calculations using this function are insufficiently reliable. Theoretical estimates with the aid of sources and sinks show that $0.875 < k < 1.0$. Reichardt obtained experimentally $k \approx 1.0$ for $\sigma < 0.1$. Epshtein assumes that for low σ , $k \approx 0.9$. According to the present author, $k = 0.96 - 1.0$. It should be noted that experimental determination of k from results of experiments beneath the free surface by the method of low-velocity

cavitation involves certain difficulties. The so-called "surfacing" of a cavity results in some increase in its diameter; a large-diameter cavity in the vicinity of the free surface deforms the latter and produces optical distortions which result in an apparent increase in diameter. Experiments with immersions of $\frac{H}{d_n} \approx 15-30$ and Froude numbers $Fr = \frac{V_0}{\sqrt{gd_n}} = 12-19$ showed that k is close to unity as $\sigma \rightarrow 0$. Subsequently k will be regarded as close to unity ($k \approx 0.96-1.0$).

Formula (5.8) yields an expression for the maximum cavity cross section

$$S_k = S_n \frac{c_x}{k\sigma} = \frac{W_0}{k\Delta p} \quad (5.9)$$

which can be used to calculate the diameter of an axisymmetric cavity

$$D_k = d_n \sqrt{\frac{c_{x0}(1+\sigma)}{k\sigma}}.$$

The theoretical results and data obtained experimentally by this author are compared in Figure 55. The experimental data were obtained for different depths of disk immersion: $\frac{H}{d_n} = 16-30$ (1), $\frac{H}{d_n} = 15$ (2), and $\frac{H}{d_n} = 3$ (3). Due to deformation of the free surface and optical distortions the cavity diameter is overestimated for small σ .

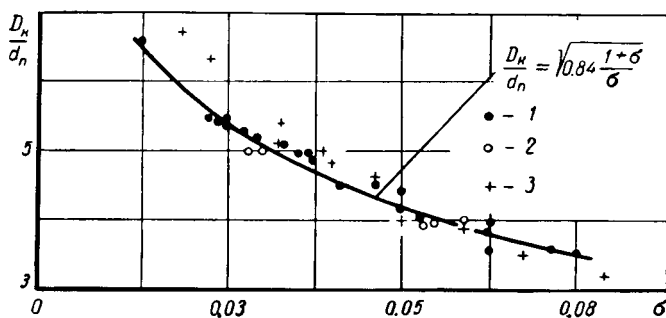


FIGURE 55.

We considered only axisymmetric flow. However, the momentum theorem can also be used for calculating the effect of an asymmetric flow subjected to gravity or lift forces.

5. General equation for cavity expansion

It is impossible to obtain an exact equation for the profile of an axisymmetric cavity. However, since cavities at low σ are highly elongated it is possible to derive an approximation equation for their profile. Let us follow the expansion of some cross section $S_x(t)$ of a cavity within stationary

where allowance is made for the fact that the velocity potential at the cavity boundary is $\varphi = - \int_R^{\infty} \tilde{v}_y \tilde{y}$.

Expression (5.7) of the momentum theorem contains the integral $I_x(x)$, which is taken into account by the expression $k_x = 1 - \frac{I_x(x)}{\Delta p S_x}$, which takes on the value of k at the maximum cross section of the cavity. It can be shown that along any straight line, parallel to the x axis and at a distance from it larger than R_k , velocity v_x attains its maximum in the plane of the maximum cross section of the cavity. Hence we shall assume that in the central part of the cavity $k_x \approx k$, and since the value of k is close to unity k_x is also close to unity. Quantities k and k_x serve as correction factors.

Expression (5.7) of the momentum theorem can now be expressed in the form

$$\frac{W_0}{k} = \Delta p S_k(t_k) = \Delta p S_x(t) - \frac{1}{2} \varrho \Phi(t) \frac{\partial S_x}{\partial t} \Phi(t). \quad (5.10)$$

Here, in addition to the above, it is assumed that $\frac{k_x}{k} = 1$. "Correction" function $\Phi(t)$ has been introduced in order to replace the preceding inequality for $I_y(x)$ by

$$\frac{1}{k} I_y(x) = - \frac{1}{2} \varrho \Phi(t) \frac{\partial S_x}{\partial t} \Phi(t).$$

It is clear that $k\Phi(t) < 1.0$ along the entire cavity. As the cavitation number is decreased for a fixed velocity of a flow with $\Delta p \rightarrow 0$, the term $\Delta p S_x \rightarrow 0$ for all finite x . If it is further assumed that $\Phi(t) \rightarrow \frac{1}{k}$, then equation (5.10) is transformed into equation (5.3). Hence one may conclude that the "correction" function should depend on the cavitation number σ .

Since the expansion of section S_x is considered in the stationary plane Σ'_2 , then taking as the time origin ($t = 0$) the instant when this plane is passed by point (x_1, R_1) of the cavity we have $V_0 t + x_1 = x$, where the origin of x is set at the center of the disk (Figure 56).

Equation (5.10) has been derived for a steady axisymmetric cavity. However, this equation can be interpreted as a general energy equation. The sum of the potential $(\Delta p S_x = \frac{\partial U_0}{\partial x})$ and kinetic $(\frac{\partial T_0}{\partial x} = - \frac{1}{2} \varrho \Phi \frac{\partial S_x}{\partial t})$ energy per unit length of cavity is equal to the work of forces overcoming the drag as the body moves through the same unit length $(\frac{\partial E_0}{\partial x} = - W_0)$. This yields the approximate equation of the cavity

$$\frac{\partial}{\partial x} (U_0 + T_0 + E_0) = 0.$$

The velocity potential φ in the preceding equations can be calculated if the potential at a given point of the cavity surface is known. Since the cavity is symmetric relative to the maximum cross section, it can be assumed that for points $x = x_k = L_k$ (see Figure 56) $\varphi_k = 0$. For a steady cavity

$$\varphi(x) = - \int_s^{s_k} v_s ds = - \int_s^{s_k} (V_k - V_0 \cos \alpha) ds = - V_k (s_k - s) + V_0 (x_k - x), \quad (5.11)$$

where x_k and s_k are respectively the abscissa and length of arc of the maximum cross section, while x and s are the abscissa and length of arc of cross section S_x .

Potential φ can also be calculated by considering the absolute motion of points on contour s_x on the basis of the Cauchy-Lagrange integral

$$\frac{\partial \varphi}{\partial t} + \frac{1}{2} v^2 = \frac{\Delta p}{\rho}.$$

Derivative $\frac{\partial \varphi}{\partial t}|_{\text{stat}}$ or a stationary point in space is expressed in terms of derivative $\frac{\partial \varphi}{\partial t}|_{\text{move}}$ at the point moving together with the boundary by the expression $\frac{\partial \varphi}{\partial t}|_{\text{stat}} = \frac{\partial \varphi}{\partial t}|_{\text{move}} - \frac{\partial \varphi}{\partial y} \cdot \frac{dy}{dt}$, where $\frac{dy}{dt} = \frac{\partial R}{\partial t}$, since the points of the contour lie in the plane Σ_2 . Hence $\frac{\partial \varphi}{\partial t} = \frac{\Delta p}{\rho} + \dot{R} \frac{\partial R}{\partial t} - \frac{1}{2} v^2$. Integrating with respect to time and assuming $\varphi = 0$ when $t = t_k$ finally gives

$$\varphi(t) = -\frac{\Delta p t_k}{\rho} \left(1 - \frac{t}{t_k}\right) + \int_t^{t_k} \left(\dot{R} \frac{\partial R}{\partial t} - \frac{1}{2} v^2 \right) dt. \quad (5.12)$$

For a steady cavity expressions (5.11) and (5.12) are identical.

6. Approximation equation of the cavity profile and length

The simplest solution of equation (5.10) can be obtained by setting

$\varphi = -\frac{\Delta p t_k}{\rho} \left(1 - \frac{t}{t_k}\right)$ and taking the "correction" function equal to some constant, $\Phi(t) = \kappa$. In fact $\frac{dR^3}{R_k^2 - R^2} = \frac{\frac{2}{\kappa} du}{u}$, where $u = 1 - \frac{t}{t_k}$. The constant of integration should be found from the condition that the cavity contour passes through some specified point $R = R_1$ at $t = 0$. As a result

$$\frac{R^2 - R_k^2}{R_1^2 - R_k^2} = \left(1 - \frac{t}{t_k}\right)^{\frac{2}{\kappa}}. \quad (5.13)$$

The contour equation $R(t)$ and the derivative $\dot{R}(t)$ is found from (5.13):

$$R = R_k \sqrt[2/\kappa]{1 - \left(1 - \frac{R_1^2}{R_k^2}\right) \left(1 - \frac{t}{t_k}\right)^{2/\kappa}}; \quad (5.14)$$

$$\dot{R} = \frac{R_k^2}{R t_k} \left(1 - \frac{R_1^2}{R_k^2}\right) \frac{1}{\kappa} \left(1 - \frac{t}{t_k}\right) \left(1 - \frac{t}{t_k}\right)^{\frac{\kappa(1-\kappa)}{\kappa}}.$$

Here it is the absolute value $\left(1 - \frac{t}{t_k}\right)$ which is raised to the fractional power. Formulas (5.14) in this form make it possible to calculate the cavity profile also when $\frac{t}{t_k} > 1$, but usually when $\frac{t}{t_k} > 1.5$ the boundaries of the cavity are indeterminate, since they start breaking up and foam begins to form.

The second of formulas (5.14) can be used to determine the half-length of the cavity, more precisely, $l_k = V_{d,k}$. For this we match at $t = 0$ the contour expressed

by (5.14) with that of the leading part of the "empirical" cavity $R = R_n \left(1 + 3 \frac{x}{R_n}\right)^{\frac{1}{3}}$ which, as was noted in Section 2, is universal in the sense that at low x it does not depend on σ . As in Section 3, by selecting $x_1 = 2R_n$ as our matching point we obtain $R_1 = 1.92R_n$ and $RR' = \frac{R_n^2}{R}$. Using these conditions and employing (5.9) we have $\left(\frac{R_k}{R_n}\right)^2 = \frac{c_{x_0}(1+\sigma)}{k\sigma}$, and substitution into the second of formulas (5.14) at $t = 0$ yields

$$\frac{l_k \sigma}{R_n} = \frac{R_1}{R_n} \cdot \frac{c_{x_0}(1+\sigma)}{k} \left(1 - \frac{R_1^2 k \sigma}{R_n^2 c_{x_0}(1+\sigma)}\right) \frac{1}{x}.$$

If the abscissa of the matching point is $x = x_1$, then the cavity half-length is $L_k = l_k + x_1$, in which case

$$\frac{L_k \sigma}{R_n} = \left\{ \frac{R_1}{R_n} \frac{c_{x_0}}{k} + \sigma \left(\frac{R_1}{R_n} \frac{c_{x_0}}{k} - \frac{R_1^3}{R_n^3} + \frac{x_1}{R_n} \kappa \right) \right\} \frac{1}{x} = a - b\sigma. \quad (5.15)$$

Calculation of constants a and b requires selecting the "correction" factor κ and matching point $R_1 = R(x_1)$ on the cavity contour at $\sigma = 0$, or if $\frac{x_1}{R_n}$ is a small quantity, at the "empirical" contour $R = R_n \left(1 + 3 \frac{x}{R_n}\right)^{\frac{1}{3}}$. In principle the matching point should be selected so as to satisfy the condition $\frac{dL_k}{dx_1} = 0$, since the cavity length cannot depend on the purely arbitrary point (x_1, R_1) . If we select $x_1 = 2R_n$ and $\kappa = 0.85$, then the experimental data will be satisfactorily expressed by (5.13), as is evident from Figure 57, taken from [4]. Under these conditions one obtains to some degree of approximation the expression $\frac{L_k \sigma}{R_n} = 1.92 - 3\sigma$, which is compared with experimental data in Figure 58.

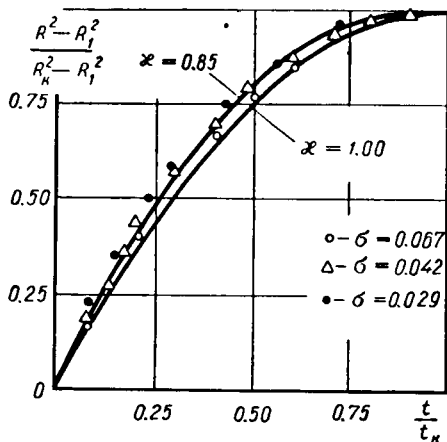


FIGURE 57.

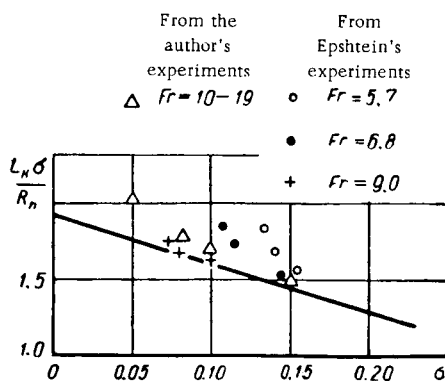


FIGURE 58.

Figure 53 shows the outlines of a cavity at $\sigma = 0.1$, $\sigma = 0.05$ and $\sigma = 0.01$ calculated from formulas (5.14) at $\kappa = 0.85$, $\bar{x}_1 = 2$. When the cavity is not formed behind a disk but past some other symmetric body, such as a cone, formulas (5.14) are also valid, but then a and b should be calculated for the specific case, since L_k will now be somewhat different.

The values of coefficients a and b in (5.15) can be calculated also from other considerations, as well as by reduction of experimental data. Values of $a = 1.53$ and $b = 0.42$ were obtained in 1952 from the potential distribution along boundaries of the cavity and disk [4]. On the basis of his experiments at low relative velocities for a weightless fluid, Epshtein recommends the formula

$$\frac{L_k \sigma}{R_n} = 1.67 \sqrt{\frac{c_{x_0}}{k}}.$$

All studies yield an estimate of the cavity half-length in the form

$\frac{L_k \sigma}{R_n} = a - b\sigma$; according to different sources, coefficients a and b have different but close values (see Figure 58).

7. Cavitation energy

Differentiating the sum of specific potential and kinetic energies $U' + T'$ along the cavity axis and adding to it the kinetic energy of the fluid along a streamline-formed surface separating from the disk edges and equal to $m^* \frac{V_0^2}{2}$ we obtain the total energy

$$E = \int_{L_k} (U' + T') dx + m^* \frac{V_0^2}{2}.$$

For a highly elongated cavity ($\sigma \rightarrow 0$) $E \approx W_0 L_k \approx k \Delta p S_k L_k$, i. e., the work expended by the external energy source in overcoming the drag W_0 is spent on statically expanding the cavity to a volume $O_k = \beta S_k L_k$ (β is the filling factor, the work is expressed as $U = \int_{L_k} U' dx = \Delta p O_k$) and on imparting kinetic energy $T = \int_{L_k} T' dx + m^* \frac{V_0^2}{2}$ to the fluid. Using the standard notation, we can express the kinetic energy in terms of the induced mass $\lambda_{11} = \frac{2T}{V_0^2}$ of the entire cavity.

Setting $k = 1$, we find for half the cavity

$$\lambda_{11} \approx q \sigma S_k L_k (1 - \beta) \approx q \frac{\pi}{2} R_n^3 \frac{1}{\sigma}. \quad (5.16)$$

The filling factor is $\beta = \frac{1}{S_k L_k} \int_{L_k} \pi R^2 dx$; integration of (5.14) yields the

value $\beta \approx 0.7$ as $\sigma \rightarrow 0$ and $\kappa = 0.85$. The expression on the right-hand side of (5.16) was obtained by substitution of S_k and L_k from (5.9) and (5.15).

The induced mass λ_{11} and the kinetic energy of absolute motion of the fluid about the cavity, expressed by this quantity, cannot be changed by instantaneously varying the motion of the disk. The cavity retains the "motion

The cavitation induced mass of the disk m^* is equal to $2.52 q R_n^3 / 4$.

history" of the body with its associated phenomenon of "heredity." Had a solid body been constructed which coincided with the cavity boundary, then the induced mass λ_{ii} for such a body would have had the usual meaning; the flow of the fluid and the kinetic energy T in this case would have been determined uniquely by the motion of the body.

It can be concluded from formula (5.16) that the longitudinal induced mass for elongated bodies coinciding with the boundaries of the disk and cavity is quite small: the volume of the induced mass, referred to the volume of the body, is approximately $\lambda_{ii}/\varrho O_k \approx 0.43\sigma$.

8. The principle of "independent expansion" of a cavity

The principle of "independent expansion" of a cavity consists in the following: each cross section of the cavity expands relative to the path of the body center almost independently of the subsequent or preceding motion of the body, and is governed by a relationship which depends only on the difference between the pressure at infinity and in the cavity, on the velocity, and on the dimensions and the drag of the body at the time it passes the plane of the cavity cross section under study. This postulate is essentially approximate and cannot be proven rigorously, but is more exact, the closer the body motion is to being rectilinear and uniform.

The preceding discussion is involved in the formulation of the independence principle; derivation of the law of expansion of an infinite cavity (Section 3) of a finite cavity (Sections 5 and 6) and, directly, the energy equation (5.10) for a given cavity cross section, which is just the formulation of the principle of independent expansion. Suppose we wish to establish the law of expansion of some cross section $S_x = S'_x(t - t_1)$ of a cavity, the plane of which was traversed by the body at time t_1 . At this time the body possessed dimension R_1 , velocity V_1 , drag W_1 , pressure in the cavity $\Delta p = \text{const}$, and fluid density ϱ . Applying formally the principle of independence, $S_x = \pi R^2(\xi, t)$ can be calculated from (5.14), which yields $R(\xi, t) = R_k f\left[\frac{W_1}{\varrho R_1^2 \Delta p}, \frac{t - t_1}{t_k}\right]$, where $R_k = \sqrt{\frac{W_1}{\pi \Delta p}}$, while t_k is found from the expression $\frac{2\Delta p t_k}{\varrho R_1 V_1} = a - b \frac{2\Delta p}{\varrho V_1^2}$, obtainable from (5.15).

This creates the impression that the principle of independence disregards entirely the effect of neighboring cross sections $\xi_1, \xi_2, \dots, \xi_n$ of the cavity on the motion of section ξ under study. In fact, the motion of cross section ξ is affected, in addition to quantities R_1, V_1 and W_1 corresponding to the time of passing of cross section ξ , also by the motion of the adjoining layers. In principle this effect can be expressed by some "correlation function," which takes into account the effect of deviations in the radius of the body, velocity and drag on R_1, V_1 and W_1 during the preceding and subsequent times. When using formulas (5.14) and (5.15) to calculate an unsteady cavity on the basis of the independence principle we simply assume that the correlation function for an unsteady cavity remains the same as it was for the steady cavity. We shall now illustrate some applications of the principle of independence.

1. Suppose a disk moves in a straight line with constant acceleration $\frac{dV}{dt} = w$ and that at time t_0 it has velocity V_0 . Had this velocity remained constant, then over a period $t = t_1 - t_0$ the disk would have moved distance $x_1 = V_0 t$ from section S_1 under study; this can be determined, for example, from (5.14). Since it moves with some acceleration, the disk will actually travel a distance $x_1' = V_0 t + \frac{wt^2}{2} = x_1 \left(1 + \frac{w x_1}{2V_0^2}\right)$, when the law governing the expansion of S_1 remains the same as for motion with constant velocity ($V = V_0$). Hence the cavity is more elongated during acceleration and more compressed during retardation.

In actual calculations it is required to find for points $x_1, x_2, x_3, \dots, x_i$ traversed by the body the velocities $V_1, V_2, V_3, \dots, V_i$ and times $t_1, t_2, t_3, \dots, t_i$ at which these points are traversed. The expansion of the cross section at path point x_i can be obtained from (5.14) by substituting for t the difference $t - t_i > 0$. The time of complete expansion t_{kt} can be found from the expression

$$t_{kt} = \frac{q R_n V_i}{2 \Delta p} \left(a - b \frac{2 \Delta p}{q V_i^2} \right) \quad (5.17)$$

The maximum cavity radius is obtained from

$$R_{kt} = \sqrt{\frac{W_i}{\pi k \Delta p}}.$$

and the radius of the cross section from

$$R_i(t - t_i) = R_{kt} f\left(\frac{R_{kt}}{R_n}, \frac{t - t_i}{t_{kt}}\right);$$

the form of the function, on the basis of the independence principle, remains the same as for a steady cavity.

2. For a disk moving in a curved path but with constant speed, the contour of a steady cavity is constructed with the path treated as the body axis. The cavity for accelerated motion over a curved path is constructed in Figure 59. Experimental checks of the independence principle under different conditions have always yielded satisfactory results [4].

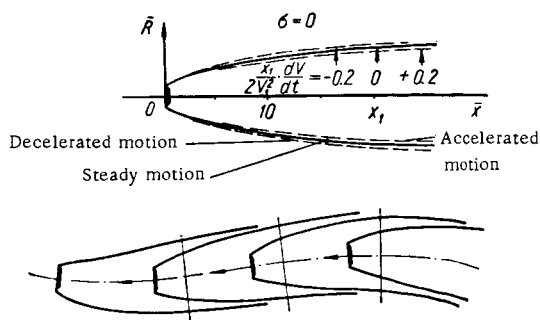


FIGURE 59.

On impact acceleration or stopping of the disk the boundaries of the cavity at the disk break up and are highly distorted; farther parts of the cavity remain, for some time, the same as if the disk would have continued moving /4/.

9. Cavity sealing and wake flow

The cavity at its central part is approximately symmetric relative to its maximum cross section. Hence in the theoretical calculation of the cavity contour the ratio $\frac{t}{t_k}$ can range from zero at the matching point (x_1, R_1) to approximately 1.5; at high $\frac{t}{t_k}$ the cavity is usually very agitated, filled with spray and foam, which is ejected from the region of wake formation. However, the length of a "smooth" cavity, free of spray and foam, is not fully defined and depends to a large extent on the conditions of formation and conditions of sealing of the cavity.

From the standpoint of the principle of independence the formation of a cavity can be schematized as follows. A body upon passing through some stationary plane generates an elementary cavity which expands by inertia, overcoming the external excess pressure $\Delta p = p_0 - p_k$. After some time (t_k) the kinetic energy supply is exhausted, the cavity attains its maximum cross section, after which the cavity starts narrowing down due to pressure Δp . This compression distorts the cross section and wake flow forms as a result of collision of the opposing boundaries.

Experiments show that the trailing part of the cavity is essentially unsteady; it periodically stretches and contracts, leaving behind eddy clusters of various dimensions, containing bubbles of gases ejected from the cavity. It is interesting to note that the theoretically postulated reentrant-jet model does not represent the actual flow pattern within the cavity, apparently due to the inherent instability of this type of flow. However, if a high-speed motion picture is taken of the trailing part of the cavity and then projected at the usual speed, one notices the periodic appearance and disappearance of reentrant jets, which flow forward from the cavity sealing region.

In a heavy fluid even the leading part of the cavity does not remain symmetric; its cross sections are distorted and the cavity rises somewhat. Under certain conditions hollow vortices form in the trailing part of a free cavity which does not close at some solid body. The generation of these vortices, which are not always visible, occurs also in flows past an inclined disk or other body, i. e., at the onset of lift. The rate of gas ejection from a cavity depends on the flow pattern which develops in its trailing part.

10. Structural details of cavities in a heavy fluid

The structure of cavities in a heavy fluid, in a gravity field with gravitational acceleration g , differs somewhat from that of the previously discussed cavities in a weightless fluid. The most elementary considerations show

that a cavity with volume O_k should have a buoyancy lift of $A_v = \rho g O_k$. However, a constant pressure p_k acts within the cavity, and the projection of resultant pressure forces at the boundaries of the cavity and disk along the y axis is found to be zero. The Bernoulli equation, composed for streamlines extending along the top and the bottom boundaries of a cavity, yields

$$p_0 + \frac{\rho V_0^2}{2} = \underbrace{p_k + \frac{\rho V_1^2}{2} + \rho g y_1}_{\text{Top } y_1 > 0} = \underbrace{p_k + \frac{\rho V_2^2}{2} + \rho g y_2}_{\text{Bottom } y_2 < 0},$$

and hence the tangential velocity $V_2 > V_1$ and a velocity circulation $\Gamma = \oint v_s ds$ 131a takes place about the cavity. The lift of cavity layer dz is, according to Zhukovskii's formula, $\rho \Gamma V_0 dz$; this force acts downward on the cavity and is balanced by the buoyancy force $\rho g S^* dz$, where S^* is the area of the section cut in the cavity by plane x, y (Figure 60). From these considerations $\Gamma = \frac{g S^*}{V_0}$. A similar result is obtained from the Bernoulli equation.

Since $\frac{V_1 + V_2}{2} (V_1 - V_2) + g(y_1 - y_2) = 0$, $d\Gamma \approx (V_2 - V_1) dx$, introduction of the average velocity $V_{av} = \frac{1}{2} (V_1 + V_2)$ and integration over the entire length of the cavity gives the expression

$$\Gamma \approx g \int_L \frac{(y_1 - y_2)}{V_{av}} dx \approx \frac{g S^*}{V_0}. \quad (5.18)$$

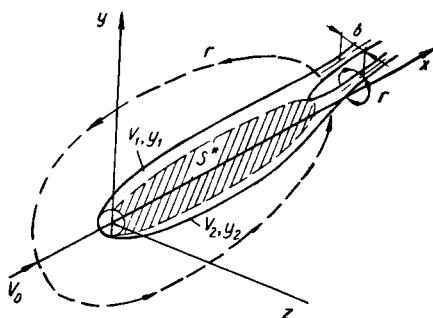


FIGURE 60.

The velocity circulation over any fluid contour encompassing each wake vortex is clearly also Γ . Actually it is quite immaterial what form is taken by the wake of the cavity, whether hollow vortices or a mixture of gas and liquid. The onset of velocity circulation Γ around a cavity in the longitudinal plane x, y also brings about the appearance of such a circulation along the contour embracing completely the single-valued wake. The circulation along a contour embracing the entire wake is zero.

Had two vortex filaments (of zero diameter) formed behind the wake, then the distance between them b_r would have been obtained from Zhukovskii's theorem, since $A_v = \rho \Gamma b_r V_0$, and from formula (5.18) $b_r = \frac{O_k}{S^*}$. These vortex

filaments would have absolute velocity $v_r = \frac{r}{2\pi b_r}$ far from the cavity, and the sine of the angle made by the filament axes with the x axis would be $\frac{v_r}{V_0}$.

The above relationships were used by Cox and Clayden /27/ and subsequently by Epshtein /7/ as a basis for the theory of loss of gas along vortex filaments. It should, however, be remembered that in the case of hollow filaments or a finite eddy region past the cavity the expressions for b_r and v_r are different.

The dimensionless criterion for the effect of fluid downstream from weight on cavitation flow can be expressed by the ratio of the drag W_0 , which virtually does not depend on weight, to the force A_v , which is entirely due to fluid weight:

$$\frac{W_0}{A_v} \approx \frac{V_0}{g d_n} \sigma^2 = \sigma^2 Fr^2. \quad (5.19)$$

The Froude number is based on the mouthpiece diameter d_n ($Fr = \frac{V_0}{\sqrt{g d_n}}$) and does not at all describe the effect of fluid weight for developed cavitating flows.

Another criterion for the effect of weight (which, however, is related to the first criterion) could be the minimum cavitation number σ_{min} . In order that a dynamic pressure minimum would not exist within the fluid it is necessary that the dynamic pressure gradient at the cavity boundaries should coincide with the normal directed into the fluid. To satisfy this condition we required $V_1 \geq V_0$ at point y_{1max} . Referring the static pressure p_0 of the free flow to the center of the disk and expressing the cavitation number as $\sigma = \frac{p_0 - p_k}{\frac{\rho V_0^2}{2}}$, we obtain

$$\frac{\rho V_0^2}{2} (1 + \sigma) = \frac{\rho V_0^2}{2} \left(\frac{V_1^2}{V_0^2} + \frac{2gy_1}{V_0^2} \right).$$

In the limiting case when $V_1 = V_0$ and $2y_{1max} = D_k$, the minimum cavitation number is

$$\sigma_{min} = \frac{g D_k}{V_0^2}. \quad (5.20)$$

Relationship (5.20) is equivalent to the condition $p_0 - p_k > \rho g R_k$; for gaseous cavitation, no matter how large the volume of gas injected, the actual cavitation number σ will always be larger than σ_{min} . It is shown below that the ratio $\frac{g L_k}{V_0^2}$ is also convenient for describing the effect of fluid weight.

11. Rising of the cavity

A cavity moving in a heavy fluid deforms and its axis acquires a curvature. Upward curving of the axis is equivalent to rising of the cavity; in the first approximation this effect can be estimated quite simply. Considering the transverse motion of unit length of a cavity

with radius R and assuming that the transverse flow is equivalent to the flow past a cylinder, we find the "momentum" $q\pi R^2 V_v$ of unit length of cavity, which should be equal to the momentum of the buoyancy forces $qg\pi \int_0^1 R^2 dt$. Thus, the vertical rise rate is $\dot{h} = V_v = \frac{g}{R^2} \int_0^1 R^2 dt$, and the extent of the rise of the cavity center relative to the center of the disk is $h = \int_0^1 V_v dt$. For a steady cavity, since $dx = V_v dt$, we have

$$\frac{V_v}{V_0} = \frac{dh}{dx} = \frac{g}{V_0^2} \cdot \frac{1}{R^2(x)} \int_0^x R^2(x) dx = \frac{gO_k(x)}{V_0^2 \pi R^2(x)},$$

where $O_k(x)$ is the cavity volume along the longitudinal-axis segment extending from 0 to x . It is possible to find some value $x = x_1$ from the consideration that $\frac{1}{x_1} O_k(x_1) = \pi R^2(x_1)$, where $x_1 > L_k$. Obviously, for all $x < x_1$ we have $h' < \frac{gx}{V_0^2}$ and the rise is $h < \frac{gx^2}{2V_0^2}$.

The cavity rise can be calculated more precisely from (5.14):

$$h = \frac{g}{\pi V_0^2} \int_0^x \frac{O_k(x)}{R^2(x)} dx. \quad (5.21)$$

In the coordinate system x, y with origin at the center of the maximum cavity cross section at $x = 1$ and $\frac{R_1^2}{R_k^2} \rightarrow 0$ (for very small σ) the rise can be calculated from the expression

$$h = \frac{gL_k^2}{V_0^2} f\left(\frac{x}{L_k}\right) \approx \frac{gL_k^2}{V_0^2} \left\{ \frac{2}{3} \ln \frac{2}{1-\zeta^2} + \frac{1}{6} (\zeta^2 - 1) \right\}, \quad (5.22)$$

where $\zeta = \frac{x}{L_k}$, and integration in (5.21) is carried out from $\zeta = -\sqrt{1 - \frac{k_0}{c_x}}$.

Table 10 lists calculated values of the relative rise $\bar{h} = \frac{h}{\frac{gL_k^2}{V_0^2}}$, calculated from formula (5.22) in a coordinate system with origin at the disk center ($x = x_0 + L_k$).

TABLE 10.

$\frac{x}{L_k}$	0	0.5	1.0	1.5	1.9
$f\left(\frac{x}{L_k}\right) = \bar{h}$	0	0.068	0.293	0.785	1.97
$\frac{1}{2} \left(\frac{x}{L_k}\right)^2 = \bar{h}_{est}$	0	0.125	0.500	1.220	1.81

Some remarks are called for on the physical nature of cavity rising. First, the above calculation of rising assumes that each section expands according to the same laws as in a weightless fluid. In fact,

the mean pressure Δp decreases as the cavity continues to rise and the law governing the expansion of the cross section will be somewhat different. Secondly, the cavity cross section deforms during rising, and a neck forms in the bottom part and breaks up into spray and foam in the sealing region. As a result of these factors the above calculation of cavity rise should be treated as an approximation, valid over approximately $\frac{2}{3}$ of the total cavity length. The results of computations are shown in Figure 61.

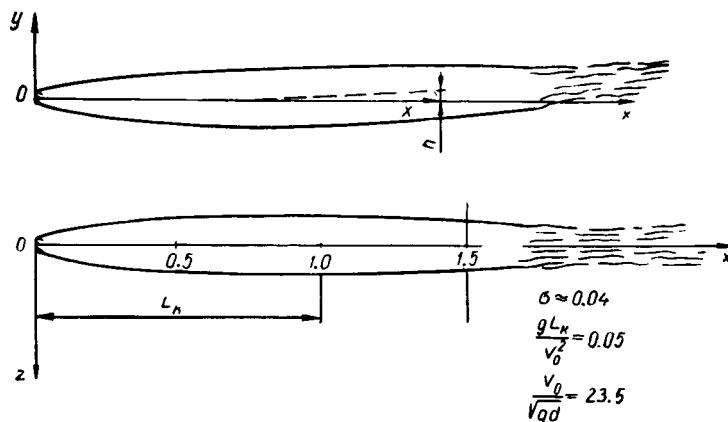


FIGURE 61.

Note. Taking note of the imperfection of the above theory of rising as applied to the trailing part of the cavity, Epshtein suggested that this phenomenon be approached from the viewpoint of the linear theory of wings with small aspect ratios. However, he failed to note that the linear theory of such wings is based on the very same momentum theorem; hence $qgO_k(x) = [q\pi R^2(x) V_y(x)]V_u$, which yields the previous formulas.

12. Cavity downwash in asymmetric flow

The lift W_y produced at a mouthpiece asymmetric to the flow results in downwash of the cavity. According to the momentum theorem, the lift momentum $W_y t$ produces an equal and oppositely directed wake momentum behind the body; for a cavity with circular cross section this momentum is approximately $V_0 t q \pi R^2 V_y$. This yields the expression for the inclination of the cavity axis

$$y' = \frac{V_y}{V_0} = - \frac{W_y}{q \pi R^2 V^2}. \quad (5.23)$$

For a steady cavity the expression for $R(x)$ is also obtainable from (5.14) and the linear travel is obtained by integrating equation (5.23):

$$h = \int_0^x y'(x) dx = -\frac{W_y}{\pi \rho V_0^2} \int_0^x \frac{dx}{R^2(x)}. \quad (5.24)$$

The formulas of this section are valid to the same degree as those of Section 11 for cavity rise. These conclusions cannot be applied directly to the rear of the cavity.

13. The general case of transverse motion of a cavity

The cavity motions examined in Sections 11 and 12 are the most elementary cases from a wide class of possible transverse deformations of a cavity. Transverse deformations are associated with rising and the onset of lift, as well as other perturbing factors. In order to show that this is so, we shall express the momentum theorem for the same control surface as was considered in Section 3 (see Figure 54), but shall now determine the force acting on the body and cavity along the y axis. Since the integrals of motion along control surfaces Σ_1 and Σ_2 do not yield force components along the y axis, we derive the following expression for the momentum flux:

$$W_y = \int_{\Sigma_1} \rho (V_0 + v_x) v_y d\Sigma - \int_{\Sigma_2} \rho (V_0 + v_x) v_y d\Sigma.$$

We recall that V_0 is the flow velocity at an infinite distance upstream, while v_x and v_y are perturbed velocities, which in this case refer to planes Σ_1 and Σ_2 .

When plane Σ_1 is moved upstream to infinity, if the flow at infinity is a doublet, the integral of $V_0 v_y$ at this plane will be zero. Even at the cavity boundaries $v_x \ll V_0$, and hence the integral of $V_0 v_y$ over plane Σ_2 can be neglected compared with the integral of $v_x v_y$.

The following should be noted as regards integral $\int_{\Sigma_2} v_y d\Sigma$. In Section 3 we considered axisymmetric flows, and hence velocity \tilde{v}_y was radial. In the case at hand we consider a flow and cavity symmetric relative to the x, y plane, and hence $W_z = 0$, while v_y is simply the vertical component of that part of the perturbed velocity which is due to asymmetry of the flow. Consequently, the integral $\rho \int_{\Sigma_2} v_y d\Sigma = K_y$ can be treated as the y component of the fluid momentum in a layer of unit thickness.

The transverse motion of a highly elongated cavity is now treated approximately by means of the principle of plane sections. As is known,

the momentum of a plane section is $K_y = -\rho \int \varphi \cos \theta ds + B_{y\infty}$, where

the integral designated as B_y is taken over the inner contour s of the cavity, formed by a section of the Σ_2 plane, while $B_{y\infty}$ is a similar integral, taken over an infinitely far contour embracing contour s (see Section 9 of

Chapter Two). By selecting an external contour in the Σ_2 plane it is possible to obtain the condition $B_{y\infty} = 0$.

Thus, the momentum theorem yields the approximate expression

$$W_y \approx qV_0 \int \varphi \cos \theta ds = -V_0 B_y. \quad (5.25)$$

Condition (5.25) should be satisfied for any section of the cavity cut by a plane parallel to the yz plane. Here, for a cavity with circular cross section $ds = R d\theta$, where θ is the angle between the positive y direction and the normal to the boundary at point s .

In flow past a disk at angle δ force W_y is directed upward (it is greater than zero), while the perturbed motion of the cavity is directed downward. When the cavity rises the hydrodynamic force is directed downward (opposing the buoyancy force), while the perturbed motion of the cavity is upward.

In order to gain a clearer insight into the perturbed motion of the cavity boundaries we shall consider this problem in more detail, assuming that the almost plane potential fluid flow in the transverse plane is generated as a result of small departures of the boundary from its initial circular cross section.

Above we replaced integral $I_y(x)$ by kinetic energy $T_0 = -\frac{1}{2} q \varphi \frac{dS_x}{dt} > I_y(x)$

within a flow tube. Now we denote the velocity potential at the cavity boundary, corresponding to radial expansion, by φ_0 . The perturbed motion and deformation of the cavity contour generate almost plane potential flow, for which the velocity potential, symmetric relative to the xy plane, can be represented by the series $\varphi_n = A_n r^{-n} \cos n\theta$.

We thus express the velocity potential of perturbed flow as

$\varphi = \varphi_0 + \varphi_1 + \varphi_2 + \dots + \varphi_n$. The potential $\varphi_1 = A_1 r^{-1} \cos \theta$ at cavity surface $r = R$ generates the normal velocity $v_1 = \frac{\partial \varphi_1}{\partial r} = -\frac{A_1}{R^2} \cos \theta$. If $A_1 = -R^2 V_y$, then potential φ_1 corresponding to a simple doublet will satisfy the kinematic boundary conditions for motion of the cavity without deformation of its circular cross section, with center velocity V_y . Integral (5.25) for φ_1 is equal to the momentum

$$B_y = -q \int_0^{2\pi} \varphi_1 d(R\theta) \cos \theta = q\pi R^2 V_y$$

and is zero for all φ_n , with the exception of φ_1 . Hence the momentum B_y of unit length of cavity is determined entirely by the motion of the cross section with area $S = \pi R^2$ as a nondeformed circle. This result shows that the estimated rise and downwash of the cavity examined in Sections 11 and 12 is valid irrespective of the deformation of the cavity cross section.

Denoting the radial rates of deformation of the cylinder by $\dot{\xi}_2, \dot{\xi}_3, \dots, \dot{\xi}_n$, we find that constants A_1, A_2, \dots, A_n satisfy the equation $A_n = -\frac{1}{n} R^{n+1} \dot{\xi}_n$, provided the deformations $\xi_2, \xi_3, \dots, \xi_n$ are zero.

The kinetic energy corresponding to each harmonic is given by

$$T_n = -\frac{q}{2} \int \varphi_n \frac{\partial \varphi_n}{\partial n} ds = \frac{\pi R^3}{n} \cdot \frac{q \dot{\xi}_n^2}{2}.$$

For the first harmonic

$$T_1 = \pi R^2 \frac{\rho V_y^2}{2}.$$

We now consider in more detail the case when the cavity axis is subject to downwash due to the onset of lift. Momentum $B_y = \rho \pi R^2 V_y$ along the cavity remains constant but, due to change in cavity radius R , the velocity V_y and kinetic energy of the fluid $T_1 = B_y \frac{V_y}{2} = \frac{W_y^2}{2V_0^2 \rho \pi R^2}$ vary. The approximate energy equation for a cavity subject to downwash by lift has, by analogy with equation (5.10), the form

$$W_x \approx \pi R^2 \Delta p + T_0 + \underbrace{\frac{W_y^2}{2V_0^2 \rho \pi R^2}}_{T_1} + \underbrace{\rho \pi R^2 \sum_{n=2}^{\infty} \frac{\dot{w}_n^2}{2n}}_{T_2 + T_3 + \dots} - I_x(x). \quad (5.26)$$

The average radius R satisfies the condition $\pi R^2 = S_x(t)$, where the cavity cross section is not necessarily a circle. Forces W_x and W_y for flow past an inclined disk are given by the formulas of Section 1; here the circular cross section of the cavity is deformed. The sum of perturbing energies $\sum T_n$ is not equal at the maximum cross section of the cavity (here it is postulated that $T_0 = 0$). Hence formula (5.9), relating the drag of a disk placed perpendicularly to the flow to the maximum cross-sectional area of the cavity $\pi R_k^2 = S_k$, is now invalid.

We assume that when the cavity streamlines separate from the disk ($t=0$) the entire lateral-motion energy $\sum_{n=1}^{\infty} T_n$ is given by the term $T_1(t=0)$. As the cavity cross section moves away from the disk, the energy is redistributed, the value of T_1 decreases, while the values of higher-order terms increase, but in such a manner that the sum $T_1 + T_2 + \dots$ remains constant and equal to $T_1(t=0)$ along the entire cavity.

Then, for any $t > 0$,

$$\frac{W_y^2}{2V_0^2 \rho \pi R^2(t)} + \rho \pi R^2(t) \sum_{n=2}^{\infty} \frac{\dot{w}_n^2}{2n} = \frac{W_y^2}{2V_0^2 \rho \pi R_n^2} = T_1(t=0).$$

The drag and lift coefficients for an inclined disk will be $c_x = c_{x0}(1 + \sigma) \cos^2 \delta$ and $c_y = c_{x0}(1 + \sigma) \cos \delta \sin \delta$, where $c_{x0} = 0.82$. Treating the inclined disk as an airfoil, we note that its aspect ratio is $\lambda = \frac{D_n^2}{S_n} = \frac{4}{\pi}$ and the induced drag coefficient is $c_{xi} = \frac{c_y^2}{\pi \lambda} = \frac{c_y^2}{4}$. Substituting these relationships into equation (5.26), on the assumption that $k = 1 - \frac{I_x}{\pi R_k^2 \Delta p}$ has the value given in Section 4, the maximum cavity cross-sectional area S_k and the average cavity radius R_k are found. For $T_0 = 0$ we obtain

$$\begin{aligned} \frac{S_k}{S_n} &= \frac{1}{k\sigma} \left(c_x - \frac{1}{4} c_y^2 \right); \\ \frac{R_k^2}{R_n^2} &= \frac{c_{x0}(1 + \sigma) \cos^2 \delta}{k\sigma} \left[1 - \frac{1}{4} c_{x0}(1 + \sigma) \sin^2 \delta \right]. \end{aligned} \quad (5.27)$$

Table 11 lists the ratios $\frac{S_k^{(\delta)}}{S_k^{(0)}}$ of the maximum cavity cross sections and the drag ratios $\frac{W_x^{(\delta)}}{W_0}$ as a function of the disk inclination angle δ .

TABLE 11.

δ	0	5	10	15	20	30
$\frac{S_k^{(\delta)}}{S_k^{(0)}}$	1	0.993	0.96	0.92	0.86	0.71
$\frac{W_x^{(\delta)}}{W_0}$	1	1.0	0.97	0.93	0.88	0.75

If the respective diameters of the maximum cavity cross section in the plane of angle δ and in the perpendicular plane are $2R_1$ and $2R_2$, then noting that (by definition) $R_k^2 = R_1 R_2$ and also (from Tseitlin's experiments)

$\frac{R_1}{R_2} \approx \cos \delta$ in the leading part of the cavity, we have approximately

$$R_2 = \frac{R_k}{\sqrt{\cos \delta}}, \quad R_1 = R_k \sqrt{\cos \delta}.$$

The contour of the cavity for $\delta \neq 0$ can be constructed from the contour at $\delta = 0$. If the contour radius for point x for $\delta = 0$ is $R = R(x)$, then $R_{av} = R \cos \delta$, and $R_1 = R \cos^{\frac{3}{2}} \delta$ and $R_2 = R \cos^{\frac{1}{2}} \delta$. The construction is shown in Figure 62. This method yields the maximum deformation. It is, however, possible that the true deformation for small σ will be smaller.

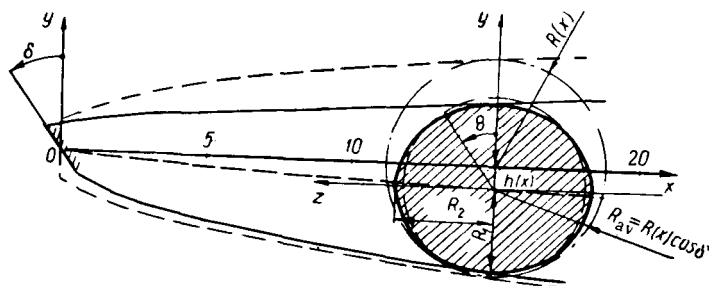


FIGURE 62.

Since R in the expression for B_v should equal R_2 , the actual downwash velocity V_v of the cavity axis relative to that calculated from formula (5.23) is as $\cos \delta$ to unity.

In the present section we presented only the most general relationships governing the motion of a perturbed cavity. Actually, however, the perturbed motion is much more complicated and has been insufficiently studied.

14. Equation of motion for the perturbed motion of a cavity

The study of the perturbed motion of a cavity can be extended somewhat by using the hypothesis of constancy of pressure at the boundary. We shall again consider the absolute motion of an almost cylindrical element of cavity length with all the perturbed motions of 1st, 2nd, 3rd, ..., n th order treated as plane, while the overall expansion is assumed to be the same as for an undisturbed axisymmetric cavity.

Assuming that the potentials φ_0 of expansion velocities and all the perturbation potentials $\varphi_1, \varphi_2, \dots, \varphi_n$ are specified in a moving coordinate system, the origin of which moves with velocity $V_y = \dot{h}$ along the y axis, the contour of the perturbed cavity in polar coordinates r, θ can be represented in the form

$$r = R + \xi_2 \cos 2\theta + \xi_3 \cos 3\theta + \dots + \xi_n \cos n\theta = R + \xi.$$

Quantities $\xi_2, \xi_3, \dots, \xi_n$ and velocities $\dot{\xi}_2, \dot{\xi}_3, \dots, \dot{\xi}_n$ can be regarded as being very small compared with R and \dot{h} .

Defining the static pressure p_0 for the initial ($h=0$) center of the cavity and treating pressure p_k as constant, we obtain an expression for the Cauchy-Lagrange integral:

$$\frac{\partial \varphi}{\partial t}|_{\text{stat}} + \frac{1}{2} (\text{grad } \varphi)^2 + \frac{p_k}{\rho} = \frac{p_0}{\rho} - g(h + R \cos \theta).$$

Derivative $\frac{\partial \varphi}{\partial t}$ should be calculated for stationary points in space with which the boundary coincides at the given time, since potentials

$\varphi_n = -\frac{R^{n+1} \dot{\xi}_n \cos n\theta}{nr^n}$ are assumed to be specified in a moving coordinate system traveling with velocity $\dot{\xi}_1 = \dot{h}$ along the y axis. Hence for the undistorted circle, when $\xi_n = 0$, we have for $n \geq 2$

$$\frac{\partial \varphi}{\partial t}|_{\text{stat}} = \frac{\partial \varphi}{\partial t}|_{\text{move}} - \frac{\partial \varphi}{\partial y} \dot{h}.$$

At the cylinder surface $r = R$ the radial velocity is $v_n = \dot{\xi}_n \cos n\theta$ and the transverse velocity is $u_n = \dot{\xi}_n \sin n\theta$; the other velocities are $v_1 = \dot{h} \cos \theta$ and $u_1 = \dot{h} \sin \theta$. Projecting these velocity components on the y axis gives

$$\dot{h} \frac{\partial \varphi}{\partial y}|_{r=R} = (\dot{R} + v_1 + v_2 + \dots + v_n) v_1 - (u_1 + u_2 + \dots + u_n) u_1.$$

In addition

$$v_1 v_n - u_1 u_n = \dot{h} \dot{\xi}_n [\cos \theta \cos n\theta - \sin \theta \sin n\theta] = \dot{h} \dot{\xi}_n \cos(n+1)\theta.$$

These expressions yield

$$h \frac{\partial \varphi}{\partial y}|_{r=R} = \dot{R} h \cos \theta + \sum_{n=1}^{\infty} \dot{h} \dot{\xi}_n \cos(n+1)\theta.$$

In order to make allowance for deformation of the cylindrical surface, it should be remembered that

$$\frac{\partial \varphi}{\partial t}|_{R+\xi} = \frac{\partial \varphi}{\partial t}|_R + \frac{\partial}{\partial r} \left(\frac{\partial \varphi}{\partial t} \right) \xi = \frac{\partial \varphi}{\partial t}|_R + \frac{\partial}{\partial t} \left(\frac{\partial \varphi}{\partial r} \right) \xi = \frac{\partial \varphi}{\partial t}|_R + \dot{R} (\dot{\xi}_2 \cos 2\theta + \dot{\xi}_3 \cos 3\theta + \dots).$$

The square of the velocity is given by

$$(\text{grad } \varphi)^2 = (\dot{R}_1 + v_1 + v_2 + \dots + v_n)^2 + (u_1 + u_2 + \dots + u_n)^2.$$

Collecting the terms and applying simple trigonometric formulas, we find that

$$\begin{aligned} (\text{grad } \varphi)^2 = & \dot{R}_1^2 + \dot{h}^2 + \dot{\xi}_2^2 + \\ & + \dots + \dot{\xi}_n^2 + 2\dot{R} \sum_1^{\infty} \dot{\xi}_n \cos n\theta + \sum_{n=1}^{\infty} \sum_{m=1}^{\infty} \dot{\xi}_m \dot{\xi}_{n+m} \cos n\theta. \end{aligned}$$

Substituting all the above expressions into the Cauchy-Lagrange integral and collecting terms with multiple angles, we have to within first-order infinitesimals

$$\begin{aligned} & \left\{ \frac{\partial \varphi_0}{\partial t} + \frac{1}{2} (\dot{R}^2 + \dot{h}^2 + \dot{\xi}_2^2 + \dots) + gh - \frac{p_0 - p_k}{\rho} \right\} + \\ & + \left\{ -\frac{1}{R} \cdot \frac{d}{dt} (R^2 \dot{h}) + gR + \dot{h} \dot{\xi}_2 + \dots \right\} \cos \theta + \\ & + \left\{ -\frac{1}{2} \cdot \frac{d}{dt} (R \dot{\xi}_2) + \dot{R} \dot{\xi}_2 - \dot{h} (\dot{h} - \dot{\xi}_2) + \dots \right\} \cos 2\theta + \\ & + \left\{ -\frac{1}{n} \cdot \frac{d}{dt} (R \dot{\xi}_n) + \dot{R} \dot{\xi}_n - \dot{h} (\dot{\xi}_{n-1} - \dot{\xi}_{n+1}) + \dots \right\} \cos n\theta + \dots = 0. \end{aligned}$$

Each expression in braces should be equal to zero. Obviously, the first term defines symmetric expansion of the cavity in the absence of disturbances. If we disregard the small quantity $\dot{h} \dot{\xi}_2 + \dots$, the first term will exactly conform to results obtained in Sections 11 and 12. In a heavy fluid $\dot{h} = \frac{g}{R^2} \int_0^t R^2 dt$, as was pointed out in Section 11. If the fluid is weightless

($g = 0$), quantity $R^2 \dot{h}$ remains constant and this case corresponds to skewing of the cavity due to lift (Section 12). In general, as long as the perturbations are small, we have linear superposition of perturbations of various orders. The perturbation of order \dot{h} is in principle excited by perturbations due to products of \dot{h} and perturbations of orders $n-1$ and $n+1$.

Experiments show that the three-dimensional cavity is sensitive to various disturbances, which markedly deform its cross sections, particularly in the trailing part. The above analysis of perturbed motion illustrates only the main aspects of the method and is apparently suitable for estimating the

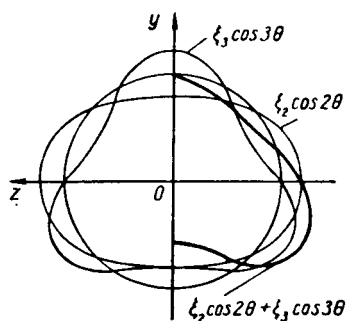


FIGURE 63.

few harmonics. An example of the addition of two harmonics of equal amplitudes is shown in Figure 63.

15. Effect of the free surface and walls

The effect of the free surface, bottom and walls of the water tunnel on the cavity dimensions is quite appreciable; however, in the majority of cases it has not been determined exactly. Treating the cavity in its absolute motion as an ensemble of stationary sources of variable strength, it can be concluded that each cavity cross section is "attracted" to the free surface during expansion and "repelled" from it during compression, i. e., in the trailing part. When moving near a solid surface this picture is reversed, i. e., the cavity is attracted to the surface during compression. Obviously, during horizontal motion in a shallow tank the trailing part of the cavity may be strongly attracted to the body. The above conclusions are obtained from elementary considerations, by taking the boundary condition at the free surface as $\frac{\partial \varphi}{\partial t} = 0$ and as $\frac{\partial \varphi}{\partial n} = 0$ at the wall; this is equivalent to placing above the free surface image sources of opposite sign and sources of the same sign behind the wall.

The axisymmetric flow past a mouthpiece in a circular tunnel with cross section S_0 can be treated by means of the momentum theorem in the same manner as in Section 3. The expressions for the maximum cavity cross section $W_0 = S_k(p_0 - p_k) - \int_{S_k} \frac{\rho v_x^2}{2} dS$ and $V_0 S_k = \int_{S_k} v_x dS$ are valid also in this case. However, the continuity equation yields inequality $V_0 S_k < (S_0 - S_k)V_k$, since between the cavity boundary and the tunnel wall the velocity decreases from V_k at the free boundary to some lower value at the tunnel wall.

Since $V_k = V_0 \sqrt{1 + \sigma}$, we should have $\frac{S_k}{S_0} < 1 - \frac{1}{\sqrt{1 + \sigma}}$. If it is desired, for example, to attain a cavitation number $\sigma = 0.1$ in the tunnel, then it is necessary that $\frac{S_0}{S_k}$ be greater than 20 and the cavity diameter should not exceed approximately 0.22 of the tunnel diameter. Even then it cannot be claimed that the effect of the walls on the cavity dimensions and shape is insignificant.

16. Different stages of developed cavitation and the loss of gas from a cavity

Developed cavitation can be (although somewhat arbitrarily) subdivided into three characteristic phases, depending on the predominance of a given factor. The first phase is dominated by the fluid's weight, when a developed cavity forms at the lower velocity limit. This phase can be termed "gravity" cavitation. The third phase, close to vaporous cavitation arises at very high velocities, when the effect of weight is unimportant. This "velocity" cavitation is close to developed cavitation in a weightless fluid. The second, transition phase, is midway between the first and third phases.

A graphic insight into the three cavitation stages can be obtained from Figure 64, where lines I—I of the minimum cavitation number

$\sigma_{\min} = \frac{g D_k}{V_0^2}$ and lines III—III of vaporous cavitation $\sigma_v = \frac{2(p_0 - p_k)}{\rho V_0^2}$. Obviously

the value of σ obtained with any gas-injection ratio \bar{Q} cannot lie outside these limits. The three basic parameters, Froude number $Fr = \frac{V}{\sqrt{gd}}$, injection ratio $\bar{Q} = \frac{Q}{Vd^2}$ and cavitation number $\sigma = \frac{2(p_0 - p_v)}{\rho V^2}$, are found to be insufficient for describing the cavitating flow. The minimum cavitation number according to (5.20) is related to the Froude number by the expression $\sigma_{min}^3 Fr^4 \approx \text{const.}$ Consequently, the lower limit of cavitating flow depends on the linear dimensions of the body, for example, on the disk diameter d_n . The upper limit, i. e., vaporous cavitation, does not depend on d_n , but on the pressure difference $p_0 - p_v$. The value of p_v , the water-vapor pressure at 20°C, amounts to only 0.0174 dyne/cm² and is therefore insignificant at $p_0 \approx 1$ atm. Hence the vaporous cavitation number σ_v is an additional and important parameter of cavitating flow.

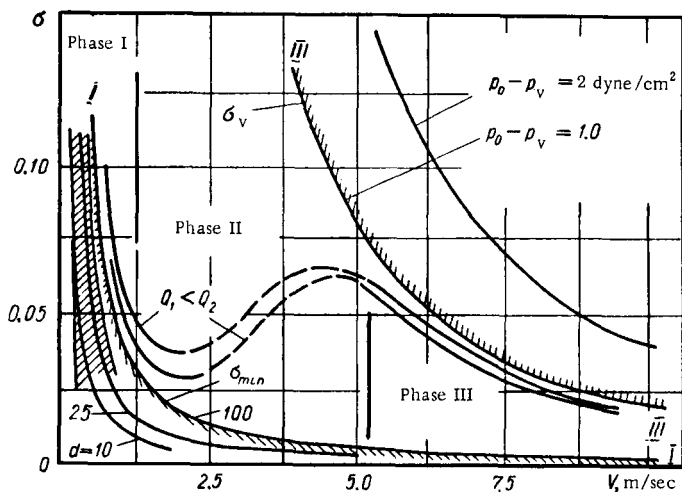


FIGURE 64.

As the difference $p_0 - p_v$ decreases the vaporous cavitation limit approaches the limit of the minimum cavitation number. Since for given $p_0 - p_v$ we have $\sigma_v \approx \frac{1}{V^2}$, while for given d_n we have $\sigma_{min} \approx \frac{1}{V^{4/3}}$, there always exists a point of intersection between the limits σ_v and σ_{min} . For example, if $p_0 - p_v = 0.1$ dyne/cm² and $d_n = 100$ mm, this will occur for a velocity of about 90 m/sec at $\sigma \approx 0.002$. Apparently the cavitation number cannot be reduced further, since this point of intersection corresponds to the attainment of pressure p_v at the upper point of intersection corresponds to the cavity. It was assumed in the above discussion that the fluid cannot sustain absolute pressures below p_v and that the flow is horizontal.

The Reynolds number and, in general, the effects associated with the viscosity of the fluid and gas have virtually no effect on the drag of bodies such as a disk and on the formation of free boundaries of the cavity.

However, the formation of gas-liquid mixtures in the rear part of the cavity and entrainment of gas there can be highly affected by the viscosity, i.e., the Reynolds number and capillary properties of the liquid.

Since the entrained gas is ejected into the cavity wake in the form of small bubbles, it is natural to expect (due to the high specific heat of the water) that the entrainment will not depend on the temperature of the gas entering the cavity. It can be assumed that the loss of gas from the cavity is affected markedly by the volumetric velocity (flow rate) Q , referred to the wake pressure p_0 and the absolute water temperature θ_0 . The kinetics of these processes in the wake will be of importance for soluble or condensing gases. Since this problem has not been studied, we shall consider below only the loss of insoluble and noncondensing gases.

Since highly elongated cavities are usually obtained at low σ , it is natural to assume that the removal of gas from the cavity is unaffected by the flow pattern at the disk, but rather by the principal dimensions of the cavity. Defining the cavity by its maximum diameter and eliminating the body diameter d , and also assuming that the gas flow does not affect the shape of the cavity boundaries, it is natural to seek the gas-loss law in the form

$$Q = VD_k^2 f\left(\sigma_{\min}, \sigma_v, \sigma, \frac{V_0 D_k}{v}, \frac{H}{D_k}\right). \quad (5.28)$$

The effect of the Reynolds number $\frac{V_0 d_k}{v}$ and of the relative immersion H/D_k of the cavity beneath the free surface, as well as the capillary forces remain virtually unexplored, and there is no complete theory of the loss of gas from a cavity.

Gravity cavitation was studied quite extensively. The attempt to construct a theory of gas loss by hollow vortices is due to Cox and Clayden /27/ and Epshtein /25/. Transition from the first form of gas loss by vortex filaments to the second form of loss by periodically ejected portions was noted by Krylov /8/, who put forward certain theoretical considerations pertaining to the frequency of ejection of these portions.

Water-tunnel experiments for determining gas loss from cavities were carried out by this author in 1948–1950 at $\frac{H}{d_n} \approx 30$ and velocities up to 8 m/sec at Froude numbers up to 19 and disk diameters of 10–20 mm. In these experiments the disk was fastened to a cylindrical tube and no free vortices were observed. Experiments showed that at some constant flow rate Q the curve of σ (Fr) follows the curve of $\sigma_{\min}(\text{Fr})$ at low Fr, and then deviates from it; σ attains a minimum and then starts increasing. This effect was also observed experimentally by Epshtein.

Gas loss by vortex filaments was studied experimentally by Epshtein, Blyumin, and Starodubtsev /26/, as well as by Krylov (1958–1961). cavitation, when hollow vortices are produced downstream of the cavity and the gas flows within the cavity do not markedly affect the configuration of cavity boundaries and of the eddies, one may expect, for high $\frac{H}{d_n}$ and $\frac{\sigma_v}{\sigma}$, an expression of the form

$$\frac{\sigma}{\sigma_m} = f\left(\frac{Q}{V_0 D_k^2}\right).$$

Figure 65 is a plot (in coordinates $\frac{\sigma}{\sigma_m}$ and $\tilde{Q} = \frac{Q}{V_0 d_n^2} \approx \frac{Q}{V_0 d_k^2}$) of the experimental points obtained from studies of gas loss by vortices [8, 26]. The curve was calculated from the expression

$$\frac{\sigma}{\sigma_m} = \frac{3}{2} \left(1 + \frac{0.05}{\tilde{Q}} \right)^{1/3}. \quad (5.29)$$

The points are very scattered. This empirical formula reflects the fact that increasing the injection ratio reduces the values of σ only to a

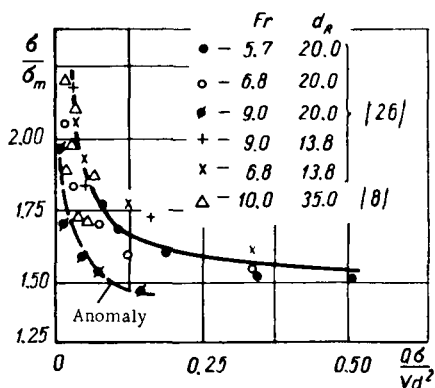


FIGURE 65.

certain limit, close to $\frac{\sigma}{\sigma_m} \approx 1.5$.

Reduction of the injection ratio to a value below $\tilde{Q} = 0.02$ usually results in the disappearance of the cavity.

Developing the Cox-Clayden theory, assuming that the vortex tube which forms "entrains" gas

from the cavity so that $Q = 2 \frac{\pi}{4} a^2 V_0$,

using the expression $p_0 - p_k - \rho g h = \frac{\rho \Gamma^2}{2\pi a^2}$

for the pressure at the boundaries of a hollow vortex, and finally substituting the expression for Γ from Section 10, Epshtein determined the gas flow rate from the expression

$$\tilde{Q} = \frac{0.27}{\sigma [\sigma^3 Fr^4 - 2]}. \quad (5.30)$$

Formulas (5.29) and (5.30) have fully identical structures. Setting $\sigma_m^3 Fr^4 = 0.96$, formula (5.29) yields

$$\tilde{Q} = \frac{0.162}{\sigma [\sigma^3 Fr^4 - 3.2]}. \quad (5.31)$$

Formulas (5.30) and (5.31) are qualitative expressions of the relationships governing gas losses by hollow vortices in the gravity cavitation stage. However, there are usually substantial differences between the calculated and observed values of \tilde{Q} . The causes for these differences should be sought in the inaccuracy of calculations as well as in the fact that some factors were disregarded in the processing of the experimental data (for example, $\frac{H}{D_k}$, Re, etc.).

When the vortices form due to lift, $\Gamma \approx \frac{\pi}{8} c_y d V_0$. Substitution into the expression $p_0 - p_k - \rho g h = \frac{\rho \Gamma^2}{2\pi a^2}$ as $V_0 \rightarrow \infty$ gives $\frac{Q\sigma}{V_0 d^2} \approx 0.025 c_y^2$. It is possible that this loss occurs in addition to losses due to other causes.

For velocity cavitation near the curve of σ_v the weight effect is unimportant provided $\sigma/\sigma_{min} \gg 1$. At $\sigma = \sigma_v$ the gas flow rate is $Q = 0$; the value of Q should increase with increasing σ_v/σ even for $V_0 S_k = \text{const}$.

The following relationship is to the first approximation:

$$Q = k V_0 S_k \left(\frac{\sigma_v}{\sigma} - 1 \right). \quad (5.32)$$

Estimates show that the "gas injection constant" $k \approx 0.008 - 0.01$.

It should be remembered that the relationships governing the loss of gas from cavities are approximate and thus provide only estimates. The rate of gas loss depends to such an extent on the specific features of the flow pattern in the cavity sealing zone that it is impossible to suggest a universal method for the theoretical determination of gas loss.

The above considerations and conclusions suffice only for gaining some approximate understanding of flows with developed cavitation. At the same time various methods for obtaining theoretical estimates of cavitation effects have been worked out. The main attention was paid to providing a logical correlation of theoretical estimates and experimental data; however, this was not always found to be possible.

The method of gaseous cavitation allows experiments to be conducted at a relatively low velocity and large cavities to be obtained. A large amount of experimental data has been accumulated in this region of gravity cavitation. However, these data should not be overestimated, since the conditions of cavity formation vary markedly with increasing velocity and the decreasing role of weight. Section 16 concerning gas loss from a cavity is only in the nature of a general survey.

Chapter Six

METHOD OF PLANE SECTIONS AND ITS APPLICATION FOR CALCULATING HYDRODYNAMIC FORCES

The method of plane sections, by its nature, is some approximation of the physical picture, the degree of approximation being the higher, the more the body is elongated. However, this method is attractive by its simplicity and generality, while in the majority of cases exact calculation of hydrodynamic forces is so complicated that it cannot be implemented and most likely cannot justify the corresponding volume of work.

In hydrodynamics the method of plane sections underlies the theory of finite-span wings and of wings with low aspect ratio. This method is used for calculating forces during planing of profiles and motion of ships. The principal results of the theory of three-dimensional cavitation were also obtained in conjunction with the method of plane sections. Other examples of successful application of this method could also be cited. However, restricting ourselves to the above we note that practical utilization of this method involves a number of fine points, which should be considered in deriving design equations. Although this is to the detriment of formal generality, we shall consider the two-dimensional motion of slender bodies of revolution within a fluid in continuous flow, partial cavitation and streamline separation, as well as the simplest cases of planing.

The idea of applying the method of plane sections to the calculation of the lift for planing profiles is due to Pavlenko (1932). At this time the theory of water entry [immersion] of profiles was still unknown, and the impact induced mass was used for calculating forces and moments. Hence agreement with experimental results was obtained only in some limiting cases (small β , partial width). This circumstance resulted in scepticism concerning the method of plane sections as a whole. Later, in 1957 — 1958, Tikhonov, Sokolov, Kolosov, and the present author also used the method of plane sections for calculating lift during planing, but employed the Wagnerian expression of lift for the uniform immersion of a wedge as the "cornerstone." Agreement with experimental results was satisfactory only at small angles of attack. At the same time work was carried out for refining the method of plane sections, resulting in the displacement theory presented here.

Two approaches are presented in the literature to the application of the method of plane sections. The first of these consists in calculating the induced masses by plane sections, whereupon the inertial hydrodynamic forces are calculated from the known rule /7/ in the same manner as for an ideal fluid, i. e., forces due to the properties of the real fluid are in some way added to these forces. The second approach is based on the concept of the "pierced layer", when the pressure is determined on an elementary "layer" through which the body passes; the total effect is obtained by integration.

The theory of planing of profiles and of three-dimensional cavitation which was lately developed [14], as well as the known linear theory of small aspect ratio wings are actually based on the concept of the pierced layer; this makes it possible to construct a physical pattern of the motion of bodies in a real fluid which is close to reality. Hence preference is given here to the concept of the pierced layer. Approaches to a given problem from different points of view are useful, since it makes it possible to determine details in the mechanism of the phenomenon; this method is used here.

1. Basic conditions and principles

First, for simplicity we shall consider the two-dimensional motion of a slender body of revolution in an infinite fluid. The coordinate system x, y, z associated with the body (Figure 66) is arranged so that the x axis coincides with the axis of symmetry of the body, while the motion occurs in the xy plane; unit vectors along the moving axes are denoted by i, j, k . The velocity vector of the origin is therefore $\bar{V} = iV_x + jV_y$ and the angular velocity vector is $\bar{\omega} = k\omega_z$.

The more complicated cases (partial cavitation, planing, rebound, etc.) will be considered from the same points of view. Calculations under other, more complex conditions of motion can be carried out without much difficulty.

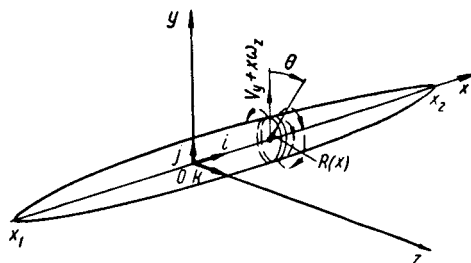


FIGURE 66.

It is known from the theory of motion of a body in an ideal incompressible fluid that the hydrodynamic problem of finding the velocity potential ϕ can be solved uniquely provided the velocity of all the points on the body surface $S(\bar{r})$ is specified and it is stated that the motion of the fluid is due only to the body. Hence the fluid at infinite distance from the body is at rest ($\text{grad } \phi \rightarrow 0$ as $r = \sqrt{x^2 + y^2 + z^2} \rightarrow \infty$). It follows from substitution and solution of the problem that stopping the body results in instantaneously stopping the fluid motion. The Laplace equation $\Delta\phi = 0$ governing the motion of the fluid shows that the velocity of a fluid particle at point $\bar{r} = lx + jy + kz$ is uniquely defined by the boundary conditions at the body surface $S(\bar{r})$, which for a given shape of body are defined uniquely by velocity \bar{V} of the coordinate origin and angular velocity $\bar{\omega}$. Hence the fluid surrounding the body can be treated as a system of material points related by ideal (internal energy equal to zero) holonomic constraints to the body possessing six degrees of freedom ($V_x, V_y, V_z, \omega_x, \omega_y, \omega_z$), i. e., respectively six generalized coordinates in Lagrange equations of the

second kind which, apparently, are applicable to this case /10/. However, all this is valid rigorously only as long as the fluid is ideal and incompressible.

A body moving in a real fluid leaves behind it a wake containing energy and momentum, and then the entire motion of the fluid can no longer be stopped by instantaneously stopping the body. Consequently the particle constraints are not holonomic. Although the fluid in the vicinity of the body outside the wake can still be treated as potential, it remains unclear to what extent the wake modifies the flow and to what degree the Lagrange equations are applicable.

In discussing the method of plane sections one must state specifically what this term means. We shall now imagine a plane section as a physical layer, isolated from the fluid by two neighboring planes perpendicular to the longitudinal axis of the body. Such a concept would not be very useful, since the flow within this layer is two-dimensional and the widening of a hole pierced by the body in this layer would require infinite energy. Hence this layer will be thought of as a fluid annulus, embracing the body in a transverse plane and bounded within the fluid by a stream surface supported by the edges of the annulus. It is assumed that the inner surface of the fluid annulus has a velocity potential ϕ and normal velocities induced by the body motion.

If we consider, for example, the transverse motion of a body of revolution, then the potential at the boundaries of the annulus, in the hole within the layer, is assumed to be the same as that of a moving similar element of length belonging, however, to a cylinder; the stream surfaces here are close to the previously mentioned planes. As the body moves longitudinally, the stream surfaces sliding off the ends of an annular element of the layer will intersect the plane of the maximum section of the body, singling out a volume formed by the rotation of two close streamlines relative to the longitudinal axis of the body.

The representation of flow past bodies by sources and sinks and, for transverse flows, also by doublets located on the axis of the body and in its wake, is known /7/. It is easy to show that the potential of transverse flow for a slender body is close to the potential of a cylinder. The kinetic energy of transverse flow in a unit annulus, determined by the boundary values of ϕ and $\frac{\partial \phi}{\partial n}$, changes instantaneously with variation in the velocity of the annulus center. It can hence be assumed that the relationships between particles within the annulus are holonomic, and that the Lagrange equation of the second kind is still applicable to it, while their application to a body as a whole with its wake is doubtful. These considerations are valid if there is no separation within the annulus; in the case of separation an energy and momentum flux to the wake flow is produced within the annulus proper.

If the body is different from a body of revolution, then for the case of flow past a part of the body with cavitation, planing and rebound all the above remains valid, but in each specific case the flow must be divided into two parts: one subject to holonomic constraints and the other determined by the momentum and energy fluxes in the body wake.

2. Approximate calculation of induced masses.

Motion in an ideal fluid

We recall the principal postulates of the theory of motion of a body in an ideal fluid; the induced masses will be calculated by the method of plane sections. As is known, the velocity potential of a flow generated by the motion of a body in the xy plane within an unbounded fluid, at rest at infinity,

is $\varphi = V_x \varphi_1 + V_y \varphi_2 + \omega_z \varphi_3$; the normal velocity is $\frac{\partial \varphi}{\partial n} = V_x \frac{\partial \varphi_1}{\partial n} + V_y \frac{\partial \varphi_2}{\partial n} + \omega_z \frac{\partial \varphi_3}{\partial n}$. The kinetic energy of the fluid is

$$T = -\frac{1}{2} \rho \iint_S \varphi \frac{\partial \varphi}{\partial n} dS = \lambda_{11} \frac{V_x^2}{2} + \lambda_{22} \frac{V_y^2}{2} + \lambda_{12} V_x V_y + \lambda_{16} V_x \omega_z + \lambda_{26} V_y \omega_z + \lambda_{66} \frac{\omega_z^2}{2}. \quad (6.1)$$

Using Green's theorem it can be shown that the induced masses are determined from the expressions

$$\lambda_{ik} = \lambda_{ki} = -\rho \iint_S \varphi_i \frac{\partial \varphi_k}{\partial n} dS = -\rho \iint_S \varphi_k \frac{\partial \varphi_i}{\partial n} dS \\ (i = 1, 2, 6; k = 1, 2, 6).$$

If it were possible to find potential φ , then one could calculate the induced masses λ_{ik} exactly, and hence compute the kinetic energy T and the hydrodynamic forces applied to the fluid by the body surface. However, the forces thus calculated would correspond to the actual values only in the case of an ideal fluid. These results would not be correct for a real fluid; in addition, it is difficult to actually determine the value of φ exactly even for a slender body of revolution. All these reasons taken together make it necessary to use approximate methods for calculating induced masses, and then also of hydrodynamic forces with allowance for properties of the real fluid. However, we shall start by applying the method of plane sections to the calculation of induced masses for a slender body, treating the fluid as ideal.

For a slender body $\frac{\partial \varphi_1}{\partial n} = \cos(\hat{n}, \hat{x}) = -\sin(\hat{s}, \hat{x}) \approx \frac{dR}{dx} = R'$ is assumed to be a small quantity. Hence $\frac{\partial \varphi_2}{\partial n} \approx \cos \theta$, where angle θ is measured in the plane parallel to the yz plane; $\frac{\partial \varphi_3}{\partial n} = x \cos(\hat{n}, \hat{y}) - y \cos(\hat{n}, \hat{x}) \approx x \cos \theta$. Induced mass λ_{11} for slender bodies is quite small and usually comprises several per cent of the mass of the fluid displaced by the body, for which reason it is assumed that $\lambda_{11} = 0$. As a result one derives the following approximate expression for the normal velocity at the surface of a slender body of revolution: $\frac{\partial \varphi}{\partial n} \approx (V_y + x \omega_z) \cos \theta = v_y \cos \theta$, where $v_y = V_y + x \omega_z = j \bar{V}_y(x)$ (\bar{V}_y is the transport [reference frame] velocity of points on the x axis of symmetry of the body). It is assumed in using the method of plane sections that the velocity potential at the surface of a quasicylindrical element $R = R(x)$ of the body is $\varphi = V_y \varphi_2 + \omega_z \varphi_3 = (V_y + \omega_z x) \varphi'_2$, where $\varphi'_2 = -R \cos \theta$, i. e., the potential is the same as for an infinite cylinder of radius R , moving with velocity v_y perpendicular to its axis; the specific induced mass is $-\rho \int_0^{2\pi} \varphi'_2 \cos \theta d(R\theta) = \rho \pi R^2(x)$.

The induced masses for a body with volume O_b and with end abscissas x_1 and x_2 are

$$\left. \begin{aligned} \varphi_2 &= \varphi_2'; \quad \frac{\partial \varphi_2}{\partial n} = \cos \theta; \\ \lambda_{22} &\approx -\varrho \int_L dx \int_0^{2\pi} R^2 \cos^2 \theta d\theta = \varrho \int_{x_1}^{x_2} \pi R^2 dx; \\ \varphi_2 &= \varphi_2'; \quad \frac{\partial \varphi_2}{\partial n} = x \cos \theta; \\ \lambda_{26} &\approx \int_{x_1}^{x_2} x \varrho \pi R^2 dx; \\ \varphi_6 &= x \varphi_2'; \quad \frac{\partial \varphi_6}{\partial n} = x^2 \cos \theta; \\ \lambda_{66} &\approx \int_{x_1}^{x_2} x^2 \varrho \pi R^2 dx. \end{aligned} \right\} \quad (6.2)$$

On the assumptions made $\lambda_{11} \approx 0$ and $\lambda_{16} = 0$. It is clear that if we do not consider the motion of a body of revolution, but of some other body, the transverse members of which are symmetric relative to the xy plane and the specific induced mass of the transverse member is $m_y^*(x)$, then (6.2) will also be valid, but then $\varrho \pi R^2(x)$ in them should be replaced by $m_y^*(x)$.

After the induced masses are calculated, the momenta and forces exerted by the body on the fluid are calculated by the known method using Lagrange equations of the second kind: $\frac{d}{dt} \frac{\partial T}{\partial \dot{q}_i} - \frac{\partial T}{\partial q_i} = Q_i$. In fact, expressing the kinetic energy as $T = \lambda_{22} \frac{V_y^2}{2} + \lambda_{26} V_y \omega_z + \lambda_{66} \frac{\omega_z^2}{2}$ and assuming that $\dot{q}_1 = V_y$ and $\dot{q}_2 = \omega_z$, we find the momentum

$$\bar{B} = j [\lambda_{22} V_y + \lambda_{26} \omega_z]$$

and the angular momentum

$$\bar{I} = k [\lambda_{26} V_y + \lambda_{66} \omega_z].$$

As is known, the force vector \bar{F} and the moment vector \bar{M} exerted by the body on the fluid are calculated from the expressions

$$\bar{F} = \frac{d\bar{B}}{dt} = \frac{\partial \bar{B}}{\partial t} + [\bar{\omega} \times \bar{B}]; \quad (6.3)$$

$$\bar{M} = \frac{d\bar{I}}{dt} = \frac{\partial \bar{I}}{\partial t} + [\bar{\omega} \times \bar{I}] + [\bar{V} \times \bar{B}].$$

Symbol $\frac{\partial}{\partial t}$ here has the meaning of differentiation of vectors \bar{B} and \bar{I} without rotation of axes, i. e., assuming unit vectors i, j and k to be constant. In our case $\bar{V} = iV_x + jV_y$ and $\bar{\omega} = k\omega_z$. Elementary computations yield

$$\begin{aligned} \bar{F} &= iF_x + jF_y = -i[\lambda_{22} V_y \omega_z + \lambda_{26} \omega_z^2] + j \left[\lambda_{22} \frac{dV_y}{dt} + \lambda_{26} \frac{d\omega_z}{dt} \right]; \\ \bar{M} &= kM_z = k[\lambda_{22} V_x V_y + \lambda_{26} V_x \omega_z] + k \left[\lambda_{26} \frac{dV_y}{dt} + \lambda_{66} \frac{d\omega_z}{dt} \right]. \end{aligned} \quad (6.4)$$

If the solid slender body proper has distributed masses $m'(x)$ along its length, then, designating the mass of the body by $m = \int_L m'(x) dx$, the centrifugal moment of inertia by $a_{26} = \int_L x m'(x) dx$ and the moment of inertia relative to the z axis by $a_{66} = \int_L x^2 m'(x) dx$, the kinetic energy of the body proper is

$$T_1 = m \left(\frac{V_x^2}{2} + \frac{V_y^2}{2} \right) + a_{26} V_y \omega_z + a_{66} \frac{\omega_z^2}{2}.$$

When the origin is placed at the center of gravity of the body, $a_{26} = 0$. The Lagrange equations yield expressions for the momentum and angular momentum applied to the body:

$$\begin{aligned} \bar{B}_1 &= imV_x + j[mV_y + a_{26}\omega_z]; \\ \bar{I}_1 &= k[a_{26}V_y + a_{66}\omega_z]. \end{aligned} \quad (6.5)$$

The equations of motion of a body in an ideal fluid due to an external force \bar{F}_{ext} and moment \bar{M}_{ext} are

$$\frac{d}{dt}(\bar{B} + \bar{B}_1) = \bar{F}_{\text{ext}}; \quad \frac{d}{dt}(\bar{I} + \bar{I}_1) = \bar{M}_{\text{ext}}. \quad (6.6)$$

If the fluid is ideal, incompressible and continuous, and the body is solid, the entire inexactness of this theory consists only in the inaccuracy of calculating induced masses by the method of plane sections. For a slender body this can usually be tolerated. In order for equations (6.6) to be valid, \bar{F}_{ext} and \bar{M}_{ext} must be external relative to the body-fluid system.

In all cases of practical importance pertaining to the motion of a body in a real fluid, the conditions underlying the preceding conclusions are (as previously pointed out) not satisfied, and hence these conclusions are for the most part invalid. In a real fluid, as a result of its viscosity and the resulting boundary layer, as well as in cases of discontinuities (when such occur), the body leaves behind it a wake, containing a certain momentum and energy, which can no longer be changed by instantaneously changing the body velocity. The presence of boundary layer separation and of a wake make it impossible to satisfy conditions under which Lagrange equations of the second kind can be applied to an ideal and incompressible fluid. Hence actually, hydrodynamic forces should not be calculated in the manner indicated above; their values may differ from those given by equations (6.4). It may appear that, in order to make allowance for properties inherent only to real fluids, it is sufficient to supplement equations (6.6) by viscosity force terms, leaving unchanged all the forces corresponding to the inertia effect of an ideal fluid. However, this is not the case. Below we shall consider the principal aspects of the problem of the motion of a body in a real fluid.

3. The concept of the pierced layer

It would appear at first sight that one can avoid using the above Lagrange equations for calculating forces by first calculating the forces acting at the boundary of the hole in the fluid layer pierced by the body and then integrating to find the total forces. We shall consider this problem in more detail and again in reference to a slender body of revolution still treating the fluid as ideal.

The pressure distribution at the surface of a cylinder moving with velocity $v_y = v_y(t)$ is obtained from the Cauchy-Lagrange equation

$$\frac{\partial \Phi}{\partial t} + \frac{v^2}{2} + \frac{p}{\rho} = F(t).$$

The velocity potential at the surface of a quasicylindrical hole in the layer pierced by the body can be represented as the sum of two potentials:

$\Phi = \Phi_1 + \Phi_2$. The boundary conditions at the surface of a slender body are $\frac{\partial \Phi}{\partial n} \approx \frac{\partial \Phi}{\partial r} = \dot{R} + \frac{\partial \Phi_2}{\partial r_{r=R}}$ and $\frac{\partial \Phi}{\partial s} = \frac{\partial \Phi}{R \partial \theta} = \frac{\partial \Phi_2}{\partial s}$. We thus assume that potential Φ_1 corresponds to expansion of hole $R = R(t)$, while potential Φ_2 is determined by the motion of the hole in the plane of the annulus formed by penetrating the layer. According to Section 2, it is assumed that $\Phi_2 \approx -\frac{v_y R^2 \cos \theta}{r}$, where r is the distance from the x axis. Derivative $\frac{\partial \Phi}{\partial t}$ in the Cauchy-Lagrange equation is taken as a stationary point in the space, while the potential is specified in the moving coordinate system. Hence

$$\frac{\partial \Phi}{\partial t}|_{\text{stat}} = \left\{ \frac{\partial \Phi_1}{\partial t} + \left[-\frac{\cos \theta}{r} \cdot \frac{d}{dt} (v_y R^2) \right] \right\}_{x,y,z} - v_y \frac{\partial \Phi}{\partial y},$$

where

$$\frac{\partial \Phi}{\partial y} = \frac{\partial \Phi}{\partial r} \cos \theta - \frac{\partial \Phi}{\partial s} \sin \theta = \dot{R} \cos \theta + v_y (\cos^2 \theta - \sin^2 \theta)_{r=R}.$$

The square of the absolute velocity at the cylinder surface in the Cauchy-Lagrange equation is

$$v^2 = (\dot{R} + v_y \cos \theta)^2 + (v_y \sin \theta)^2 = \dot{R}^2 + v_y^2 + 2v_y \dot{R} \cos \theta.$$

The time function $F(t)$ is determined from the same considerations, i.e., the disturbed motion of the fluid at infinity from the body disappears, i.e., $\frac{\partial \Phi}{\partial t}$ and v^2 tend to zero as $r = \sqrt{x^2 + y^2 + z^2} \rightarrow \infty$. Hence, as $r \rightarrow \infty$, $p \rightarrow p_0$; consequently $F(t) = \frac{p_0}{\rho}$. Substitution of these results into the Cauchy-Lagrange equation yields

$$\frac{p - p_0}{\rho} = \frac{\cos \theta}{R} \cdot \frac{d}{dt} (v_y R^2) + \frac{v_y^2}{2} (1 - 4 \sin^2 \theta) - \left\{ \frac{\partial \Phi_1}{\partial t} + \frac{1}{2} \dot{R}^2 \right\}.$$

According to the postulates of Section 2, $\Phi_1 = V_x \varphi_1$ and $\frac{\partial \Phi_1}{\partial n} \approx \frac{\partial \Phi_1}{\partial r} \approx R' V_x \approx \dot{R}$. Evidently when $V_x = \text{const}$, $\frac{\partial \Phi_1}{\partial t} = \frac{\partial \Phi_1}{\partial x} \cdot \frac{\partial x}{\partial t} = -V_x \frac{\partial \Phi_1}{\partial x}$.

In considering the stationary layer pierced by the body we neglect the absolute velocity $\frac{\partial \Phi_1}{\partial x}$ of travel of the layer proper, while in Section 2 we neglected the longitudinal induced mass λ_{11} . Both these assumptions are equivalent and standard in the theory of slender bodies. In addition, the pressure defined by the expression in braces does not depend on angle θ and does not have a component along the y axis. Hence in calculating forces acting on a slender body of revolution we shall take into account only that part of the pressure which is due to motion along the y axis. Thus, the pressure difference which generates the lateral forces can be expressed as

$$p - p_0 = \frac{v_y^2}{2} (1 - 4 \sin^2 \theta) + \frac{q \cos \theta}{R} \cdot \frac{d}{dt} (R^2 v_y). \quad (6.7)$$

We shall be concerned with two excess pressure integrals. The first defines the pressure force of the cylinder on the fluid:

$$dF_y = dx \int_0^{2\pi} (p - p_0) \cos \theta d(R\theta) = \frac{d}{dt} (q\pi R^2 v_y) dx,$$

and the second the "circular pressure" on the fluid:

$$dQ = dx \int_0^{2\pi} (p - p_0) d(R\theta) = -2\pi R \frac{v_y^2}{2} dx.$$

For a slender body $\frac{dR}{dx} = R'$ is a small quantity; hence $dF_x = -R'dQ = 2\pi R \frac{v_y^2}{2} dR$. Obviously, $dM_z = x dF_y$. When the body pierces the stationary layer $\frac{d}{dt} = \frac{d}{dx} \cdot \frac{dx}{dt}$, where $\frac{dx}{dt} = -V_x$. Therefore

$$dF_y = \left\{ 2\pi R \frac{dR}{dx} (V_y + x\omega_z)(-V_x) + q\pi R^2 \left(\frac{dV_y}{dt} + x \frac{d\omega_z}{dt} - V_x \omega_z \right) \right\} dx.$$

In integrating dF_y and dM_z along the longitudinal axis of the body we will encounter integrals of the form

$$\left. \begin{aligned} \int_{x_1}^{x_2} q 2\pi R \frac{dR}{dx} dx &= q [\pi R^2]_{x_1}^{x_2} = \lambda^*; \\ \int_{x_1}^{x_2} q 2\pi R \frac{dR}{dx} x dx &= q [x\pi R^2]_{x_1}^{x_2} - \int_{x_1}^{x_2} q\pi R^2 dx = -\lambda_{22}^*; \\ \int_{x_1}^{x_2} q 2\pi R \frac{dR}{dx} x^2 dx &= q [x^2\pi R^2]_{x_1}^{x_2} - \int_{x_1}^{x_2} q\pi R^2 2x dx = -2\lambda_{36}^*. \end{aligned} \right\} \quad (6.8)$$

Integrating the elementary forces and moments along the body axis from $x = x_1$ to $x = x_2$, we find the projections of forces on the body axes x and y , as well as the projections of the moment vector on the z axis.

Equations (6.8) yield the following expressions for the forces and the moment:

$$\left. \begin{aligned} F_{x2} &= [\varrho \pi R^2 x_1^2] \frac{V^2}{2} + \{[\varrho \pi R^2 x_1^2] - \lambda_{22}\} V_y \omega_z + \{[\varrho \pi R^2 x_1^2] - 2\lambda_{26}\} \frac{\omega_z^2}{2}; \\ F_{y2} &= -[\varrho \pi R^2 x_1^2] V_x V_y - [\varrho \pi R^2 x_1^2] V_x \omega_z + \lambda_{22} \frac{dV_y}{dt} + \lambda_{26} \frac{d\omega_z}{dt}; \\ M_{x2} &= -[\varrho \pi R^2 x_1^2] V_x V_y + V_x (\lambda_{22} V_y + \lambda_{26} \omega_z) - [\varrho \pi R^2 x_1^2] V_x \omega_z + \\ &\quad + \lambda_{26} \frac{dV_y}{dt} + \lambda_{66} \frac{d\omega_z}{dt}. \end{aligned} \right\} \quad (6.9)$$

For a slender body with sharp ends, when there is no separation of fluid from the body surface and derivative R' is very small along the entire body, all the expressions in brackets in (6.8) and (6.9) vanish, since $R(x_1) = R(x_2) = 0$. Here $\lambda' = 0$, $\lambda_{22} = \lambda_{26}$, $\lambda_{26} = \lambda_{66}$, and formulas (6.9) reduce to (6.4). We note that the result as such is quite natural, since instead of calculating the pressure one can use the expression for the kinetic energy for the pierced layer,

$T' = \varrho \pi R^2 \frac{v_y^2}{2}$, and then calculate from the Lagrange equation the quantity

$$\frac{a}{dt} \cdot \frac{\partial T'}{\partial v_y} = F'_y \text{ and } \frac{\partial T'}{\partial R} = -Q'.$$

It is clear that the result is the same irrespective of the sequence of operations.

Hence, both the method of initial computation of induced masses (Section 2) and the method using the concept of the pierced layer (Section 3) for an ideal fluid and continuous flow past bodies yield the same final results.

4. Flow with streamline separation

Suppose a slender body has a pointed nose, so that $R(x_2) = 0$, and is truncated by a perpendicular plane at $x = x_1$, where $R(x_1) = R_1$. When such a body moves in a real fluid, flow past the sharp corner at R_1 is replaced by separation of free streamlines which, together with the fluid left behind by the body, form a wake; in some cases a cavity may form behind the body. In such a flow the terms in brackets in formulas (6.9) will no longer vanish but be equal to their value at x_1 . Denoting by $\lambda'_1 = \varrho \pi R_1^2$ the specific induced mass at $x = x_1$ in the plane of streamline separation, and the projection of the transport velocity of point x_1 on the y axis, as above, by $v_{y1} = V_y + x_1 \omega_z$, collection of terms expressing forces in expressions (6.9) gives

$$\left. \begin{aligned} F_{x2} &= -\lambda'_1 \frac{v_{y1}^2}{2} + F_{x1}; \\ F_{y2} &= \lambda'_1 V_x v_{y1} + F_{y1}; \\ M_{x2} &= \lambda'_1 x_1 V_x v_{y1} + M_{x1}. \end{aligned} \right\} \quad (6.10)$$

Expressions for F_x , F_y and M_x in (6.10) are determined from (6.4) in the same manner as for an ideal fluid and continuous flow past the body. Velocity $V_y + x_1 \omega_z = v_{y1}$ is the velocity of the separation point x_1 in the y direction, for which reason $\lambda_1 v_{y1} = B'_{y1}$ is the specific momentum in the plane of separation while $V_x B'_{y1}$ is the momentum flux shed from the rear end of the body. Equations (6.10) show that force F_{y2} and moment M_{x2} of the body pressure on

the fluid are composed of time derivatives of the momentum and the angular momentum associated with the body and calculated in the same manner as for the flow of an ideal fluid past the body from formula (6.4) and from fluxes of momenta and angular momenta shed from the body.

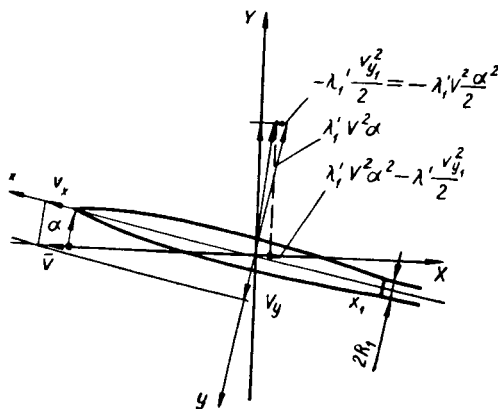


FIGURE 67.

On converting to a moving coordinate system, the suction force $-\lambda'_1 \frac{v_{y1}^2}{2} = -\lambda'_1 V^2 \frac{\alpha^2}{2}$, together with the projection of force $-\lambda'_1 V_x v_{y1}$ in the direction of the velocity, yields the induced drag $\lambda'_1 V^2 \alpha^2 - \lambda'_1 \frac{v_{y1}^2}{2}$, equal to the specific energy of the transverse motion of the wake (Figure 67).

Example. Let a circular cone with small central angle 2μ move in such a manner that $V_y = -\alpha V_x$, where $\alpha < \mu$. Let velocities V_x and V_y be constant and let the angular velocity be zero. The induced masses relative to the origin placed at the center of cone base R_1 are

$$\lambda_{22} = \frac{\pi \rho}{3} \cdot \frac{R_1^3}{\operatorname{tg} \mu}; \quad \lambda_{26} = \frac{\pi \rho}{12} \cdot \frac{R_1^4}{\operatorname{tg}^3 \mu}; \quad \lambda_{66} = \frac{\pi \rho}{30} \cdot \frac{R_1^5}{\operatorname{tg}^5 \mu};$$

the separation induced mass is $\lambda'_1 = \pi \rho R_1^2$.

The forces and moments exerted by the fluid on the cone are:
induced drag

$$-F_{x2} = \rho \pi R_1^2 \frac{V^2 \alpha^2}{2};$$

lift

$$-F_{y2} = \rho \pi R_1^2 V^2 \alpha;$$

moment

$$-M_{x2} = \frac{\rho \pi}{3} \cdot \frac{R_1^3}{\operatorname{tg} \mu} V^2 \alpha.$$

As known, the induced mass of a plate of width $2R_1$ is also πR_1^2 . Hence the preceding expressions apply equally to a delta wing and express the known linear theory of small-aspect-ratio wings.

5. Further refinements of the theory

The introduction of the separation induced mass λ'_1 explains to a large degree the appearance of hydrodynamic forces when a body moves in a real fluid. The pierced-layer concept thus makes it possible to estimate the hydrodynamic forces produced by the presence of viscosity forces in real fluids. However, in Section 3 we presented only the simplest scheme of force computation on the assumption that the layer is stationary at each given time and does not deform relative to the fluid at rest, and that viscosity does not induce fluid separation within the pierced layer proper.

Actually, however, when using the concepts of the pierced layer theory consideration must be given to the longitudinal transport of the layer which, for a slender body, occurs with absolute velocity $\frac{\partial \varphi}{\partial x} = u$, where the local transport velocity is $u = u(x, \theta)$. The average value of the velocity $u_{av} = \frac{1}{2\pi} \int_0^{2\pi} u d\theta$ can be treated as the rate of transport of the layer center along the x axis. When this transport is considered the relative velocity of the layer is $V_{rel} = \frac{dx}{dt} = -V_x + u_{av}$. Obviously, the appearance of the transport velocity modifies the magnitude of forces calculated in Section 3.

Let us now calculate the transport velocity for a slender body of revolution in continuous flow. The velocity potential at the body surface was expressed in Section 2 as $\varphi = -(V_y + \omega_z x) R \cos \theta + \Phi_1$. The absolute longitudinal velocity of the fluid is $\frac{\partial \varphi}{\partial x} = -R' (V_y + \omega_z x) \cos \theta - \omega_z R \cos \theta + \frac{\partial \Phi_1}{\partial x}$. Obviously, for any values of V_y and ω_z for a slender body of revolution $u_{av} = 0$, since $\int_0^{2\pi} \cos \theta d\theta = 0$, and the transport velocity $\frac{\partial \Phi_1}{\partial x}$ is usually insignificant. It can be concluded from this that the mean transport of layers for the forward part of a thin, sharp-nosed body of revolution, where there is no lateral separation of fluid from the body surface, is zero. For the case of planing and fully cavitating flow past bodies the transport of layers at the lateral surface can be quite appreciable.

It is known that if a body starts moving from rest, then the boundary layer and the drag associated with its formation do not arise all at one time, but gradually. Following the fluid particles belonging to the layer pierced by the sharp-nosed body of revolution it is seen that the particles adjoining the body are moved aside by it and the center of the fluid annulus is transported with velocity $V_y + x\omega_z = v_y$.

If the amount of center drift $\int_0^t v_y dt$ during passage along the body is very high compared with the body radius R , then an ordinary wake will develop behind the body and one may expect the appearance of lateral drag w_y , close to the drag of a cylinder placed in a flow with velocity v_y . If, however, the body moves with velocity v_y small compared with V_x , particularly if the

transport distance is smaller than the body radius, which is defined by the inequality $\frac{v_y(x_1 - x)}{V_x} < R(x)$, then there will be almost no separation to the rear of circle $R(x)$ and drag w_y can be neglected. In general the lateral drag will differ from zero and be proportional to qv_y^2 for each element, but the drag coefficient C_c will be a complex function of the transport of the center, expansion of the radius, and the Reynolds number; this function is unknown. Coefficient C_c ranges (depending on the case) from zero to a maximum and then decreases to some steady value. The lateral drag and its moment for the entire body are

$$w_y = \int_{x_1}^{x_2} C_c 2R \frac{qv_y^2}{2} dx = C_{22} \frac{V_y^2}{2} + C_{26} V_y \omega_z + C_{66} \frac{\omega_z^2}{2};$$

$$m_z = \int_{x_1}^{x_2} C_c 2R \frac{qv_y^2}{2} x dx = C_{26} \frac{V_y^2}{2} + C_{66} V_y \omega_z + C_{66}^* \frac{\omega_z^2}{2}.$$

These forces and moment can be added to expressions (6.10) of hydrodynamic forces.

The separation induced mass λ'_1 and its corresponding separation momentum B'_y need not necessarily be regarded as the effect of free streamlines separating from a body with a butt of radius R_1 . For any body at $v_{y1} \neq 0$, even in the case of quite smooth sharp outlines, viscosity causes the shedding of a vortex system from the body surface (Figure 68). The vortices start at different points on the body surface, but behind the body they form a vortex pair with momentum B'_y and kinetic energy $B'_y \frac{v_{y1}}{2}$ per unit length. The separation induced mass λ'_1 can be treated as the equivalent of such a vortex system.

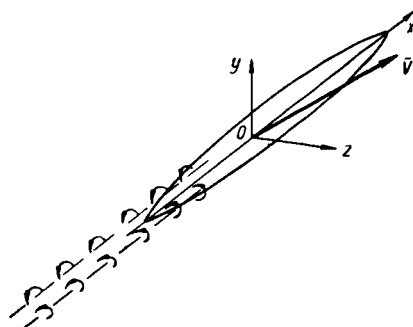


FIGURE 68.

For clarity of the analogy between forces $\lambda_1 V_x V_y$ and $\lambda'_1 \frac{v_y^2}{2}$ and forces acting on a wing, Figure 67 shows transition to the moving axes X, Y . For small angles of attack $\alpha = -\frac{V_y}{V_x}$ at $\omega_z = 0$, in the xy plane, the forces exerted by the fluid on the body are

$$F'_y = -\lambda_1 V^2 \alpha \text{ and } F'_x = \lambda_1 V^2 \frac{\alpha^2}{2};$$

the projections of these forces on the moving axes are

$$Y = \lambda_1 V^2 \alpha + \dots,$$

$$X_i = \lambda_1 V^2 \alpha^2 - \lambda_1 V^2 \frac{\alpha^2}{2} = \lambda_1 V^2 \frac{\alpha^2}{2}.$$

Force X_i is none other than the induced drag.

With consideration of the above, as well as of the fact that, in addition to the above forces, there acts along the x axis a force overcoming the drag

$\omega_x = C_x S_m \frac{v_{y1}^2}{2}$, which is due to friction and incomplete recovery of pressure, the system of forces acting on the fluid takes the form

$$\left. \begin{aligned} F_x^* &= -\lambda_1 \frac{v_{y1}^2}{2} + F_x + \omega_x; \\ F_y^* &= \lambda_1 V_x v_{y1} + F_y + \omega_y; \\ M_z^* &= \lambda_1 x_1 V_x v_{y1} + M_z + m_z. \end{aligned} \right\} \quad (6.11)$$

In these formulas force F_x^* , whose magnitude is equal to the drag for slender bodies of revolution, depends very little on the transverse flow, determined by velocities V_y and ω_z . The drag coefficient is usually determined from wind-tunnel tests or is calculated with consideration of friction and pressure induced drag.

The expressions needed to construct equations of motion of the body are the last two of system (6.11). Ignoring nonlinear terms and making use of the fact that $v_{y1} = V_y + x_1 \omega_z$,

$$\begin{aligned} F_y^* &= \lambda_{22} \frac{dV_y}{dt} + \lambda_1 V_x V_y + \lambda_{26} \frac{d\omega_z}{dt} + \lambda_1 x_1 V_x \omega_z; \\ M_z^* &= \lambda_{26} \frac{dV_y}{dt} + (\lambda_{22} + \lambda_1 x_1) V_x V_y + \lambda_{66} \frac{d\omega_z}{dt} + (\lambda_{26} + \lambda_1 x_1^2) V_x \omega_z. \end{aligned} \quad (6.12)$$

Force F_y^* and moment M_z^* are exerted by the body on the fluid. Usually steady hydrodynamic forces exerted by the fluid on the body are expressed in terms of coefficients c_y and m_z by the formulas

$$Y = c_y S_m \frac{v_{y1}^2}{2}; \quad M_z = m_z S_m L \frac{v_{y1}^2}{2},$$

where S_m and L are respectively the characteristic area and length of the body. In the linear approximation

$$\begin{aligned} c_y &= c_y^a \alpha + \bar{c}_y^{\bar{\omega}} \bar{\omega}; \\ m_z &= m_z^a \alpha + \bar{m}_z^{\bar{\omega}} \bar{\omega}. \end{aligned}$$

The dimensionless angular velocity is $\bar{\omega} = \frac{L\omega_z}{V}$.

The position coefficients c_y^a and m_z^a are determined by wind-tunnel testing of rectilinear models. Quantities $\bar{c}_y^{\bar{\omega}}$ and $\bar{m}_z^{\bar{\omega}}$ can be determined experimentally by wind-tunnel testing of curvilinear models, the method of oscillations, and rate-table tests.

Equating the steady-state force components from (6.12) to their expressions in terms of coefficients c_y and m_z , and noting that for small angles of attack $\alpha = -\frac{V_y}{V_x}$, we obtain

$$\begin{aligned} \lambda_1^* &= c_y^a S_n \frac{L}{2}; \quad (\lambda_1^* x_1)_2 = -c_y^{\bar{w}} S_n L \frac{L}{2}; \\ (\lambda_{22} + (\lambda_1^* x_1)_3) &= m_2^a S_n L \frac{L}{2}; \quad (\lambda_{26} + (\lambda_1^* x_1)_4) = -m_2^{\bar{w}} S_n L^2 \frac{L}{2}. \end{aligned} \quad (6.13)$$

Formally (according to the preceding conclusions) the values of the separation induced mass λ_1^* and of the separation abscissa x_1 should be the same in all the terms of (6.12). However, comparison with wind-tunnel results shows that the values of λ_1^* and x_1 obtained from different formulas of system (6.13) vary, for which reason the products of λ_1^* and x_1 in these expressions are subscripted.

As an illustration consider a slender body of revolution of length L , consisting of a cylinder with cross section S_n and ellipsoids of revolution in the forward part with major semiaxis $L/2$. The induced masses are easily calculable relative to the center $L/2 = x_1$:

$$\lambda_{22} = \frac{5}{6} \rho S_n L; \quad \lambda_{26} = -\frac{1}{16} \rho S_n L^2; \quad \lambda_1^* = \rho S_n.$$

Formulas (6.13) define the theoretical values of the coefficients:

$$\begin{aligned} c_y^a &= 2.0; \quad m_2^a = \frac{2}{3}, \\ c_y^{\bar{w}} &= 1.0; \quad m_2^{\bar{w}} = -\frac{3}{8}. \end{aligned}$$

Experiments show that the actual values of these coefficients differ somewhat from the above; however, they are close to theoretical values.

It was found by measuring the pressure distributions that at low angles of attack the hypothesis of a pierced layer holds quite satisfactorily at the leading, widening part of a slender body of revolution. Integration of pressure over the contour of the cross section at the cylindrical part of the body does not yield a stable value of the specific pressure force. This may be attributed to separation of flow at the "leeward" side of the cylinder.

6. Forces on a partly wetted body

At sufficiently high velocities, part of the slender body may be wrapped in a cavity (Figure 69). The leading part of the cavity has no clear boundaries, due to the pulsating, unsteady nature of the flow. It is hence impossible to single out precisely the points at which the flow is no longer separated and, in addition, the flow pattern past the body used in calculations is also some approximation of the actual situation. However, an approximate expression for forces can still be found using the pierced-layer analogy.

The projection of forces on the traveling x axis now has a value differing from that given by expressions (6.9). Due to the break in medium continuity, the "circular pressure" q_c is zero. The projection on the x axis of friction forces on the rear part of the body and of the pressure forces on the wetted leading part will be denoted by w_x , keeping in mind that this quantity is determined from relationships of cavitating flow.

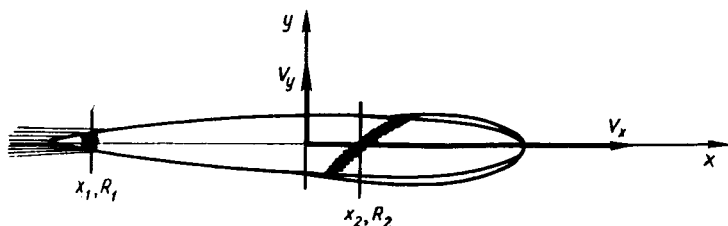


FIGURE 69.

The force F_y and moment M_z can be calculated from (6.8) and (6.9) on the assumption that the average wetted-boundary abscissa is x_2 and the separation-boundary abscissa is x_1 . Here two remarks are in order. First, when integrating dF_y and $dM_z = x dF_y$ along the x axis the specific induced mass $\varrho\pi R^2$ will be referred to the wetted part of the body. If it is the cylindrical part of the body which is wetted, then $\lambda_{22} = \varrho\pi R^2(x_2 - x_1)$; $\lambda_{26} = \frac{1}{2} \varrho\pi R^2(x_2^2 - x_1^2)$, and $\lambda_{66} = \frac{1}{3} \varrho\pi R^2(x_2^3 - x_1^3)$. Second, it may appear at first sight that the expressions in brackets in (6.9) are simply equal to the difference of the upper and lower values of the quantity in the brackets. For example, if $R_1 = R_2$, then $[\varrho\pi R^2]_1^2 = 0$. However, this is not so. The point is that, according to the principle of independent expansion of a cavity, the center of the cavity-pierced layer is stationary relative to the quiescent fluid. This layer therefore acquires a velocity $V_y + x_2\omega_z$ only upon collision with the body, which imparts to it momentum $\lambda'_2(V_y + x_2\omega_z)$, while the momentum flux $\lambda'_2(V_y + x_2\omega_z)V_x$ is equal to the pressure force on the fluid due to the setting into motion of layers at $x = x_2$. As a result of the change in momentum as the layer moves from x_2 to x_1 , there will appear (as in Section 3) a force which is determined from the expression in brackets in (6.9), but with consideration of the upper and lower limits. The force and moment are thus

$$\begin{aligned}
 F_{y2} &= -[\varrho\pi R^2(V_y + x\omega_z)]_{x_1}^{x_2} V_x + \varrho\pi R_2^2(V_y + x_2\omega_z) V_x + \\
 &\quad + \lambda_{22} \frac{dV_y}{dt} + \lambda_{26} \frac{d\omega_z}{dt} = \lambda'_1 V_x v_{y1} + \lambda_{22} \frac{dV_y}{dt} + \lambda_{26} \frac{d\omega_z}{dt}; \\
 M_{z2} &= -[\varrho\pi R^2 x(V_y + x\omega_z)]_{x_1}^{x_2} V_x + \varrho\pi R_2^2 x_2(V_y + x_2\omega_z) V_x + \\
 &\quad + (\lambda_{22} V_y + \lambda_{26} \omega_z) V_x + \lambda_{26} \frac{dV_y}{dt} + \lambda_{66} \frac{d\omega_z}{dt} = \lambda'_1 x_1 V_x v_{y1} + (\lambda_{22} V_y + \\
 &\quad + \lambda_{26} \omega_z) V_x + \lambda_{26} \frac{dV_y}{dt} + \lambda_{66} \frac{d\omega_z}{dt}.
 \end{aligned} \tag{6.14}$$

These expressions are fully analogous to formulas (6.10), the only exception being that now the induced masses λ_{22} , λ_{26} and λ_{66} have different numerical values. It is interesting that the cavitation force and moment are precisely the same as for continuous flow past the entire body.

Above we assumed a value of the specific induced mass $\varrho\pi R^2$, corresponding to transverse continuous motion of the pierced layer along the body. For partially cavitated flow cases are possible of separation of the fluid from the body in the low-pressure region, and this will result in a reduction in the induced masses.

7. Planing. Principal considerations

When dealing with a profile planing on the free surface of a fluid (Figure 70) one may in principle make the same assumptions which were postulated in considering the motion of a body submerged in a fluid. However, differences between these cases do exist. First, the three kinematic quantities V_x , V_y and ω_z describing the motion must now be supplemented by two more: depth of immersion of some point of the body (for example, of the planing element h_k), and the angle φ_k made by the x axis with the horizontal, equal to the angle of attack α . Second, it should be remembered when using the pierced-layer concept that the force exerted by the profile on the fluid during submergence is not the total time derivative of the fluid momentum $/2/$. If the induced mass in the direction of velocity of immersion \dot{h} of some profile is m^* , then the momentum of the fluid is $m^*\dot{h}$, but the force is not $\frac{d}{dt}(m^*\dot{h})$ (see Chapter IV).

Consider the planing of a plane, fin-shaped plate with deadrise angle β , in the xy plane of symmetry. The x axis is directed along the planing element, while the origin is placed at the trailing point of the planing element. The immersion of the planing step and the rate of immersion are denoted by h_k and $\dot{h}_k = -V_y$; the angle of attack is α (Figure 71).

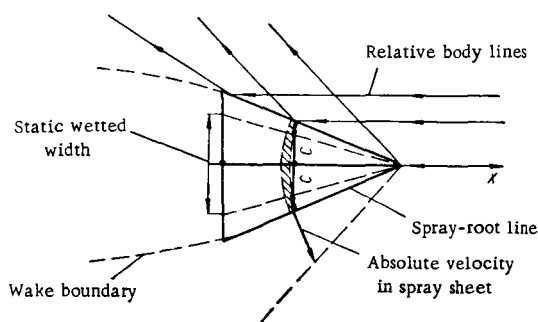


FIGURE 70.

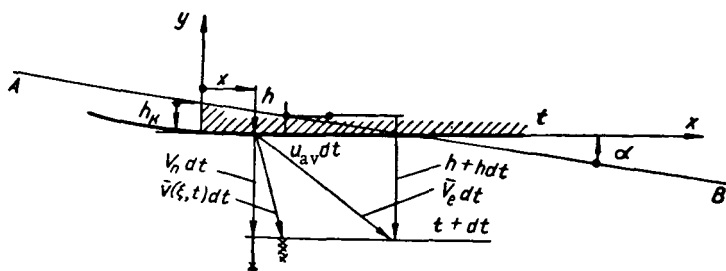


FIGURE 71.

The pressure force of a planing plate on a fluid is

$$dP_n = \pi \left(\frac{n}{2\beta} - 1 \right)^2 \left\{ \varrho h \dot{h}^2 + \left(1 - \frac{1}{2} \cos \beta \right) \varrho h^2 \dot{h}' \right\} dx \dots \quad (6.15)$$

The simplified method of plane sections as applied to this case would have consisted in calculating the force $F_y = - \int_h dP_n$, where $\dot{h} = V_n = -(V_y + x\omega_z)$.

However, in the case of planing the longitudinal travel of fluid layers is substantial and the method of plane sections yields incorrect results.

We recall the principles of the theory of immersion (see Chapter IV). When a profile is immersed symmetrically through a free fluid surface the latter curves upward and terminates in a spray sheet which carries with it energy and momentum flux. The energy and momentum thus carried away are nonholonomic in the sense that changing the velocity of the profile cannot change the velocity of particles in the spray sheet and, consequently, also the energy and momentum carried by the spray sheet cannot be changed in this manner.

Another part of the energy and momentum is imparted by the moving profile to the main flow, the flow pattern within which is close to that induced by impact of a profile, albeit in the case of a free surface distorted by a previous immersion. This part of the flow can be treated as holonomic, the energy and momentum of this region can change instantaneously with a change in the velocity of the profile and is determined by means of an induced mass basically in the same manner as for a body fully submerged in an ideal fluid.

If the rate of profile submersion is \dot{h} , while the impact induced mass is m^* , then the pressure force of the profile on the fluid is (see (4.42))

$$P = m^* \ddot{h} + \frac{dM}{dt} \dot{h} = \frac{d}{dt} (m^* \dot{h}) - f(\beta) \dot{h}^2 \frac{dm^*}{dh}. \quad (6.16)$$

The impact and apparent induced masses m^* and M are related by the integral expression $m^* = \int_0^M \frac{2(1+k)}{2k+1} dM$, where $k \approx \frac{v_\infty}{2h \sin \beta}$, v_∞ being the tangential velocity in the spray sheet and β the angle made by the spray sheet with the horizontal. For a symmetric wedge $\frac{1+k}{2k+1} \approx 1 - \frac{1}{2} \cos \beta$. The impact induced mass m^* and the apparent induced mass per unit length of the wedge are expressed by the approximate formulas

$$m^* = \frac{\pi}{2} \rho h^2 \left(\frac{\pi}{2\beta} - 1 \right)^2 (2 - \cos \beta);$$

$$M = \frac{\pi}{2} \rho h^2 \left(\frac{\pi}{2\beta} - 1 \right)^2; \quad f(\beta) = \frac{1 - \cos \beta}{2 - \cos \beta}.$$

Using these expressions we can derive expression (6.15) from (6.16).

The flow in each plane parallel to the yz plane during planing is approximately the same as on immersion. Hence planing can be treated as an ensemble of immersions of length elements dx of the planing profile. Since the two-dimensional theory of immersion of a profile pertains in essence to a fluid layer, in the theory of planing based on the theory of immersion one must follow the migration of a thin pierced layer, which travels ahead of the planing surface. We emphasize again that the concept of the "pierced layer" is conditional in the sense that reference is not actually had to a physical layer, but to a mechanically equivalent effect.

The transport velocities at points z are different and fluid particles which form strip dx lying along the z axis form (at a subsequent time instant) a curved strip. Hence we shall not refer to the local, but rather to the average velocity of layer travel.

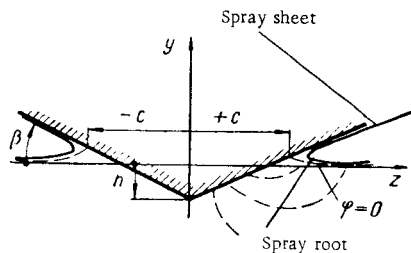


FIGURE 72.

We now calculate the velocity of longitudinal transport. The velocity potential φ at the center of the wetted surface of a wedge (Figure 72) or of some other submerging profile is negative; near the spray root at $z = c\zeta_k$ the potential is zero. At the lateral faces of the wedge, at the inner and outer surfaces of the spray sheet, the potential is positive. The impact induced mass is approximately given by

$$m^* \dot{h} = -\rho \int_{-c\zeta_k}^{+c\zeta_k} \varphi dz$$

when $\beta \rightarrow 0$, $\zeta_k \rightarrow 1$. Since $\varphi(c\zeta_k) = 0$, for small β

$$\frac{\partial}{\partial x} (m^* \dot{h}) = -\rho \frac{\partial}{\partial x} \int_{-c}^{+c} \varphi dz = -\rho 2cu_{av}.$$

At some point x of the planing element the normal velocity is $V_n = -(V_y + x\omega_z)$, while the rate of submersion of the fluid pierced layer (when its abscissa is x) is \dot{h} . At time $t+dt$ point x will move through segment $\dot{V}_n dt$, while the layer will move through segment $jV_n dt + u_{av} dt$, which yields $h = V_n - u_{av} \tan \alpha$. Using the expression for u_{av} the effective immersion rate is found to be

$$h = \frac{V_n}{1 - \frac{\tan \alpha}{2\rho c} \cdot \frac{\partial (m^* \dot{h})}{h \partial x}}.$$

Using the Wagnerian expression $\frac{dc}{dh} = \frac{\pi}{2 \tan \beta}$ and noting that for small α and β the induced mass is $m^* < \frac{\pi}{2} \rho c^2$, we derive the greatest transport effect in the form

$$\kappa(\alpha, \beta) = 1 - \frac{\tan \alpha}{2\rho c} \cdot \frac{\partial (m^* \dot{h})}{h \partial x} = 1 + \frac{\pi^2}{4} \cdot \frac{\alpha^2}{\tan \beta} + \frac{\pi^2}{8} \cdot \frac{\alpha}{\tan \beta} \cdot \frac{h\omega_z}{\dot{h}}.$$

At large β the induced mass is relatively somewhat smaller, since the longitudinal transport is also smaller. The condition for separation-free flow should consist in the fact that the velocity at all points be directed into the fluid; hence $\dot{h}_k - \kappa \omega_k$ should be greater than zero.

The acceleration \ddot{h} of the layer is defined as the projection, on the plane of the layer, of the absolute velocity of a point moving along the x axis with relative velocity $\bar{V}_n = i \frac{dx}{dt} = i(-V_x + u_{av})$. The projection of the acceleration on the inner normal is

$$\frac{dV_n}{dt} = - \left\{ \frac{dV_y}{dt} + x \frac{d\omega_z}{dt} + \omega_z \left(2 \frac{dx}{dt} + V_x \right) \right\}.$$

The acceleration of the layer is $\ddot{h} = \frac{1}{\kappa^*} \cdot \frac{dV_n}{dt}$, where function κ^* can have a value different from that given above; only in particular cases, when $\omega_z = 0$, does one obtain $\kappa^* = \kappa(\alpha, \beta)$. The general expression for the pressure force and moment of a planing surface of an arbitrary profile on the fluid is

$$F_y = - \int_{l_k} \left\{ \frac{m^*}{\kappa^*} \cdot \frac{dV_n}{dt} + \frac{dM}{dh} \cdot \frac{V_n^2}{\kappa^2} \right\} dx; \quad M_z = - \int_{l_k} x dF_k. \quad (6.17)$$

For an arbitrary motion of some profile the calculation of force F_y and moment M_z reduces to the calculation of $m^*(h)$ and $M(h)$ corresponding to the values of κ^* and $\kappa(\alpha, \beta)$, as well as to numerical integration along the length.

8. Equations for calculating the planing of a profile

A fin-shaped plate lands on the water surface at constant angle of attack $\alpha = \text{const}$ ($\omega_z = 0$). The velocity vector V_0 is inclined to the horizontal angle θ , so that $V_x = V_0 \cos(\alpha + \theta)$; $V_n = V_0 \sin(\alpha + \theta)$; $\frac{dV_n}{dt} = \frac{dV_0}{dt} \sin(\alpha + \theta) + V_0 \cos(\alpha + \theta) \frac{d\theta}{dt}$. We denote for brevity

$$\Phi(\alpha, \beta) = \pi \frac{\left(\frac{\pi}{2\beta} - 1 \right)^2}{\left(1 + \frac{\pi^2}{4} \cdot \frac{\alpha^2}{\lg \beta} \right)^2};$$

$$\xi = \left(1 - \frac{1}{2} \cos \beta \right) \left(1 + \frac{\pi^2}{4} \cdot \frac{\alpha^2}{\lg \beta} \right).$$

The pressure force on the fluid, $F = -F_y$, is found to be

$$F_n = \Phi(\alpha, \beta) \left[\frac{\rho h_k}{2 \lg \alpha} V_n^2 + \xi(\alpha, \beta) \frac{\rho h_k^3}{3 \lg \alpha} \cdot \frac{dV_n}{dt} \right] + \dots \quad (6.18)$$

For small α and θ , when $V_0 = \text{const}$, we have $V_n \approx V_0(\alpha + \theta)$; $\theta \approx \frac{\dot{h}}{V_0}$ and $\frac{dV_n}{dt} \approx V_0 \frac{d\theta}{dt} = \ddot{h}_k$. Substitution of these expressions into (6.18) yields

$$F_n = \Phi(\alpha, \beta) \left[\frac{\rho V_0^2}{2} h_k^2 \alpha \left(1 + \frac{\dot{h}_k}{V_0 \alpha} \right)^2 + \xi(\alpha, \beta) \frac{\rho h_k^3}{3 \alpha} \ddot{h}_k \right]. \quad (6.19)$$

Theoretically the moment is $M_z = \frac{1}{3} l_k F_n \approx \frac{1}{3} \cdot \frac{h_k}{\alpha} F_n$; actually, however, it can be somewhat higher due to the pressure drop at the transom. Comparison of theoretical results obtained from formulas (6.18) and (6.19) with experimental data on steady planing, as well as on rebounds, usually gives satisfactory agreement at angles of attack of up to $12-15^\circ$ /14/. Sedov /20/, as well as Sedov and Vladimirov /21/, present much experimental data on the planing of fin-shaped plates (at $\beta = 22.5^\circ$) over their partial width. An experimental relationship was established of the form $\frac{l_k}{\sqrt{\frac{2\Delta}{\rho V^2}}} = f(\alpha)$, where l_k is the wetted length along the planing element, and $\Delta = P_n \cos \alpha$ is the load on the water.

Expression (6.18) yields

$$\frac{l_k}{\sqrt{\frac{2\Delta}{\rho V^2}}} = \frac{1}{\sqrt{\Phi(\beta, \alpha) \sin^2 \alpha}} = \frac{1 + \frac{\pi^2}{4} \cdot \frac{\alpha^2}{\operatorname{tg} \beta}}{\left(\frac{\pi}{2\beta} - 1\right) \sqrt{\pi \sin^2 \alpha}}.$$

With this relationship one can compare the experimental results of /20, 21/ with those obtained from the simplified theory and with the "transport theory" developed here (Table 12).

TABLE 12

α , deg	$l_k / \sqrt{\frac{2\Delta}{\rho V^2}}$		
	experiment	simplified theory	"transport theory"
2	27	28.2	28.0
4	10.1	10.7	10.4
6	6.0	6.31	5.94
8	4.15	4.75	4.15
12	2.62	3.16	2.52
16	1.82	2.71	1.87

A similar comparison was made with the experimental results of Kolosov /21/. The excellent agreement between experimental data and results obtained from the transport theory point to the fact that it incorporates the main features of the effect.

We now compare (6.18) with equations (6.10). The first term of (6.18) contains the expression $\Phi(\alpha, \beta) \rho h_k^2 V_n = \frac{M V_n}{x^2} = B_n'$, representing the separation momentum, i. e., the specific momentum imparted to the fluid layer approaching the transom. The rate of momentum production at the transom is $\frac{V_n}{\operatorname{tg} \alpha} = \frac{V_0 \sin(\alpha + \theta)}{\operatorname{tg} \alpha}$; it is composed of two velocities: the velocity of impulse discharge $V_0 = \cos(\alpha + \theta)$, and the rate of increment of the momentum "tied"

$$F_n \approx \frac{\pi}{4} \rho R^2 V^2 \alpha. \quad (6.21)$$

The above considerations can be used for an approximate calculation of the lift in other cases of interest.

9. Equations of motion

The equations of two-dimensional motion are expressed in vectorial form as

$$\frac{d\vec{B}_1}{dt} + \vec{F}^* = \vec{F}_{\text{ext}}; \quad \frac{d\vec{J}_1}{dt} + k\vec{M}_1^* = \vec{M}_{\text{ext}}. \quad (6.22)$$

The expressions for the force vector $\vec{F}^* = i\vec{F}_x^* + j\vec{F}_y^*$ and for the moment \vec{M}_1^* contain terms determined by the momentum flux rolling off the body according to (6.11) and (6.12). These equations differ from equations (6.6), which are valid for an ideal fluid.

It is sometimes possible to consider the motion of a body along the x axis independently from the transverse motion and to establish a relationship between velocity V_x and time t or the travel distance s . The two other equations (if we omit ω_y and m_z), after division by the constant velocity V_x (since $ds = V_x dt$), assume the form

$$\begin{aligned} (\lambda_{22} + m) \frac{dV_y}{ds} + \lambda_{11} V_y + \lambda_{26} \frac{d\omega_z}{ds} + (m + [\lambda_{11} x_1]_1) \omega_z &= \frac{F_{y\text{ext}}}{V_x}, \\ (\lambda_{66} + a_{66}) \frac{d\omega_z}{ds} + (\lambda_{26} + [\lambda_{11} x_1^2]_4) \omega_z + \lambda_{26} \frac{dV_y}{ds} + (\lambda_{22} + [\lambda_{11} x_1]_3) V_y &= \frac{M_{z\text{ext}}}{V_x} \end{aligned} \quad (6.23)$$

Analysis of system (6.23) is not difficult. The use of these equations provides for convenient calculation of the path traveled by the body inside the fluid. The characteristic equation of system (6.23) is

$$\begin{vmatrix} (\lambda_{22} + m) p + \lambda_{11} & \lambda_{26} p + (m + \lambda_{11} x_1) \\ \lambda_{26} p + (\lambda_{22} + \lambda_{11} x_1) & (\lambda_{66} + a_{66}) p + (\lambda_{26} + \lambda_{11} x_1^2) \end{vmatrix} = A_0 p^2 + A_1 p + A_2 = 0,$$

where

$$\begin{aligned} A_0 &= (\lambda_{22} + m)(\lambda_{66} + a_{66}) - \lambda_{26}^2, \\ A_1 &= (\lambda_{22} + m) \lambda_{11} x_1^2 + (\lambda_{66} + a_{66}) \lambda_{11} - 2\lambda_{26} \lambda_{11} x_1, \\ A_2 &= (\lambda_{26}^2 - m\lambda_{22}) - (\lambda_{22} + m) \lambda_{11} x_1 \end{aligned}$$

The induced mass λ_{22} for bodies of revolution is equal to the mass of the displaced fluid; $\lambda_{26} = r_c \lambda_{22}$, where r_c is the abscissa of the center of the volume; $\lambda_{66} = r_i^2 \lambda_{22}$, where r_i is the radius of inertia.

If ρ_1 and ρ_2 , the roots of the characteristic equation, are negative and real, or have a negative real part, then steady motion of the body is possible in which $\frac{dV_y}{ds} \rightarrow 0$ and $\frac{d\omega_z}{ds} \rightarrow 0$, while V_y and ω_z asymptotically attain steady values, which are independent of the initial conditions but are determined from the right-hand side of equation (6.23).

For planing with fixed α the approximate equation of motion with small immersion of the planing element is obtained quite simply: $m\ddot{h} + F_n = F_{ext}$. The external force F_{ext} may here be the gravity force gm . It is found that rebounds of a fin-type plate moving with high translational velocities are damped out quite slowly.

10. Vibrations of a slender body. The flapping wing

It is of interest to estimate the characteristics of a vibrating or deforming slender body from the standpoint of the generation of thrust and its operation as a flapping wing. This study can explain to some extent the swimming mechanism of sea animals.

The vortex theory of a finite flapping wing /16/ has not been sufficiently developed, and practical calculations using it are made difficult by the fact that the forces at each instant are determined not only by the instantaneous state of the motion, but also by the vortex trail left behind by the wing, which contains the "history of motion." The theory of a slender body with separation at the trailing edge and the pierced-layer theory make it possible to avoid difficulties involved in the construction of a model and calculation of forces.

As is known from the preceding, element ds of body length is acted on by the inertia force $dF_n = \frac{d}{dt}(m^*v_n)ds$ and suction force dF_s , determined by the "circular pressure"; the integrals of the projections of these forces on the average direction of motion ξ and on the normal to it η yield resultant forces F_ξ and F_η (Figure 74). Induced separation mass λ'_i separates from the "tail" of the body ($x = x_i$) which has a tangential velocity V_s . This mass carries into the wake a separation momentum per second of $\lambda'_i v_{n1} V_s$, directed along the normal separation velocity v_{n1} . The reaction force acting on the body is $-\lambda'_i v_{n1} V_s$. In addition, the body is acted on by suction force P_ξ . The kinetic energy remaining in the wake per unit path of the "tail" is $\lambda'_i \frac{v_{n1}^2}{2}$.

In the case of periodic vibrations of a body moving in the ξ direction with velocity V_ξ , the average useful power over period τ is equal to the sum of powers developed by suction force P and impulsive force I :

$$\{P_\xi V_\xi\} + \{[\lambda'_i v_{n1} V \cos(\xi, v_{n1})] V_\xi\} = \{P\} + \{I\} = \{A\}. \quad (6.24)$$

The kinetic energy of the wake averaged over the period is given by

$$\frac{1}{\tau} \int_0^\tau \lambda'_i \frac{v_{n1}^2}{2} V_s dt = \left\{ \left[\lambda'_i \frac{v_{n1}^2}{2} \cdot \frac{V_s}{V_\xi} \right] V_\xi \right\} = \{E\}. \quad (6.25)$$

At the start and termination of each period ($0, \tau, 2\tau, \dots$) the kinetic energy "bound" to the body is the same, but still another wake wave containing energy $\{E\} \tau$ is added over the period. The thrust, over path $V_\xi \tau$, performs an amount of work equal to $\{A\} \tau$. Consequently, the external energy source over the period should perform work $\{N\} \tau = \{A + E\} \tau$, and the hydrodynamic efficiency is

$$\{\eta_p\} = \frac{\{A\}}{\{A\} + \{E\}} = \frac{\{A\}}{\{N\}}. \quad (6.26)$$

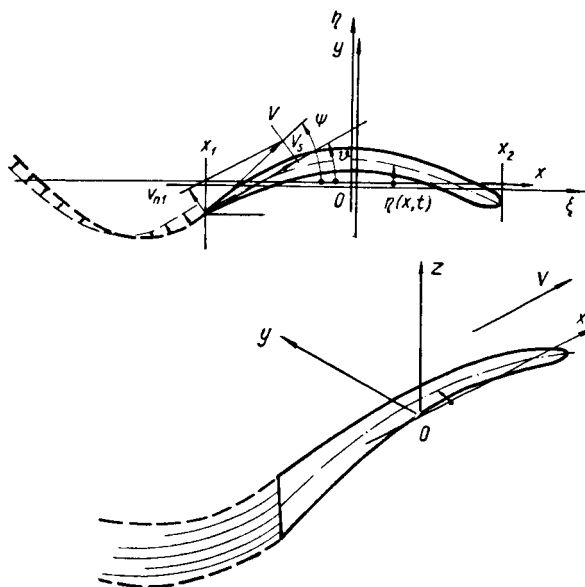


FIGURE 74.

This simple theory is the first approximation of reality. Apparently partial separation occurs at the lateral surface of the body, and this separation is also disregarded. However, the boundary layer at the surface of a vibrating and deforming body apparently forms differently than in ordinary cases, and the suction force can be more efficient. Some simple cases are considered below.

11. Small vibrations of a solid slender body

We assume that the coordinate system ξ, η, ζ is associated with the stationary fluid, while system x, y, z is associated with the body (for example, with a delta wing possessing small aspect ratio). We shall consider two-dimensional motions, when the z and ζ axes are parallel, the motion of the body center O occurs on the average along the ξ axis, the absolute magnitude of the velocity of the center is $V = V_\xi = \text{const}$, but the velocity vector makes an angle $\psi(t)$ with the ξ axis, while the x axis of the body is inclined at angle $\vartheta(t)$. It is assumed that angles ψ and ϑ are sufficiently small so that the sines and tangents can be assumed equal to the angles, while the cosines can be taken as unity. Under these conditions

$$V_x = V; \quad V_y = V(\psi - \vartheta) = \dot{\eta} - V\dot{\vartheta}; \quad v_{n1} = v_{y1} = V(\psi - \vartheta) + x_1\dot{\vartheta}; \quad \omega_z = \dot{\vartheta}.$$

Velocity v_{y1} , as above, is the normal velocity at the separation edge, the abscissa of which is $x = x_1$. If the span of the sharp rear edge $2R_1$

is aligned along the z axis, then the separation induced mass is $\lambda_1' = \varrho \pi R_1^2$ (for example, a delta wing).

If we assume the above velocities, the hydrodynamic forces exerted by the fluid on the body, in their projections on the moving axes, can be determined from (6.4) and (6.10) as $-F_x$, $-F_y$, $-M_z$. These formulas (with subscript 2 omitted) are

$$F_x = -\lambda_{22} V_y \omega_z - \lambda_{26} \omega_z^2 - \lambda_1' \frac{v_{y1}^2}{2};$$

$$F_y = \lambda_{22} \frac{dV}{dt} + \lambda_{26} \frac{d\omega_z}{dt} + \lambda_1' V_x v_{y1};$$

$$M_z = \lambda_{22} V_x V_y + \lambda_{26} V_x \omega_z + \lambda_{26} \frac{dV}{dt} + \lambda_{66} \frac{d\omega_z}{dt} + \lambda_1' x_1 V_x v_{y1}.$$

We recall that these formulas yield forces acting on the fluid. We shall be interested in forces acting on the body projected onto the ξ and η axes:

$$F_\xi = -(F_x \cos(x, \xi) + F_y \cos(y, \xi)) \approx -F_x + F_y \vartheta;$$

$$F_\eta = -(F_x \cos(x, \eta) + F_y \cos(y, \eta)) \approx -F_x \vartheta - F_y.$$

The kinetic energy remaining per unit length of the wake is $\frac{\lambda_1'}{2} [V(\psi - \vartheta) + x_1 \dot{\vartheta}]^2 = E$. This energy is equal to the work performed by suction force P over unit path length along the ξ axis. Substitution of the velocities and accelerations into these expressions gives

$$\left. \begin{aligned} F_\xi &= \lambda_{22} V(\psi \dot{\vartheta} + \dot{\psi} \vartheta - 2\vartheta \dot{\vartheta}) + \lambda_{26}(\dot{\vartheta}^2 + \vartheta \ddot{\vartheta}) + \frac{\lambda_1'}{2} V^2 \left[\left(\psi + \frac{x_1 \dot{\vartheta}}{V} \right)^2 - \vartheta^2 \right]; \\ F_\eta &= - \left[\lambda_{22} V(\dot{\psi} - \dot{\vartheta}) + \lambda_{26} \ddot{\vartheta} + \lambda_1' V^2 \left(\psi + \frac{x_1 \dot{\vartheta}}{V} - \vartheta \right) \right]; \\ M_z &= - \left[\lambda_{22} V^2(\psi - \vartheta) + \lambda_{26} V \dot{\psi} + \lambda_{66} \ddot{\vartheta} + x_1 \lambda_1' V^2 \left(\psi + \frac{x_1 \dot{\vartheta}}{V} - \vartheta \right) \right]. \end{aligned} \right\} \quad (6.27)$$

The energy expended in moving the body can be expressed in the form

$$\begin{aligned} N = -F_\eta \dot{\eta} - M_z \dot{\vartheta} &= A + E = \lambda_{22} V^2(\psi \dot{\psi} - \vartheta \dot{\vartheta}) + \lambda_{26} V(\dot{\psi} \dot{\vartheta} + \dot{\psi} \ddot{\vartheta}) + \\ &+ \lambda_1' V^3 \left[\psi^2 - \vartheta \psi + 2\psi \frac{x_1 \dot{\vartheta}}{V} - \vartheta \frac{x_1 \dot{\vartheta}}{V} + \left(\frac{x_1 \dot{\vartheta}}{V} \right)^2 \right]. \end{aligned}$$

The instantaneous efficiency is then

$$\eta_M = \frac{A}{N},$$

where $A = F_\xi V$.

We now consider simple cases.

1. Rectilinear and uniform motion of a body (wing). In this case $\dot{\psi} = \dot{\vartheta} = 0$. Consequently

$$\frac{A}{V} = F_\xi \approx \frac{\lambda_1' V^2}{2} (\psi^2 - \vartheta^2); \quad \frac{N}{V} = \lambda_1' V^2 (\psi - \vartheta) \psi.$$

The efficiency $\eta_p = \frac{\psi + \vartheta}{2\psi}$ tends to unity if ϑ tends to ψ ; at $\vartheta = 0$, $\eta_p = \frac{1}{2}$. For this case Figure 75 shows graphs of the variation in quantities N , E , P and I , divided by $\lambda_1 V^3$, as well as of η_p as a function of ϑ at $\psi = 20^\circ$.

2. Harmonic oscillations of a body. We assume that $\eta = a \sin kt$, or $\dot{\eta} = V\psi = V\psi_0 \cos kt$, and $\vartheta = \vartheta_0 \sin(kt + \theta)$.

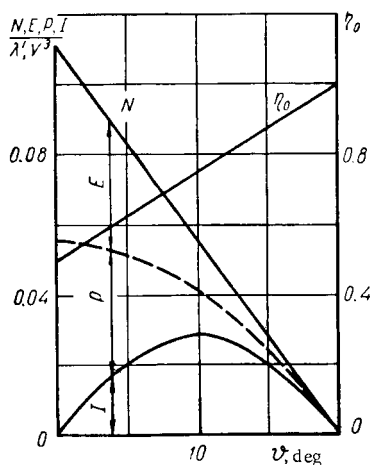


FIGURE 75.

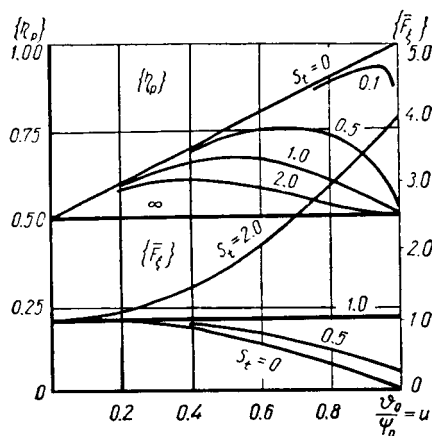


FIGURE 76.

Calculations yield the following average useful power over period τ :

$$\{A\} = \{F_k V\} = \frac{\lambda_1 V^3}{4} \left[\psi_0^2 + \left(\frac{x_1 k}{V} \right)^2 \vartheta_0^2 + 2 \frac{x_1 k}{V} \psi_0 \vartheta_0 \cos \theta - \vartheta_0^2 \right].$$

The average wake energy is

$$\{E\} = \frac{\lambda_1 V^3}{4} \left[\psi_0^2 + \left(\frac{x_1 k}{V} \right)^2 \vartheta_0^2 + 2 \frac{x_1 k}{V} \psi_0 \vartheta_0 \cos \theta - 2 \psi_0 \vartheta_0 \sin \theta + \vartheta_0^2 \right];$$

the average expended power is

$$\{N\} = \frac{\lambda_1 V^3}{2} \left[\psi_0^2 + \left(\frac{x_1 k}{V} \right)^2 \vartheta_0^2 + 2 \frac{x_1 k}{V} \psi_0 \vartheta_0 \cos \theta - \psi_0 \vartheta_0 \sin \theta \right];$$

the average efficiency is

$$\{\eta_p\} = \frac{\psi_0 + \left(\frac{x_1 k}{V} \right) \vartheta_0^2 + 2 \frac{x_1 k}{V} \psi_0 \vartheta_0 \cos \theta - \vartheta}{2 \left[\psi_0^2 + \left(\frac{x_1 k}{V} \right)^2 \vartheta_0^2 + 2 \frac{x_1 k}{V} \psi_0 \vartheta_0 \cos \theta - \psi_0 \vartheta_0 \sin \theta \right]} \quad (6.28)$$

It is seen from these expressions that in order for the body (wing) to have thrust during purely torsional oscillations, when $\psi_0 = 0$, the Strouhal number $S_t = \frac{x_1 k}{V}$ should be larger than unity. According to Nekrasov /16/ the condition for production of thrust for an infinite wing with allowance for the vortex trail is $S_t > 0.942$.

The previous formula yields, for $\psi_0 = 0$, the expression $\{\eta_p\} = \frac{1}{2} \left(1 - \frac{1}{S_i^2}\right)$ for the "impulsive" thrust $\{F_\xi\} = \frac{\lambda_1 V^2}{4} \psi_0^2 (S_i^2 - 1)$. For example, a delta wing with a span of 0.5 m and a chord of 1 m should, at $|x_1| = 0.5$ m, vibrate with frequency $k > 10$ radians/sec in order to develop thrust at velocity $V = 5$ m/sec. At $\psi_0 = 0.1$ radian (5.73°) and $k = 20$ sec $^{-1}$, for this case, when moving in water, obtains a thrust of 3.75 dynes at efficiency $\{\eta_p\} = 0.375$.

Setting $u = \frac{\psi_0}{\psi_0}$, and making use of the fact that the separation edge is usually located at the trailing part of the body of revolution ($x_1 < 0$), and introducing the Strouhal number S_i , the preceding formulas can be expressed in the form

$$\begin{aligned} \{F_\xi\} &= \frac{\lambda_1 V^2}{4} \psi_0^2 [1 + u^2 (S_i^2 - 1) - 2u S_i \cos \theta]; \\ \{\eta_p\} &= \frac{1 + u^2 (S_i^2 - 1) - 2u S_i \cos \theta}{2[1 + u^2 S_i^2 - 2u S_i \cos \theta - u \sin \theta]} \end{aligned} \quad (6.29)$$

The characteristics of a wing with small aspect ratio, at $\theta = \frac{\pi}{2}$, are shown in Figure 76. It is interesting that the efficiency is the highest at $S_i = 0$, i. e., for quasisteady motion of the wing. The impulsive thrust coefficient increases with increasing S_i ; however, the validity of the principal hypothesis for high S_i requires a more careful check.*

12. Motion of a flexible body

In this case it is best to use the inertial coordinate system x, y, z which moves in a straight line and uniformly relative to the quiescent fluid (the ξ, η, ζ system) with velocity $V_x = V$, while the flexible body occupies the x axis segment from $x = x_1$ to $x = x_2$ (Figure 74). The ordinate of the body along the y axis is denoted by $\eta = \eta(x, t)$. If the cross-sectional shape is assumed to be unchanged, then the specific induced masses will depend only on the abscissa x , and in general $m^* = m^*(x) = K_0 R^2$, where K is some constant for each specific cross sectional shape. In the case of a circular or elliptical cross section with major semiaxis R , $K = \pi$. The velocity of the hole in the pierced layer normal to the curvilinear axis is $v_n = \frac{\partial \eta}{\partial t} - V \frac{\partial \eta}{\partial x} = \eta_t - V \eta_x$; the specific momentum of the fluid is $m^*(x) v_n(x, t)$.

The specific normal force acting on the body, generated upon its passage through the pierced layer, is

$$\begin{aligned} -dF_n &= \frac{a}{dt} [m^*(x) v_n(x, t)] ds = \left[-\frac{dm^*}{dx} V (\eta_t - V \eta_x) + \right. \\ &\quad \left. + m^* (\eta_{tt} - 2V \eta_{tx} + V^2 \eta_{xx}) \right] ds \end{aligned}$$

In addition to the normal force, element ds is acted upon by the "circular pressure" $-2\pi R \frac{v_n^2}{2}$, which yields the arbitrary force applied to the body

* The author is unaware of experiments with high-frequency fluctuations of a wing in a flow. However, the method of high-frequency oscillations is used to determine the induced mass, and consequently, a near-ideal flow is attained. All the assumptions of the pierced layer hypothesis are, however, valid at relatively low S_i .

$$dF_s = \left[-2\pi R \frac{v_n^2}{2} \cdot \frac{dR}{dx} \right] ds = -\frac{v}{2} (\eta_l - V\eta_x)^2 \frac{dS}{dx} ds, \quad (6.30)^*$$

where S is the area of the induced mass (πR^2).

The projections of elementary forces on the x and y axes are

$$\begin{aligned} dF_x &= dF_s - \eta_x dF_n, \\ dF_y &= dF_n + \eta_x dF_s. \end{aligned} \quad (6.31)$$

The total instantaneous forces acting on the entire body are obtained by integration:

$$F_x = \int_{x_1}^{x_2} dF_x, \quad F_y = \int_{x_1}^{x_2} dF_y$$

According to Section 10, the calculation of forces F_x and F_y for periodic motion can be avoided by integrating equations (6.31). For this it suffices to use the characteristics of the wake, which can be calculated if the trajectory of the "tail" is known. However, suction force $|P|$ must still be calculated.

The instantaneous value of the suction force, according to equations (6.31) is

$$P = - \int_{x_1}^{x_2} \frac{v_n^2}{2} \cdot \frac{d}{dx} [\pi R^2(x)] dx.$$

The specific results depend on the form of functions $\eta(x, t)$ and $R(x)$.

The wake momentum $\lambda_1' v_n V_s$ can be calculated in the same manner as for a solid body. In fact $v_n = V(\psi - \vartheta)$. The instantaneous force generated by the momentum flux is

$$IV = \lambda_1' V^2 (\psi - \vartheta) \vartheta = \lambda_1' V (\eta_l - V\eta_x) \eta_x \quad \text{for } x = x_1,$$

and the energy of the wake is

$$E' = \frac{\lambda_1'}{2} (\eta_l - V\eta_x)^2.$$

Let us assume that a wave travels along the flexible body in the negative x direction with phase velocity c and constant amplitude η_0 . Then

$$\eta = \eta_0 f \left(\frac{ct}{L} - \frac{x_2 - x}{L} \right).$$

Clearly

$$v_n = \eta_l - V\eta_x = \frac{\eta_0}{L} (c - V) f' \left(\frac{ct}{L} - \frac{x_2 - x}{L} \right).$$

The normal velocity of the "tail" at $x = x_1$, for a body of length $L_p = x_2 - x_1$, is

* The circular pressure is given by this expression for a circle and all the ellipses (including a plate) with semiaxis R for motion at velocity v_n along the perpendicular axis.

$$v_{n1} = \frac{\eta_0}{L} (c - V) f' \left(\frac{ct}{L} - \frac{L_p}{L} \right).$$

We assume

$$f' \left(\frac{ct}{L} - \frac{x_2 - x}{L} \right) = \sin \left(\frac{ct}{L} - \frac{x_2 - x}{L} \right)$$

and

$$\pi R^2(x) = \pi R_1^2 \frac{x_2 - x}{L_p}.$$

Hence

$$\frac{d}{dx} (\pi R^2) = - \frac{\pi R_1^2}{L_p}.$$

Simple calculations yield values averaged over some period:

$$\left. \begin{aligned} \langle I \rangle &= \frac{\lambda_1'}{2} V^3 \left(\frac{\eta_0}{L} \right)^2 \left(\frac{c}{V} - 1 \right); \\ \langle P \rangle &= \frac{\lambda_1'}{4} V^3 \left(\frac{\eta_0}{L} \right)^2 \left(\frac{c}{V} - 1 \right)^2 = \langle E \rangle; \\ \langle A \rangle &= \frac{\lambda_1'}{4} V^3 \left(\frac{\eta_0}{L} \right)^2 \left[\left(\frac{c}{V} \right)^2 - 1 \right]; \\ \langle N \rangle &= \frac{\lambda_1'}{2} V^3 \left(\frac{\eta_0}{L} \right)^2 \left[\frac{c}{V} \left(\frac{c}{V} - 1 \right) \right]; \\ \langle \eta_p \rangle &= \frac{1}{2} \left(1 + \frac{V}{c} \right). \end{aligned} \right\} \quad (6.32)$$

Simple calculations show that a fish with a tail span of 0.5 m ($\lambda_1' = 20$ kg/m) and relative amplitude $\frac{\eta_0}{L} = 0.1$ develops, at velocity 10 m/sec for $\frac{V}{c} = 0.4$, on the average 3750 joules/sec of power and produces a thrust of about 26 dynes (of which 45% is due to the suction force) at a mechanical efficiency of about 0.7. The length of the fish is $L_p = 2\pi nL$, where n is the number of waves over length L .

The pierced layer concept makes it possible to estimate forces for a large variety of cases of bodies in a fluid. It is seen from comparison with experimental data that these estimates are sufficiently accurate and reliable. This makes it possible to expect that these methods, when applied to cases for which experimental data are unavailable, will yield results close to reality.

Chapter Seven

CAVITATING HYDROFOILS

When hydrofoils move at high speed, cavitation may arise at the low-pressure part of their surface. Cavitation, which is related to the formation of gas and vapor bubbles, markedly modifies the hydrodynamic forces. As the velocity is increased, bubble-type cavitation transforms into developed cavitation, when larger cavities with smooth inner boundaries are continuously cast off the foil [also known as supercavitation]. The development of cavities extending far past the hydrofoil is also aided by their entrainment of atmospheric air.

Studies show that the work performed by a cavitating hydrofoil is, from the mechanical standpoint, identical to the work corresponding to continuous flow past the hydrofoil. Hence the well-known theory of wings with finite span is for the most part applicable also to cavitating hydrofoils, irrespective of whether the cavity forms at the rear of the foil or whether it extends over the entire upper surface of the foil. The specific features of a hydrofoil consist in the effect exerted by the close-by free surface, which primarily affects the induced drag and downwash, as well as the lift of the profile. However, for thin cavitating hydrofoils the proximity of the free surface is primarily equivalent to the effect of the upper wing of a biplane on its lower wing.

Usually hydrofoils and (all the more so) cavitating hydrofoils operate at such high velocities that the weight of the water has no appreciable effect. Hence here the entire theory pertains to the motion of the foil at infinite Froude numbers. However, for cavitating hydrofoils, particularly at small immersion depths, when the upper streamline markedly distorts the free surface, the asymptotic theory, which is analogous to the theory of a wing in a continuous medium, must be substantially modified to conform to the special features of hydrofoils.

1. Flow past a profile and past finite-span hydrofoils

Figure 77 shows four patterns of flow past a hydrofoil profile. Pattern I corresponds to continuous flow, when the Chaplygin-Zhukovskii condition is satisfied at the trailing edge. The streamline flowing down from the upper part of the profile moves with the same velocity as the lower streamlines; both streamlines merge at the back of the profile. Pattern II depicts cavitating flow downstream of a curved wedge; the streamlines flowing down the upper and lower parts of the profile are now separated,

resulting in the formation of a cavity behind the profile. Since the flow velocity along the cavity boundary is constant everywhere, the Chaplygin-Zhukovskii condition is always satisfied at the trailing edge at the top and bottom of any cavitating profile. Pattern III differs from pattern II only by the fact that separation of the top streamline does not occur at the trailing edge point D, but at point E at the upper surface of the profile. Pattern IV corresponds to Rayleigh flow past an inclined plate AB, when the upper streamline separates at point A. Obviously, flow patterns III and IV are not, in principle, different than pattern II, since in all these cases we can consider the flow past curved wedge ABD.

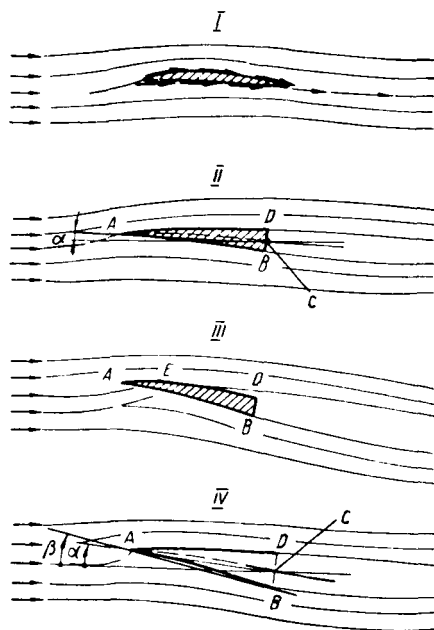


FIGURE 77.

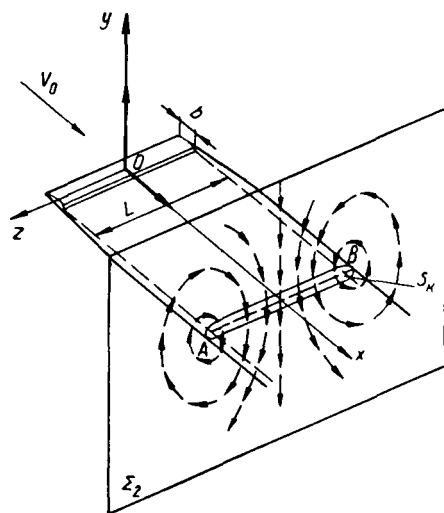


FIGURE 78.

The idea of constructing a noncavitating profile with a trailing cavity consists in the following. Calculations of cavitating flow past a thin wedge, due to Bobylev /10/, show that the pressure at the edges of the wedge is elevated; hence the disturbed velocities at the edges oppose the free-stream direction. It may be assumed that a vortex sheet with vortex strength γ is distributed along the lateral surface (or approximately along the axis of symmetry) of the wedge. This sheet induces velocities coinciding with the free flow direction at the upper edge and opposing the free-flow direction at the lower edge. The vortex-induced velocities are added to the perturbation velocities produced by the wedge in such a manner that the velocity opposing the free stream decreases at the top and increases at the bottom. As a result the pressure at the top edge of the wedge decreases and at the bottom wedge increases; this produces lift. If the resultant pressure at each point of the upper edge is still higher than in the free stream, then

there will be no cavitation at this edge. It will be seen below that in order to obtain flow about a wedge with a vortex sheet, the wedge axis must be curved in some appropriate manner.

Figure 78 shows the flow pattern about a finite-span foil in an infinite flow. The cavity developing at the rear of the foil will cut a hole S_k in plane Σ_2 , perpendicular to the flow velocity. Had the flow past the foil been noncavitating, then the free vortices cast off the foil (in the idealized formulation) would have been aligned along the dashed line AB. Actually, both the vortex sheet AB and cavity S_k behind the foil perform a complex motion and roll up at the edges, with resultant departure from symmetry relative to the z axis. However, as in the vortex theory of airfoils [6], we shall estimate the effect of the cavity by assuming it to be symmetrical relative to the y and z axes. The lift Y on the foil is the reaction of the foil pressure on the fluid which, in the wake behind the foil, induces downwash of the wake and its surrounding fluid. The field of absolute velocities in the Σ_2 plane is shown in Figure 78.

For a hydrofoil moving at depth h close to the free surface, the flow pattern behind the foil in the Σ_2 plane is shown in Figure 79. Below we shall show that such a flow arises past a biplane when the distance between its wings is $2h$.

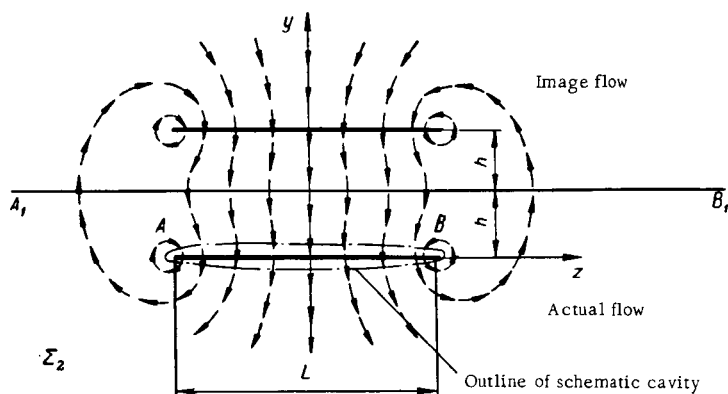


FIGURE 79.

It is clear without going into proofs that when the top and bottom boundaries of a cavity are merged, a vortex sheet is produced corresponding to continuous flow past a foil, and the entire theory of ordinary airfoils will fully apply to this case. The existence of cavitation modifies the flow about a hydrofoil; these changes are considered below.

2. Lift and induced drag

We now apply the momentum theorem to the control surface formed by two infinite planes Σ_1 and Σ_2 parallel to the y, z coordinate plane, where plane Σ_1 moves ahead of the foil while Σ_2 intersects the wake in the manner shown in Figure 78. The free stream velocity is V_0 , and is directed along the x axis; the projections of the perturbed velocity vector \vec{v} on the coordinate axes are v_x , v_y and v_z .

From the momentum theory the drag X and lift Y are

$$\begin{aligned} X &= \int_{\Sigma_1} [\rho(V_0 + v_x)^2 + P]_1 d\Sigma - \int_{\Sigma_2} [\rho(V_0 + v_x)^2 + P]_2 d\Sigma; \\ Y &= \int_{\Sigma_1} [\rho(V_0 + v_x)v_y]_1 d\Sigma - \int_{\Sigma_2} [\rho(V_0 + v_x)v_y]_2 d\Sigma. \end{aligned} \quad (7.1)$$

The pressure in the Σ_1 and Σ_2 planes is obtained from the Bernoulli theorem, for example, $P_2 = C - \frac{\rho}{2}[(V_0 + v_x)^2 + v_y^2 + v_z^2]$. The expression for lift does not contain the pressure, since the control surface is perpendicular to the flow.

Note. The application of the momentum theorem to the calculation of forces acting on a foil requires care in selecting the control surface. It is known that the vortex system trailing the foil is equivalent to doublets distributed along the surface subtending the vortex. If the foil is replaced by an equivalent vortex L with velocity circulation Γ , leaving behind it tip vortices (horseshoe vortex), then the equivalent vortex sweeps out per unit time an area $V_0 L$, the momentum of the fluid increases by an amount $\rho \Gamma V_0 L = Y$, and this quantity is equal to the increase in the moment of a doublet whose axis is directed oppositely to Y . The moment of the doublet is then $Yl = \rho \Gamma L l_k$, where l_k is the total cavity length. Velocity v in the Σ_1 plane is of the order of $\frac{l_k}{r_0^3}$, where r_0 is the distance from the coordinate origin to the Σ_1 plane. Integrals over Σ_1 , which contain the velocity v_x or v_y to the first power, will be of the order of $\frac{l_k}{r_0^3}$, since the area of plane Σ_1 increases with increasing r_0 as r_0^2 . In order for these integrals to tend to zero it is required that $\frac{l_k}{r_0} \rightarrow 0$, and this can happen if r_0 is of a higher order than l_k (for example, $r_0 = l_k^2$).

We now apply the continuity equation

$$\int_{\Sigma_1} V_0 d\Sigma - \int_{\Sigma_2 - S_k} (V_0 + v_x) d\Sigma = V_0 S_k - \int_{S_k} v_x d\Sigma = 0.$$

Noting that the pressure in plane Σ_1 is $p_1 = C - \frac{\rho V_0^2}{2}$ while the pressure within the cavity is p_k , and substituting these results in (7.1), we derive

$$\begin{aligned}
 X &= S_k(\rho_0 - \rho_k) + \frac{\rho}{2} \int_{S_k}^{\infty} (v_y^2 + v_z^2) d\Sigma - \frac{\rho}{2} \int_{S_k}^{\infty} v_x^2 d\Sigma; \\
 Y &= -\rho V_0 \int_{S_k}^{\infty} v_y d\Sigma - \rho \int_{S_k}^{\infty} v_x v_y d\Sigma.
 \end{aligned}
 \tag{7.2}$$

The largest cavity, and consequently the greatest effect on the flow about the hydrofoil, is obtained at zero cavitation number and $\rho_0 = \rho_k$. Integral

$\frac{\rho}{2} \int_{S_k}^{\infty} (v_y^2 + v_z^2) d\Sigma = T$ expresses (from the physical point of view) the kinetic energy of the absolute motion of the fluid in unit-thickness layer Σ_z ;

integral $\rho \int_{S_k}^{\infty} v_y d\Sigma = B_y$ represents the momentum of the fluid within that layer.

The fluid motion in the transverse plane Σ_z far downstream of the body is found to be virtually two-dimensional [6/.

Note. We show that integrals

$$I_1 = \frac{\rho}{2} \int_{S_k}^{\infty} v_x^2 d\Sigma \quad \text{and} \quad I_2 = \rho \int_{S_k}^{\infty} v_x v_y d\Sigma$$

tend to zero as plane Σ_z is moved downstream of the foil to infinity with x of the order of $\frac{l_k}{2}$. Velocity v_x is at its maximum at the cavity boundary,

where it is proportional to $\frac{1}{2} y_k'^2$, provided that $y_k = f(x)$ is the equation of the cavity contour in the xy plane. Hence

$$I_2 < v_{xk} \rho \int_{S_k}^{\infty} v_y d\Sigma = v_{xk} B_y.$$

In fact the hydrofoil is trailed by a three-dimensional cavity, which expands slower than a plane cavity. The ordinate of the plane cavity increases as \sqrt{x} , and consequently $y_k'^2$ decreases faster than $1/x$, and as $x \rightarrow \infty$, I_2 tends to zero not slower than $\frac{1}{x}$. Hence I_1 decreases not slower than $\frac{1}{x^2}$.

Neglecting integrals I_1 and I_2 due to their relative smallness we obtain

$$X = T; Y + V_0 B_y = 0. \tag{7.3}$$

As is known, for a foil with elliptical lift distribution over the span the momentum in continuous flow is $B_y = m^* V_y$, where m^* is the induced mass per unit length of plate with width L , equal to $\rho \frac{\pi}{4} L^2$, while V_y is the vertical wave velocity far downstream of the foil. Clearly in this case the kinetic energy is $T = m^* \frac{V_y^2}{2}$.

The induced drag and lift are related by an expression obtainable from (7.3) by eliminating V_y :

$$X_i = \frac{Y^2}{2m^*V_0^2}. \quad (7.4)$$

The lift and induced drag can also be expressed by the standard equations

$$X_i = c_{xi} S_{cr} \frac{vV_0^2}{2}; \quad Y = c_y S_{cr} \frac{vV_0^2}{2}$$

Noting that the aspect ratio is $\lambda = \frac{L^2}{S_{cr}}$ and substituting the above expressions for X_i and Y into formula (7.4), we obtain the expression for the induced drag coefficient known from [thin] wing theory, $c_{xi} = \frac{c_y^2}{\pi\lambda}$. The flow downwash angle in the plane of the lifting vortex is $\alpha_i = \frac{c_y}{\pi\lambda}$; the downwash angle far downstream of the foil is $2\alpha_i = -\frac{V_y}{V_0} = 2\frac{c_y}{\pi\lambda}$.

3. Effect of cavity on the downwash

We now represent the velocity potential of absolute flow in plane Σ_2 by the sum of two potentials $\varphi_1 + \varphi_2$, assuming that φ_1 corresponds to the general descending motion of the cavity while potential φ_2 corresponds to its expansion. Integration over the closed loop enclosing the cavity in the plane Σ_2 (with allowance for our assumptions) yields

$$\oint \frac{\partial \varphi_1}{\partial n} ds = 0, \quad \oint \varphi_2 \cos(y, \hat{n}) ds = 0.$$

The momentum component is

$$B_y = - \oint v \varphi_1 \cos(y, \hat{n}) ds, \quad (7.5)$$

while the specific kinetic energy is

$$T = -\frac{\rho}{2} \oint (\varphi_1 + \varphi_2) \left(\frac{\partial \varphi_1}{\partial n} + \frac{\partial \varphi_2}{\partial n} \right) ds. \quad (7.6)$$

Since potentials φ_1 and φ_2 satisfy the Laplace equation, we have on the basis of Green's theorem

$$I = \oint \varphi_1 \frac{\partial \varphi_2}{\partial n} ds = \oint \varphi_2 \frac{\partial \varphi_1}{\partial n} ds.$$

For a slender cavity integration over contour s can be replaced by integration over camber [mean] line AB (Figure 78), traversing it in both

directions. Denoting the values of φ and $\frac{\partial\varphi}{\partial n}$ above line AB by a plus sign and those below line AB by a minus sign, $\varphi_{l(+)} = -\varphi_{l(-)}$ and $\frac{\partial\varphi_1}{\partial n_{l(+)}} = -\frac{\partial\varphi_1}{\partial n_{l(-)}}$, while $\varphi_{2(+)} = \varphi_{2(-)}$ and $\frac{\partial\varphi_2}{\partial n_{l(+)}} = \frac{\partial\varphi_2}{\partial n_{l(-)}}$. Consequently, $l = 0$ and the kinetic energy consists of two independent terms:

$$T = -\frac{Q}{2} \oint \varphi_1 \frac{\partial\varphi_1}{\partial n} ds - \frac{Q}{2} \oint \varphi_2 \frac{\partial\varphi_2}{\partial n} ds = T_1 + T_2. \quad (7.7)$$

This expression can be given the following mechanical interpretation: energy T_1 corresponds to the general motion of the cavity with velocity V_y and its deformation when moving away from the coordinate origin. As was pointed out $T_1 = m^* \frac{V_y^2}{2}$, the corresponding momentum being $B_y = m^* V_y / 15$. Energy T_2 pertains to the expansion of the cavity and numerically should be equal to the Bobylev drag, induced for cavitated flow past an undistorted wedge or other profile.

We shall now clarify the effect of the cavity on the value of the induced velocity in the plane of the lifting vortex. For this we use the potential theory in the form

$$\varphi = \frac{1}{4\pi} \iint \frac{\partial\varphi}{\partial n} \cdot \frac{ds}{r} + \frac{1}{4\pi} \iint \varphi \frac{\partial}{\partial n} \left(\frac{1}{r} \right) ds.$$

We take as the cavity-surface element ds a strip of the contour contained between planes Σ_2 and Σ'_2 separated by distance $\delta\xi$. The distance between the far point $A(x, y, z)$ and the point $B(\xi, \eta, \zeta)$ on contour s in plane Σ_2 is $r = \sqrt{(x-\xi)^2 + (y-\eta)^2 + (z-\zeta)^2}$, while the distance between point A and the center of the cavity cross section in plane Σ_2 is $r_1 = \sqrt{(x-\xi)^2 + y^2 + z^2}$. For distances r and r_1 large compared with η and ζ we have approximately

$$\frac{1}{r} \approx \frac{1}{r_1} + \frac{y\eta + z\zeta}{r_1^3}; \quad \frac{\partial}{\partial n} \left(\frac{1}{r} \right) = \frac{1}{r_1^3} \left(y \frac{\partial\eta}{\partial n} + z \frac{\partial\zeta}{\partial n} \right).$$

As a result of substituting these expressions into that for the potential and making use of the properties of potential φ_1 and of the symmetry relative to the xy plane, integration over s gives

$$\delta\varphi_1 = -\frac{1}{4\pi} \left(S_k V_y + \frac{B_y}{Q} \right) \frac{y}{r_1^3} \delta\xi.$$

The induced-velocity increment at the center of the lifting line ($x = 0$, $y = 0$, $z = 0$) due to the motion of a cavity element of length $\delta\xi$ is

$$\delta v_i = \delta \frac{\partial\varphi_1}{\partial y} = -\frac{1}{4\pi} \left(S_k V_y + \frac{B_y}{Q} \right) \frac{\delta\xi}{\xi^3}. \quad (7.8)$$

For continuous noncavitating flow past a foil $S_k = 0$ and the moment of an elementary doublet is $\frac{B_y}{Q}$ rather than $S_k V_y + \frac{B_y}{Q}$. We denote the induced

velocity arising at the center of the lifting line on cavitated flow past the foil by v_i , and the induced velocity of the same foil with the same lift but without cavitation by v'_i ; the cavity cross-sectional area at point $x = \xi_1$ is denoted by $S_k(\xi_1)$. Since the induced velocities are proportional to the strength of doublet moments

$$v_i = v'_i \left[1 + \frac{q S'_k(\xi_1) V_y}{B_y} f(\xi_1) \right].$$

Had the cross-sectional area of the cavity been $S_k(\xi_1)$ over its entire length, then correction function $f(\xi_1)$ would have been unity. However, for $\xi > \xi_1$ the cavity is wider than at point $x = \xi_1$, and over the range $0 < \xi < \xi_1$ it is narrower than at point ξ_1 ; hence $f(\xi_1)$ differs from unity. In order to take into account the effect of an infinite expanding cavity, we shall first subtract the effect of a cavity with constant cross section $S_k(\xi_1)$ at the axis segment from ξ_1 to infinity, and then add the effect of an expanding cavity.

The expansion of a plane cavity is governed by $y_k = \sqrt{\frac{bc_x}{\pi}} \sqrt{\xi}$, where b is the foil chord and c_x is its drag coefficient. For a delta-shaped foil the Bobylev drag coefficient is $c_x = c_{x0} = \frac{8}{\pi} \mu^2 / 10$. A cavity forming behind a finite hydrofoil expands slower than a plane cavity, and therefore for a wedge-shaped profile $S_k < \frac{4}{\pi} \mu L^2 \sqrt{\frac{2}{\lambda}} \sqrt{\frac{\xi}{L}}$. Hence

$$f(\xi_1) = 1 + \int_{\xi_1}^{\infty} \frac{d\xi}{\xi^3} - \int_{\xi_1}^{\infty} \sqrt{\xi} \frac{d\xi}{\xi^3} = \frac{5}{6} \text{ at } \xi_1 = 1.$$

Here ξ denotes the distance from the origin, referred to the span L . The induced velocity is

$$\frac{v_i}{v'_i} \approx 1 + \frac{5}{6} \cdot \frac{q S_k(\xi_1) V_y}{B_y} \approx 1 + \frac{4}{3} \mu \sqrt{\frac{2}{\lambda}} = 1 + \tau \dots \quad (7.9)$$

For slender delta-shaped foils with large aspect ratio the velocity ratio $\frac{v_i}{v'_i}$ is close to unity. For example, if $2\mu = 0.1$ radians and the aspect ratio $\lambda = 5$, then $\frac{v_i}{v'_i} \approx 1.042$, i. e., the induced drag increases by 4.2% as compared with a noncavitating hydrofoil.

4. Effect of hydrofoil immersion depth

The derivation of the momentum theorem presented in Section 2 applies unchanged also to a hydrofoil moving horizontally at depth h , and so formulas (7.3) and (7.4) are applicable also to this case. Observations show that a cavity behind a hydrofoil has no large transverse deformation over a large length and is similar to Prandtl's "board"; at the rear, where the cavity breaks up, it degenerates into clearly defined vortices with

gas-bubble and foam-filled cores. The generation of a cavity is shown schematically in Figure 80. Hence, introducing the induced mass m^* of the wake and treating the flow behind the hydrofoil as induced by "impact of a plate," we derive a pattern close to the actually observed flow pattern.

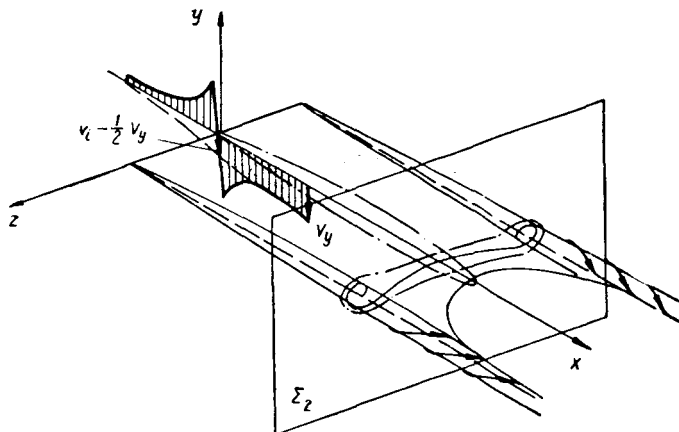


FIGURE 80.

The effect of the proximity of the free surface, which consists in increasing the induced drag, can be quite graphically attributed to the reduction in the induced mass at the wake with reduction between the hydrofoil and the free surface, and consequently, the need to impart to the wake a higher transverse velocity for exciting the same lift. The induced mass of the plate at infinite depth ($h/L \rightarrow \infty$) is $m_\infty^* = \rho \frac{\pi}{4} L^2$, while at the surface ($h/L \rightarrow 0$) the induced mass is half as large and equal to $m_1^* = \rho \frac{\pi}{8} L^2$.

Thus $m^* \left(\frac{h}{L} \right) = m_\infty^* / k \left(\frac{h}{L} \right)$. The induced drag coefficient c_{xi} and the induced downwash angle α_i are related by the expression

$$c_{xi} = \frac{c_y^2 S_{cr} \rho}{4m^* \left(\frac{h}{L} \right)} = \frac{c_y^2}{\pi \lambda} k_1 \left(\frac{h}{L} \right) = c_y \alpha_i. \quad (7.10)$$

Function $k_1 \left(\frac{h}{L} \right)$ can be calculated by solving the problem of impact of plates separated by a distance $2h$ (see Figure 79). The values of k_1 calculated by Fedorov are given in Table 13. At times the quantity $\kappa_1 = \frac{1}{k}$ will be required.

TABLE 13

$\frac{h}{L}$	0.0346	0.0588	0.185	0.393	0.557	1.434
k_1	1.715	1.610	1.308	1.137	1.08	1.032

The effect of hydrofoil immersion can also be calculated from other considerations. For infinitesimal disturbances of the free surface the condition of pressure constancy at the surface yields for the boundary condition of the perturbed velocity potential φ at $y = h$ the expression

$$\frac{\partial^2 \varphi}{\partial x^2} + \frac{g}{V_0^2} \cdot \frac{\partial \varphi}{\partial y} = 0. \text{ For very high velocities (more precisely as } V_0 \rightarrow \infty)$$

the second term drops out and condition $\frac{\partial^2 \varphi}{\partial x^2} = 0$ consists in the fact that

perturbed velocity $u = \frac{\partial \varphi}{\partial x}$ is constant at the free surface, but since $u = 0$ at $x = -\infty$, we concluded that $u = 0$ everywhere. In order to satisfy this boundary condition it may be imagined that the upper half-space is also filled with a fluid, while vortices and sinks with potential $\tilde{\varphi}$ are placed at the image points with respect to the free surface. Potential $\tilde{\varphi}$ should be selected so that the total potential $\varphi + \tilde{\varphi}$ satisfies the Laplace equation $\Delta(\varphi + \tilde{\varphi}) = 0$ and the above boundary condition at the free surface. In particular, the vortex in the bottom half-space will be mapped onto the upper space with circulation Γ of the same sign, while the sources are mapped with sign reversal. The motion of a hydrofoil at depth h is thus equivalent to flow past such a foil in an unstaggered biplane cell with interfoil distance of $2h$.

Since the actual and image foils have the same circulation and therefore the same lift, the free-surface proximity effect is equivalent to mutual induction of the biplane foils. The induced drag of a hydrofoil is greater than in an infinite fluid and is obtained from the expression

$$X_i = \frac{Y^2}{2m_\infty V^2} (1 + \sigma). \quad (7.11)$$

Quantity $(1 + \sigma)$, taken from biplane theory /17/, is equal to the value of k_1 , calculated by Fedorov from the problem of twin-plate impact /24/.

For small depth of hydrofoil immersion, the free surface above the foil becomes distorted and the thickness h of the water layer on top of the foil differs from the value of h_{st} of a stationary foil. The free surface in relative motion is a streamline; hence the central streamline ($z = 0$) satisfies the

equation $\frac{dx}{V_0} = \frac{dy}{v_y}$. Velocity v_y is induced by the vortex system of the hydrofoil proper, as well as by the image system. Calculations yield the approximate formula

$$h_{st} = h - \frac{c_y b}{2\pi} \left(\ln \frac{L}{h} - 1 \right). \quad (7.12)$$

Strictly speaking, the perturbations of the free surface due to the hydrofoil motion should have been taken into account in mapping the vortices and in constructing the biplane pattern, as in calculating the induced wake mass. In addition, some reduction occurs in the velocity of flow past the hydrofoil due to the image induction ($V_0 = V_\infty - \frac{\Gamma}{4\pi h}$). However, a theory for taking these effects into account has not yet been developed, and so we shall restrict ourselves to the above remarks.

5. The lift of a profile at small immersion depth

In addition, the increased induced downwash near the free surface or the closeness of the second wing of a biplane results in reducing the derivative of the lift coefficient with respect to the angle of attack. This effect is taken into account by introducing the function $\kappa_2\left(\frac{2h}{b}\right) = \frac{c_y^a}{c_y^{a\infty}}$. Data obtained from calculating function κ_2 from Carafoli's formula [6] (carried out by Fedorov [24]) are presented in Table 14.

TABLE 14

$\frac{h}{L}$	0	0.1	0.2	0.3	0.4	0.5	1.0
κ_1	0.5	0.68	0.78	0.84	0.89	0.92	0.97
$\frac{2h}{b}$	0	0.2	0.4	0.6	0.8	1.0	2.0
κ_2	0.5	0.62	0.71	0.77	0.82	0.86	0.95

We shall consider a second, quite simple derivation of the expression for function $\kappa_2\left(\frac{2h}{b}\right)$, based on the Lagrange equation of the second kind.

Suppose a plate with width $2a = b$ has velocity $\bar{V} = iV_x + jV_y$ relative to the stationary fluid (Figure 81a). The motion of an incompressible fluid is determined uniquely by the motion of the plate, and hence the fluid can be treated as a system of material points with ideal holonomic constraints. For translational motion of the plate we have two obvious generalized coordinates, which are the motions along the y and x axes. We introduce a third generalized coordinate a , equal to half the width of the plate, and determine the suction force. The kinetic energy of the fluid will be

$T = \pi \rho a^2 \frac{V_y^2}{2}$, where $\pi \rho a^2 = m^*$ is the known expression for the induced mass.

Applying the Lagrange equation $\frac{d}{dt} \frac{\partial T}{\partial \dot{q}_i} - \frac{\partial T}{\partial q_i} = Q_i$ to the generalized coordinate a , we derive

$$Q_a = -\pi \rho a V_y^2.$$

This generalized force Q_a is applied to the fluid; at each end of the plate it is equal to $\frac{1}{2} Q_a$ and is directed toward the origin along the x axis. The

suction force acting at each end of the plate will be $P_{\pm} = -\frac{1}{2} Q_a$. It is produced by infinite velocities at points $\pm a$. We select the velocity circulation Γ in such a manner that the suction force at point $x = -a$ disappears. Evidently, here the velocity at point $x = +a$ is doubled from symmetry conditions, while the suction force increases fourfold as compared with a plate without circulation. Thus $P_{-a} = 0$ and $P_{+a} = 2\pi \rho a V_y^2$.

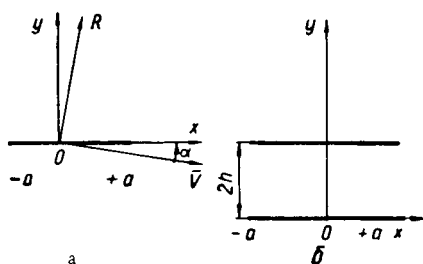


FIGURE 81.

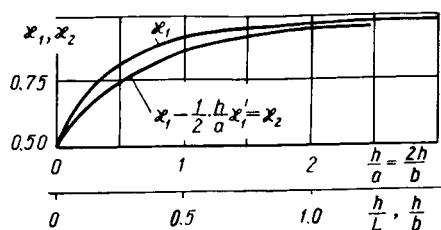


FIGURE 82.

Since by the formulation of the problem $V_y = -V \sin \alpha$, and for flow past a plate with circulation the absolute value of the resultant force is

$R = \rho V \Gamma = \frac{P}{\sin \alpha}$, we have finally

$$P = 2\pi a \rho V^2 \sin \alpha; \\ \Gamma_\infty = 2\pi a V \sin \alpha; \quad c_{y_\infty}^a = 2\pi.$$

These formulas express known properties of a plate placed in an infinite flow with circulation. The solution of the problem of impact of two biplane plates (Figure 81b) can be represented as an expression for the induced masses of each plate:

$$m_y^* \left(\frac{h}{a} \right) = m_{y_\infty}^* \kappa_1 \left(\frac{h}{a} \right) = \pi \rho a^2 \kappa_1 \left(\frac{h}{a} \right).$$

From physical considerations $\frac{1}{2} < \kappa_1 < 1$ when $0 < \frac{h}{a} < \infty$, since the induced mass for a plate floating on the free surface is one-half that for a plate in an infinite fluid.

Applying the Lagrange equation to the kinetic energy of one plate $T = \pi \rho a^2 \kappa_1 \left(\frac{h}{a} \right) \frac{V^2}{2}$ and denoting the derivative of function $\kappa_1 = \kappa_1 \left(\frac{h}{a} \right)$ with respect to the argument by κ_1' , we have

$$\frac{\partial T}{\partial a} = \pi \rho a \kappa_1 V^2 - \pi \rho h \kappa_1' \frac{V^2}{2} = \pi \rho a V^2 \left(\kappa_1 - \frac{1}{2} \cdot \frac{h}{a} \kappa_1' \right) = -Q_a.$$

Repetition of all the preceding considerations for different angles of attack yields

$$\frac{\Gamma \left(\frac{2h}{b} \right)}{\Gamma_\infty} = \frac{c_{y_\infty}^a \left(\frac{2h}{b} \right)}{c_{y_\infty}^a} = \left[\kappa_1 \left(\frac{2h}{b} \right) - \frac{h}{b} \kappa_1' \left(\frac{2h}{b} \right) \right] = \kappa_2 \left(\frac{2h}{b} \right). \quad (7.13)$$

It is thus found that the reduction in the lift of a hydrofoil when approaching the free surface is due to a reduction in the suction force. The graph of functions κ_1 and κ_2 is given in Figure 82. Satisfaction of the Chaplygin-Zhukovskii condition at the trailing edge of the foil requires a smaller

velocity circulation and consequently a smaller lift. All these conclusions pertain to a hydrofoil in continuous flow, as well as to a cavitating hydrofoil, but in the case when the cavity is situated at the rear of the foil.

6. Hydrodynamic features of hydrofoils

The hydrodynamic forces of a hydrofoil in both noncavitated and cavitated flow are calculated from the same hypothesis of a plane section which is generally postulated in the theory of large-span foils. It is assumed that foil-span element dz has the same lift as a similar element of an infinite foil placed at an effective angle of attack. The depth of hydrofoil immersion reduces c_y^a of the profile, increases the induced flow downwash α_i , and changes the effective angle of attack due to the profile thickness.

It will be shown below that a wedge-shaped profile with wake cavitation (Figure 77, flow pattern II) has properties close to those of a profile in noncavitated flow. However, angle of attack α , measured from the chord line, is smaller than the angle of attack measured from the chord by the amount μ (Figure 83). When the profile moves at a large depth, μ does not affect the lift, but as the foil approaches the free surface, the effect of the profile taper demonstrates itself in increasing the effective angle of attack by the amount $\mu\lambda\left(\frac{2h}{b}\right)$. As shown by Fedorov $\chi\left(\frac{2h}{b}\right) \approx \kappa_2^{-1}\left(\frac{2h}{b}\right) - 1$.

For an ideal foil $c_{y\infty}^a = 2\pi$; however, it was found experimentally that $c_{y\infty}^a$ is somewhat smaller than 2π and therefore we shall set $c_{y\infty}^a = 2\pi k_0$, where $k_0 < 1.0$.

Using the above results we express the lift coefficient as

$$c_y = \frac{2\pi k_0 \kappa_2 [\alpha + \alpha_1 + \mu\chi]}{1 + \frac{2k_0}{\lambda} \cdot \frac{\kappa_2}{\kappa_1} (1 + \tau)}, \quad (7.14)$$

where $\kappa_1 = \kappa_1\left(\frac{h}{L}\right)$ and $\kappa_2 = \kappa_2\left(\frac{2h}{b}\right)$. For an infinite fluid $\kappa_1 = 1$ and $\kappa_2 = 1$. For a very small immersion depth κ_1 and κ_2 tend to 0.5, while c_y is halved. Angle α_1 depends on the profile camber; this angle will be defined below.

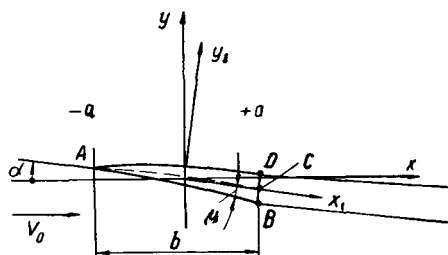


FIGURE 83.

The induced drag and induced downwash are determined from (7.10). If the foil is not thin and a wide cavity forms behind it, then the additional downwash due to the cavity (see Section 3) can be calculated from the expression

$$\frac{v_i}{v_i'} = \frac{v_i' + \Delta v_i}{v_i'} = 1 + \tau.$$

The induced drag coefficient and the downwash angle are finally obtained from the expression

$$c_{xi} = \frac{c_y^2}{\pi \lambda \alpha_i} (1 + \tau) = c_y \alpha_i. \quad (7.15)$$

The value of $1 + \tau$ for a wedge-shaped [tapered] profile is found from formula (7.9). This quantity has been incorporated into (7.14). In addition to the induced drag the foil is acted upon by the Bobylev drag (see Section 9), the friction drag and Zhukovskii [form] drag.

The Zhukovskii drag arises as a result of loss of suction force at the profile nose. In round-nosed airfoils a large part of the suction force actually materializes and the Zhukovskii drag is low. In order to prevent cavitation and flow separation, hydrofoils are usually designed with a sharp leading edge, at which the suction force does not materialize. Flow past this sharp edge produces a vortex which is carried away by the flow. The calculation of Zhukovskii drag is given below.

It can be concluded from the above that from the hydrodynamic standpoint a cavitating hydrofoil differs from one without cavitation only by the Bobylev drag and by a usually quite insignificant increase in the induced drag due to expansion of the cavity.

7. Flow past a wedge-shaped profile

We now consider the flow past a thin tapered profile with a cavity, applying all the standard hypotheses of thin-wing theory (Figure 83). The $x_1 y_1$ coordinate system associated with the profile is oriented so that the origin is located at the middle of foil chord b and the x_1 axis coincides with the chord line AB of profile ABD . The profile is wedge-shaped and in general the angle made by the camber line with the wedge generatrix is $\pm \mu$, which is a quantity dependent on the abscissa x_1 . The equation of the profile camber line is $y_1 = l(x_1)$ and the angle of attack is α . If the flow is assumed to be potential, then the normal velocities at the lower (-) and upper (+) boundaries are

$$\begin{aligned} \frac{\partial \varphi}{\partial n_{(-)}} &= V_0 [\alpha - l'(x_1) + \mu] = -v_1 - v_2; \\ \frac{\partial \varphi}{\partial n_{(+)}} &= V_0 [\alpha - l'(x_1) - \mu] = -v_1 + v_2. \end{aligned}$$

Angle α , $l'(x_1)$ and μ for a slender profile are very small; hence the profile can be moved to the x axis on the assumption that the boundary conditions

$$\alpha + \frac{v_1}{V_0} = f'(x), \quad \pm \mu \pm \frac{v_2}{V_0} = 0 \quad (7.16)$$

are satisfied on the x -axis segment from $-a$ to $+a$, where $a = \frac{b}{2}$. The first of boundary conditions (7.16) is the ordinary condition of thin-wing theory and pertains to the camber line. The second boundary condition pertains to an uncambered wedge.

If it is assumed that a vortex of strength $\gamma = \gamma(x)$ is situated on segment b of the x axis, then an elementary vortex located at point ξ of this axis has a circulation $d\Gamma = \gamma(\xi) d\xi$. According to the Biot-Savart law the following velocity is induced at point x :

$$dv_1(x) = \frac{-\gamma(\xi) d\xi}{2\pi(x-\xi)}.$$

Integrating, and substituting the result into the first of equations (7.16), the known equation of thin-wing theory is obtained:

$$\alpha + \frac{1}{2\pi V_0} \int_{-a}^{+a} \frac{\gamma(\xi) d\xi}{\xi - x} = f'(x). \quad (7.17)$$

Function $f'(x)$ can be found by specifying function $\gamma(\xi)$ with the aid of equation (7.17). A second integration then yields the airfoil equation $y = f(x)$. Equation (7.17) can be solved by the well-known Glauert method. Traversing a vortex sheet element along the edges of rectangle 1, 2, 3, 4 (Figure 84) yields

$$u_{1(-)} dx + v_1 dy - u_{1(+)} dx - v_1 dy = -\gamma dx.$$

Since v_1 is continuous when crossing the x axis, $u_{1(-)} - u_{1(+)} = -\gamma$ or, by virtue of symmetry, $\gamma = 2 u_{1(+)}$. The tangential velocity thus possesses a discontinuity when crossing the x axis.

It is assumed that a cavity rolls off the edges of the wedge and that the free streamlines I and II extend to infinity. According to the preceding definitions the velocity circulation is

$$\Gamma = \int_{-a}^{+a} \gamma(\xi) d\xi = \int_{-a}^{+a} (u_{1(-)} - u_{1(+)}) d\xi.$$

Figure 84 shows the flow pattern and flow boundaries. Since contours I-IV-II and I-(-a)-II-II', V, I' and I were drawn within the potential flow, the linear velocity integrals over these contours are zero, and hence $\Gamma + \Gamma_1 = 0$ and $\Gamma + \Gamma_2 = 0$, or $\Gamma_1 = \Gamma_2$. The linear integrals over cavity

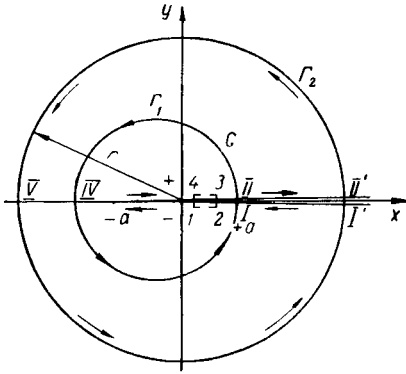


FIGURE 84.

segments I—I' and II—II' cancel. Contours II—IV—I and II'—V—I' are termed regular contours, since they intersect the cavity at equal abscissas. Taylor's [Kelvin's] theorem claims that the velocity circulation in steady motion is the same over any regular contour encompassing the profile /3/.

8. Application of the Sedov theory to cavitating hydrofoils

Sedov's theory /19/ can be used for determining the hydrodynamic characteristics of a hydrofoil provided that its profile equation $y = f(x)$ is known. From the physical point of view the flow in the vicinity of a thin curved profile can be approximately treated as the superposition of two flows — one induced by the vortex strength $\gamma(x)$, distributed along the segment $(-\frac{b}{2}, +\frac{b}{2})$, and another, corresponding to cavitated flow past the profile and generated by sources $q(x) \approx 2 v_2$, distributed along the segment $(-\frac{b}{2}, +\infty)$.

In order to construct the theory of a thin cavitating hydrofoil we assume in the case under study that $W_1(z)$ is a complex potential in the vicinity of the vortex sheet ($W_1(z) = \varphi_1 + i\psi_1$), while $W_2(z)$ is a complex potential of symmetric cavitated flow ($W_2(z) = \varphi_2 + i\psi_2$). In keeping with boundary conditions (7.16) we have the following symmetry conditions: $F_1(z) = \frac{dW_1}{dz} = u_1 - iv_1$. Here, when approaching segment b from the top (+) and the bottom (-), $u_{1+} = -u_{1-}$, while $v_{1+} = v_{1-}$ and $F_2(z) = \frac{dW_2}{dz} = u_2 - iv_2$. Also $u_{2+} = u_{2-} = u_2$; $v_{2+} = -v_{2-}$ at interval $(-\frac{b}{2}, +\infty)$, since by definition the cavity extends to infinity.

We apply the Cauchy formula $F(z) = \frac{1}{2\pi i} \oint \frac{F(\zeta)}{\zeta - z} d\zeta$ to the contour delineating region G and proceeding from point $z = -a$ along the top surface of the profile and cavity to the large circle $z = -\infty$, then along this circle to the lower boundary of the cavity, and then along it and along the lower surface of the profile to point $z = -a$ (see Figure 84).

At the large circle's circumference $\frac{dW_1}{dz} = \frac{i\Gamma}{2\pi z}$; consequently, the contribution to the integral in the Cauchy formula along this circle is zero. The cavity boundaries from $x = +a$ to $x = -\infty$ were moved onto the x axis; velocities u_1 and v_1 at the upper and lower boundaries have the same sign, while the direction of traverse of the upper and lower boundaries is opposite. Consequently the contribution to the integral along the cavity boundaries is also zero.

Thus, the only nonzero part of the integral is obtained only by traversing the profile contour from the lower to the upper separation point. Since from symmetry $F_1(\zeta)_+ - F_1(\zeta)_- = u_{1+} - u_{1-} = \gamma(\zeta)$,

$$F_1(z) = \frac{1}{2\pi i} \int_{-a}^{+a} \frac{\gamma(\zeta)}{\zeta - z} d\zeta = u_1(z) - iv_1(z).$$

Substitution of $v_1(x, 0)$ into the first linearized boundary condition yields (7.17).

The idea underlying the Sedov solution consists in selecting auxiliary function $g(z)$ in such a manner that the integrand in the Cauchy formula applied to function $F_1(z)g(z)$ would contain only the imaginary part of $F_1(z)$. It is clear that function $g(z)$ must be continuous in region G , and analytical function $F_1(z)g(z)$ should decrease at infinity not slower than $1/z$. Function $g(z)$ to both sides of the cut $(-a, +a)$ should have a different sign so that $g(x_1 + i0)$ would be equal to $-g(x_1 - i0)$. Under these conditions the Cauchy integral applied to function $F_1(z)g(z)$ will have the form

$$F_1(z) = \frac{1}{2\pi i} \cdot \frac{1}{g(z)} \int_{-a}^{+a} \frac{-i2v_1 g(\xi + i0)}{\xi - z} d\xi.$$

We introduce, in the assumed coordinate system, the function $g(z) = \sqrt{\frac{z+a}{z-a}}$, the root taking a minus sign at $x < -a$. This function is continuous over the entire region G and at the boundaries of the segment. If the root is taken with the appropriate signs it will have the form $g(x + i0) = -g(x - i0) = i\sqrt{\frac{a+\xi}{a-\xi}}$. Hence

$$-i2v_1 g(\xi) = 2v_1 \sqrt{\frac{a+\xi}{a-\xi}}.$$

The Sedov formula can be expressed in the following final form in the assumed coordinate system:

$$F_1(z) = u_1 - iv_1 = \frac{i}{2\pi} \sqrt{\frac{z-a}{z+a}} \int_{-a}^{+a} \frac{2v_1}{\xi - z} \sqrt{\frac{a+\xi}{a-\xi}} d\xi. \quad (7.18)$$

The expansion of F_1 as $z \rightarrow \infty$ is $\frac{dW_1}{dz} = \frac{i\Gamma}{2\pi z} + \dots$. Expression (7.18) with the first of boundary conditions (7.16) yields

$$\Gamma = - \int_{-a}^{+a} 2v_1 \sqrt{\frac{a+\xi}{a-\xi}} d\xi = bV_0 \int_{-1}^{+1} [\alpha - f'(t)] \sqrt{\frac{1+t}{1-t}} dt \dots \quad (7.19)$$

The lift of the profile is

$$\begin{aligned} Y &= qV_0\Gamma = 2\pi b \frac{\rho V_0^2}{2} (\alpha + \alpha_1); \\ \alpha_1 &= -\frac{1}{\pi} \int_{-1}^{+1} f'(t) \sqrt{\frac{1+t}{1-t}} dt. \end{aligned} \quad (7.20)$$

The suction force acting on the profile in the vicinity of $z = -a$ is also found from the Sedov formula

$$P = -q\pi \left[(z+a) \left(\frac{dW_1}{dz} \right)^2 \right]_{z=-a}.$$

Simple calculations yield

$$P = -2\pi b \frac{qV_0^2}{2} (\alpha + \alpha_2)^2; \quad (7.21)$$

$$\alpha_2 = -\frac{1}{\pi} \int_{-1}^{+1} \frac{f'(t)}{\sqrt{1-t^2}} dt.$$

In a real, discontinuous fluid a Zhukovskii vortex forms at the sharp leading edge, a sheet of such vortices rolls off the profile surface, and the suction force vanishes. This produces the Zhukovskii drag $X_i = -P$; the Zhukovskii drag coefficient is

$$c_{xi} = 2\pi(\alpha + \alpha_2)^2.$$

The complex velocity $F_z(z)$ due to sources $q(x) = 2v_z = 2V_0\mu(x)$ distributed along segment $-a < x < +\infty$ can also be obtained from the Cauchy formula. On the basis of the assumed symmetry $F_z(z)$ can be expressed as

$$F_z(z) = u_z - iv_z = -\frac{1}{2\pi} \int_{-a}^{+\infty} \frac{v_{z+} - v_{z-}}{\zeta - z} d\zeta. \quad (7.22)$$

The integration in (7.22) is carried out only along the profile and cavity axes, which were moved to the x axis. In spite of the fact that the drag for a cambered wedge is not obtainable from the Bobylev formula and cannot be calculated by the same method, we shall still call it the Bobylev drag.

For a plane cavity the contour of free boundaries at high x is $/3/$

$$y = \pm \frac{2}{V_0} \sqrt{\frac{X_0}{\pi q}} \sqrt{x}.$$

Bobylev's drag coefficient $c_{x0} = \frac{X_0}{b \frac{qV_0^2}{2}}$ for an uncambered wedge is obtained directly from the above solution and, for small angle μ and $\sigma = 0$, is equal to

$$c_{x0} = \frac{8}{\pi} \left(1 - \frac{2}{\pi} \mu\right) \mu^2. \quad (7.23)$$

According to the Sedov formula, which is valid only for slender bodies, the drag coefficient at $\sigma > 0$ is approximately equal to $c_{x0} + \sigma$.

As a result we obtain the following general conclusion: a slender profile with wake cavitation has the same lift and drag as the profile camber-line section in noncavitating flow, but with the Bobylev drag calculated for the same but uncambered profile added to the camber-line section drag.

9. Estimating the hydrodynamic features of a noncavitating wedge-shaped profile

Figure 85 shows the pressure distribution along the edges of the wedge. The solid curve corresponds to the pressure distribution $\bar{p} = \frac{2(p - p_0)}{qV_0^2}$ over

the edges of a symmetric wedge (Bobylev's problem). The dashed curves for $\bar{p}_{(-)}$ and $\bar{p}_{(+)}$ show the pressure distributions respectively for the lower (-) and upper (+) boundaries of a cambered wedge; the area bounded by these curves is proportional to the lift. An obvious condition for the absence of cavitation at the upper edge is $\bar{p}_{(+)} > 0$, i.e., the pressure at the surface of this edge should be higher than the static pressure.

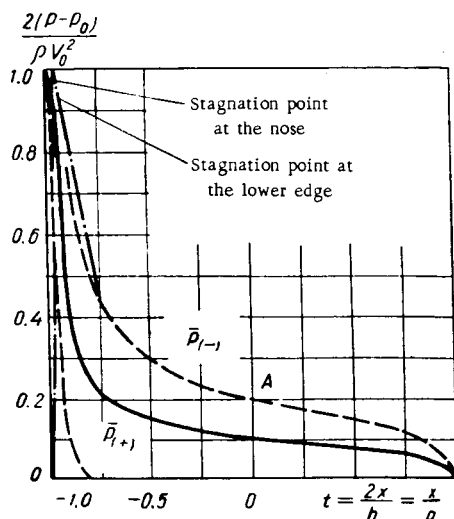


FIGURE 85.

We shall clarify the limiting conditions for noncavitated flow past a wedge-shaped profile. We designate the tangential velocity of flow past the edges of an uncambered wedge by $V_s = V_0 + u_s$ and the additional tangential velocity induced by the vortex sheet (profile camber) by u_1 . The resultant tangential velocity is then:

at the upper edge

$$V_{s(+)} = V_0 + u_2 + u_1;$$

at the lower edge

$$V_{s(-)} = V_0 + u_2 - u_1.$$

The pressure at the upper and lower edges is obtained from the Bernoulli equation

$$p_s - p_0 = -\rho V_0 (u_2 \pm u_1) - \frac{1}{2} \rho (u_2 \pm u_1)^2.$$

The condition for noncavitated flow at the upper edge is $p_+ = p_0$ or $u_2 + u_1 = 0$. Velocity u_s for an uncambered wedge is negative, and hence $V_0 + u_2 < V_0$; the resultant velocity at the nose stagnation point is zero and hence $V_0 + u_2 = 0$ and $u_2 = -V_0$.

Using the pressure distribution over the edges, we determine the lift and the Bobylev drag. Retaining [only] first-order infinitesimals,

$$\begin{aligned} Y &= \int_{-a}^{+a} (p_{(-)} - p_{(+)}) dx = \int_{-a}^{+a} \varrho (V_0 + u_2)(u_{1(+)} - u_{1(-)}) dx, \\ X_0 &= \int_{-a}^{+a} (p_{(-)} + p_{(+)}) \mu dx = -2 \int_{-a}^{+a} [\varrho V_0 u_2 + \frac{\varrho}{2} (u_2^2 + u_1^2)] \mu dx. \end{aligned} \quad (7.24)$$

By definition $u_{1(+)} - u_{1(-)} = \gamma$ (see Section 7). Consequently, the elementary circulation at chord point x is $d\Gamma = \gamma dx = 2u_{1(+)} dx$, while according to Zhukovskii's theorem the elementary lift is $dY = \varrho (V_0 + u_2) d\Gamma$, where $V_0 + u_2 = V_0$ is the velocity past the vortex $d\Gamma$. It was assumed in the preceding sections that for an infinitely thin wedge ($\mu \rightarrow 0$) $u_2 = 0$; for a wedge with finite angle μ , u_2 and V_0 are functions of abscissa x . Consequently, the refined form of equation (7.17) is

$$\alpha + \frac{1}{2\pi V_0'(x)} \int_{-a}^{+a} \frac{\gamma(\xi) d\xi}{\xi - x} = f'(x). \quad (7.17a)$$

Theoretically the maximum lift corresponding to the cavitation boundary ($p_+ = p_0$) can be obtained when $u_{1(+)} = -u_2$. Hence from (7.24)

$$Y_{\max} = -\varrho V_0^2 b \int_{-1}^{+1} \left[\frac{u_2}{V_0} + \left(\frac{u_2}{V_0} \right)^2 \right] dt.$$

The drag of an uncambered wedge from (7.24) is

$$X_0 = -\varrho V_0^2 b \int_{-1}^{+1} \left[\frac{u_2}{V_0} + \frac{1}{2} \left(\frac{u_2}{V_0} \right)^2 \right] \mu dt.$$

However, Bobylev's solution yields directly

$$X_0 = \frac{8}{\pi} \left(1 - \frac{2}{\pi} \mu \right) \mu^2 b \frac{\varrho V_0^2}{2} = \left(\frac{4}{\pi} \mu - \frac{8}{\pi^2} \mu^2 \right) \mu b \varrho V_0^2.$$

Equating both these expressions for X_0 we can set

$$-\int_{-1}^{+1} \left(\frac{u_2}{V_0} \right) dt = \frac{4}{\pi} \mu; \quad \int_{-1}^{+1} \left(\frac{u_2}{V_0} \right)^2 dt = \frac{16}{\pi^2} \mu^2.$$

With the above expressions we find the limiting formulas for a cambered wedge when the pressure at the upper edge equals the static pressure in the flow:

$$\begin{aligned} X_{0\text{cam}} &= \underbrace{\frac{8}{\pi} \mu^2 \left(1 - \frac{4}{\pi} \mu \right) b \frac{\varrho V_0^2}{2}}_{c_{x0}}; \\ Y_{\max} &= \underbrace{\frac{8}{\pi} \mu \left(1 - \frac{4}{\pi} \mu \right) b \frac{\varrho V_0^2}{2}}_{c_{y\max}}. \end{aligned} \quad (7.25)$$

If the profile curve of the wedge is curved along an arc segment with camber f , then in order to obtain $c_{y \max} = 0$ at $\alpha = 0$ we require that $\frac{f}{b} = \frac{2}{\pi^2} \mu \left(1 - \frac{4}{\pi} \mu\right)$. The Sedov formula for a circle-arc segment gives $\alpha_2 = 0$ and $\alpha_1 = 2 \frac{f}{b}$, and therefore when $\alpha = 0$ we have impact-free entry and the Zhukovskii drag is zero.

TABLE 15

μ , deg	2	3	5	7	9
$c_{y \max}$	0.085	0.124	0.197	0.264	0.318
$\frac{f}{b}$	0.00675	0.01	0.0157	0.021	0.025
$K_{a \max}$	28.5	19.0	11.5	8.2	6.4

Table 15 lists values of $c_{y \max}$ and corresponding values of f for wedges with different μ . The lower row gives values of the theoretical lift/drag ratio $K_{a \max} = \frac{y_{\max}}{x_\delta}$. Actually the value of $K_{a \max}$ is much lower, since the Bobylev drag should be supplemented by the frictional resistance and the Zhukovskii drag.

The maximum lift from (7.25) is defined subject to the condition that at the upper edge $u_2 + u_{1(+)} = 0$, while at the lower edge $u_2 + u_{1(-)} = 2 u_2$. As a result the tangential velocity at the lower edge is $V_{s(-)} = V_0 + 2 u_2$.

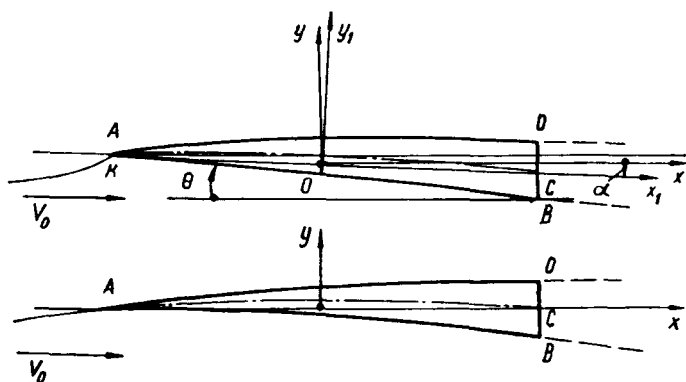


FIGURE 86.

At the stagnation point $V_s = 0$; consequently $V_0 + 2 u_2 = 0$, and this point is situated at abscissa x_k , where $u_2 = -\frac{1}{2} V_0$, while the excess pressure for

an uncambered wedge is $3/4$ of the velocity head. Hence the lift which can be actually attained at the upper edge in the absence of cavitation is somewhat lower than that calculated from (7.25). In general it is always desirable to attain impact-free entry under operating conditions, i. e., one should strive to locate the stagnation point at the nose in the manner shown at the bottom of Figure 86.

10. Polar diagram of hydrofoil and experimental data

Figure 87 shows the hydrodynamic characteristics of a delta-shaped foil with opening [wedge] angle $2\mu = 10^\circ$, span $L = 320$ mm, chord $b = 100$ mm, angle $\alpha_1 = 3^\circ$ (see equation (7.20)), $\alpha_2 \approx 0$. Such hydrofoils were tested by Fedorov and the experimental data were compared with experimental results [24]. The models in these experiments were towed at 8 m/sec with relative immersion depths of $\frac{h}{b}$ equal to 0.955, 0.445 and 0.255. The principal quantities needed for calculating c_y were obtained from formula (7.14) with $k_0 = 0.8$; the principal results are listed in Table 16.

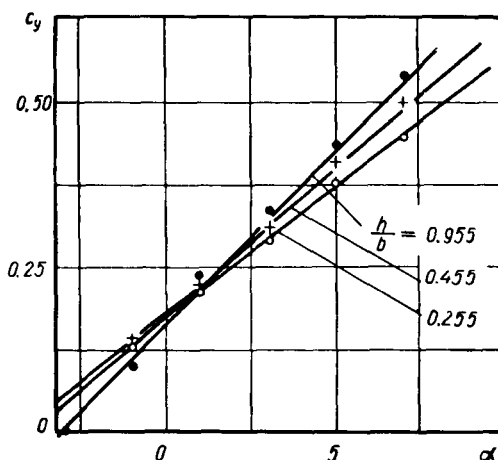


FIGURE 87.

It is seen from Figure 87 that the experimental data (points) are very close to the theoretical results (lines). The last two columns of Table 16 list the averaged experimental data on c_y^a and on the zero lift angle $\alpha_0 = -\alpha_1 - \mu\chi$. Comparison with theoretical results shows that they are in satisfactory agreement with experimental data.

The drag coefficient is calculated from the expression

$$c_x = c_{x0} + c_{x1} + c_{xI} + 2c_{f1}$$

the Bobylev drag is given by

$$c_{x0} = \frac{8}{\pi} \left(1 - \frac{4}{\pi} \mu \right) \mu^2 = 0.172;$$

the induced drag is

$$c_{xi} = \frac{c_y^2}{\pi \lambda \alpha_1} (1 + \tau) \begin{cases} 0.13 c_y^2, & \frac{h}{b} = 0.955; \\ 0.15 c_y^2, & \frac{h}{b} = 0.455; \\ 0.165 c_y^2, & \frac{h}{b} = 0.255; \end{cases}$$

and the Zhukovskii drag is given by

$$c_{xj} = 2\pi (\alpha + \mu\lambda + \alpha_2 + \alpha_i)^2.$$

TABLE 16

$\frac{h}{b}$	$\frac{h}{L}$	α_1	α_i	$1 + \tau$	$2\pi k_0 \alpha_1$	$1 + \frac{2k_0 \alpha_1}{\lambda \alpha_1} \times (1 + \tau)$	$\frac{\alpha}{c_y}$	$\mu\lambda$	Experiment	
									$\frac{\alpha}{c_y}$	$\alpha_1 + \mu\lambda$
0.955	0.300	0.95	0.84	1.092	4.78	1.62	2.94	0.25°	3.01	3.15
0.455	0.142	0.85	0.73	1.092	4.28	1.645	2.60	0.90°	2.56	3.90
0.255	0.080	0.75	0.66	1.092	3.78	1.63	2.31	1.65°	2.29	4.50

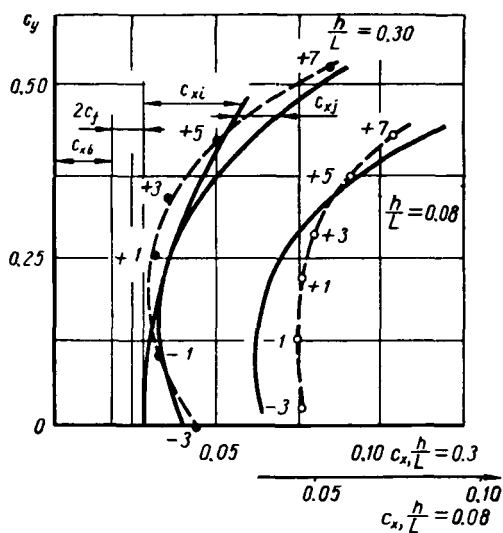


FIGURE 88.

In the given case $\alpha_2 = 0$, the frictional resistance is $2c_f = 0.01$. In general the frictional resistance is calculated either from the Prandtl-Schlichting formula, or from experimental data.

Figure 88 shows polar diagrams for immersion depths of $\frac{h}{L} = 0.3$ and $\frac{h}{L} = 0.08$. It is seen by comparing these curves that the experimental data differ to a greater degree from the calculated results than those for the lift.

The approximate theory of cavitating hydrofoils thus expresses satisfactorily the lift, and somewhat less satisfactorily (but still correct in a qualitative respect) the total drag.

11. Fully stalled profile

A plate in Rayleigh flow (Figure 77, IV), a cambered airfoil or profile, flow past which involves streamline separation from the upper surface (Figure 77, III), can be identified with flow past a tapered profile and the above theory can be applied to these cases. It was pointed out in Section 1 that free streamline AD and line AB can be treated as the walls of profile ABD and it, in turn, can be interpreted by means of the theory of profiles with cavitated wakes.

The mean (camber) line AC (dashed line) [of a wedge] and the mean chord AC of a plate should perform the same function as for a tapered profile. Hence the lift actually developed in a flow past a plate can be determined in two ways: on the one hand, from Rayleigh equations for plate AB, placed in a flow at angle θ , and on the other hand, for equations of the wing theory referred to angle of attack α for chord AC of the camber line. As for wedge-shaped profiles these considerations are valid primarily for small angles of attack, when the angle between the plate and the free streamline is small. The lift coefficient referred to chord b is then given by

$$c_y = \frac{\partial c_y}{\partial \theta} \theta = \frac{\partial c_y}{\partial \alpha} \alpha.$$

The solution of the problem of streaming flow past a plate at some angle of attack /10/ yields the following expressions for the lift and drag:

$$\begin{aligned} Y &= \frac{2\pi \sin \theta \cos \theta}{4 + \pi \sin \theta} b \frac{\rho V_0^2}{2}; \\ X &= \frac{2\pi \sin^2 \theta}{4 + \pi \sin \theta} b \frac{\rho V_0^2}{2}. \end{aligned} \quad (7.26)$$

The lift and drag coefficients for small θ are respectively $c_y = \frac{\pi}{2} \theta$ and $c_x = \frac{\pi}{2} \theta^2$.

Equating the lift and drag coefficients obtained from the streamline-flow theory and from the wing theory we find that

$$\begin{aligned} c_y &= 2\pi (\alpha + \alpha_1) = \frac{\pi}{2} \theta; \\ c_x &= 2\pi (\alpha + \alpha_2)^2 + c_{x0} = \frac{\pi}{2} \theta^2. \end{aligned}$$

According to the first expression the effective angle of attack is $\alpha + \alpha_1 = \frac{1}{4} \theta$.

A plate in streaming flow can be treated as a deforming wedge-shaped profile, the upper surface of which rises with an increase in θ such that the effective angle of attack $\alpha + \alpha_1$ increases four times as slowly as angle θ .

It is possible to select a wedge-shaped profile with angle μ which has the same lift as a plate at some angle of attack, in which case

$$c_y \approx \frac{8}{\pi} \mu \approx \frac{\pi}{2} \theta.$$

If this profile is cambered so that $\alpha + \alpha_2 = 0$, the drag coefficient will

become $c_x = \frac{8}{\pi} \mu^2$ and the lift/drag ratio will be $K_a = \frac{1}{\mu}$, while for a plate

$K_a = \frac{1}{\theta} = \frac{\pi^2}{16} \cdot \frac{1}{\mu}$. We conclude from this that in the case of equal lift a cambered tapered profile in noncavitated flow at the upper edge should have a lift/drag ratio which is at most a factor of $\frac{16}{\pi^2}$ greater than a plate with the same chord with streamline separation.

This situation can be explained as follows (Figure 89). The dependence of coefficients c_y and c_x on angle θ for a plate in streaming flow is expressed

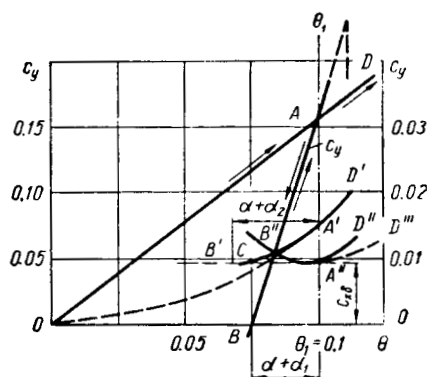


FIGURE 89.

by straight line OA and parabola OA' . If we imagine that, upon attaining an angle of θ_1 (in Figure 89, $\theta_1 = 0.1$ rad), the free streamline above the plate solidifies, and the solid wedge thus formed rotates so as to reduce angle θ , then the value of c_y will change along straight line AB while that of c_x will vary along parabola $A'B'$. Clearly $\theta_1 - \theta_B = \alpha + \alpha_1$. If the profile has a bottom camber selected in such a manner that the lift corresponds to point A and the Zhukovskii drag is zero, then at $\theta = \theta_1$ only the Bobylev drag c_{x0} will remain.

When the angle of attack is reduced c_y will change along straight line AB (with slope 2π), while c_x will vary along the left branch of the

Zhukovskii-drag parabola $B'A'D''$. When the angle of attack is increased ($\theta > \theta_1$) flow separation will occur at the upper surface. In both cases the values of c_y will vary along straight line AD (with slope $\frac{\pi}{2}$), and c_x respectively along curve $A'D'$ for flow past a plate and curve $A'D''$ for flow past a cambered plate or wedge. It is thus found that, when rotated so as to reduce angle θ , a plate with solidified streamline above it and the cambered wedge behave like an airfoil, while when rotated so as to increase the angle of attack they behave as a plate in streaming flow.

Separation from the top surface is sometimes delayed and occurs at some angle of attack $\theta > \theta_1$; the lift drops sharply upon separation. However, this separation delay occurs at a relatively low velocity and cannot be expected at high flow velocities.

12. Application of wing theory to the calculation of a cavitating plate

The validity of the correspondence of lift coefficients $c_y = 2\pi(\alpha + \alpha_1) = \frac{\pi}{2}\theta$ for a cavitating plate and for a camber-line arc of a wedge-shaped airfoil can be established by direct calculation of angle α_1 . This angle is now calculated from the Sedov formula (7.20), while the mean line of a profile formed by a plate and the free streamline above it will be calculated from Fedorov's formulas /23/.

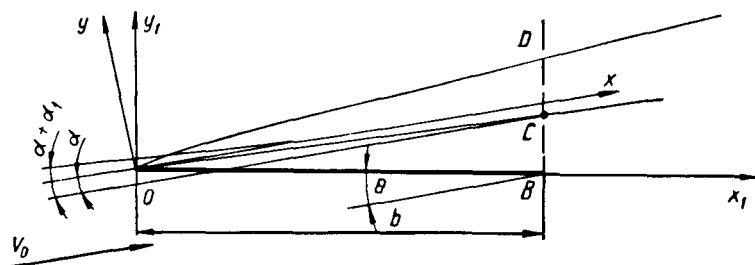


FIGURE 90.

Figure 90 depicts the plate and free streamlines for $\theta = 10^\circ$, the coordinates of which were taken from /23/. The free streamline makes a large angle with the plate, the mean-line chord has also a relative length of 1.0, and hence the abscissa of point D does not coincide with 1.0. At low θ , in the limit as $\theta \rightarrow 0$, the abscissa of point D tends to infinity. The above remarks pertain to very small angles θ .

In the coordinate system shown in Figure 90 the equation of the free streamline contour behind the plate is expressed by Fedorov's formulas

$$\begin{aligned} \frac{x_1}{b} &= \frac{1}{4 + \pi \sin \theta} \left[\frac{\cos \theta}{2} (\operatorname{ch} 2\tau - 1) - 2(\operatorname{ch} \tau - 1) \right]; \\ \frac{x_2}{b} &= \frac{1}{4 + \pi \sin \theta} \left[\frac{\cos \theta}{2} (\operatorname{ch} 2\tau - 1) + 2(\operatorname{ch} \tau + 1) + \pi \sin \theta \right]; \\ \frac{y}{b} &= \frac{\sin \theta}{4 + \pi \sin \theta} \left(\frac{\operatorname{sh} 2\tau}{2} - \tau \right), \end{aligned}$$

where τ is a parameter varying from zero to infinity. For small θ we have approximately $\cos \theta = 1$ and $\sin \theta = \theta$. It can be shown by calculations that, as $\theta \rightarrow 0$, the free-streamline point above the trailing edge of the plate

($\frac{x_1}{b} = 1$) is obtained at $\tau_0 \approx 1.76$.

Using these expressions, we find the correspondence between the angle of attack α of the chord line and the angle of attack θ of the plate. For small angles of attack

$$\alpha = \theta - \frac{1}{2} \cdot \frac{y}{x_{\tau=\tau_0}} = \theta - \frac{1}{2} \theta \frac{\operatorname{sh} 2\tau_0 - 2\tau_0}{\operatorname{ch} 2\tau_0 - 4\operatorname{ch} \tau_0 + 3} = \theta(1 - 0.85) = 0.15\theta.$$

For the mean line we may set $f(x) = \theta\psi'(x)$, where

$$\psi'(x) = \frac{1}{2} \cdot \frac{dy}{dx_1} - \frac{1}{2} \cdot \frac{y}{x_{\tau=\tau_0}} = \frac{1}{2} \left[\frac{\operatorname{ch} 2\tau - 1}{\operatorname{sh} 2\tau - 2\operatorname{sh} \tau} - \frac{\operatorname{sh} 2\tau_0 - 2\tau_0}{\operatorname{ch} 2\tau_0 - 4\operatorname{ch} \tau_0 + 3} \right].$$

With the aid of (7.20) and various computations, we derive

$$\frac{\alpha_1}{\theta} = -\frac{1}{\pi} \int_{-1}^{+1} \psi'(t) \sqrt{\frac{1+t}{1-t}} dt \approx 0.1.$$

Hence, by direct calculations, $\alpha + \alpha_1 = \frac{1}{4}\theta$.

The drag of a cavitating plate is $c_x = \frac{\pi}{2}\theta^2$. Since $\alpha = 0.15\theta$, the wedge formed by the plate and streamline OD will have a wedge angle of $2\mu = 2(\theta - \alpha) = 1.7\theta$. Bobylev's drag for this wedge is $\epsilon_{x0} = (0.85)^2 \theta^2 = 1.83\theta^2$, i. e., 16.5% overrated. Consequently in practice the drag of a plate is equivalent to the drag of a wedge formed by the plate and the free boundary.

13. Stalled foil of finite span

Flow past a stalled foil of finite span, as past an ordinary foil, involves the appearance of an induced velocity and an induced downwash $\alpha_i = \frac{c_p}{\pi\lambda x_1}$. However, the upper surface of a stalled foil is formed by the free boundary, which reacts to the downwash by coming close to the trailing edge of the profile by an amount $a_i b$. Hence the angle of attack of the chord line increases by $\frac{1}{2}\alpha_i$ due to the approach of the boundary and decreases by an amount α_i due to the downwash proper. Thus, if the angle of attack of the chord line at $\lambda = \infty$ is denoted by α , then the effective angle of attack of the chord line for a finite-span foil is

$$\alpha_{ef} = \alpha + \frac{1}{2}\alpha_i - \alpha_i = \alpha - \frac{1}{2}\alpha_i = 0.15(\theta - \alpha_i).$$

The value of α_i for the profile formed by the plate and the free boundary is proportional to α , i. e., $\frac{\alpha_i}{\alpha} = \frac{0.1}{0.15} = \frac{2}{3}$. Hence the effective angle of attack for a finite span is

$$(\alpha + \alpha_i)_{ef} = \left(1 + \frac{2}{3}\right) \left(\alpha - \frac{1}{2}\alpha_i\right) = \frac{1}{4}(\theta - \alpha_i).$$

The lift coefficient c_y when the immersion depth h is so great that $\kappa_2 \approx 1$ but κ_1 still differs from unity, will have the following form when the additional, cavitation-induced downwash is taken into account:

$$c_y = \frac{\frac{\pi}{2} \theta}{1 + \frac{1}{2\lambda\kappa_1} (1 + \tau)}. \quad (7.27)$$

This yields the induced downwash angle $\alpha_i = \frac{\theta}{1 + \frac{1}{2\lambda\kappa_1} (1 + \tau)}$ in the vicinity of a stalled hydrofoil. It can be shown that the stalled and ordinary foils have the same downwash angle provided they have equal λ and c_y .

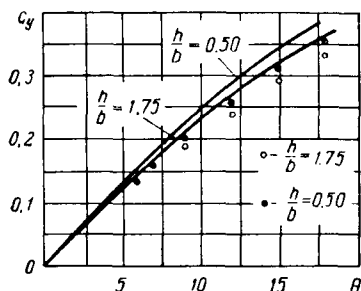


FIGURE 91.

Using Fedorov's formulas /22/, Kryukov /9/ obtained an approximate expression for the lift coefficient of an infinite plate ($\lambda = \infty$) as it approaches the surface. Denoting the streamline thickness at infinity by $\bar{\delta} = \frac{\delta}{b}$, the Kryukov equation assumes the form

$$c_y = \frac{2\pi \sin \theta \cos \theta}{4 + \pi \sin \theta} \left(1 + \frac{\cos \theta}{1 + 3.3 \sqrt{\bar{\delta}}} \right).$$

Using (7.26), we derive an expression for the function which takes into account the variation in c_y as the free surface is approached ($\cos \theta \rightarrow 1$):

$$\kappa_3 = \frac{c_y(\bar{\delta})}{c_{y\infty}} = 1 + \frac{1}{1 + 3.3 \sqrt{\bar{\delta}}}.$$

For not too small immersion depths $\bar{\delta}$ can be replaced by the relative immersion depth $\bar{h} = \frac{h}{b}$. Function κ_3 increases as the free surface is approached and equals 2 at $\bar{\delta} = 0$.

The lift coefficient is now

$$c_y = \frac{\frac{\pi}{2} \kappa_3 \theta}{1 + \frac{\kappa_1}{2\lambda\kappa_1} (1 + \tau)}. \quad (7.28)$$

For planing $\bar{\delta} = 0$, $\kappa_3 = 2$, $\kappa_1 = 0.5$ and $\tau = 0$; hence

$$c_y = \frac{\frac{\pi \theta}{2}}{1 + \frac{1}{\lambda}}.$$

At large depths $\kappa_3 = 1$ and $\kappa_1 = 1$; consequently

$$c_y = \frac{\frac{\pi}{2} \theta}{1 + \frac{1}{2\lambda} (1 + \tau)}.$$

Figure 91 compares Kryukov's /9/ experimental data with those obtained from (7.28), in which, however, $c_{y\infty}$ was calculated from (7.26), since angles θ , which in the experiments were as high as 18° , cannot be treated as small. It was assumed in these calculations that $1 + \tau = 1.0$ and $\lambda = 4$. This comparison shows that the theoretical values of c_y are higher than those obtained experimentally. As this comparison was conducted for wedge-shaped foils, it may be assumed that $c_{y\infty} = \frac{\pi \sin 2\theta}{4 + \pi \sin \theta} k_0$ and that the correction factor is $k_0 \approx 0.8 - 0.9$.

The above fundamentals of the theory of cavitating hydrofoils allow one to carry out practical calculations for high-aspect-ratio foils. Comparison of the theoretical results with experimental data shows that the theory describes the actual flow quite accurately. It should be noted that in examining cavitating hydrofoils we considered only the simplest scheme. This amounted to assuming everywhere that the lift distribution over the span is elliptical; the induced velocity and the dynamic surface rise were taken into account only for the center of the foil. The method for including the effect of the cavity width on the induced downwash in the vicinity of the hydrofoil is quite approximate. A number of other simplifications made in constructing the theory can be listed. However, in spite of all these approximations the theoretical and experimental results are in quite satisfactory agreement, and this makes it safe to claim that in other cases the construction of an approximate theory based on the same principles will yield satisfactory results.

Bibliography

1. Birkhoff, G. Hydrodynamics.— New York, Dover Publications. 1950
2. Golovin, S. Eksperimental'noe issledovanie pogruzheniya profilei v zhidkost' (Experimental Study of the Immersion of Profiles into a Fluid).— In: Sbornik "Trudy TsAGI,"* 807. Moskva. 1960.
3. Golubev, V. V. Lektsii po teorii kryla (Lectures on Wing Theory).— Moskva, Gostekhizdat. 1949.
4. Gurevich, M. I. Obtekaniya osesimmetricheskogo polutela konechnogo soprotivleniya (Flow Past a Finite-Drag Axisymmetric Half-Body).— Prikladnaya matematika i mekhanika, 11, 1. 1947.
5. Gurevich, M. I. Udar plastinki pri obtekani plastinki s otryvom strui (Impact of a Plate in Separated Flow Past a Plate).— Prikladnaya matematika i mekhanika, 21, 1. 1952.
6. Carafoli, E. High-Speed Aerodynamics, Compressible Flow.— New York, Pergamon Press. 1956.
7. Kochin, N. E., I. A. Kibel', and N. V. Roze. Teoreticheskaya gidromekhanika (Theoretical Hydromechanics), Part 1.— Moskva, OGIZ. 1948.
8. Krylov, V. V. Eksperimental'nye materialy po unosu gaza s kaverny, obrazovannoi metodom podduva (Experimental Data on the Ejection of Gas from a Ventilated Cavity).— In: Sbornik "Trudy TsAGI," 824. Moskva. 1961.
9. Kryukov, G. M. Raschet gidrodinamicheskikh kharakteristik kryl'ev s ploskoi nizhnei poverkhnost'yu pri struinom rezhime obtekaniya (Calculation of the Hydrodynamic Characteristics of Flat-Bottomed Hydrofoils in Streaming Flows).— In: "Sbornik rabot po gidrodinamike." Izdatel'stvo TsAGI. Moskva. 1959.
10. Lamb, H. Hydrodynamics.— New York, Dover Press. 1945.
11. Logvinovich, G. V. Pogruzhenie tel v zhidkost' i dvizhenie s razvitoi kavitatsiei (Entry of Bodies into a Fluid and Fully Cavitated Motion).— In: "Sbornik rabot po gidrodinamike." Moskva, Izdatel'stvo TsAGI. 1959.
12. Logvinovich, G. V. Pogruzhenie profilei v zhidkost', udar i glissirovanie (Entry of Profiles into a Fluid, Impact and Planing).— In: Sbornik "Trudy TsAGI," 707. Moskva. 1958.
13. Logvinovich, G. V. Progruzhenie tel v zhidkost' i nestatsionarnoe glissirovanie (Entry of Bodies into a Fluid and Unsteady Planing).— In: Sbornik "Trudy TsAGI," 807. 1960.
14. Logvinovich, G. V. Tcheniya s razvitoi kavitatsiei (Fully Cavitated Flows).— Inzhenernoi Zhurnal, 1, 1. 1961.

* [Tsentral'nyi Aerogidrodinamicheskii Institut imeni N. E. Zhukovskogo — Central Aerohydrodynamic N. E. Zhukovskii Institute.]

15. Logvinovich, G.V. Voprosy teorii kavitiruyushchikh klinovykh krylev (Problems in the Theory of Cavitating Wedge-Shaped Hydrofoils).— In: Sbornik "Trudy TsAGI," 842. Moskva. 1962.
16. Nekrasov, A.I. Teoriya kryla v nestatsionarnom potoke (Wing Theory in Unsteady Flow).— Moskva, Izdatel'stvo AN SSSR.* 1947.
17. Prandtl, L. and O.G. Tietjens. Applied Hydro- and Aeromechanics.— New York, Dover Press. 1957.
18. Riman, I.S. and R.L. Kreps. Prisoedinennye massy tel razlichnoi formy (Induced Masses of Bodies of Different Shapes).— In: Sbornik "Trudy TsAGI," 635. Moskva. 1947.
19. Sedov, L.I. Ploskie zadachi gidrodinamiki i aerodinamiki (Two-Dimensional Problems in Hydrodynamics and Aerodynamics).— Moskva, Gostekhizdat. 1950.
20. Sedov, L.I. Metody podobiya i razmernosti v mekhanike (Methods of Similitude and Dimensional Analysis in Mechanics).— Moskva-Leningrad, Gostekhizdat. 1951.
21. Sedov, L.I. and A.N. Vladimirov. Vliyanie mekhanicheskikh parametrov i yavlenie ustanovivshegosya i neustanovivshegosya glissirovaniya kilevatoi plastiny (Effect of Mechanical Parameters and the Phenomenon of Steady and Unsteady Planing of a Wedge-Shaped Plate).— Doklady AN SSSR, 33, 2. 1941.
22. Fedorov, E.A. Dvizhenie plastinki bezkonechnogo razmakha vblizi svobodnoi poverkhnosti ideal'noi nevesomoi zhidkosti (Motion of an Infinite Plate in the Vicinity of the Free Surface of an Ideal Weightless Fluid).— In: Sbornik "Trudy TsAGI," 711. Moskva. 1958.
23. Fedorov, E.A. O forme svobodnykh strui za plastinkoi i za klinom beskonechnogo razmakha (On the Shape of Free Streamlines Past a Plate and Past an Infinite Wedge).— In: "Sbornik rabot po gidrodinamike." Moskva, Izd. TsAGI. 1959.
24. Fedorov, E.A. Raschet gidrodinamicheskikh kharakteristik podvodnykh kryl'ev s klinovym profilem (Calculating the Hydrodynamic Characteristics of Wedge-Shaped Hydrofoils).— In: Sbornik "Trudy TsAGI," 842. Moskva. 1962.
25. Epshtein, L.A.— In: Sbornik "Stat'i po voprosam kavitatsionnykh techenii." Trudy TsAGI, 824. Moskva. 1961.
26. Epshtein, L.A., V.I. Blyumin, and P.S. Starodubtsev. Vliyanie chisel kavitatsii i Fruda na razmery kaverny i kolichestvo vozdukha neobkhodimogo dlya ee podderzhaniya (Effect of the Cavitation and Froude Numbers on Cavity Dimensions and the Amount of Air Needed for Maintaining It).— In: Sbornik "Trudy TsAGI," 824. Moskva. 1961.
27. Cox, P.N. and W.A. Clayden. Air Entrainment of the Rear of a Steady Cavity.— Cavitation in Hydrodynamics. Proc. Sympos. Held at the Nat. Phys. Lab., London. 1955.

* [Akademiya Nauk SSSR — Academy of Sciences of the USSR.]

28. Pierson, J.D. The Penetration of a Fluid Surface by a Wedge.—
Inst. Aeronaut. Sci., Rep. No. 381. 1950.
29. Plesset, M.S. and P.A. Shaffer Jr. Drag in Cavitating Flow.—
Rev. Mod. Phys., Vol. 20, pp. 228. 1948.
30. Watanabe, Shumpei. Resistance of Impact on Water Surface.—
Sci. Papers Inst. Phys. Chem. Res., 11, 221—227; 12,
251—267. 1930.
31. Wagner, H. Über Stoss- und Gleitvorgänge der Oberfläche von
Flüssigkeiten.— ZAMM, 4, 199—215. 1932.